Transition Metal Hydrides that Mediate Catalytic Hydrogen Atom Transfers

Deven P. Estes

Submitted in partial fulfillment of the requirements for

the degree of Doctor of Philosophy

in the Graduate School of Arts and Sciences

COLUMBIA UNIVERSITY

2014

ABSTRACT

Transition Metal Hydrides that Mediate Catalytic Hydrogen Atom Transfers

Deven P. Estes

Radical cyclizations are important reactions in organic chemistry. However, they are seldom used industrially due to their reliance on neurotoxic trialkyltin hydride. Many substitutes for tin hydrides have been developed but none have provided a general solution to the problem.

Transition metal hydrides with weak M–H bonds can generate carbon centered radicals by hydrogen atom transfer (HAT) to olefins. This metal to olefin hydrogen atom transfer (MOHAT) reaction has been postulated as the initial step in many hydrogenation and hydroformylation reactions. The Norton group has shown MOHAT can mediate radical cyclizations of α,ω dienes to form five and six membered rings. The reaction can be done catalytically if 1) the product metalloradical reacts with hydrogen gas to reform the hydride and 2) the hydride can perform MOHAT reactions. The Norton group has shown that both $CpCr(CO)_3H$ and $Co(dmgBF_2)_2(H_2O)_2$ can catalyze radical cyclizations. However, both have significant draw backs.

In an effort to improve the catalytic efficiency of these reactions we have studied several potential catalyst candidates to test their viability as radical cyclization catalysts. I investigate the hydride $CpFe(CO)_2H$ (FpH). FpH has been shown to transfer hydrogen atoms to dienes and styrenes. I measured the Fe–H bond dissociation free energy (BDFE) to be 63 kcal/mol (much higher than previously thought) and showed that this hydride is not a good candidate for catalytic radical cyclizations.

I have investigated the dynamics of $Co(dmgBF_2)_2(H_2O)_2$ under hydrogen gas to attempt to observe its hypothesized cobalt hydride. Under large pressures up to 70 atm we see two species one which we assign as the cobalt hydride and one which we assign as a ligand protonated Co(I) complex. These are supported by high pressure NMR studies of the same complexes. By varying the H_2 pressure, we can calculate the hydrogen atom donor ability of the mixture formed under H_2 as 50 kcal/mol. This makes this mixture a very good H• donor.

The Norton group has shown that vanadium hydrides have very weak V–H bonds that donate H• rapidly. However, they cannot be made catalytic under hydrogen gas. I have attempted to regenerate these vanadium hydrides by a sequential reduction then protonation of the metalloradical. With $HV(CO)_4$dppe this only produced hydrogen gas, presumably by one electron reduction of $HV(CO)_4$dppe. However, with $HV(CO)_4$dppf this does not readily occur and this hydride could potentially be a catalyst for radical cyclizations.

Many radical cyclizations involve vinyl (sp^2) radicals. I have shown that both the $CpCr(CO)_3H$ and the $Co(dmgBF_2)_2(H_2O)_2$ systems can catalytically perform metal to alkyne hydrogen atom transfers (MAHAT's) and that these reactions can be used to perform radical cyclizations very efficiently.

TABLE OF CONTENTS

List of Schemes

List of Tables

List of Figures

ACKNOWLEDGMENTS

I would like to give a big thanks to my advisor Jack Norton for welcoming me into his laboratory five years ago. Jack has always been a great mentor, a brilliant chemist, and a great guy to work for. I thank him for giving me the freedom to work on interesting chemistry and to create my own research agenda at Columbia, and for his friendship.

I would also like to thank the rest of my committee members who were gracious enough to read and give feedback on my thesis and provide help and support over all the years. I would like to especially thank the late Prof. Nicholas Turro who served on my committee until my fourth year. He was a brilliant man and a superb committee member and will be deeply missed. I would also like to thank Prof. Ged Parkin for stepping in in Prof. Turro's absence and for becoming an important part of my committee. I also thank Prof. Jon Owen who has been a great source of advice about chemistry over the years and who is always ready to provide suggestions and comments. I also thank Prof.'s John Sowa and Jay Groves for serving on my committee and reading my thesis.

I am also deeply indebted to my various collaborators. I would like to especially thank Dr. Steffen Jockusch for help with EPR spectroscopy. I am also grateful for the help of Dr. David Grills at BNL who helped with and taught me about high pressure spectroscopy and how to safely handle a high gas pressure apparatus. This proved invaluable in my progress toward this dissertation. I am also thankful to the research group of Prof. Dennis Lichtenberger, especially Prof. Aaron Vannucci, with whom I collaborated on the Fe–H pK_a measurements. I am also

thankful to the Columbia NMR staff, John Decatur and Michael Apple, who were always willing to set up the odd ^{59}Co NMR experiment for me and for giving me leave to do my high pressure experiments in the wide bore. I would like to thank Prof. John Bercaw (Caltech), Prof. Jon Owen, and Dr. Aaron Appel (PNNL) for assistance and advice in setting up the high pressure NMR capabilities which proved vital to my project.

I have been fortunate to work with some great people over the years in the Norton group. I would like to especially thank Dr. John Hartung, Dr. James Camara, Dr. Tony Shaw, Michael Eberhart, Gang Li, and the rest of the Norton lab for their contributions to my research and for just being good company. I'm also grateful to the Parkin group members who helped with chemistry and with crystallography, especially Wes and Aaron Sattler, Josh Palmer, Serge Ruccolo, Yi Rong, and Ahmed Al-Harbi.

I would never have been able to do all this without the tireless support of my wife, Kelli. She has been there through thick and thin and provided emotional support, helped me get away from problems in the lab, and on a few occasions even given me some ideas to try in the lab. She is always willing to listen and for that I'll be eternally grateful. Our two cats have also made this an easier and more enjoyable time. I am also deeply indebted to my family for listening to me, supporting me, and calling to talk whenever they can.

Chapter 1: Introduction to Transition Metal Hydrides that Mediate Catalytic Hydrogen Atom Transfers

1.1 Radical Reactions in Organic Chemistry

1.1.1 Elementary Reactions of Organic Radicals

Organic radicals react quickly, due to the unpaired electron on carbon. The reactions of alkyl reactions are often diffusion controlled and the lifetimes of alkyl radicals in solution can be less than a nanosecond.[1] They decompose by disproportionation (eq 1.1), radical combination (eq 1.2), or H• abstraction from the solvent (eq 1.3).

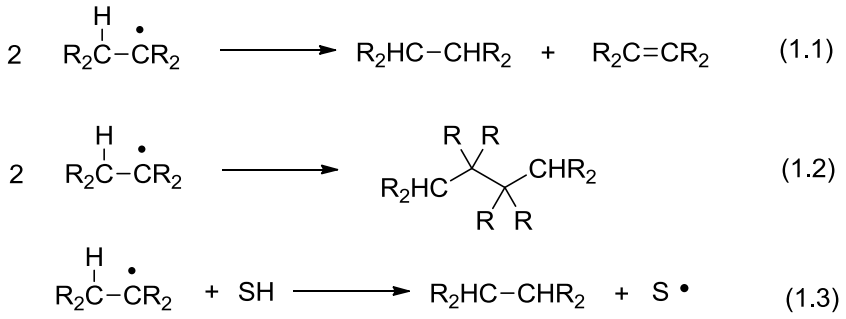

By choosing conditions in which the radical concentration remains low (1.1 – 1.2) and by choosing an appropriate solvent (1.3), the processes in eq 1.1–1.3 become unimportant. This can lead the way for these radicals to do synthetically useful reactions.[2] One example of a radical reaction which is synthetically useful, the radical addition, is discussed below.

1.1.2 Radical Additions to Unsaturated Carbon Substrates

The addition of a radical to an unsaturated carbon bond to make a new carbon – carbon bond is shown in eq 1.4.

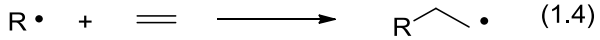

The rate of addition is controlled by a variety of factors.[3] The most important is thermodynamics. Less stable radicals react faster. For example, methyl radical adds to 1–butene (**1.1**) 230 times faster than benzyl radical (eq 1.5) — the reaction with methyl radical is more exothermic than with benzyl radical.

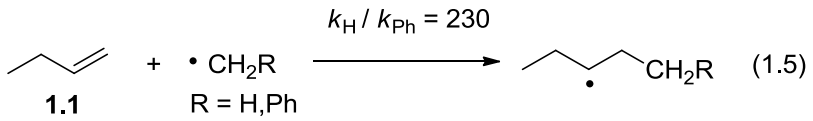

1.1

Radical addition forms a new CC σ bond and breaks a CC π bond, resulting in a new carbon radical. The regiochemistry of the addition is controlled by the stability of the radical formed (or to put it another way, the regioselectivity of radical addition is determined by the strength of the CC bonds formed). The result is that radicals usually add to the carbon with fewer substituents (or the carbon with fewer radical stabilizing groups). For example, when radicals add to styrene the benzylic radical (**1.2**) is formed preferentially (eq 1.6).

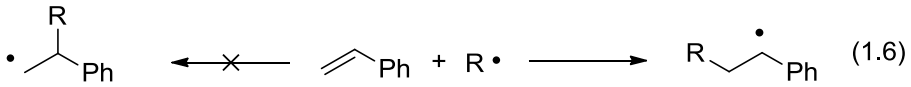

1.2

Other factors also affect the rate of radical additions. Radicals can be defined as either nucleophilic (electron rich) or electrophilic (electron poor), depending on the energy of the singly occupied molecular orbital (SOMO).[4] Nucleophilic radicals react more rapidly with electron–poor double bonds than with electron–rich double bonds. The high energy SOMO of the nucleophilic radical matches the energy of the π* orbital of an electron–poor alkene, resulting in some charge transfer in the transition state (Figure 1.1). The opposite is true for electrophilic

radicals reacting with electron–rich double bonds.[3] In other words, the transition states of polar radical addition reactions have partial charge transfer character.

Figure 1. 1 Orbital Diagram for Nucleophilic Radical Addition

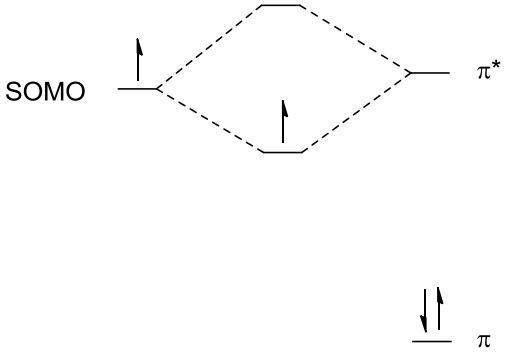

Steric interference between the radical and the alkene will slow the reaction.[3] For example, addition of a methyl radical to 2–methylpropene is four times faster than to 2–methylbut–2–ene (eq 1.7). By the same token, t–butyl radical adds to ethylene almost three times more slowly than methyl radical (eq 1.8).

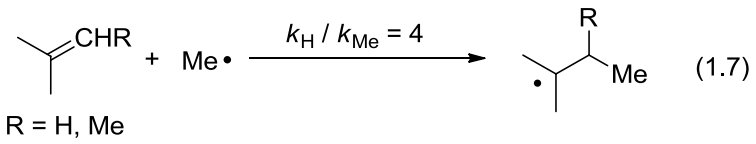

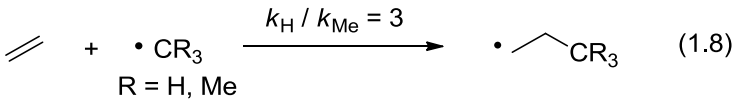

1.1.3 Radical Cyclizations

In the examples above, the radical and the alkene were reacting in a bimolecular fashion. If the radical and the receiving double bond are in the same molecule their intramolecular reaction will result in formation of a ring (eq 1.9). These ring–forming steps can occur with high

regio– and diastereoselectivity.[2] They can also make highly substituted C–C bonds, that are difficult to make by other methods.[5] Since the radical addition results in a new radical, another cyclization is possible, like that used for the total synthesis of hirsutene (eq 1.10).[6]

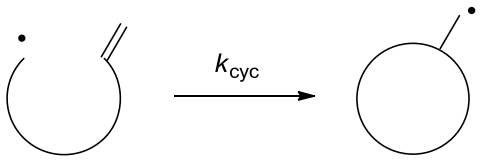

(1.9)

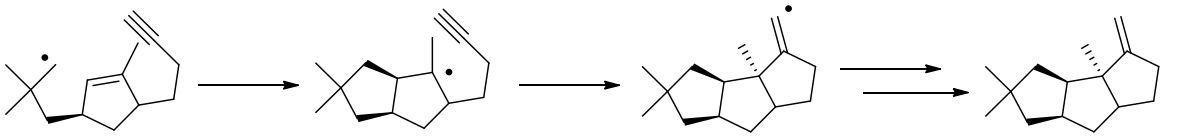

(1.10)

These qualities make radical cyclizations quite useful synthetically. They have become part of the standard repertoire of the synthetic chemist. Many natural products have been synthesized with radical cyclizations.[7-11] Some examples are shown in figure **1.2**.

Figure 1. 2 Natural Products Synthesized by Radical Cyclizations

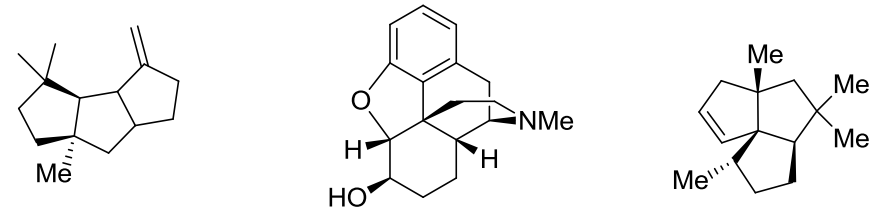

$\Delta^{9,12}$ Capnellene dihydroisocodeine silphinene

The rate constants for many radical cyclizations have been measured.[12-15] Radical cyclizations are inherently radical additions and are subject to all the same limitations. Their rates also depend on additional factors, such as linker length and linker rigidity. For example, in the cyclization of 5–hexenyl (**1.3**) the rate of five–membered ring formation is much faster than the rate of six membered ring formation (eq 1.11).[12] It has been proposed that the transition state

for 5–exo cyclizations is a chair (**1.4**) and the same energetic concerns which govern substituents on cyclohexyl rings govern the energies of various 5–exo transition states.[16] Guidelines have been proposed for the viability of different types of radical cyclizations.[17]

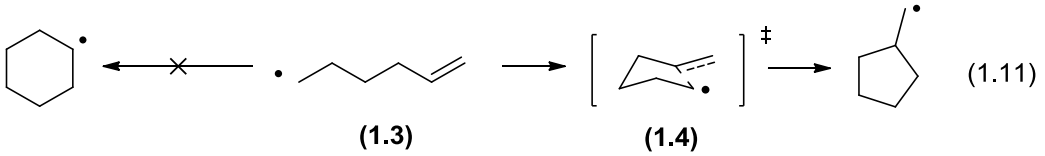

1.2 Generation of Organic Radicals

1.2.1 Trialkyltin Hydride

Typically radicals are generated from radical initiators at high temperatures, such as azobisisobutyronitrile (AIBN) or benzoyl peroxide. The radicals produced then abstract a hydrogen atom from tributyltin hydride (eq 1.12) (Sn–H bond dissociation enthalpy (BDE) = 78 kcal/mol).[18] This tin radical then abstracts a group with a large atom (usually a Br, I, S, or Se) to make the desired organic radical (eq 1.13). This allows for the selective formation of any radical that might be desired.

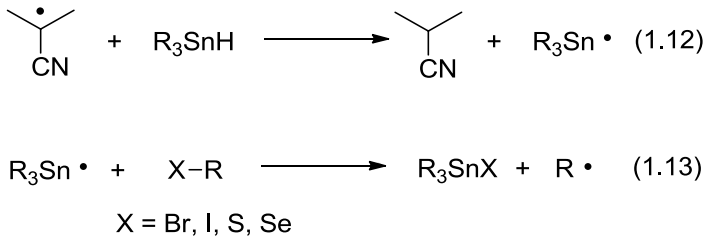

However, there are many drawbacks to the use of alkyl tin reagents, such as their acute toxicity,[19] their lack of atom economy (large amounts of SnX waste are produced),[20-21] and the harsh conditions which are required to produce the desired reaction (usually > 100°C). This has led researchers to search for tin replacements (using elements like Ge,[22] In,[23] Si,[24] and B[25]) or to

make a tin reagent that is easier to separate from the final product.[26-27] However, none of them has proven a general solution to the problem.

1.3 Radical Reactions of Transition–Metal Hydrides

Transition–metal hydrides can be used as H• donors to organic substrates. This generates organic radicals and could make such hydrides alternatives to tin hydrides in synthesis. By regenerating the M–H bond under H_2, these reactions could be catalytic.

1.3.1 Hydrogen Atom Transfers to Unsaturated Carbon Substrates

Feder and Halpern proposed that hydrogenation of anthracene by $HCo(CO)_4$ proceeds via reversible H• transfer (Scheme 1.1).[28] They based this proposal on several observations. 1) When using $DCo(CO)_4$, H/D exchange at the 9 and 10 positions is faster than hydrogenation. 2) Introduction of alkyl groups at the 9 and 10 positions caused a rate increase, due to formation of a more stable radical. 3) Introduction of alkyl groups at the 9 and 10 position leads to equal mixtures of cis and trans dialkyldihydroanthracene (**1.5**). They also proposed that hydrogenations by $[HCo(CN)_5]^{3-}$, showing effects similar to those listed above went through free radical intermediates.[29]

Scheme 1. 1 Hydrogenation of Anthracene with $HCo(CO)_4$

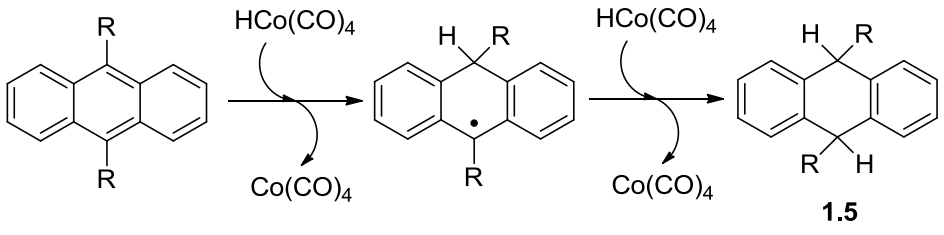

Sweany and Halpern later observed the hydrogenation of α–methylstyrene by $HMn(CO)_5$. Kinetic studies indicated that it was 1st order in both alkene and in hydride, but had no dependence on added CO. They proposed that the hydrogenation went by H• transfer from Mn to the alkene (eq 1.14) followed by a fast H• transfer to the carbon radical (eq 1.15).[30] This hypothesis was supported by several pieces of mechanistic evidence.

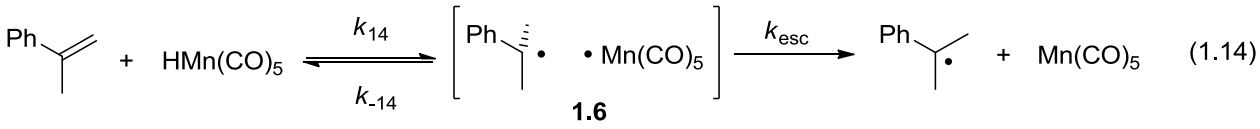

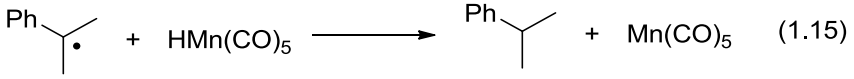

They observed Chemically Induced Dynamic Nuclear Polarization (CIDNP) when the reaction was performed inside a magnetic field. In order for this to occur a caged radical pair must be formed and cage escape (k_{esc}) must compete with radical recombination (k_{-14}).[31] The proton spins on the hydrogenated product become polarized due to hyperfine coupling with the organic radical. This causes either ^{1}H NMR signal enhancement or emissive behavior (negative peak).

$DMn(CO)_5$ showed both deuterium incorporation into the product and H/D exchange into the reactant alkene (eq 1.16). Instead of the radicals combining with each other (to form a Mn–C bond) the Mn can reabstract H• from the organic radical (eq 1.16).

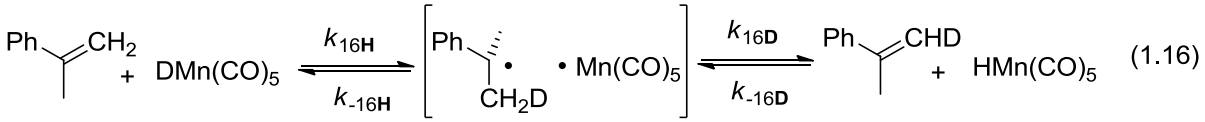

They also measured an inverse isotope effect of 0.4 with H/DMn(CO)$_5$. The cause of this inverse isotope effect is still unclear, but is a general characteristic of these reactions. Most metal hydrides have M–H BDE's between 60 and 70 kcal/mol,[32] while the β–CH bonds of most carbon centered radicals have BDE's between 37 and 50 kcal/mol.[33-35] As a result, reaction 1.14 is estimated to be thermodynamically uphill by ~10 kcal/mol.[34-35] Sweany and Halpern rationalized the isotope effect by comparing the vibrational frequencies of Mn-H (~1800 cm^{-1}) with those of radical β – C–H bonds (average for ethyl radical 2803 cm^{-1}).[36] Since the formation of the radical cage pair is probably rapidly maintained, the observed first order rate constant $k_{obs} = K_{14}k_{esc}$, where the isotope effect is due to the equilibrium of radical cage formation. They proposed that eq 1.14 should have an inverse equilibrium isotope effect since the difference in ground state H/D vibrational energies is larger in the product than in the reactant (Figure 1.3). (Of course, this is a first approximation since we've only examined the stretching frequencies rather than all vibrational modes.)

Figure 1. 3 Energy Diagram for HAT from Mn to Olefin

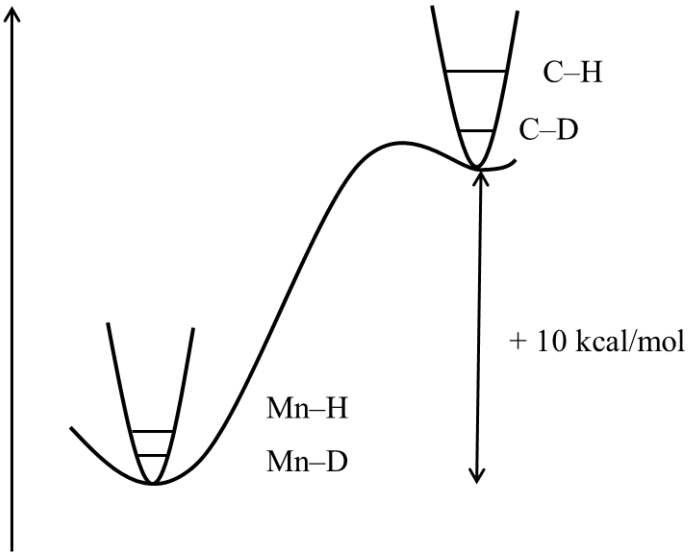

Since these two reports, many other cases of HAT from metal hydrides to unsaturated carbon substrates have been found using a range of hydrides and a range of substrates.[37-52] These various studies have led to additional observations about HAT from hydrides to olefins.

Roth and Orchin found that added CO does not inhibit the hydrogenation of 1,1 diphenylethylene by $HCo(CO)_4$ (eq 1.17),[37] implying that the hydrogen atom transfer is "outer–sphere".

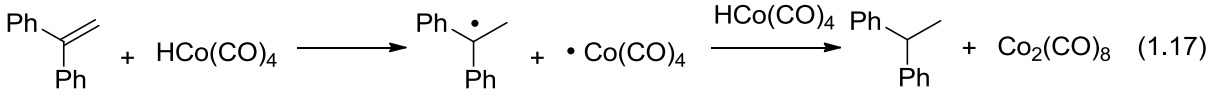

(1.17)

Solvent viscosity plays a role in the reaction.[46-47] During the stoichiometric hydroformylation of styrene by $HCo(CO)_4$ under CO (Scheme 1.2), Ungvary and coworkers found that changing the solvent from octane to Nujol significantly changed the product ratios of hydrogenated product **1.7** to hydroformylated product **1.8**. Since **1.7** is the product of cage escape and **1.8** is the product of radical combination to form organometallic complex **1.9**, high viscosity solvent (Nujol) slows the rate of cage escape and favors the product of radical combination, **1.8**.

Scheme 1. 2 The Role of Cage Escape in Hydroformylations

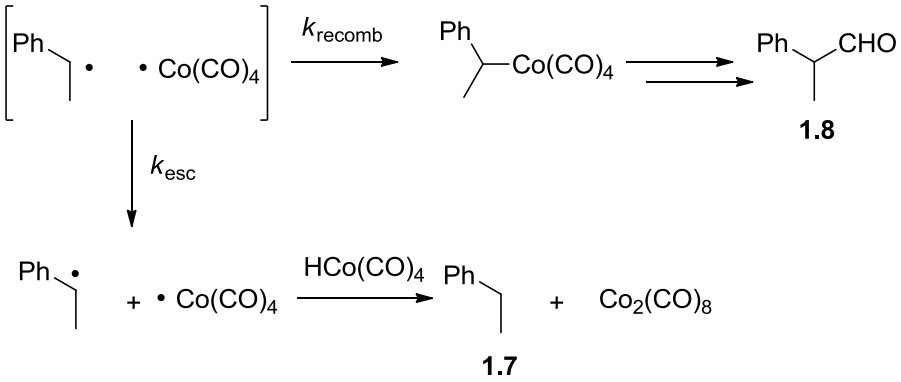

Bullock and Samsel measured the 2nd order rate constant for hydrogenation (k_H in eq 1.18) of α–cyclopropylstyrene by a series of stable transition metal hydrides.[52] They observed both the cyclopropyl ring opened product (**1.9**) and an inverse H/D isotope effect for k_H, meaning that this reaction goes via metal to olefin HAT. The rate of transfer was heavily influenced by the strength of the M–H bond, weaker bonds transferring much faster than stronger ones. For example, k_H of $CpCr(CO)_3H$ (Cr–H bond dissociation free energy (BDFE) = 56.7 kcal/mol)[53] was 3.4×10^{-3} $M^{-1}s^{-1}$ at 22°C whereas for $CpW(CO)_3H$ (W–H BDFE = 68 kcal/mol)[53] it was 6.2×10^{-5} $M^{-1}s^{-1}$ at 100°C.

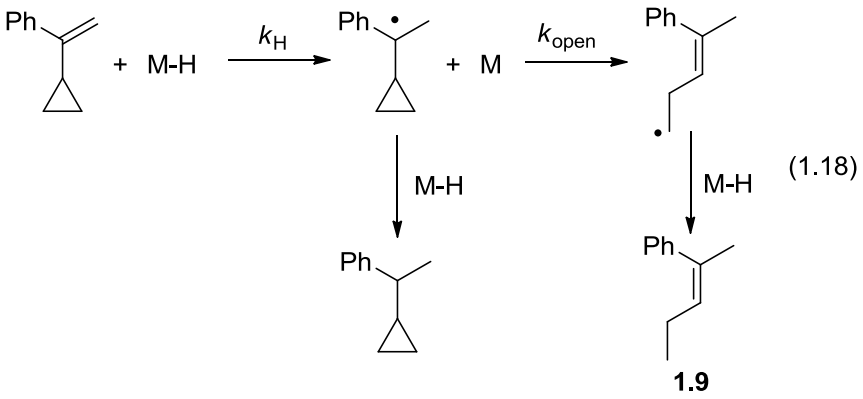

(1.18)

The Norton group has examined the effect of the organic substrate on the rate of HAT to olefins.[35, 54] They measured the rate constant (k_H) of HAT from $CpCr(CO)_3H$ to an excess of a variety of olefins. They found that k_H could be measured in two separate cases. If only hydrogenation occurred (i.e. $k_{19} >> k_{-H}$) then equation 1.20 could be used to calculate k_H from the pseudo-first order rate constant k_{obs}.

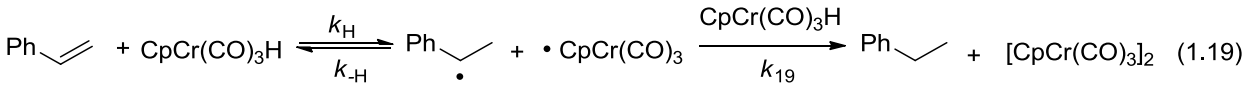

(1.19)

$$k_{obs} = 2k_H\left[olefin\right] \qquad (1.20)$$

If only exchange occurred (i.e. $k_{-H} >> k_{19}$) then k_H could be measured by isotopic exchange of $CpCr(CO)_3H$ with excess deuterated olefin. This was the case for methylmethacrylate-d_5 (**1.10**). Applying a statistical correction (S) for the reabstraction of H versus D (using k_{-H}/k_{-D} for a related compound) (eq 1.22) gave a good estimate of k_H to methylmethacrylate.

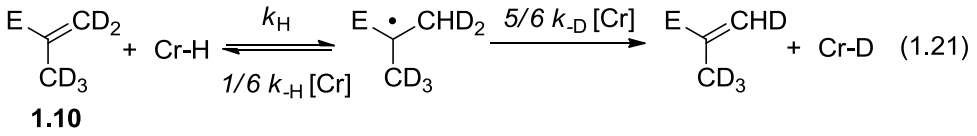

$$k_H = Sk_{obs} \text{ where for MMA } S = \frac{\frac{5}{6}k_{-D}[Cr\bullet]}{\frac{1}{6}k_{-H}[Cr\bullet] + \frac{5}{6}k_{-D}[Cr\bullet]} = \frac{5}{5 + \frac{k_{-H}}{k_{-D}}} \qquad (1.22)$$

According to their measured values of k_H (Table 1.1),[34, 54] HAT rates share many attributes with radical additions to olefins. For example, HAT to **1.11** is 780 times faster than to **1.13**, meaning that these reactions are sensitive to sterics at the double bond. Changing one phenyl group of **1.11** to a methyl group as in **1.12** decreases the rate by a factor of 6. With only alkyl substituents, the rate was too slow to measure accurately and only upper limits of 10^{-6} and 10^{-7} $M^{-1}s^{-1}$ could be estimated.

Table 1. 1. Rate constants (k_H) for HAT from $CpCr(CO)_3H$ to Substituted Olefins at 323 K

Compound	Structure	k_H ($M^{-1}s^{-1}$)	Relative Rate
1.11		$4.6(6) \times 10^{-1}$	780
1.12		$7.9(3) \times 10^{-2}$	134
Styrene		$1.58(6) \times 10^{-2}$	27
MMA	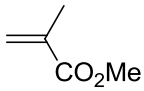	$1.4(3) \times 10^{-2}$	24
1.13	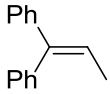	$5.9(2) \times 10^{-4}$	1
1.14	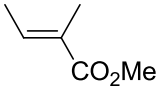	$(0.8 – 1.6) \times 10^{-5}$	~0.02
1.15	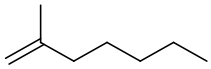	$\leq 3.2 \times 10^{-6}$	≤ 0.005
1.16	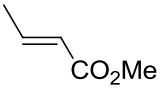	$\leq 3.2 \times 10^{-7}$	≤ 0.0005
1.17	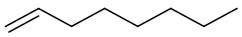	$\leq 1.1 \times 10^{-7}$	≤ 0.0002

These studies have yielded some general characteristics which seem to be shared by all Metal to Olefin HAT (MOHAT) reactions.

(1) The rate of these reactions is sensitive to thermodynamics

a. Weaker M–H bonds transfer H• faster

b. H• transfers faster when the product radical is more stable

(2) Steric hindrance (both at the olefin and at the metal) has a large effect on the rate of MOHAT

(3) MOHAT results in a caged radical pair, which causes CIDNP and solvent viscosity dependence.

(4) MOHAT reactions have an inverse isotope effect for M–H/D.

(5) MOHAT is reversible. If M–D is used then H/D exchange can be observed

(6) MOHAT reactions appear to be outer sphere, there is no rate dependence on added ligand

1.4 Radical Cyclizations Mediated by Metal Hydrides

The MOHAT reaction is a useful alternative to tin–based methods for generating carbon radicals for synthesis. The Norton Group has used this method to do radical cyclizations of various α,ω dienes in good yields.[55-59] Compound **1.18** provides a useful example. The reaction of **1.18** with two equiv of $CpCr(CO)_3H$ does the cyclization in eq 1.23 to produce **1.19**, **1.20**, and **1.21** in 34, 11, and 6% yields, respectively, with 49% unreacted starting material.[60]

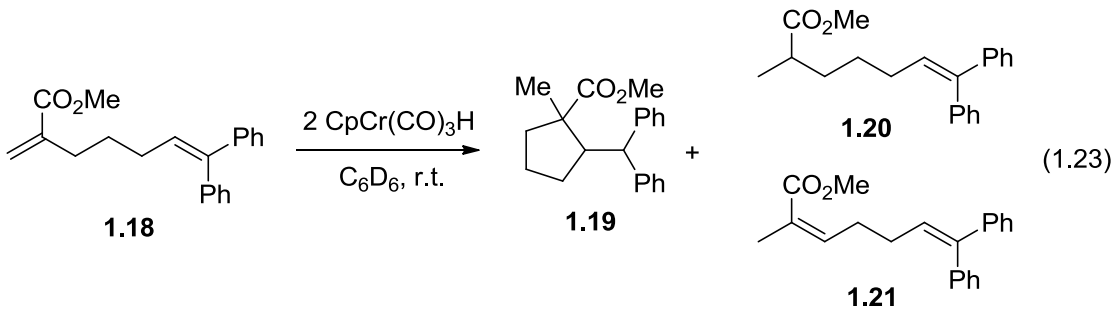

(1.23)

MOHAT is the rate–determining step in these radical cyclization reactions. Vanadium hydrides react faster than Cr–H.[57] For example, the weak V–H bond in $HV(CO)_4$dppe (BDFE = 52 kcal/mol)[57] does MOHAT to styrene 10 times faster than Cr–H (56.7 kcal/mol). Increasing the rate of MOHAT (k_H) will shorten the reaction time for radical cyclizations. The reaction of two equiv $HV(CO)_4$dppe with **1.18** yielded 77% cyclized product.[60]

These studies lead to a mechanistic picture for this reaction, shown below in Scheme 1.3. The unsubstituted acrylate is the kinetic site for MOHAT, according to the measured rate constants in Table 1.1. In order to form one radical selectively, there must be a substantial difference in the HAT rates of the two olefins. After HAT the radical formed can do one of three things: cyclize, isomerize, or hydrogenate. In order to maximize our yield of cyclized product the rate of cyclization (k_{cyc}) must be faster than the rates of isomerization (k_{isom}[Cr•]) and hydrogenation (k_{hydr}[Cr–H]).

Scheme 1. 3 Cyclization of 1.18

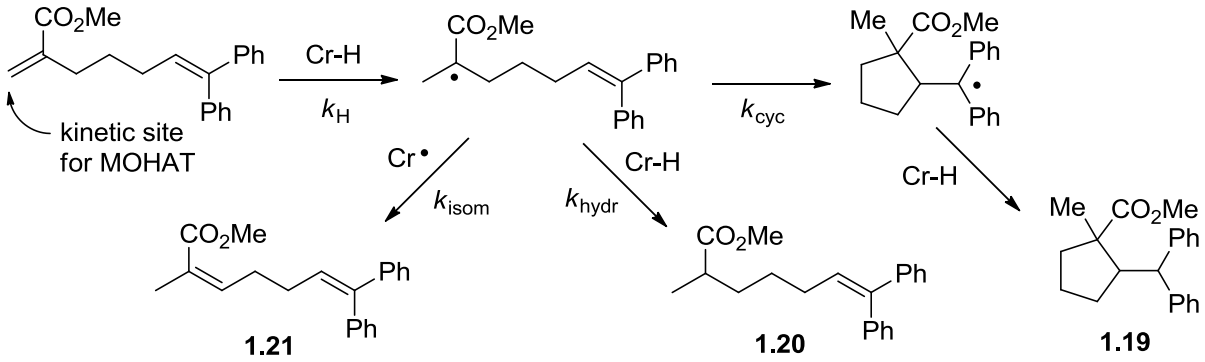

1.4.1 Increasing the Rate of Cyclization (k_{cyc})

One way to maximize the yield of cyclized material is to increase the cyclization rate. By adding substituents to the backbone of **1.18**, the rate of cyclization can be increased (Thorpe-Ingold Effect).[61-62] Treatment of **1.22** with two equiv $CpCr(CO)_3H$ gives cyclized product **1.23** in 65% yield, the balance being unreacted starting material. [60] This offers a two-fold improvement in yield over **1.18**.

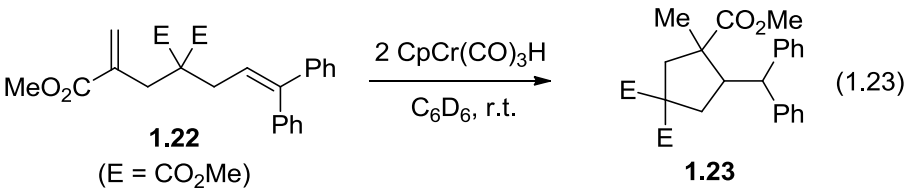

The Norton group has examined the effect of the double bond substituents on both the yield of cyclized product and the rate of cyclization (eq 1.24).[59] The results are shown in Table 1.2. Radical–stabilizing substituents on the receiving double bond increase the rate of cyclization and consequently the yield of cyclized product. However, steric crowding also drives the cyclization rate down. Adding two phenyls (**1.29**) slows the rate of cyclization below that of one phenyl (**1.27**). The non-planarity of the phenyl rings adds additional steric hindrance to the "b" double bond, which slows the cyclization.

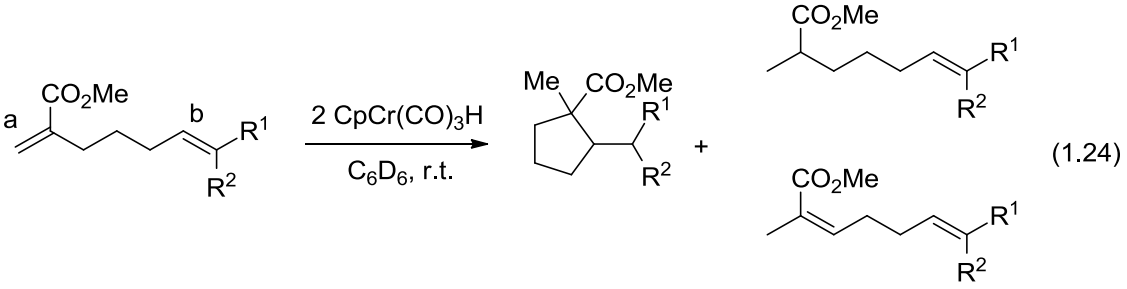

Table 1. 2. Calculated Cyclization Rate Constants and Product Yields from eq 1.24

Substrate	R^1	R^2	% Cyclization	% Hydrogenation	% Isomerization	Calculated k_{cyc} (s^{-1})
1.24	H	H	5	76	19	5.80×10^2
1.25	Me	H	16	56	28	2.47×10^3
1.26	Me	Me	18	51	31	1.66×10^3
1.27	Ph	H	52	37	11	6.03×10^5
1.28	H	Ph	53	38	9	6.18×10^4
1.29	Ph	Me	41	49	10	3.45×10^4
1.30	Ph	Ph	27	55	18	1.75×10^4

1.4.2 Decreasing the Rates of Side Reactions

The other way to increase cyclization yield is to decrease the rates of the side reactions, hydrogenation and isomerization. The Norton group has measured the hydrogen atom transfer rates (k_{HAT}) from M–H to the monomeric trityl radical **1.31** below (eq 1.25).[63-64] They found that k_{HAT} is mostly determined by steric factors and that, while M–H bond dissociation free energy (BDFE) plays a role, it is not a large one.

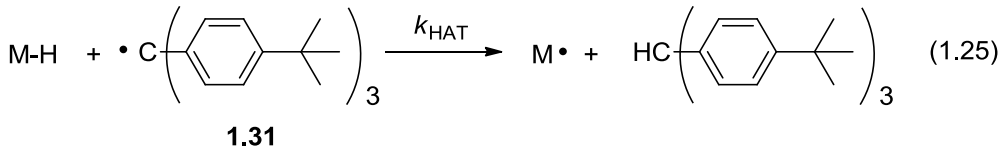

1.31

Franz and coworkers have measured the absolute rates of HAT from $CpMo(CO)_3H$ to simple organic radicals using radical clock methods.[65] This study led to a similar conclusion, that the rates of HAT from MH to carbon radicals are primarily controlled by sterics.

Less is known about the rates of isomerization reactions. The Norton group has used metalloradicals to catalyze chain transfer during radical polymerizations.[66-69] The key step of this process is the abstraction of a β–H from a polymer radical **1.32** by chromium metalloradicals. The chain transfer constant C_s — the ratio of k_{tr} (the rate constant for chain transfer in eq 1.26) to k_P (the chain propagation rate constant in eq 1.27) — can be determined by plotting the inverse of the number averaged degree of polymerization versus the ratio of chain transfer agent to monomer used. Since k_P for methyl methacrylate is constant, C_s is a measure of the relative rate constant for chain transfer.

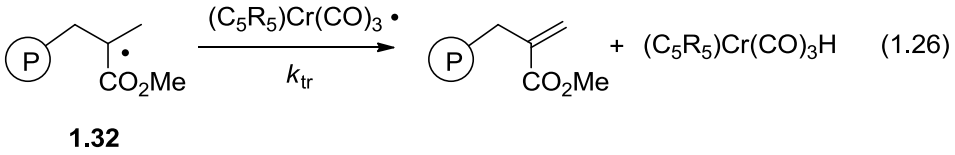

1.32

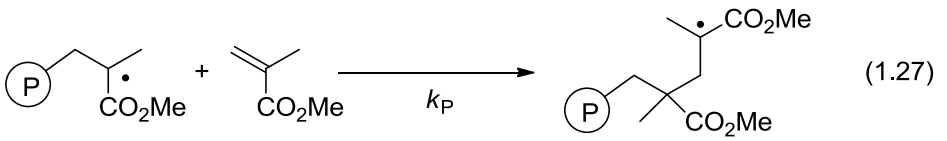

1.32

C_s values for a series of Cr and Mo metalloradicals are shown in Table 1.3.[67] Sterics largely control k_{tr}. For example moving from $(C_5H_5)Cr(CO)_3$• to $(C_5Me_5)Cr(CO)_3$• lowers C_s by a factor of four (and thus lowers k_{tr} by a factor of four). The M–H BDFE probably has a smaller effect on the rate but this has not been studied.

Table 1. 3. Apparent Chain Transfer Constants and M–H BDE's for Cr and Mo Radicals

Metalloradical	C_s[67]	M–H BDFE (kcal/mol)[32, 34]
$(C_5Ph_5)Cr(CO)_3$•	1040	59.2
$(C_5Ph_5)Cr(CO)_2PMe_3$•	3.7	—
$(C_5Ph_5)Cr(CO)_2P(OMe)_3$•	35.7	—
$(C_5Me_5)Cr(CO)_3$•	6300	57.6
$(C_5Me_5)Cr(CO)_2PMe_3$•	4200	—
$(C_5H_5)Cr(CO)_3$•	25000	56.7
$(C_5H_5)Cr(CO)_2PPh_3$•	1210	55.0
$TpMo(CO)_3$•	52	57.3
$Tp^*Mo(CO)_3$•	22	54.5

1.4.3 Catalytic Radical Cyclizations with Metal Hydrides

As can be seen in equation 1.20, radical cyclizations with stoichiometric metal hydrides produce metalloradicals as well as organic radicals. If M–H were reformed from the metalloradical M•, the reaction would be catalytic (eq 1.28). It could be possible to do this with H_2 (eq 1.28) which would act as a source of two H•.

$$2\ M\bullet\ +\ H_2 \underset{}{\overset{k_{H2}}{\rightleftharpoons}} 2\ M\text{-}H \qquad (1.28)$$

The reaction in eq 1.28 is known for a few metalloradicals.[70-77] These complexes and their kinetic parameters are shown in Table 1.4. These reactions share some characteristics with each other.

1) *The reactions are termolecular, characterized by a rate law involving two metals and one molecule of H_2.*
2) *They have almost no temperature dependence, with a very small $\Delta H^{\ddagger}$ (typically < 5 kcal/mol) and a large negative $\Delta S^{\ddagger}$ (between -25 and -55 eu), as expected for a termolecular transition state.*
3) *The H_2/D_2 isotope effects tend to be rather small (about 1.4)*
4) *The reaction occurs best with metal centers that have **only** weak association with one another.*

Table 1. 4. The kinetic parameters for metalloradicals reacting with hydrogen

M•	k_{H2} at 25°C ($M^{-2}s^{-1}$)	$\Delta H^{\ddagger}$ (kcal/mol)	$\Delta S^{\ddagger}$ (e.u.)
$[Co(CN)_5]^{3-}$	40	-1	-55
Rh(TMP)	3	5	-40
$Cp^*Cr(CO)_3$	330	0	-47
$CpCr(CO)_3$	12	8*	-25*

*These numbers were calculated from a limited data set at only two temperatures

The reaction is thought to be the product of the linear transition state **1.33**. This transition state is the one which best accounts for the data above and has been proposed for most of these reactions.

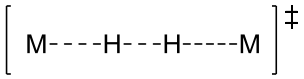

1.33

Since $CpCr(CO)_3$• reacts with hydrogen gas to reform $CpCr(CO)_3H$, $CpCr(CO)_3H$ can be used to catalyze the radical cyclizations of the dienes like **1.22** (eq 1.29).[55-56] With 7 mol% Cr–H and 2 atm H_2, **1.22** is quantitatively converted to **1.23**.

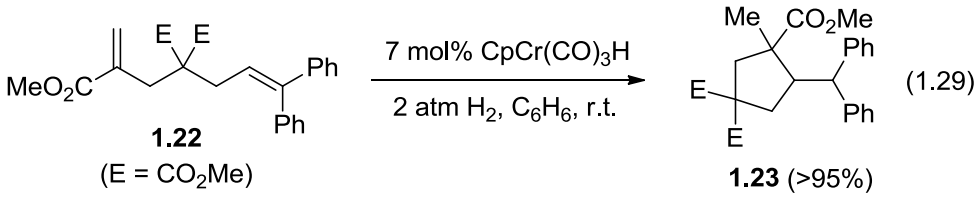

1.22 (E = CO_2Me)

1.23 (>95%)

(1.29)

Catalytic cyclization of **1.18** under similar conditions (eq 1.30) yields 62% cyclized product **1.19**, 26% hydrogenated product **1.20**, and 12% isomerized product **1.21**.[60] The yield of cyclized product is greatly improved under these conditions. Since H_2 converts M• to M–H, the isomerization rate (k_{isom}[Cr•] from Scheme 1.3) will be smaller. In addition the total concentration of M–H is lower in the catalytic reaction, which lowers the rate of hydrogenation (k_{hydr}[Cr–H] from Scheme 1.3).

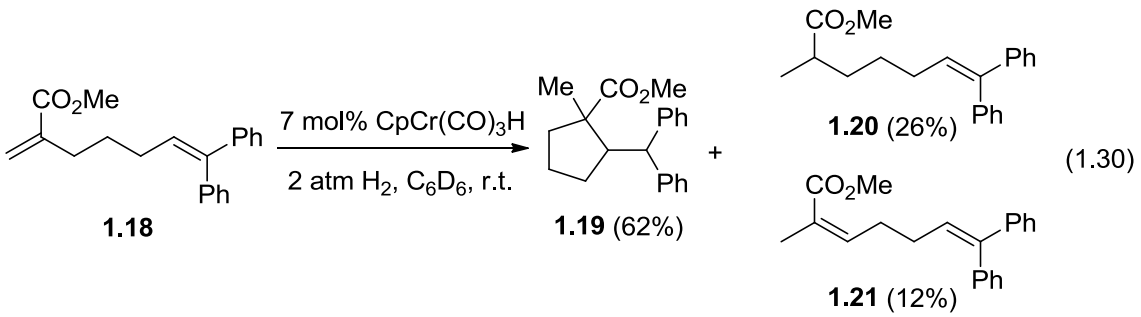

(1.30)

The vanadium hydrides above do not react with hydrogen gas. No reaction was observed when **1.22** was mixed with catalytic V–H (7 mol% $HV(CO)_4$dppe) under 5.5 atm H_2.

Why does V• not react with H_2? 1) The V–H bond formed (52 kcal/mol) might be too weak for two V• to react with H_2. 2) The activation of H_2 may be sterically inaccessible. Despite their thermodynamic instability, bimolecular loss of H_2 from two V–H is slow (these hydrides are stable). Since bimolecular H_2 loss is the microscopic reverse of the termolecular H_2 activation step (eq 1.28), the barrier to both the forward and reverse reactions must be substantial. $HV(CO)_4$dppx (x = m,e,p,b) complexes are 7 coordinate and the steric barrier to bringing two octahedral •$V(CO)_4$dppx molecules together would be high.

Cobaloximes (**1.34**) also catalyze radical cyclizations.[58] Catalytic reaction of **1.34** (7 mol%) with **1.18** under 5.5 atm H_2, yields 11% cyclization (**1.19**), 3% hydrogenation (**1.20**), and 86% isomerization (**1.21**). These cobalt complexes have been shown to perform chain transfer polymerization of methyl methacrylate and are thought to have very high C_s values.[78-80] Therefore, the predominance of the isomerization pathway is not surprising. Blocking isomerization by using **1.22** (due to steric bulk from the CO_2Me groups) gives quantitative cyclization to **1.23**.

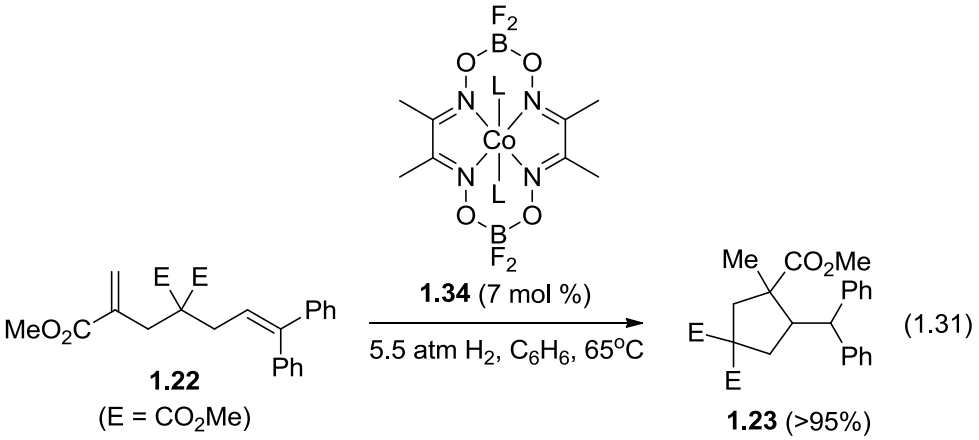

(1.31)

A good catalyst for radical cyclization of α,ω dienes must have the following characteristics.

1) *The metal hydride catalyst must have a weak M–H bond (BDFE < 60 kcal/mol) for MOHAT to proceed at an appreciable rate.*
2) *The corresponding M• must react with H_2 to regenerate M–H. The M–H bond must be strong enough (BDFE > 52 kcal/mol) for H_2 splitting to be thermodynamically viable. M• must interact weakly with itself.*
3) *The rate of isomerization (k_{isom}) by M• must be slow. This is reflected by a small chain transfer constant (C_s).*
4) *The rate of hydrogenation (k_{hydr}) by M–H must also be slow. (Both 3 and 4 can be obtained by adding steric bulk to the hydride).*

These rules will be useful in the search for new catalysts and in improving our existing catalysts. Drawbacks of our current catalysts: $CpCr(CO)_3H$ produces large amounts of side products and does MOHAT relatively slowly; the cobalt catalyst **1.34** has a high C_s and little is known about the presumed Co–H formed under H_2 or how fast it can transfer H•. The vanadium hydrides have weak V–H bonds which transfer H• quickly but cannot be regenerated under H_2. It

is the goal of this thesis to discover new catalysts and improve existing radical cyclization catalysts.

1.5 References

1. Weiner, S. A.; Hammond, G. S., Rates of recombination of carbon radicals in solution. *J. Am. Chem. Soc.* **1969,** *91*, 986-991.

2. Curran, D. P.; Porter, N. A.; Giese, B., *Stereochemistry of Radical Reactions: Concepts, Guidelines, and Synthetic Applications*. VCH Publishers: New York, 1996.

3. Fischer, H.; Radom, L., Factors Controlling the Addition of Carbon-Centered Radicals to Alkenes—An Experimental and Theoretical Perspective. *Angew. Chem., Int. Ed.* **2001,** *40*, 1340-1371.

4. Fleming, I., *Frontier Orbitals and Organic Chemical Reactions*. John Wiley & Sons: 1976.

5. Curran, D. P., Radical Cyclizations and Sequential Radical Reactions. In *Comprehensive Organic Synthesis*, Trost, B. M.; Fleming, I.; Semmelhack, M. F., Eds. Pergamon Press: Oxford, 1991; Vol. 4, pp 779-831.

6. Curran, D. P.; Rakiewicz, D. M., Tandem Radical Approach to Linear Condensed Cyclopentanoids - Total Synthesis of (±)-Hirsutene. *J. Am. Chem. Soc.* **1985,** *107*, 1448-1449.

7. Jasperse, C. P.; Curran, D. P.; Fevig, T. L., Radical Reactions in Natural Product Synthesis. *Chem. Rev.* **1991,** *91*, 1237–1286.

8. Curran, D. P.; Chen, M.-H., Radical-initiated polyolefinic cyclizations in condensed cyclopentanoid synthesis. Total synthesis of (±)-Δ9(12)-capnellene. *Tetrahedron Lett.* **1985,** *26*, 4991-4994.

9. Parker, K. A.; Fokas, D., Convergent Synthesis of (±)-Dihydroisocodeine in 11 Steps by the Tandem Radical Cyclization Strategy. A Formal Total Synthesis of (±)-Morphine. *J. Am. Chem. Soc.* **1992,** *114*, 9688–9689.

10. Rao, Y. K.; Nagarajan, M., Formal Total Synthesis of (±)-Silphinene via Radical Cyclization. *J. Org. Chem.* **1989,** *54*, 5678–5683.

11. Stork, G.; Baine, N. H., Cyclization of Vinyl Radicals: a Versatile Method for the Construction of Five- and Six-membered Rings. *J. Am. Chem. Soc.* **1982,** *104*, 2321-2323.

12. Beckwith, A. L. J.; Moad, G., Intramolecular Addition In Hex-5-enyl, Hept-6-enyl, and Oct-7-enyl Radicals. *J. Chem. Soc.-Chem. Commun.* **1974**, 472-473.

13. Newcomb, M., Competition Methods and Scales for Alkyl Radical Reaction Kinetics. *Tetrahedron* **1993,** *49*, 1151–1176.

14. Newcomb, M.; Horner, J. H.; Filipkowski, M. A.; Ha, C.; Park, S. U., Absolute Rate Constants for Reactions of α-Carbethoxy and α-Cyano Radicals. *J. Am. Chem. Soc.* **1995,** *117*, 3674-3684.

15. Newcomb, M.; Filipkowski, M. A.; Johnson, C. C., Alpha-Ethoxycarbonyl and Alpha-Methoxy Substituted Radical Clocks. *Tetrahedron Lett.* **1995,** *36*, 3643-3646.

16. Spellmeyer, D. C.; Houk, K. N., A Force-Field Model for Intramolecular Radical Additions. *J. Org. Chem.* **1987,** *52*, 959–974.

17. Beckwith, A. L. J.; Easton, C. J.; Serelis, A. K., Some Guidelines for Radical Reactions. *J. Chem. Soc., Chem. Commun.* **1980**, 482–483.

18. Luo, Y.-R., *Handbook of bond dissociation energies in organic compounds*. CRC Press: Boca Raton, Florida, 2002; p 380.

19. Baguley, P. A.; Walton, J. C., Flight from the Tyranny of Tin: The Quest for Practical Radical Sources Free from Metal Encumbrances. *Angew. Chem., Int. Ed. Engl.* **1998,** *37*, 3072–3082.

20. Trost, B. M., The Atom Economy- A Search for Synthetic Efficiency. *Science* **1991,** *254*, 1471-1477.

21. Trost, B. M., Atom Economy — A Challenge for Organic Synthesis: Homogeneous Catalysis Leads the Way. *Angew. Chem., Int. Ed. Engl.* **1995,** *34*, 259-281.

22. Bowman, W. R.; Krintel, S. L.; Schilling, M. B., Tributylgermanium Hydride as a Replacement for Tributyltin Hydride in Radical Reactions. *Org. Biomol. Chem.* **2004,** *2*, 585–592.

23. Inoue, K.; Sawada, A.; Shibata, I.; Baba, A., Indium (III) Chloride–Sodium Borohydride System: A Convenient Radical Reagent for an Alternative to Tributyltin Hydride System. *J. Am. Chem. Soc.* **2002,** *124*, 906–907.

24. Chatgilialoglu, C., Organosilanes as Radical-Based Reducing Agents in Synthesis. *Acc. Chem. Res.* **1992,** *25*, 188–194.

25. Mikami, S.; Fujita, K.; Nakamura, T.; Yorimitsu, H.; Shinokubo, H.; Matsubara, S.; Oshima, K., Triethylborane-Induced Radical Reactions with Gallium Hydride Reagent $HGaCl_2$. *Org. Lett.* **2001,** *3*, 1853–1855.

26. Curran, D. P.; Hadida, S.; Kim, S.-Y.; Luo, Z., Fluorous Tin Hydrides: A New Family of Reagents for Use and Reuse in Radical Reactions. *J. Am. Chem. Soc.* **1999,** *121*, 6607–6615.

27. Curran, D. P.; Yang, F.; Cheong, J., Relative Rates and Approximate Rate Constants for Inter- and Intramolecular Hydrogen Transfer Reactions of Polymer-Bound Radicals. *J. Am. Chem. Soc.* **2002,** *124*, 14993–15000.

28. Feder, H. M.; Halpern, J., Mechanism of the Cobalt Carbonyl-Catalyzed Homogeneous Hydrogenation of Aromatic Hydrocarbons. *J. Am. Chem. Soc.* **1975,** *97*, 7186-7188.

29. Kwiatek, J., Reactions Catalyzed by Pentacyanocobaltate(II). *Catalysis Reviews* **1968,** *1*, 37-72.

30. Sweany, R. L.; Halpern, J., Hydrogenation of α-Methylstyrene by Hydridopentacarbonylmanganese(I). Evidence for a Free-Radical Mechanism. *J. Am. Chem. Soc.* **1977,** *99*, 8335-8337.

31. Kochi, J. K., *Free Radicals*. John Wiley & Sons: New York, NY, 1973; Vol. I.

32. Tilset, M., Organometallic Electrochemistry: Thermodynamics of Metal-Ligand Bonding. In *Comprehensive Organometallic Chemistry III*, Robert, H. C.; Mingos, D. M. P., Eds. Elsevier: Oxford, 2007; pp 279-305.

33. Blanksby, S. J.; Ellison, G. B., Bond Dissociation Energies of Organic Molecules. *Acc. Chem. Res.* **2003,** *36*, 255–263.

34. Tang, L.; Papish, E. T.; Abramo, G. P.; Norton, J. R.; Baik, M.-H.; Friesner, R. A.; Rappé, A., Kinetics and thermodynamics of H• transfer from (η^5-C_5R_5)$Cr(CO)_3H$ (R = Ph, Me, H) to methyl methacrylate and styrene (vol 125, pg 10093, 2003). *J. Am. Chem. Soc.* **2006,** *128*, 11314.

35. Tang, L.; Papish, E. T.; Abramo, G. P.; Norton, J. R.; Baik, M.-H.; Friesner, R. A.; Rappé, A., Kinetics and Thermodynamics of H• Transfer from (η^5-C_5R_5)$Cr(CO)_3H$ (R = Ph, Me, H) to Methyl Methacrylate and Styrene. *J. Am. Chem. Soc.* **2003,** *125*, 10093-10102.

36. Pacansky, J.; Dupuis, M., Assignment of the infrared spectrum for the ethyl radical. *J. Am. Chem. Soc.* **1982,** *104*, 415-421.

37. Roth, J. A.; Orchin, M., The stoichiometric hydrogenation of 1,1-diphenylethylene with hydridocobalt tetracarbonyl; differences from the hydroformylation reaction. *J. Organomet. Chem.* **1979,** *182*, 299-311.

38. Sweany, R. L.; Comberrel, D. S.; Dombourian, M. F.; Peters, N. A., The hydrogenation of α-methylstyrene by tricarbonyl(cyclopentadienyl)hydride compounds of tungsten and molybdenum; support for a radical mechanism. *J. Organomet. Chem.* **1981,** *216*, 37-63.

39. Sweany, R. L.; Butler, S. C.; Halpern, J., The Hydrogenation of 9,10-Dimethylanthracene by Hydridopentacarbonylmanganese(I). Evidence for a Free-Radical Mechanism. *J. Organomet. Chem.* **1981,** *213*, 487-492.

40. Nalesnik, T. E.; Orchin, M., The stoichiometric hydrogenation of 9-methylidenefluorene and related compounds with hydridocobalt tetracarbonyl. *J. Organomet. Chem.* **1980,** *199*, 265-269.

41. Nalesnik, T. E.; Orchin, M., Free Radical Reactions of Tetracarbonylhydridocobalt. *Organometallics* **1982,** *1*, 222-223.

42. Roth, J. A.; Wiseman, P., The stoichiometric hydrogenation of substituted phenyl alkenes by hydridocobalt tetracarbonyl. *J. Organomet. Chem.* **1981,** *217*, 231-234.

43. Ungváry, F.; Markó, L., Reaction of $HCo(CO)_4$ and CO with styrene. Mechanism of (alpha-phenylpropionyl)- and (beta-phenylpropionyl)cobalt tetracarbonyl formation. *Organometallics* **1982,** *1*, 1120-1125.

44. Bockman, T. M.; Garst, J. F.; King, R. B.; Markó, L.; Ungváry, F., CIDNP evidence for radical intermediates in the hydroformylation and reduction of styrene by $HCo(CO)_4$/CO. *J. Organomet. Chem.* **1985,** *279*, 165-169.

45. Bockman, T. M.; Garst, J. F.; Ungváry, F., Reaction of Cobalt Tetracarbonyl Hydride with Phenylacetylene. *J. Organomet. Chem.* **1999,** *586*, 41-47.

46. Jacobsen, E. N.; Bergman, R. G., Synthesis and chemistry of a bridging vinylidenedicobalt complex- evidence for a nonchain radical mechanism in its reaction with metal-hydrides to give heteronuclear clusters. *J. Am. Chem. Soc.* **1985,** *107*, 2023-2032.

47. Ungváry, F.; Markó, L., Effect of solvent viscosity on the reaction of styrenes with $HCo(CO)_4$ and CO. *J. Organomet. Chem.* **1983,** *249*, 411-414.

48. Connolly, J. W., Reaction between hydridotetracarbonyl(trichlorosilyl)iron, $HFe(CO)_4SiCl_3$, and conjugated dienes. Evidence for a free radical mechanism. *Organometallics* **1984,** *3*, 1333-1337.

49. Thomas, M. J.; Shackleton, T. A.; Wright, S. C.; Gillis, D. J.; Colpa, J. P.; Baird, M. C., Evidence for the radical pair mechanism in insertion reactions of transition metal hydrides with conjugated dienes. *J. Chem. Soc., Chem. Commun.* **1986**, 312-314.

50. Wassink, B.; Thomas, M. J.; Wright, S. C.; Gillis, D. J.; Baird, M. C., Mechanisms of the hydrometalation (insertion) and stoichiometric hydrogenation reactions of conjugated dienes effected by manganese pentacarbonyl hydride: processes involving the radical pair mechanism. *J. Am. Chem. Soc.* **1987,** *109*, 1995-2002.

51. Shackleton, T. A.; Baird, M. C., The radical pair mechanism in hydrometalation and stoichiometric hydrogenation reactions of dicarbonyl(cyclopentadienyl)iron hydride [eta-^{5}-$C_5H_5Fe(CO)_2H$] with conjugated dienes. *Organometallics* **1989,** *8*, 2225-2232.

52. Bullock, R. M.; Samsel, E. G., Hydrogen Atom Transfer Reactions of Transition-metal Hydrides. Kinetics and Mechanism of the Hydrogenation of α-Cyclopropylstyrene by Metal Carbonyl Hydrides. *J. Am. Chem. Soc.* **1990,** *112*, 6886-6898.

53. Wayner, D. D. M.; Parker, V. D., Bond Energies in Solution from Electrode Potentials and Thermochemical Cycles - A Simplified and General Approach. *Acc. Chem. Res.* **1993,** *26*, 287-294.

54. Choi, J.; Tang, L.; Norton, J. R., Kinetics of Hydrogen Atom Transfer from (η^5-C_5H_5)$Cr(CO)_3H$ to Various Olefins: Influence of Olefin Structure. *J. Am. Chem. Soc.* **2007,** *129*, 234-240.

55. Smith, D. M.; Pulling, M. E.; Norton, J. R., Tin-free and Catalytic Radical Cyclizations. *J. Am. Chem. Soc.* **2007,** *129*, 770-771.

56. Hartung, J.; Pulling, M. E.; Smith, D. M.; Yang, D. X.; Norton, J. R., Initiating Radical Cyclizations by H• Transfer from Transition Metals. *Tetrahedron* **2008,** *64*, 11822-11830.

57. Choi, J.; Pulling, M. E.; Smith, D. M.; Norton, J. R., Unusually Weak Metal-Hydrogen Bonds in $HV(CO)_4$(P-P) and Their Effectiveness as H• Donors. *J. Am. Chem. Soc.* **2008,** *130*, 4250-4252.

58. Li, G.; Han, A.; Pulling, M. E.; Estes, D. P.; Norton, J. R., Evidence for Formation of a Co-H Bond from $(H_2O)_2Co(dmgBF_2)_2$ under H_2. Application to Radical Cyclizations. *J. Am. Chem. Soc.* **2012,** *134*, 14662-14665.

59. Han, A.; Spataru, T.; Hartung, J.; Li, G.; Norton, J. R., Effect of Double-Bond Substituents on the Rate of Cyclization of α-Carbomethoxyhex-5-enyl Radicals. *J. Org. Chem.* **2014,** *79*.

60. Pulling, M. E. Hydrogen Atom Transfer from Transition-Metal Hydrides: Applications to Radical Cyclization. Columbia University, 2009.

61. Beesley, R. M.; Ingold, C. K.; Thorpe, J. F., CXIX.—The formation and stability of spiro-compounds. Part I. spiro-Compounds from cyclohexane. *Journal of the Chemical Society* **1915,** *107*, 1080-1106.

62. Kaneti, J.; Kirby, A. J.; Koedjikov, A. H.; Pojarlieff, I. G., Thorpe-Ingold Effects in Cyclizations to Five-membered And Six-membered Rings Containing Planar Segments. The Rearrangement of N(1)-alkyl-substituted Dihydroorotic Acids to Hydantoinacetic Acids in Base. *Org. Biomol. Chem.* **2004,** *2*, 1098-1103.

63. Eisenberg, D. C.; Lawrie, C. J. C.; Moody, A. E.; Norton, J. R., Relative Rates of H. Transfer from Transition-Metal Hydrides to Trityl Radicals. *J. Am. Chem. Soc.* **1991,** *113*, 4888-4895.

64. Eisenberg, D. C.; Norton, J. R., Hydrogen-Atom Transfer-Reactions of Transition-Metal Hydrides. *Isr. J. Chem.* **1991,** *31*, 55-66.

65. Franz, J. A.; Linehan, J. C.; Birnbaum, J. C.; Hicks, K. W.; Alnajjar, M. S., Absolute Rate Expressions for Hydrogen Atom Abstraction from Molybdenum Hydrides by Carbon-Centered Radicals. *J. Am. Chem. Soc.* **1999,** *121*, 9824–9830.

66. Tang, L.; Norton, J. R.; Edwards, J. C., Inverse Temperature Dependence of Chain Transfer Rate Constant for a Chromium Metalloradical in Polymerization of MMA. *Macromolecules* **2003,** *36*, 9716–9720.

67. Tang, L.; Norton, J. R., Effect of Steric Congestion on the Activity of Chromium and Molybdenum Metalloradicals as Chain Transfer Catalysts during MMA Polymerization. *Macromolecules* **2004,** *37*, 241–243.

68. Tang, L. H.; Norton, J. R., Measurement of the rate constant for H-dot abstraction from methylisobutyryl radical by $(C_5Ph_5)Cr(CO)(_3)$dot. *Macromolecules* **2006,** *39*, 8236-8240.

69. Tang, L. H.; Norton, J. R., Factors Affecting the Apparent Chain Transfer Rate Constants of Chromium Metalloradicals: Mechanistic Implications. *Macromolecules* **2006,** *39*, 8229-8235.

70. Fischer, E. O.; Hafner, W.; Stahl, H. O., Uber Cyclopentadienyl-metall-carbonyl-wasserstoffe des Chroms, Molybdans und Wolframs. *Z. Anorg. Allg. Chem.* **1955,** *282*, 47-62.

71. Halpern, J.; Pribanic, M., Hydrogenation of pentacyanocobaltate(II) at high pressures. *Inorg. Chem.* **1970,** *9*, 2616-2618.

72. Halpern, J., Mechanism of the Splitting of Dihydrogen by Pentacyanocobalate(II). A Reappraisal. *Inorg. Chim. Acta* **1983,** *77*, L105-L106.

73. Halpern, J., Binuclear Oxidative Addition - Reductive Elimination Reactions. *Inorg. Chim. Acta* **1982,** *62*, 31-37.

74. Capps, K. B.; Bauer, A.; Kiss, G.; Hoff, C. D., The Rate and Mechanism of Oxidative Addition of H_2 to the •$Cr(CO)_3C_5Me_5$ Radical--Generation of a Model for Reaction of H_2 with the •$Co(CO)_4$ Radical. *J. Organomet. Chem.* **1999,** *586*, 23-30.

75. Vollhardt, K. P. C.; Cammack, J. K.; Matzger, A. J.; Bauer, A.; Capps, K. B.; Hoff, C. D., Thermodynamic and Kinetic Study of Oxidative Addition/Reductive Elimination of H_2 and D_2 to Fulvalene$Cr_2(CO)_6$: Evidence for Relatively Strong Metal-Metal Bonds in Fulvalenedimetals. *Inorg. Chem.* **1999,** *38*, 2624-2631.

76. Wayland, B. B.; Ba, S.; Sherry, A. E., Reactions of hydrogen or deuterium molecule with a rhodium(II) metalloradical: kinetic evidence for a four-centered transition state. *Inorg. Chem.* **1992,** *31*, 148-150.

77. Norton, J. R.; Spataru, T.; Camaoni, D.; Lee, S.-J.; Li, G.; Choi, J.; Franz, J. A., Kinetics and Mechanism of the Hydrogenation of $CpCr(CO)_3$• to $CpCr(CO)_3H$. *Organometallics* **2014,** *33*, 2496.

78. Ittel, S. D.; Gridnev, A. A. Initiation of Polymerization by Hydrogen Atom Donation. U.S. Patent 7022792, April 4, 2006.

79. Gridnev, A. A.; Ittel, S. D., Catalytic Chain Transfer in Free-Radical Polymerizations. *Chem. Rev.* **2001,** *101*, 3611–3659.

80. Gridnev, A. A., Features of the Radical Polymerization of Styrene and Methyacrylates in the Presence of Cobalt-oximes. *Polym. Sci. U.S.S.R.* **1989,** *31*, 2369–2376.

Chapter 2. The Strengths of the M–H bonds in a Family of Group 8 Hydrides

2.1 Finding New M–H bonds that Readily Transfer H•

In light of the discussions of chapter one, we set out to find new metal hydrides that would be good H• donors. As was noted in chapter one, several factors influence the rate of MOHAT. While factors such as steric hindrance of the hydride play a role, the most important is the M–H bond energy. As we saw in section **1.3.1**, weaker M–H bonds transfer H• more rapidly. So determining M–H bond strengths is critical to understanding how M–H bonds react with organic substrates.

2.1.1 $CpFe(CO)_2H$

One hydride that could be a good MOHAT catalyst is $CpFe(CO)_2H$ (FpH). Despite its early discovery in 1959 by Green and Wilkinson, FpH has not been extensively studied due to its instability.[1] Only its decomposition, ligand substitution, and a few reactions with unsaturated organic compounds have been investigated.[2-4] It has been shown to donate H• to conjugated dienes[3] as well as to styrenes.[5] The Fe–H BDFE of FpH has been measured as 53 kcal/mol while the Ru–H bond in $CpRu(CO)_2H$ (RpH) has been measured as 65 kcal/mol.[6] However, the H• transfer rate of FpH to α – cyclopropylstyrene (**2.1**) was slower than that of other hydrides with supposedly stronger M–H bonds.[5] In 1991, Bullock suggested that ". . . the actual Fe–H BDE of $HFe(CO)_2Cp$ is significantly higher than the reported value".[7]

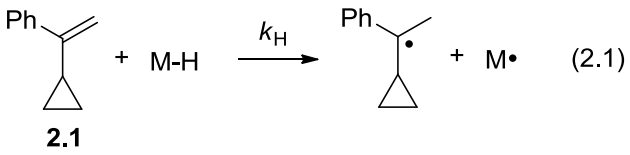

2.1

FpH is the parent of a family of iron alkyls which have a large presence in the organometallic literature.[8-14] Many transition−metal catalysts utilize M–H,[15-16] specifically Fe–H,[17] bonds in catalysis. Hence it is important to know the properties of the Fe-H bond in FpH.

Wayner and Parker calculated from thermodynamic data the metal-hydride BDFE's for 14 metal hydride complexes of W, Mn, Re, Fe, Ru, and Co.[18] Thirteen of the fourteen complexes had bond dissociation free energies between 58 and 68 kcal/mol. The only complex outside that range was FpH, with a reported BDFE of 50.8 kcal/mol.

2.2 Determination of M-H Bond Dissociation Energies Using Thermodynamic Cycles

2.2.1 Definition of the Bond Dissociation Enthalpy and Free Energy

The bond dissociation enthalpy (BDE) and bond dissociation free energy (BDFE) of transition metal hydrides represent ΔH^o of eq 2.2 and ΔG^o of eq 2.3. By convention BDE's are typically measured in the gas phase while the BDFE is usually expressed as a solution quantity. Despite this, solvation is thought to have little effect on the BDE and BDFE. Many organic BDE's are currently known from gas phase experiments.[19] However these methods are not conveniently applied to many larger molecules, particularly involving organometallic complexes.

$$M\text{-}H_{(g)} \longrightarrow M_{(g)}^{\bullet} + H_{(g)}^{\bullet} \qquad (2.2)$$

$$M\text{-}H_{(sol)} \longrightarrow M_{(sol)}^{\bullet} + H_{(sol)}^{\bullet} \qquad (2.3)$$

2.2.2 Thermodynamic Cycle for BDFE Determination

One of the most widely used methods for determining BDE and BDFE for M-H bonds has been the use of thermodynamic cycles. This strategy was first used by Breslow to estimate

the BDE's and pK_a's of C–H and O–H bonds.[20-21] It then spread through the physical organic world and was used for many organic molecules before its first application to M–H bonds by Tilset and Parker in 1989.[22-23] Since then this strategy has been used to determine the BDFE's of a wide variety of M–H bonds.[24]

$$M\text{-}H_{(sol)} \longrightarrow M^-_{(sol)} + H^+_{(sol)} \quad (2.4)$$

$$M^-_{(sol)} \longrightarrow M_{(sol)}\bullet + 1\ e^- \quad (2.5)$$

$$H^+_{(sol)} \longrightarrow H^+_{(aq)} \quad (2.6)$$

$$H^+_{(aq)} + 1e^- \longrightarrow 1/2\ H_{2(g)} \quad (2.7)$$

$$1/2\ H_{2(g)} \longrightarrow H_{(g)}\bullet \quad (2.8)$$

$$H_{(g)}\bullet \longrightarrow H_{(sol)}\bullet \quad (2.9)$$

This thermodynamic cycle is composed of the M–H pK_a, the M•/M$^-$ redox potential, and the H^+/H• potential in the solvent of choice.[25] The first two properties can be measured experimentally (eqs 2.4 and 2.5) and the third can be estimated by addition of eqs 2.6 through 2.9. Adding the free energies of eqs 2.4 – 2.9 gives a general expression of the BDFE as a function of the M–H pK_a and the M•/M$^-$ redox couple versus Fc/Fc$^+$ in acetonitrile (eq 2.10). Use of the $Fc_{(sol)}/Fc^+_{(sol)}$ reference requires conversion of the $H^+_{(sol)}/H\bullet_{(sol)}$ couple from NHE reference to $Fc_{(sol)}/Fc^+_{(sol)}$, which was worked out in acetonitrile by DuBois and coworkers.[26] The $H^+_{(sol)}/H\bullet_{(sol)}$ potential is heavily solvent dependent and so the constant in eq 2.10 is specific for acetonitrile. Acetonitrile is able to adequately solvate most charged organometallic fragments to

prevent ion pairing,[27] has a large autoprotolysis constant (as high as 44),[28] and has a large electrochemical potential window (~ 5 V)[29] making it an ideal solvent for BDFE determination.

$$BDFE(M-H) = 1.37\,pK_a + 23.06E^0_{M\bullet/M^-} + 53.6\,{}^{kcal}\!/_{mol} \qquad (2.10)$$

2.2.3 Sources of Error in BDFE Determination

When discussing errors, we must make the distinction between absolute errors and relative errors. Certain assumptions in this cycle introduce absolute errors which have been noted. The free energy change for eq 2.6 relies on the extrathermodynamic "tetraphenylarsenium tetraphenylboride assumption".[30] The free energy of solvation of the hydrogen atom (eq 2.9) has never been measured and was assumed to be equal to that of the H_2 molecule.[31-32] Another source of absolute error is the assumption that the electrolyte has negligible effect on the solvation energies above, which was shown to be correct within 2 kcal/mol.[33] However, the scale of M–H BDFE's determined by this method is self-consistent, making relative values more meaningful.

Relative errors are introduced only through the measurements of the M–H pK_a and E°(M•/M$^-$). The largest source of experimental error is in the measurement of E°(M•/M$^-$); an error of 20 mV = 0.5 kcal/mol. The electrochemical measurement must be reversible to be thermodynamically meaningful. Often it is not and the true reversible potential must be estimated. Irreversibility can be caused by subsequent reaction after the electrochemical event in a so–called EC mechanism. If the rate constant of this second step is known, then a kinetic potential shift correction can be applied to correct for the contribution of the chemical step to the

overpotential. This has been done for a variety of M•/M$^-$ using known rate constants for the dimerization reaction in eq 2.11.

$$2\ M\bullet \xrightarrow{k_{dimer}} M_2 \qquad (2.11)$$

Measurement of the pK_a must also be done carefully. The pK_a is often measured by equilibration of either M–H and B or BH$^+$ and M$^-$, to produce the equilibrium in eq 2.12.[27] Hydrides are often unstable with respect to oxidation and hydrogen loss. Care must always be taken to ensure that no decomposition occurs during the experiments. In addition, the pK_a of BH$^+$ must also be known. The pK_a of many acids have been measured in acetonitrile and put on one self–consistent scale.[34-35] Homoconjugation equilibria similar to eq 2.13 complicate the situation further. Ideally, BH$^+$ should not homoconjugate. If it cannot be avoided, BH$^+$'s with known homoconjugation constants can still give accurate pK_a's.

$$M\text{-}H + B \rightleftharpoons M^- + BH^+ \qquad (2.12)$$

$$BH^+ + B \rightleftharpoons B_2H^+ \qquad (2.13)$$

2.2.4 Conversion of BDFE to BDE

Most X–H bond energies are in the form of BDE's. To make a direct comparison, we must convert our BDFE values to BDE's. This can be accomplished using eq 2.14.[25] It is commonly assumed that both the entropic difference between M–H and M• (TS^o_f(M• – M–H)) and the difference in their solvation free energies ($\Delta\Delta G^o_{solv}$(M• – M–H) are negligible so that the only terms which need be considered when converting BDFE to BDE are the free energy of

solvation of H• ($\Delta G^{o}_{solv}(H\bullet)$) and the entropy of formation of H• ($TS^{o}_{f}(H\bullet)$) (eq 2.15). For acetonitrile, $BDE(M–H)_g$ is 4.8 kcal/mol higher in energy than $BDFE(M–H)_S$.[25]

$$BDE\left(M-H\right)_g = BDFE\left(M-H\right)_S - \Delta G_{solv}\left(H\bullet\right) + TS^{\circ}_f\left(H\bullet\right) \\ -\Delta\Delta G_{solv}\left(M\bullet - M-H\right) + TS^{\circ}_f\left(M\bullet - M-H\right) \tag{2.14}$$

$$BDE\left(M-H\right)_g \approx BDFE\left(M-H\right)_S - \Delta G_{solv}\left(H\bullet\right) + TS^{\circ}_f\left(H\bullet\right) \\ = BDFE\left(M-H\right)_S + 4.8\,{}^{kcal}\!/_{mol} \tag{2.15}$$

The validity of this conversion was tested versus calorimetric $BDE(Cr–H)_g$ values for two different Cr–H bonds.[33] They found the correction in these cases to be 5.2 and 6.2 kcal/mol. This proves that eq 2.14 is valid to within a few kcal/mol but the contribution within that window could either be error in the estimation of $\Delta G_{solv}(H\bullet)$ or small corrections from the last two terms in eq 2.14, which would vary with the nature of the hydride. This effect can be large. Mayer and coworkers found that for some Fe complexes, a PCET reaction is coupled to a transition from low spin to high spin, making the $TS^{o}_{f}(M\bullet – M–H)$ term significant.[36] Unless a direct comparison must be made it is advisable to use $BDFE(M–H)_S$ over $BDE(M–H)_g$.

2.3 Acidity of Transition Metal Hydrides

The transition metal-hydrogen bond can react as a proton donor, and is often quite acidic. For example, $HCo(CO)_4$ was measured to be almost as acidic as HCl, making it one of the most acidic hydrides known.[27] Measuring the M–H pK_a is done by equilibrating the hydride with a base of known basicity, (eq 2.16).

$$pK_{eq} = pK_{a,hydride} - pK_{a,base} \; where \; K_{eq} = \frac{[BH^+][M^-]}{[MH][B]} \tag{2.16}$$

As noted above, the acidity must be known in order to measure the BDFE. The acidities of many metal hydride complexes have been determined using this method.[27] Since the energetics of all metal-hydrogen cleavage modes depend on the acidity, the accurate determination of metal-hydride acidities is important.

The pK_a of FpH in acetonitrile was originally determined as 19.4 by the Norton group in 1986.[27] However, the Lichtenberger group, during a study on the electrocatalytic generation of hydrogen, observed that Fp^- was able to deprotonate acids with pK_a values much greater than 19.4.[37] They estimated the pK_a of FpH as 26.7, seven orders of magnitude higher.[37] The pK_a of the ruthenium analog was originally measured to be 20.2, seemingly in agreement with the original pK_a value for FpH.[27] However, the osmium analog of this compound was determined in a separate study to have a pK_a of 32.7,[38] which seemingly supports the latter pK_a value for FpH.

In order for the chemistry of this hydride to be understood, the acidity must be determined accurately. We have, therefore, redetermined the pK_a of FpH. We have also determined the pK_a values of the Ru analog of FpH as well as the pK_a of $Cp^*Fe(CO)_2H$ (Fp*H) in order to assess the ligand and group trends.

2.4 Results and Discussion

2.4.1 M–H acidity

In collaboration with the Lichtenberger group (U. Ariz), the pK_a values of these hydrides in acetonitrile have been determined relative to bases of appropriate strength.[34] The pK_a values are shown in Table 2.1. The concentrations of each of the carbonyl containing components in the solution were measured by quantitative IR spectroscopy (molar absorptivities of each carbonyl band of the complexes used are given in Table 2.3 below). The pK_a of FpH has been determined with multiple bases including the phenolates of 4-*tert*-butylphenol (pK_a = 27.5)[39] and phenol

(pK_a = 26.6),[40,41-43] and 1,5,7 triazabicyclo[4.4.0]dec-5-ene (TBD) (pK_a = 26.03).[34] Weaker bases such as triethylamine (pK_a = 18.82)[34] and tetramethylguanidine (pK_a = 23.3)[39] are unable to deprotonate FpH.

Phenol is subject to the ternary homoconjugation equilibrium, shown in equation 2.17. The correction for this involves solving a cubic equation,[28] which can introduce uncertainty into the measurement. This equilibrium has led to contention in the literature as to the correct value for the pK_a of phenol in acetonitrile, with numbers ranging from 26.6 to 29.1 appearing in the literature.

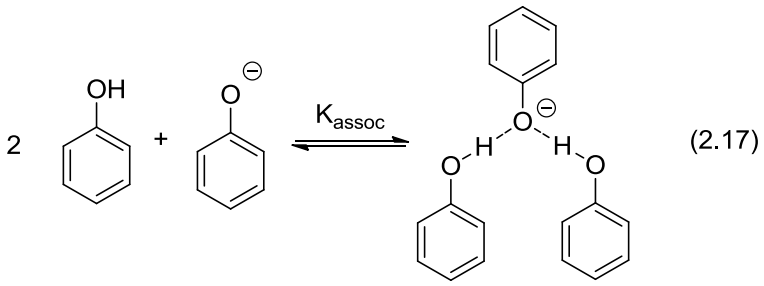

(2.17)

In contrast, TBD is a guanidine type base with no homoconjugation equilibrium; the pK_a has been unequivocally determined on the unified scale in acetonitrile. For these reasons, we prefer the pK_a value of FpH determined with TBD. Indeed, FpH is much less acidic than reported previously, with a pK_a of 27.1(2). The cause of the discrepancy in the original pK_a measurement is unclear.

Table 2.1. The pK_a's of the compounds measured, equilibrium constants, and bases used to measure them.

Compound	Base (pK_a, K_{assoc})	K_{eq}	pK_a
$CpFe(CO)_2H$	4-tertbutylphenolate (27.5, 1×10^5)[39]	0.109	26.5
$CpFe(CO)_2H$	phenolate (26.6, 6.3×10^5)[16]	0.79	26.7(3)
$CpFe(CO)_2H$	TBD (26.03, 0)[34]	0.085	27.1(2)
$CpRu(CO)_2H$	TBD (26.03, 0)[34]	0.005	28.4(1)

$CpOs(CO)_2H$[38]	Verkade's Super Base (33.53, 0)[38]	-	32.7[38]
$Cp^*Fe(CO)_2H$	phenolate (26.6, 6.3×10^5)[16]	7.4×10^{-4}	29.7

FpH is the most acidic hydride in this series, with a pK_a of 27.1, followed by the ruthenium analog (pK_a = 28.4(1)), the osmium analog being the least acidic of all (pK_a = 32.7).[38] The differences in pK_a values among these first, second, and third row hydrides are similar to the differences in pK_a values for the group six analogs $CpM(CO)_3H$ (M = Cr, Mo, W).[27] Fp*H shows a significant decrease in acidity with a pK_a of 29.7, roughly 3 units more basic than FpH, due to the electron donating nature of Cp*.

2.4.2 M–H BDFE

These pK_a values have been used to calculate the other properties of the M–H bonds. Table 2.2 shows the pK_a, BDFE, and BDE values of these compounds. The M–H BDFE increases while descending each group. The Fe–H bond of FpH (63 kcal/mol) is weaker than the Ru–H bond in RpH, which is weaker still than the Os–H bond of the related osmium hydride (one of the strongest metal-hydrogen bonds ever discovered).[38] This trend is very similar to that of analogous group six hydrides, where the Cr–H bond is weaker than both the Mo–H and the W–H bond.[6] The group eight M–H BDFE's are higher than those of group six, ($CpCr(CO)_3H$, Cr–H BDFE = 57 kcal/mol).[6] However, this trend does not extend to other groups in the transition series. These M–H bonds are much stronger than originally believed and are in better agreement with reported rate constants for hydrogen atom transfer reactions of metal hydrides.[7]

Table 2.2. Acidities, M-H BDE's, and M-H BDFE's of the M-H bonds in Group 8 Hydrides

Compound	pK_a	M-H BDE[a]	M-H BDFE[a]
$CpFe(CO)_2H$	27.1	68	63
$CpRu(CO)_2H$	28.3	77	72

$CpOs(CO)_2H$[b]	32.7	83	78
$Cp^*Fe(CO)_2H$[c]	29.7	—	—

[a] Electrochemical Data were taken from reference 13
[b] Data taken from reference 25
[c] No BDE is reported for this complex since the electrochemical analysis does not yield a straightforward oxidation potential (see reference 13)

2.4.3 Thermodynamics of Hydride Donation from $CpFe(CO)_2H$

The free energy of hydride loss from a metal hydride (known as the hydricity, shown in eq 2.21) can be determined from a different thermodynamic cycle. This cycle uses the acidity of the metal hydride complex (eq 2.18), combined with the two electron oxidation potential of the conjugate base (eq 2.19), and the two electron reduction potential of H^+ in acetonitrile (eq 2.20). Adding these potentials gives eq 2.22, which can be used to calculate the thermodynamic hydricity of a hydride. This method has been used to measure the hydricity of a series of group 10 cationic metal hydrides.[44]

$$M\text{-}H_{(sol)} \longrightarrow M^-_{(sol)} + H^+_{(sol)} \qquad (2.18)$$

$$M^-_{(sol)} \longrightarrow M^+_{(sol)} + 2\,e^- \qquad (2.19)$$

$$H^+_{(sol)} + 2\,e^- \longrightarrow H^-_{(sol)} \qquad (2.20)$$

$$M\text{-}H_{(sol)} \longrightarrow M^+_{(sol)} + H^-_{(sol)} \qquad (2.21)$$

$$\Delta G^o_{H^-} = 1.37\,pK_a + 46.1E^o_{ox,(II/0)} + 79.6\,kcal/mol \qquad (2.22)$$

We can use the same cycle to calculate the hydricity of FpH in CH_3CN, if we know $E°_{2e\,ox}(Fp^-)$, the two-electron oxidation potential of Fp^- in that solvent (eq 2.19). Tilset and Parker have estimated the potential for eq 2.23 in CH_3CN as –1.235 V vs Fc/Fc^+,[6, 23] and Pugh and Meyer have determined the potential for eq 2.24 in CH_3CN as –1.124 V vs Fc/Fc^+.[45] Averaging

these two values gives $E^{o}_{(II/0)}$ = –1.180 V vs Fc/Fc^{+}. These numbers give FpH a hydricity (ΔG_H-) of 62 kcal/mol. This value is higher than, but consistent with, the 55 kcal/mol reported by DuBois and co-workers for $CpMo(CO)_2(PMe_3)H$.[46] We expect $CpMo(CO)_2(PMe_3)H$ to be a better H^- donor than FpH, as the lower ΔG_H- of $CpMo(CO)_2(PMe_3)H$ predicts. This is consistent with the trend found for kinetic hydricities of similar compounds.[47] But, compared to common main group hydrides like $[HBEt_3]^-$ (ΔG_H- = 26 kcal/mol) FpH is a poor hydride donor.[48]

$$Fp^- \longrightarrow Fp\bullet + e^- \qquad (2.23)$$

$$Fp\bullet \longrightarrow Fp(NCCH_3)^+ + e^- \qquad (2.24)$$

2.4.4 Predicting reactivity with H_2 using the M-H BDFE

Our M–H BDFE values can be used to predict the position of equilibria for the production of molecular hydrogen from metal-hydrides as shown in eq 2.25. It has been suggested that hydride complexes with BDE's lower than 56 kcal/mol (BDFE = 52 kcal/mol) should be unstable to H_2 loss at room temperature.[49] Indeed, many hydrides (e.g., $CpCr(CO)_3H$ and $HV(CO)_4$(dppm) that have weaker M–H bonds than FpH (57 and 52 kcal/mol, respectively[50]) are isolable at room temperature — unlike FpH, which evolves H_2 in an open system despite its relatively strong M–H bond (63 kcal/mol in Table 2.2 above).

$$2\ M\text{—}H \rightleftharpoons M_2 + H_2 \qquad (2.25)$$

It is apparent from eq 2.25 that the strength of a given metal metal interaction is also important in determining the position of such equilibria. With Fp_2 the situation is complicated by the presence of several isomers (cis (μ-$CO)_2$ and trans(μ-$CO)_2$).[45] However, a useful estimate (25 kcal/mol) of the free energy of interaction between two Fp fragments has been obtained by rapid scan cyclic voltammetry.[45]

This ΔG for $Fp_2/Fp\bullet$, along with a BDFE for hydrogen of 103.6 kcal/mol,[18] leads to an estimate of -2.6 kcal/mol for the ΔG of eq 2.25. This estimate is consistent with the report by Barnett and co-workers that only significant pressures of H_2 (1000 psi of H_2/CO, 100 °C) can convert Fp_2 to FpH.[51] This also matches the earlier discussion from section **1.4.4**, where we stated that the rate of H_2 activation (k_{H2}) is slow with high metal metal interaction.

2.5 Experimental Details

All manipulations were performed under a nitrogen or argon atmosphere using standard Schlenk or inert atmosphere box techniques. IR data were recorded on either a Perkin Elmer Spectrum 2000 spectrometer using an air-free 0.1 mm path length CaF_2 solution cell or a Nicolet 380 FT-IR using an air-free (1 mm) KBr solution cell.

Acetonitrile was distilled from P_4O_{10} to remove water, then from CaH_2 to remove acidic impurities; it was purged with argon for several hours to remove oxygen, and stored in an argon atmosphere over 3Å molecular sieves. THF and benzene were purified by distillation from Na/benzophenone ketyl under nitrogen. Organic liquids were deoxygenated by performing three freeze – pump – thaw cycles under argon.

The anions $E[(\eta^5\text{-}C_5H_5)M(CO)_2]$ (M = Fe[52], Ru[53]) (E = Na, K) were prepared by literature procedures.

Preparation of $(\eta^5\text{-}C_5H_5)Fe(CO)_2H$ (FpH). To a bright red solution of $K[(\eta^5\text{-}C_5H_5)Fe(CO)_2]$ (KFp) in CH_3CN (0.1 M), was added 0.5 eq of anhydrous HCl in diethyl ether. A subsequent bulb to bulb vacuum transfer yielded a pale yellow solution of pure FpH in CH_3CN, which showed 10% decomposition over 24 h at room temperature by ^1H NMR. (CH_3CN, ν(CO): 1951, 2014 cm^{-1}). Solutions of FpH of known concentration were made by mixing an excess of an acid

known to quantitatively protonate the Fp anion (anilinium tetrafluoroborate or HCl) with a solution of KFp of known concentration.

Preparation of (η^5-C_5H_5)Ru(CO)$_2$H (RpH). Same procedure as above for FpH. IR (CH_3CN ν_{CO} : 1959, 2022 cm^{-1}).

Preparation of (η^5-C_5Me_5)Fe(CO)$_2$H (Fp*H). A solution of Fp*$_2$ in 50 ml of dry THF was stirred with two equiv of liquid sodium amalgam overnight under an inert atmosphere. Two equivalents of glacial acetic acid (i.e., one acid per Na) were then added to the THF solution which was then stirred for one hour. The THF was removed under vacuum, resulting in a dark solid which was then dissolved in pentane and filtered. Pentane was removed under vacuum to produce a gold solid. IR (CH_3CN ν_{CO} : 1929, 1992 cm^{-1}).[54]

Molar absorptivities of the carbonyl stretching frequencies were found by measuring the absorbances (baseline corrected) of the carbonyl stretches of multiple solutions of known concentrations (0.0025 – 0.02M) and fitting this data to a linear regression.

The pK_a measurements were performed by making solutions of the hydride (0.0052 M FpH, 0.015 M RpH) with the appropriate base (0.0137 M TBD) and measuring the equilibrium concentrations of all species. The equilibrium concentrations were determined by quantitative IR spectroscopy from the carbonyl stretch absorptions, given in Table 2.3. The final pK_a values are the average of three experiments.

Table 2.3. IR stretching frequencies and molar absorptivities for metal hydrides and anions

Compound	ν_{CO} (cm^{-1})	ε ($M^{-1}cm^{-1}$)
$CpFe(CO)_2H$	1951	1848
	2014	1452
$K[CpFe(CO)_2]$	1785	2167
	1861	1956

$CpRu(CO)_2H$[a]	1959	1862
	2022	1391
$Na[CpRu(CO)_2]$	1803	1570
	1888	1522
$Cp^*Fe(CO)_2H$	1929	2044
	1992	2587

[a] In all cases the integrated intensities of the carbonyl stretching bands are smaller for the neutral hydride complexes than for the deprotonated anions. As a referee has pointed out, this pattern is to be expected in view of the fact that "intensities … increase … with falling CO stretching frequency".[55] However, because the carbonyl band at 1959 cm^{-1} for RpH is sharper than the corresponding band for Rp^-, ε for that (1959 cm^{-1}) band of RpH is higher than ε for the corresponding band of Rp^-.

2.6 References

1. Green, M. L. H.; Street, C. N.; Wilkinson, G., Some New Transition Metal pi-Cyclopentadienyl Hydrides. *Zeitschrift Fur Naturforschung Part B-Chemie Biochemie Biophysik Biologie Und Verwandten Gebiete* **1959,** *14* (11), 738-738.

2. Fergusson, S. B.; Sanderson, L. J.; Shackleton, T. A.; Baird, M. C., $CpFe(CO)_2H$ - A Reassessment of the Literature. *Inorganica Chimica Acta-Articles and Letters* **1984,** *83* (2), L45-L47.

3. Shackleton, T. A.; Baird, M. C., The radical pair mechanism in hydrometalation and stoichiometric hydrogenation reactions of dicarbonyl(cyclopentadienyl)iron hydride [eta-^{5}-$C_5H_5Fe(CO)_2H$] with conjugated dienes. *Organometallics* **1989,** *8* (9), 2225-2232.

4. Shackleton, T. A.; Mackie, S. C.; Fergusson, S. B.; Johnston, L. J.; Baird, M. C., The Chemistry of (η^5-C_5H_5)$Fe(CO)_2H$ Revisited. *Organometallics* **1990,** *9* (8), 2248-2253.

5. Bullock, R. M.; Samsel, E. G., Hydrogen Atom Transfer Reactions of Transition-metal Hydrides. Kinetics and Mechanism of the Hydrogenation of α-Cyclopropylstyrene by Metal Carbonyl Hydrides. *J. Am. Chem. Soc.* **1990,** *112* (19), 6886-6898.

6. Tilset, M.; Parker, V. D., Solution Homolytic Bond Dissociation Energies of Organotransition-Metal Hydrides. *J. Am. Chem. Soc.* **1989,** *111*, 6711-6717.

7. Bullock, R. M., *Comments Inorg. Chem.* **1991,** *12*, 1.

8. Mohler, D. L.; Shell, T. A., The hydrogen peroxide induced enhancement of DNA cleavage in the ambient light photolysis of CpFe(CO)(2)Ph: A potential strategy for targeting cancer cells. *Bioorg. Med. Chem. Lett.* **2005,** *15* (20), 4585-4588.

9. Cutler, A.; Ehntholt, D.; Lennon, P.; Nicholas, K.; Marten, D. F.; Madhavarao, M.; Raghu, S.; Rosan, A.; Rosenblum, M., Chemistry of Dicarbonyl eta-5-Cyclopentadienyliron Complexes - General Syntheses of Monosubstituted eta-2-Olefin Complexes and of 1-Substituted eta-1-Allyl Complexes - Conformational Effects on Course of Deprotonation of (eta-2-Olefin) Cations. *J. Am. Chem. Soc.* **1975,** *97* (11), 3149-3157.

10. Casey, C. P.; Smith, L. J., Inversion of Stereochemistry at the Carbon Bound to Iron in Cyclopropane Formation from Threo-$C_5H_5(CO)_2FeCHDCHDCH_2S(CH_3)C_6H_5^+$. *Organometallics* **1989,** *8* (9), 2288-2290.

11. Bock, P. L.; Boschetto, D. J.; Rasmussen, J. R.; Demers, J. P.; Whitesides, G. M., Stereochemistry of Reactions at Carbon-Transition Metal Sigma Bonds - $(CH_3)_3CCHDCHDFe(CO)_2C_5H_5$. *J. Am. Chem. Soc.* **1974,** *96* (9), 2814-2825.

12. Bock, P. L.; Whitesides, G. M., Stereoselective Synthesis of 1-Substituted Organometallic Derivatives of 3,3-Dimethylbutane-1,2-D_2. *J. Am. Chem. Soc.* **1974,** *96* (9), 2826-2829.

13. Whitesides, G. M.; Boschetto, D. J., Reaction of Threo-$(CH_3)_3CCHDCHDFe(CO)_2$-π-C_5H_5 with Triphenylphosphine. *J. Am. Chem. Soc.* **1969,** *91* (15), 4313-&.

14. Whitesides, G. M.; Boschetto, D. J., Stereochemistry of Reactions Occurring at Iron-Carbon Omicron Bonds. *J. Am. Chem. Soc.* **1971,** *93* (6), 1529-&.

15. Creutz, C.; Chou, M. H.; Hou, H.; Muckerman, J. T., Hydride Ion Transfer from Ruthenium(II) Complexes in Water: Kinetics and Mechanism. *Inorg. Chem.* **2010,** *49* (21), 9809-9822.

16. Lee, J. P.; Ke, Z.; Ramírez, M. A.; Gunnoe, T. B.; Cundari, T. R.; Boyle, P. D.; Petersen, J. L., Six-, Five-, and Four-Coordinate Ruthenium(II) Hydride Complexes Supported by N-Heterocyclic Carbene Ligands: Synthesis, Characterization, Fundamental Reactivity, and Catalytic Hydrogenation of Olefins, Aldehydes, and Ketones. *Organometallics* **2009,** *28* (6), 1758-1775.

17. Casey, C. P.; Guan, H., Cyclopentadienone Iron Alcohol Complexes: Synthesis, Reactivity, and Implications for the Mechanism of Iron-Catalyzed Hydrogenation of Aldehydes. *J. Am. Chem. Soc.* **2009,** *131* (7), 2499-2507.

18. Wayner, D. D. M.; Parker, V. D., Bond energies in solution from electrode potentials and thermochemical cycles. A simplified and general approach. *Accounts of Chemical Research* **1993,** *26* (5), 287-294.

19. Luo, Y.-R., *Handbook of bond dissociation energies in organic compounds*. CRC Press: Boca Raton, Florida, 2002; p 380.

20. Breslow, R.; Balasubramanian, K., pK_a of Triphenylcyclopropene. Electrochemical Determination of an Inaccessible Equilibrium Constant. *J. Am. Chem. Soc.* **1969,** *91* (18), 5182-5183.

21. Breslow, R.; Chu, W., Thermodynamic Determination of pK_a's of Weak Hydrocarbon Acids Using Electrochemical Reduction Data. Triarylmethyl Anions, Cycloheptatrienyl Anion, and Triphenyl- and Trialkylcyclopropenyl Anions. *J. Am. Chem. Soc.* **1973,** *95* (2), 411-418.

22. Tilset, M.; Parker, V. D., Solution homolytic bond dissociation energies of organotransition-metal hydrides. *J. Am. Chem. Soc.* **1989,** *111* (17), 6711-6717.

23. Tilset, M.; Parker, V. D., Solution Homolytic Bond Dissociation Energies of Organotransition-Metal Hydrides [Erratum to document cited in CA111(11):97481d]. *J. Am. Chem. Soc.* **1990,** *112* (7), 2843-2843.

24. Tilset, M., Organometallic Electrochemistry: Thermodynamics of Metal-Ligand Bonding. In *Comprehensive Organometallic Chemistry III*, Robert, H. C.; Mingos, D. M. P., Eds. Elsevier: Oxford, 2007; pp 279-305.

25. Wayner, D. D. M.; Parker, V. D., Bond Energies in Solution from Electrode Potentials and Thermochemical Cycles - A Simplified and General Approach. *Acc. Chem. Res.* **1993,** *26* (5), 287-294.

26. Ellis, W. W.; Raebiger, J. W.; Curtis, C. J.; Bruno, J. W.; DuBois, D. L., Hydricities of BzNADH, $C_5H_5Mo(PMe_3)(CO)_2H$, and $C_5Me_5Mo(PMe_3)(CO)_2H$ in Acetonitrile. *J. Am. Chem. Soc.* **2004,** *126* (9), 2738-2743.

27. Moore, E. J.; Sullivan, J. M.; Norton, J. R., Kinetic and Thermodynamic Acidity of Hydrido Transition-Metal Complexes. 3. Thermodynamic Acidity of Common Mononuclear Carbonyl Hydrides. *J. Am. Chem. Soc.* **1986,** *108* (9), 2257-2263.

28. Kristjánsdóttir, S. S.; Norton, J. R., Acidity of Hydrido Transition Metal Complexes in Solution. In *Transition Metal Hydrides,* Dedieu, A., Ed. VCH: New York, 1992.

29. Bard, A. J.; Faulkner, L. R., *Electrochemical Methods: Fundamentals and Applications*. 2nd Edition ed.; John Wiley and Sons, Inc.: Hoboken, NJ, 2001.

30. Parker, A. J., Protic-dipolar aprotic solvent effects on rates of bimolecular reactions. *Chem. Rev.* **1969,** *69* (1), 1-32.

31. Parker, V. D., Homolytic bond (H-A) dissociation free energies in solution. Applications of the standard potential of the (H+/H•) couple. *J. Am. Chem. Soc.* **1992,** *114* (19), 7458-7462.

32. Parker, V. D., Homolytic bond (H-A) dissociation free energies in solution. Applications of the standard potential of the (H+/H•)couple. [Erratum to document cited in CA117(14):139621f]. *J. Am. Chem. Soc.* **1993,** *115* (3), 1201-1201.

33. Parker, V. D.; Handoo, K. L.; Roness, F.; Tilset, M., Electrode potentials and the thermodynamics of isodesmic reactions. *J. Am. Chem. Soc.* **1991,** *113* (20), 7493-7498.

34. Kaljurand, I.; Kutt, A.; Soovali, L.; Rodima, T.; Maemets, V.; Leito, I.; Koppel, I. A., Extension of the self-consistent spectrophotometric basicity scale in acetonitrile to a full span of 28 pK_a units: Unification of different basicity scales. *J. Org. Chem.* **2005,** *70* (3), 1019-1028.

35. Kutt, A.; Leito, I.; Kaljurand, I.; Soovali, L.; Vlasov, V. M.; Yagupolskii, L. M.; Koppel, I. A., A comprehensive self-consistent spectrophotometric acidity scale of neutral bronsted acids in acetonitrile. *J. Org. Chem.* **2006,** *71* (7), 2829-2838.

36. Mader, E. A.; Davidson, E. R.; Mayer, J. M., Large ground-state entropy changes for hydrogen atom transfer reactions of iron complexes. *J. Am. Chem. Soc.* **2007,** *129* (16), 5153-5166.

37. Felton, G. A. N.; Vannucci, A. K.; Okumura, N.; Lockett, L. T.; Evans, D. H.; Glass, R. S.; Lichtenberger, D. L., Hydrogen generation from weak acids: Electrochemical and computational studies in the (eta(5)-C5H5)Fe(CO)(2) (2) system. *Organometallics* **2008,** *27* (18), 4671-4679.

38. Zhang, J.; Grills, D. C.; Huang, K. W.; Fujita, E.; Bullock, R. M., Carbon-to-metal hydrogen atom transfer: Direct observation using time-resolved infrared spectroscopy. *J. Am. Chem. Soc.* **2005,** *127* (45), 15684-15685.

39. Izutsu, K., *Acid - Base Dissociation Conostants in Dipolar Aprotic Solvents*. Blackwell Scientific Publications: Oxford, UK, 1990.

40. There are three different values for the pKa of phenol in acetonitrile in the literature, 26.6, 27.2, and 29.1 from references 27, 28, and 29 respectively. We have chosen to use the number 26.6 in this work, as it is the most commonly cited in the literature.

41. Coetzee, J. F.; Padmanabhan, G. R., Dissociation and Homoconjugation of Certain Phenols in Acetonitrile. *J. Phys. Chem.* **1965,** *69* (9), 3193-3196.

42. Kuett, A.; Movchun, V.; Rodima, T.; Dansauer, T.; Rusanov, E. B.; Leito, I.; Kaljurand, I.; Koppel, J.; Pihl, V.; Koppel, I.; Ovsjannikov, G.; Toom, L.; Mishima, M.; Medebielle, M.; Lork, E.; Roeschenthaler, G. V.; Koppel, I. A.; Kolomeitsev, A. A., Pentakis(trifluoromethyl)phenyl, a sterically crowded and electron-withdrawing group: Synthesis and acidity of pentakis(trifluoromethyl)benzene, -toluene, -phenol, and -aniline. *J. Org. Chem.* **2008,** *73* (7), 2607-2620.

43. Kolthoff, I. M.; Chantooni, M. K.; Bhowmik, S., Acid-base indicator constants in acetonitrile. *Anal. Chem.* **1967,** *39* (3), 315-320.

44. Curtis, C. J.; Miedaner, A.; Ellis, W. W.; DuBois, D. L., Measurement of the hydride donor abilities of $[HM(diphosphine)_2]^+$ complexes (M = Ni, Pt) by heterolytic activation of hydrogen. *J. Am. Chem. Soc.* **2002,** *124* (9), 1918-1925.

45. Pugh, J. R.; Meyer, T. J., Organometallic thermodynamics. Redox couples involving metal-metal bonds. *J. Am. Chem. Soc.* **1992,** *114* (10), 3784-3792.

46. Ellis, W. W.; Raebiger, J. W.; Curtis, C. J.; Bruno, J. W.; DuBois, D. L., Hydricities of BzNADH, C5H5MO(PMe3)(CO)(2)H, and C5Me5Mo(PMe3)(CO)(2)H in acetonitrile. *J. Am. Chem. Soc.* **2004,** *126* (9), 2738-2743.

47. Cheng, T.-Y.; Bullock, R. M., Hydride Transfer from $(\eta^5\text{-}C_5Me_5)(CO)_2MH$ (M = Fe, Ru, Os) to Trityl Cation: Different Products from Different Metals and the Kinetics of Hydride Transfer. *Organometallics* **2002,** *21* (11), 2325-2331.

48. Mock, M. T.; Potter, R. G.; Camaioni, D. M.; Li, J.; Dougherty, W. G.; Kassel, W. S.; Twamley, B.; DuBois, D. L., Thermodynamic Studies and Hydride Transfer Reactions from a Rhodium Complex to BX_3 Compounds. *J. Am. Chem. Soc.* **2009,** *131* (40), 14454-14465.

49. Kiss, G.; Zhang, K.; Mukerjee, S. L.; Hoff, C. D.; Roper, G. C., Heat of Reaction of the $Cr(CO)_3(C_5Me_5)$ Radical with Hydrogen and Related Reactions. Relative and Absolute Bond Strengths in the Complexes H-$Cr(CO)_2(L)(C_5R_5)$. *J. Am. Chem. Soc.* **1990,** *112* (14), 5657-5658.

50. Choi, J.; Pulling, M. E.; Smith, D. M.; Norton, J. R., Unusually Weak Metal-Hydrogen Bonds in $HV(CO)_4$(P-P) and Their Effectiveness as H• Donors. *J. Am. Chem. Soc.* **2008,** *130* (13), 4250-4252.

51. Chang, B. H.; Coil, P. C.; Brown, M. J.; Barnett, K. W., Hydrido Cyclopentadienyl Dicarbonyliron and its Role in Olefin Hydroformylation. *J. Organomet. Chem.* **1984,** *270* (1), C23-C25.

52. Jeffrey S. Plotkin, S. G. S., Convenient Preparation and Isolation of Pure Potassium Cyclopentadienyldicarbonylferrate, K[(eta5-C5H5)Fe(CO)2]. *Inorg. Chem.* **1981,** *20*, 1.

53. Blackmore, T.; Bruce, M. I.; Stone, F. G. A., Chemistry of Metal Carbonyls 49. Dicarbonyl-π-Cyclopentadienylruthenium Fluorocarbon Complexes. *J. Chem. Soc. A* **1968,** (9), 2158.

54. Whitesides, T. H.; Shelly, J., Thermolysis and photolysis of (cyclopentadiene)iron tricarbonyl. Evidence for a radical mechanism involving iron(I). *J. Organomet. Chem.* **1975,** *92* (2), 215-226.

55. Braterman, P. S., *Metal Carbonyl Spectra*. Academic Press: London, 1975; p 168.

Chapter 3: Mechanism of the Reaction of Cobaloximes with Hydrogen

3.1 Cobaloximes as MOHAT Catalysts

In section 1.4.4, it was mentioned that cobaloximes catalyze MOHAT reactions under hydrogen gas. Compound **1.34** is a good catalyst for the radical cyclization of substrate **1.22**. However, very little is known about this process. Presumably, it involves steps similar to those proposed for $CrCr(CO)_3H$ in chapter 1. In this chapter, I report my investigations into the dynamics of complex **1.34** and analogous complexes under hydrogen gas and attempts to characterize its putative hydride.

3.1.1 Cobaloximes

Cobaloxime complexes like **3.1** have been well studied owing to the fact that they are similar to cobalt corrinoid complexes such as vitamin B_{12}.[1-3] They consist of a central cobalt surrounded by two monoanionic glyoxime ligands which form a planar macrocycle with four N donors (formally an L_2X_2 ligand). An alternate resonance structure, shown on the right below, more clearly represents the L_2X_2 nature of the macrocycle. However, crystallographic bond distances support the structure on the left which is more C=N and C–C in nature. The central Co can then be coordinated by two axial ligands to make a tetragonally distorted octahedral coordination environment. The bridging linker E is usually either H or BF_2.

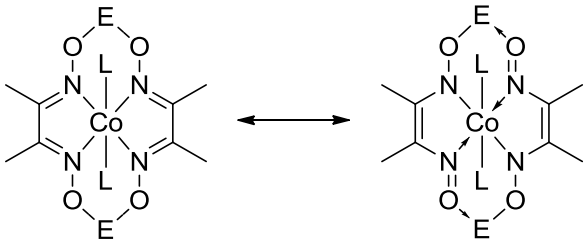

3.1 (E = BF_2)
3.2 (E = H)
a (L = CH_3CN)
b (L = THF)
c (L = H_2O)

3.1.2 Cobaloxime Hydrides

In an attempt to model the organometallic chemistry of cobalamin complexes, many alkyl cobaloxime complexes (one L = R) have been synthesized.[4-8] However, despite the large number of alkyl complexes, only one stable cobaloxime hydride **3.4d** has been reported in the literature.[9] Compound **3.4d** was originally reported to have a hydride ^{1}H NMR resonance of +6 ppm and a Co–H stretch at 2240 cm^{-1}. However, this was found to be incorrect by Artero and coworkers after remaking this molecule.[10] They found no observable Co–H stretch and a ^{1}H NMR signal at –6.40 ppm, and suggested that the originally isolated material may not have been the hydride.

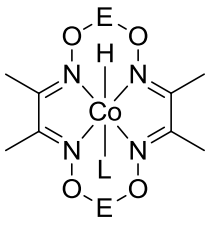

3.3 (E = BF_2)
3.4 (E = H)
a (L = CH_3CN)
b (L = THF)
c (L = H_2O)
d (L = PBu_3)

The stability of the Co–H bond seems to be affected by the identity of the other axial ligand. For example, substituting PBu_3 in **3.4d** with pyridine creates a hydride that decomposes slowly in solution.[9]

Despite their instability other cobaloxime hydrides have been proposed in a variety of catalytic reactions, for example, during electrocatalytic hydrogen evolution. Many groups have used these cobaloximes as a way to produce hydrogen gas from electrons and protons at low overpotential.[10-30] Espenson and Chao initially studied the reaction of compound **3.4d** with acid and showed that it lost hydrogen gas by two different mechanisms.[11] The first (eq 3.1) was a second order reaction of Co–H with H^+. The second was a bimolecular loss of hydrogen with no pH dependence (eq 3.2).

$$\text{Co-H} + H_3O^+ \longrightarrow {}^+\text{Co}-OH_2 + H_2 \quad (3.1)$$

$$2\ \text{Co-H} \longrightarrow 2\ \text{Co} + H_2 \quad (3.2)$$

Artero and Fontecave[18] and Peters[24] simultaneously popularized **3.1a** and **3.2a** as electrocatalysts for H_2 evolution from acidic solutions. They preferred **3.1a** due to its greater stability in acid. Three pathways were proposed, all involving the protonation of Co(I) anion **3.5** to form hydride **3.3** (Scheme 3.1).

Scheme 3.1. Possible Mechanisms of Hydrogen Evolution from Cobaloximes

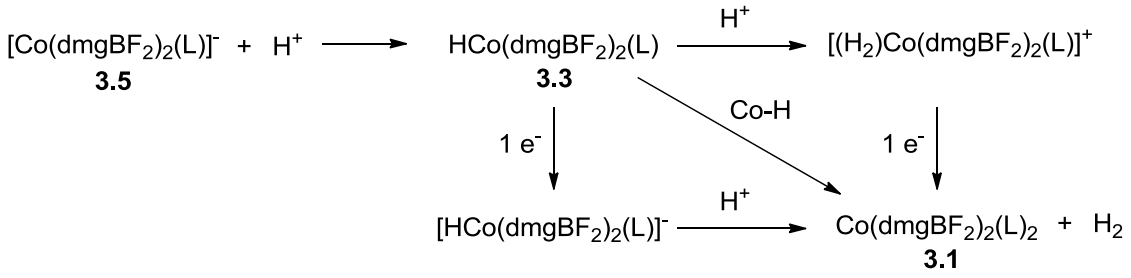

The first was the bimolecular loss of hydrogen proposed above (eq 3.2). The second was the reaction of **3.3** directly with acid to give a $[Co(H_2)]^+$ which would be reduced to **3.1**.[17] In 2010, Gray and coworkers used a photoacid to trigger rapid protonation of **3.5a** and monitored the subsequent reactions using time–resolved spectroscopy. This experiment led them to propose a third mechanism involving reduction of **3.3** to give the very hydridic cobalt hydride radical anion, that would react quickly with a proton to give **3.1** and hydrogen.[27] They also found that tethering two cobaloximes together had no effect on the rate, disproving the bimolecular mechanism.[29] The fact that the potential of the Co–H/$[Co–H]^{\bullet-}$ redox couple has been estimated to be less than that of **3.1**/**3.5** makes the mechanism in Scheme 3.2 likely under highly reducing conditions.[31] However, all three pathways can occur under certain conditions.

Scheme 3.2. Electrocatalytic production of H_2 with **3.1**

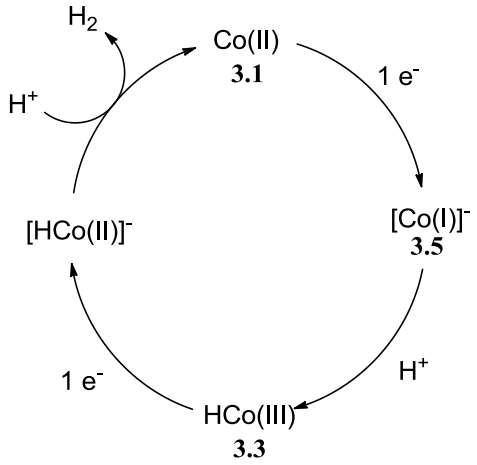

There is also disagreement in the literature on the spectroscopic features of the cobalt hydride **3.3**. Gray and coworkers expected **3.3a** to have a UV–Vis spectrum similar to that of $MeCo(dmgBF_2)_2CH_3CN$ (λ_{max} = 360 nm).[27] Indeed upon protonation of **3.5a** they observed a rapid increase in the absorbance at 405 nm and a rapid decrease of the absorbance at 610 nm (but

not its total disappearance). A similar UV–Vis spectrum having a peak at ~350 nm was calculated by Muckerman.[31]

The UV–Vis spectrum of $HCo(dmgH)_2(P^nBu_3)$ (**3.4d**) has a strong peak at approx. 325 nm similar to those in the previous paragraph.[9-10] However, it also has another peak that shifts from 506 nm in acetonitrile to 567 nm in cyclohexane. (When Artero calculated the UV–Vis spectrum of **3.4d** he found that the result is strongly dependent on the basis set used in the calculation.[10]) The more electron donating nature of the $[dmgH]^-$ and P^nBu_3 ligands on **3.4d** could change the spectrum significantly from **3.3a**. Bakac showed that when cobalt anion **3.5c** (λ_{max} = 610 nm) is acidified in a rapid mixing system, an intermediate with a similar but weaker absorbance (λ_{max} = 611 nm) is formed. They proposed that this was the hydride **3.3c**, conflicting with the observation by Gray and coworkers above.

When combined with a photosensitizer system, acid, and a sacrificial reductant these molecules produce hydrogen gas photocatalytically.[19-22] Sometimes the photosensitizer is attached to the Co via binding of an axial ligand, usually a pyridine moiety.[32] This makes knowing the coordination chemistry of **3.3** very important, since the dissociation of the photosensitizer from the cobalt would attenuate the activity.

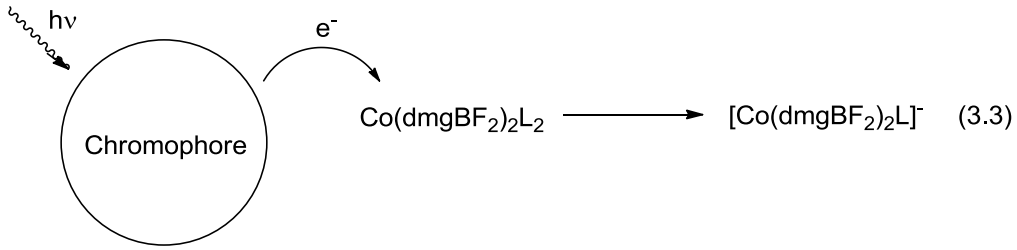

(3.3)

3.1.3 Hydrogen Activation by Cobaloximes

The Co(II) cobaloximes are known to react with hydrogen gas and have been used as hydrogenation catalysts.[33-38] In 1980, Simándi and co–workers showed that the rate law of hydrogen uptake by these complexes is overall third order, first order in [H_2] and second order in [Co] (eq 3.4).[38] This leads to the same picture for hydrogen activation seen in section 1.4.4. They also measured the rate in the presence of different amounts of various axial ligands; the initial rate varied with the identity of the ligand. The presumed hydrides all decomposed by ligand hydrogenation.

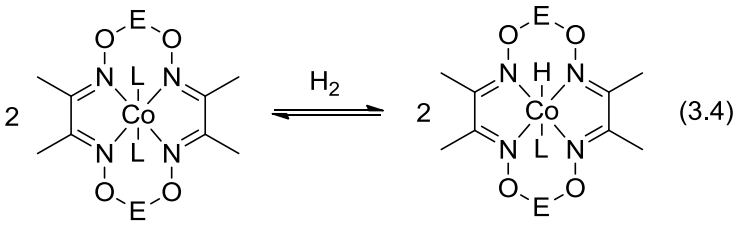

3.1 (E = BF_2)
3.2 (E = H)
a (L = CH_3CN)
b (L = THF)
c (L = H_2O)

3.3 (E = BF_2)
3.4 (E = H)
a (L = CH_3CN)
b (L = THF)
c (L = H_2O)

Gridnev and Ittel used these complexes under hydrogen gas to catalyze chain transfer during radical polymerizations and showed that they have very high chain transfer constants (C_s).[39-43] Compound **3.3** was thought to transfer H• rapidly. This suggests that despite having an unstable hydride, the MOHAT reaction can proceed rapidly with only a small equilibrium concentration of **3.3** under hydrogen gas. However, we do not know where this equilibrium lies.

Gang Li in the Norton group has recently shown that **3.1** and **3.2** can catalyze the transfer of H• to stable radicals such as TEMPO and trityl radicals (Scheme 3.3) by H_2[44] and generate radicals by H• transfer to activated alkenes[44] and alkynes[45]. The cobaloxime **3.1** can thus

generate radicals from α-substituted acrylate esters, and catalyze radical cyclohydrogenation reactions as discussed in chapter 1.[44] The rate law for the reaction in Scheme 3.3 is independent of [TEMPO], first order in [H_2], and second order in [**3.1**], suggesting that the rate-determining step — the forward reaction of an unfavorable equilibrium — involves the formation of **3.3** from H_2 and two equiv of **3.1** (eq 3.3).[44] We have gained some mechanistic insights by examining the structures of **3.1a-c**.

Scheme 3.3. Hydrogen atom transfer (HAT) from H_2 to stable free radicals (X = •CAr_3 or TEMPO) catalyzed by **3.1**

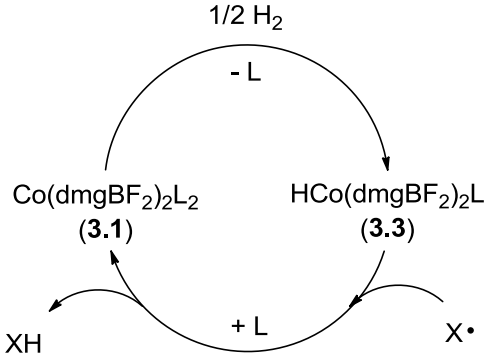

Since **3.3** is in an unfavorable equilibrium with H_2, it will not be stable at ambient conditions. I have attempted to spectroscopically observe **3.3** under large hydrogen pressures and to characterize its thermodynamic properties (i.e. its pK_a, its BDFE, etc).

3.2 Results

3.2.1 Structural effects on the mechanism of Cobaloxime H_2 Activation

When L is a neutral ligand, complex **3.1** is low spin d^7, S = ½. Coordinating two axial L ligands gives cobalt a total of 19 e^-. High field EPR studies have shown that the spin density mostly resides in Co's d_{z^2} orbital with little delocalization onto the ligand.[32] I was able to grow crystals of X–ray diffraction quality by simply dissolving diaquo complex **3.1c** in the solvent corresponding to the desired axial ligand. For example a saturated solution of **3.1c** in CH_3CN

was layered with ether, and yielded high quality crystals of **3.1a**. The molecular structure is shown in Figure 3.1. Compound **3.1b** was crystallized in a similar manner.

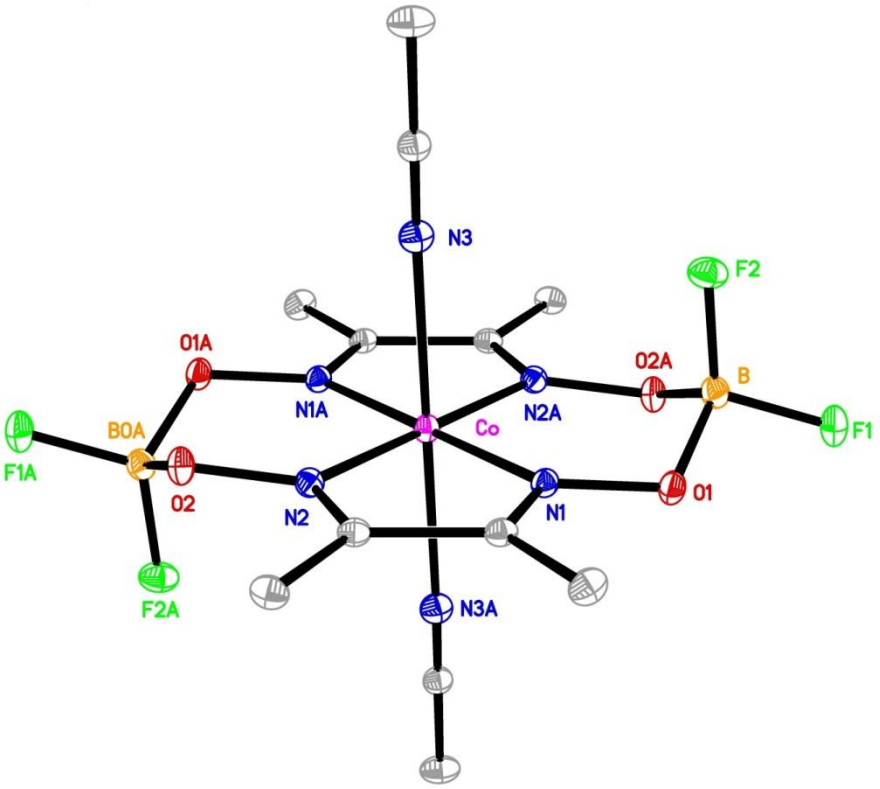

Figure 3.1. Molecular Structure of 3.1a (20% thermal ellipsoids) hydrogen atoms excluded

Gang Li has measured the rates of hydrogen uptake (k_{H2}) by various cobaloximes (eq 3.5). The results are shown in Table 3.1. The value of k_{H2} is strongly influenced by the identity of the axial ligand. For example with THF, k_{H2} is three times faster than with methanol and an order of magnitude faster than with water. This seems to be related to the Co–L bond length which is also included in Table 3.1. Complexes with longer Co–L bonds tend to react faster. Complexes with CH_3CN and PPh_3 are much slower.

$$2\ Co(dmgBF_2)_2(L)_2 + H_2 \xrightarrow{k_{H2}} 2\ HCo(dmgBF_2)_2L \quad (3.5)$$

Table 3.1. Rate constants for hydrogen activation by cobaloximes

Ligand	k_{H2} ($M^{-2}s^{-1}$)	k_7 ($M^{-2}s^{-1}$)	K_6 (M)	M–L distance (Å)
THF	$1.04(6)\times10^3$	$1.02(1)\times10^3$	1.26(6)	2.324
MeOH	343(7)	346(7)	0.128(6)	2.264[46]
H_2O	106(3)	—	—	—
PPh_3	37(5)	37(5)	—	—
CH_3CN	< 16	—	—	2.260

Gang Li also has shown that the reaction in eq 3.5 is inhibited by added ligand. When the reaction is repeated in the presence of varying concentrations of L, the rate is attenuated. So one axial ligand must dissociate (eq 3.6) before hydrogen activation can occur (eq 3.7). Values of k_7 and K_6 are included in Table 3.1 above. The nature of the ligand also has an effect on the value of k_7. The triphenylphosphine cobaloxime complex is five–coordinate, lacking an additional axial ligand.[32] Despite this, the rate constant for hydrogen activation is quite slow with PPh_3, more than 25 times slower than with THF.

Neither I nor Andrea Bakac's group have been able to crystallize the diaquocobaloxime **3.1c**.[47] Only a red powder is obtained. However, upon vapor diffusion of hexanes into a solution of **3.1c** in CH_2Cl_2, small yellow crystals suitable for X–ray diffraction were obtained. Serge Ruccolo, of the Parkin group, collected the diffraction data and solved the structure. The crystals belong to hexagonal space group P622; the details are given in Appendix II.

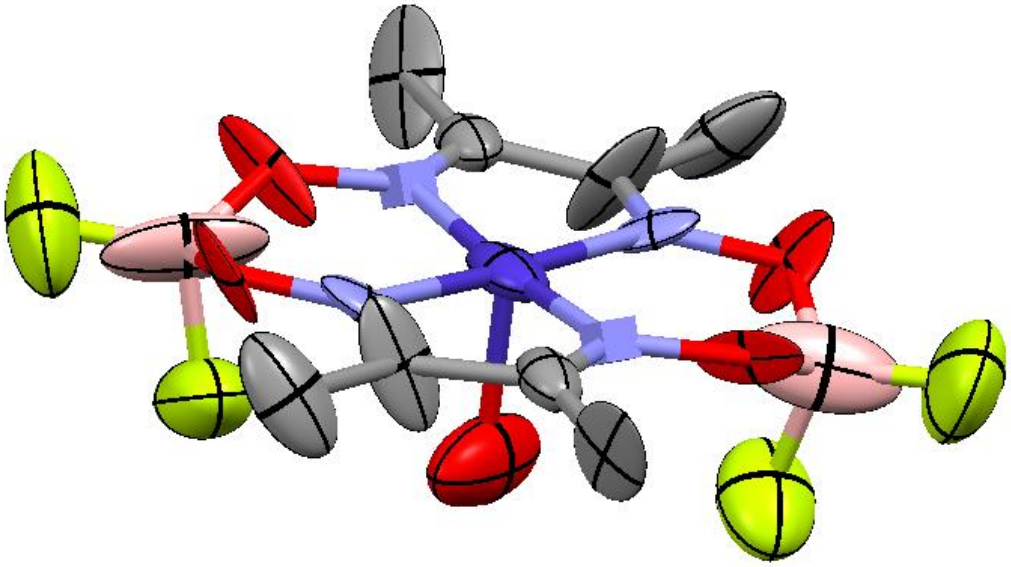

Figure 3.2. Molecular structure of $Co(dmgBF_2)_2(H_2O)$

The molecular structure of the monohydrated cobaloxime is shown in Figure 3.2. Examination of the crystal packing gives the larger secondary structure shown in Figure 3.3. The crystal has several interesting features.

1) The hexagonal structure arises from hydrogen bonding of the aquo ligands. This leads to void spaces parallel to the axis of the crystal filled with disordered solvent molecules, as seen in Figure 3.3. Indeed, these crystals collapse when exposed to vacuum. The disordered solvent cannot be modeled very effectively and leads to very strange thermal parameters for this molecule. This structure needs to be corroborated by other methods of characterization, such as solid state X-ray Absorption Spectroscopy or EPR.

2) Each five coordinate cobaloxime shares a face with another cobaloxime. Each Co atom is sunken 0.076 Å below the plane of the ligand such that the distance between the ligand planes is 2.98 Å. The ionic radius of a low spin six coordinate Co^{2+} ion is approximately 1.3 Å,[48] meaning that a Co – Co covalent bond would be around 2.6 Å. The Co—Co distance in this

structure is 3.13 Å, which suggests that this is not a metal–metal bond but a strong interaction. The electron density map also shows a small pocket of electron density half way between the Co atoms (1.56 Å away from each Co). It was suggested that this might be an atom bridging between the two Co atoms. For example if an oxygen atom was bridging the two Co atoms, this Co–O bond would be smaller than any cobalt–oxygen bond currently in the Cambridge Structural Database. Thus we think it is unlikely for an atom to reside between the Co atoms.

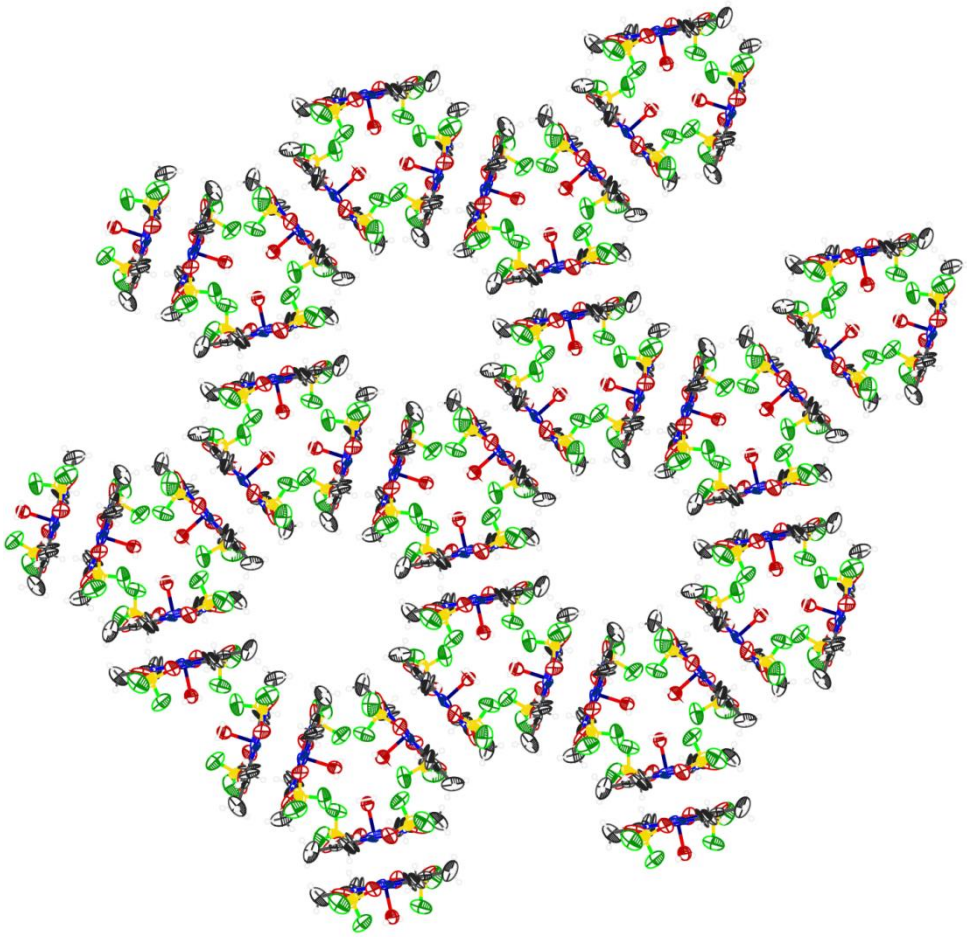

Figure 3.3. Packing structure of crystals obtained by recrystallization of 3.1c in CH_2Cl_2

The structure above is similar to known structures in the literature. Caulton and Cotton showed that the structure of $[Rh(dmgH)_2PPh_3]_2$ (shown below) was very similar to what we observe for $[Co(dmgBF_2)_2(H_2O)]_2$.[49] This cofacial rhodoxime complex has a Rh–Rh distance of

2.936 Å. Each Rh atom is sunken below the ligand plane such that the ligands are separated by a distance of 2.88 Å, much the same as what we see with Co. The ligands are twisted such that, when looking down the Rh Rh axis, the methyl groups of one dmg ligand are eclipsed with the O–H - - O group of the second ligand. This behavior is also seen for Co. However, the Rh–Rh distance that they observed is shorter than our Co–Co distance. It could be that the BF_2 group is more sterically demanding than the bridging H structure, forcing the ligands farther apart.

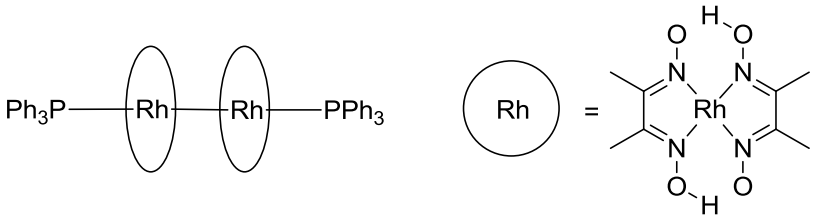

Reed and Sun saw that reduction of the proton bridged $ClCo(dmgH)_2(P\textit{n}\text{-}Bu_3)$ with BH_4^- gave a purple complex similar to $HCo(dmgH)_2(P\textit{n}\text{-}Bu_3)$.[35] It had no hydride resonance in the NMR spectrum, and the UV–Vis spectrum varied with temperature and with concentration. They proposed that this was caused by $Co(dmgH)_2(P\textit{n}\text{-}Bu_3)$ being in equilibrium with its dimer.

Similar five coordinate cofacial Co – Co complexes have been seen.[50-51] Collman and coworkers made the tethered dicobalt porphyrin complex (**3.6**). By themselves each Co center was low spin d^7 (S = ½). However, the two cobalt centers were found to undergo antiferromagnetic coupling with each other. This was reflected in the zero–field splitting observed in its EPR spectrum at low temperature. The observed zero–field splitting was 92×10^{-4} cm^{-1}, which corresponds to a metal metal separation of 6.5 Å. The fact that these Co atoms are farther apart than our system is most likely a result of the linker length.

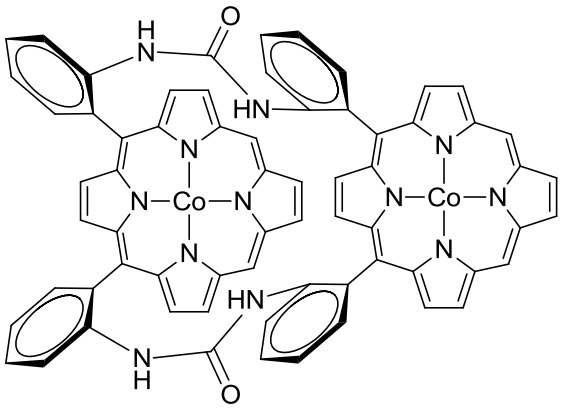

3.6

Eaton[52] and Chang[53] separately observed zero–field splittings in stacked copper porphyrin EPR spectra. These zero–field splittings gave Cu–Cu distances between 4.1 and 5.6 Å and inter–porphyrin distances of 3.9 Å, in good agreement with crystallographic data. These examples suggest that our Co–Co distance of 3.13 Å could produce a sizable antiferromagnetic coupling between the two Co centers.

The magnetic moments (Evans Method)[54] of several different cobaloxime complexes showed no conclusive evidence for interaction in solution. The results are shown in Table 3.2. The monomeric cobaloximes **3.1a – c** have magnetic moments in the expected range for monomeric S = ½ complexes. When the monoaquo crystals were dissolved in dry CD_2Cl_2, the magnetic moment was less than that of the diaquo complex. However, this neither proves nor disproves the existence of antiferromagnetic coupling since the magnetic moment of the compound is influenced by other factors besides spin, such as spin orbit coupling. A low temperature solid state magnetometry study will be conducted to characterize the magnetic behavior of these crystals.

Table 3.2. Magnetic moments of cobaloxime complexes in solution

Complex	$\mu_{eff}(\mu_B)$
$Co(dmgBF_2)_2(CH_3CN)_2$ (**3.1a**)	1.84
$Co(dmgBF_2)_2(THF)_2$ (**3.1b**)	2.06
$Co(dmgBF_2)_2(H_2O)_2$ (**3.1c**)	2.12
$Co(dmgBF_2)_2(H_2O)$ crystals in CD_2Cl_2	1.94

Antiferromagnetic coupling could be an important element in the mechanism of termolecular hydrogen activation (eq 3.5). As was discussed in section 1.4.4, one hypothesized transition state was **1.33**.

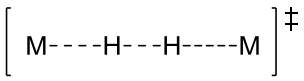

1.33

The spin state of the two metalloradicals (Figure 3.4) could have a profound effect on the reaction. If, for example, the two metal atoms have parallel spins (Labelled B in figure 3.4) then the overall spin state is S = 1. Starting from point B the reaction to produce two Co–H bonds directly is spin forbidden and would require mixing of the triplet H_2 electronic surface (state D) into the transition state — introducing a large electronic barrier.[55] Antiferromagnetic coupling of the two Co centers (state A) makes the reaction spin allowed, with the only barrier being the thermodynamic barrier to breaking H–H and making 2 Co–H (state F). Larger exchange coupling between the two Co centers increases the rate of spin reorganization before the transition state, thus avoiding the spin forbidden reaction pathway.[56] This picture of reaction 3.5 matches the observation in section 1.4.4 that these reactions have almost no enthalpic contribution to the transition state, meaning that the barrier is almost entirely entropic. The entropic component of

the barrier is due to the arrangement of the atoms to form the linear arrangement on the left side of figure 3.4.

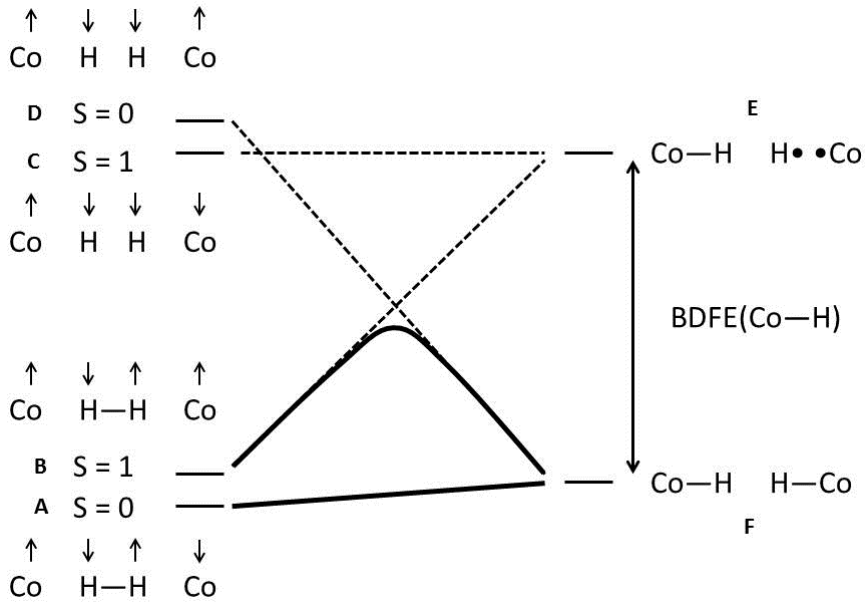

Figure 3.4. Spin state effects in the reaction of cobaloximes with H_2

3.2.2. Observation of the equilibrium of cobaloximes and hydrogen

When the diaquocobaloxime **3.1c** is dissolved in CH_3CN it gives the bisacetonitrile cobaloxime **3.1a**,[24, 57] with λ_{max} at 430 nm (3240 $M^{-1}cm^{-1}$). Under 70 atm of H_2 at room temperature, the UV-vis spectrum changes slowly (24 h) but smoothly (difference spectra shown in Figure 3.7) into one with a λ_{max} at 556 nm (7700 $M^{-1}cm^{-1}$), another at 627 nm (7460 $M^{-1}cm^{-1}$), and a small peak at 354 nm. The process is reversible; the original spectrum returns slowly (48 h) after release of the gas pressure.

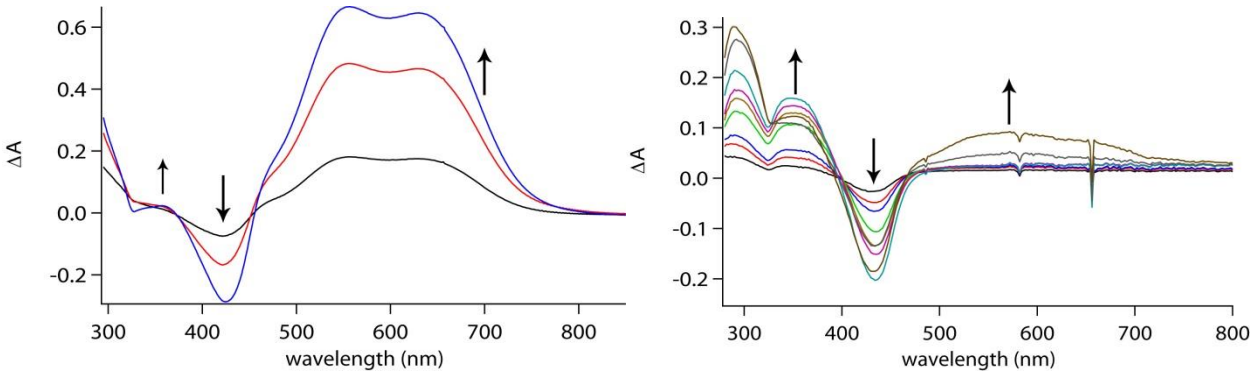

Figure 3.5. UV/vis difference spectra recorded over the course of 24 h for complex **3.1a** in CH_3CN (left) and **3.1b** in THF (right), pressurized with 70 atm of H_2 gas at room temperature.

When **3.1c** is recrystallized from THF, it forms the bis–THF complex **3.1b**,[57] with a λ_{max} at 434 nm (3200 $M^{-1}cm^{-1}$), and the behavior of **3.1b** under 70 atm of H_2 is different from that of **3.1a** (Figure 3.5). An intermediate appears (354 nm) as the 434 nm band is bleached by reaction with H_2. After 8 h, the intermediate at 354 nm begins to decrease, with a new band appearing at 580 nm.

The absorbance of the intermediate (354 nm) is similar to that observed for $Co(dmgBF_2)_2(py)Me$[58] (py = pyridine), similar to the spectrum calculated for the cobalt hydride **3.3a**,[31] and similar to the absorbance observed by Dempsey and Gray which they attributed to **3.3a**.[27] This intermediate is the hydride complex **3.3a/b** — presumably the initial product of the termolecular reaction with hydrogen.[59]

The band positions of the final spectra from the hydrogen reactions (λ_{max} = 556 and 627 nm in CH_3CN; 580 nm in THF) suggest that the products are Co(I) species. The UV–vis spectrum of $[Co(dmgBF_2)_2(CH_3CN)]^-$ (**3.5a**) has been previously reported,[27] with λ_{max} at 553 nm (4712 $M^{-1}cm^{-1}$) and 628 nm (4546 $M^{-1}cm^{-1}$); I obtain slightly higher ε values (6930 and 6780 $M^{-1}cm^{-1}$ respectively) upon spectro-electrochemical reduction of bis acetonitrile adduct **3.1a** to **3.5a** in CH_3CN (Figure 3.6). Upon spectro-electrochemical reduction of bis–THF cobaloxime **3.1b** to

the corresponding anion **3.5b**, only one new broad peak appears at 630 nm (6900 $M^{-1}cm^{-1}$). Under the conditions of the H_2 experiments, there is no base in solution with which to deprotonate the hydride **3.3a/b**, making anions **3.5a/b** unlikely products.

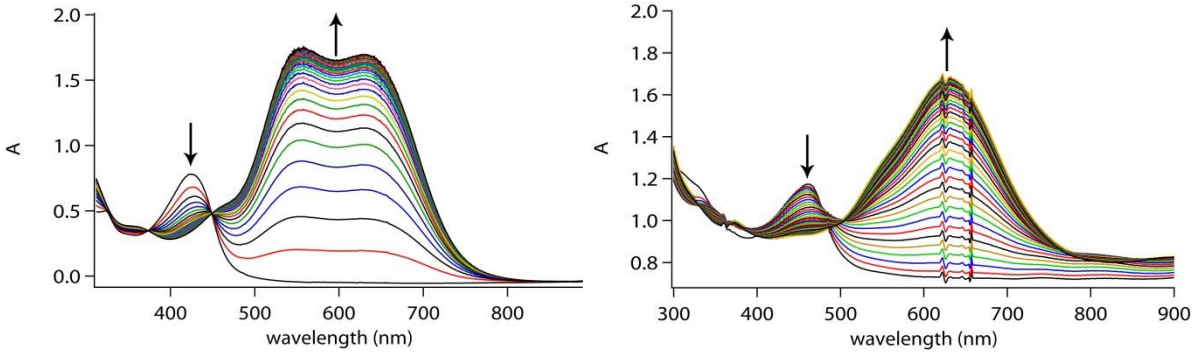

Figure 3.6. Spectro-electrochemical reduction of **3.1a** (left) and **3.1b** (right) at an applied potential of -1.0 V vs Ag wire pseudo–reference. Solutions contain 0.1 M NBu_4BF_4 as an electrolyte.

The ^{1}H NMR of **3.1a** in CD_3CN under 70 atm H_2 after 15 hours, shows sharpening of the methyl resonance (δ 2.06 ppm) and appearance of a broad peak at δ 2.5 ppm (Figure 3.7). When the pressure is released this peak disappears. In the presence of exchangeable deuterated solvents like CD_3OD this peak never appears. The peak at 2.5 ppm is probably due to the O–H in **3.**7**a**. The equivalence of the methyl resonances means that PCET from **3.7a** to **3.1a** must be fast on the NMR time scale. No evidence for a Co–H was ever seen. However, residual coupling to the ^{59}Co (I = 7/2) could render it too broad to observe. The low solubility of **3.1** may also preclude detection of low concentration species via NMR. Based on UV–Vis and NMR data, I propose that the products of the H_2 reactions (556 and 627 nm in CH_3CN; 580 nm in THF) are **3.7a/b**, tautomers of the Co–H **3.3a/b** that are formally Co(I) (eq 3.6).

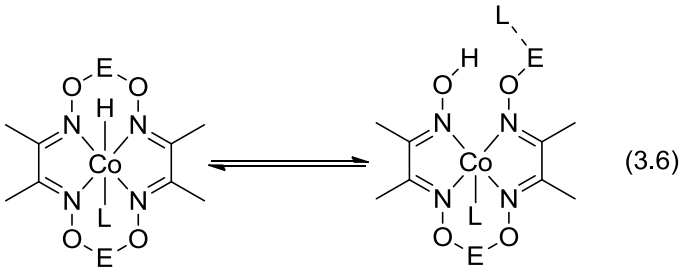

(3.6)

3.3 (E = BF_2)
3.4 (E = H)

3.7 (E = BF_2)
3.8 (E = H)

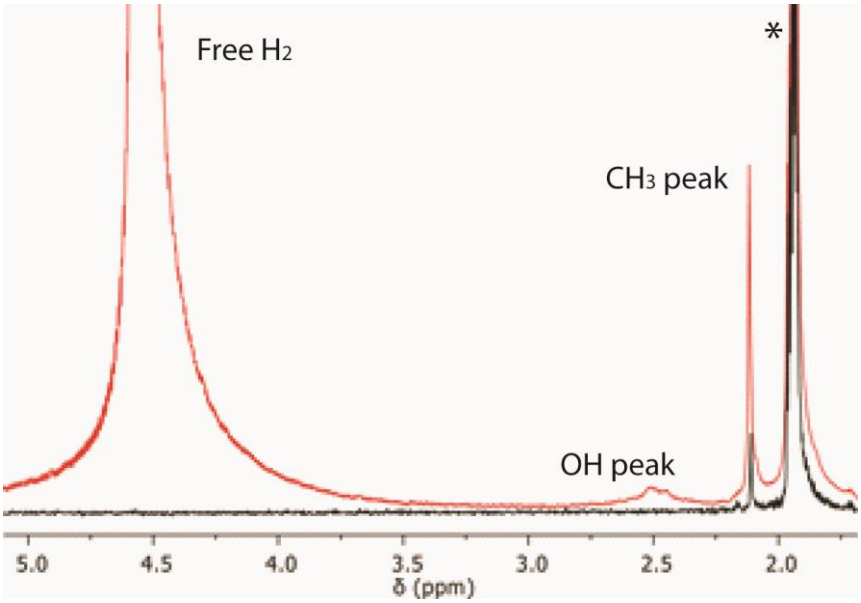

Figure 3.7. ^{1}H NMR of **3.1a** (black) at ambient conditions and (red) after 15 h under 70 atm H_2 (*CH_2DCN)

The assignment of this new species as **3.7a/b** is also supported by H_2 experiments on the proton-bridged complex **3.2a**. When **3.2a** is placed under 4 atm H_2, the solution turns red. Under 4 atm D_2, both HD and H_2 are observed (^{1}H NMR). The ^{2}H NMR of the same mixture shows D incorporation into both the bridging position and free water (eq 3.7). Artero and Fontecave observed that $HCo(dmgH)PBu_3$ does not exchange with D_2O.[10] This suggests that the Co−H bond does not exchange directly with water and that H/D exchange probably occurs through intermediate **3.8a**, although direct D_2O/Co–H exchange cannot be ruled out. A structure similar to **3.8a** has been suggested by Artero and Fontecave for the mischaracterized

"$HCo(dmgH)_2PBu_3$".[10, 44] H/D exchange also occurred with compound **3.1a**; stirring it under 50 psi of D_2 gave exchange of D into free water.

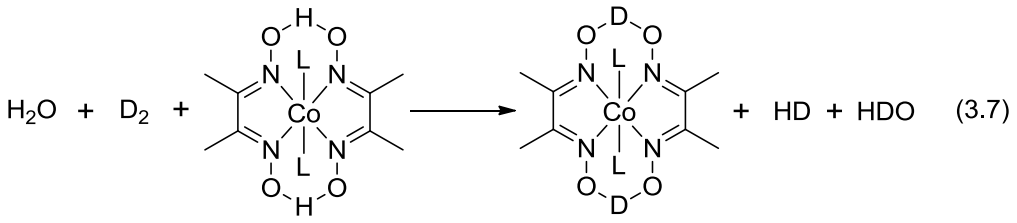

I modelled the equilibrium of **3.1a** with H_2 (eq 3.8) using the Benesi–Hildebrand method modified for a ternary equilibrium (See Appendix II for derivation).[60] By fitting the absorbance at various P_{H2} to eq 3.10 (Figure 3.8), I obtain an equilibrium constant (K_{eq})[61] of 0.014 atm^{-1}.

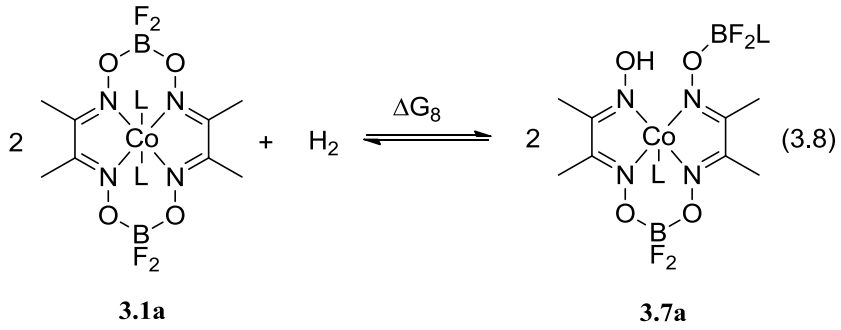

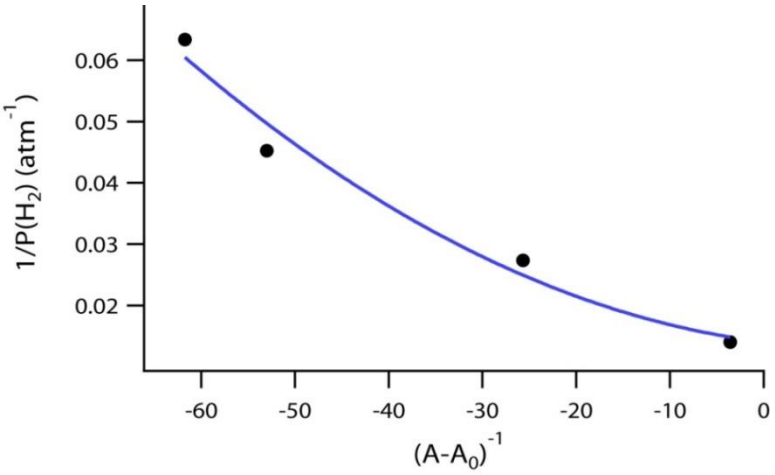

Figure 3.8. Plot of P_{H2}^{-1} vs the inverse of the change in absorbance of **3.1a** at 430 nm $(A\text{-}A_0)^{-1}$, measured in CH_3CN under different H_2 pressures. The blue curve is a fit of the data to eq 3.10.

$$K_{eq}(atm^{-1}) = \frac{[3.7a]^2}{[3.1a]^2 P_{H_2}} \qquad (3.9)$$

$$\frac{1}{P_{H_2}} = K_{eq}\left([3.1a]_0^2\Delta\varepsilon^2\left(\frac{1}{A - A_0}\right)^2 - 2[3.1a]_0^2\Delta\varepsilon^2\left(\frac{1}{A - A_0}\right) + 1\right) \quad (3.10)$$

This K_{eq} gives a ΔG_8 = 2.5 kcal/mol. Use of the bond dissociation free energy (BDFE) of H_2 (103.6 kcal/mol)[62] with eq 3.12 gives the free energy change of reaction 3.11, ΔG_{11} = 50 kcal/mol. Assuming that changes to other bonds roughly cancel, ΔG_{11} is equal to the BDFE of the O–H bond in **3.7a** (BDFE = 50 kcal/mol, BDE = 55 kcal/mol).[62] The BDE of the Co–H bond in **3.3a** is probably close to that of the O–H bond in **3.**7**a**.

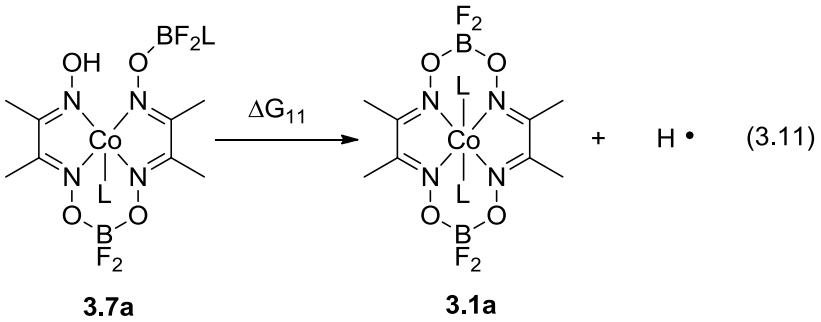

$$\Delta G_8 = \Delta G(H - H) - 2\Delta G_{11} \qquad (3.12)$$

$$BDFE = 1.37pK_a + 23.06E^0_{ox} + 53.6\frac{kcal}{mol} \qquad (3.13)$$

The thermodynamic cycle in eq 3.13[62] estimates the pK_a of ligand protonated complex **3.**7**a** as 13.4 in CH_3CN using the O–H BDFE and the potential of the $Co(I)^-$/Co(II) couple (−0.93 V vs Fc/Fc^+).[17] Artero and Fontecave's reported pK_a of 13.3 for this compound is in good agreement with our estimate.[17] This pK_a is consistent with the fact that (a) proton transfer from $HNEt_3^+$ (pK_a = 18.8 in CH_3CN)[63] to **3.5b** is slow and unfavorable (still incomplete after 8 s, see stopped-flow data in Appendix II), and (b) catalysis of hydrogen evolution by **3.1a** does not occur with acids weaker than $HNEt_3^+$.

Some observations in the literature attributed to cobalt hydride **3.3** are better explained by the ligand protonated complex **3.7**. In the reaction of **3.1a** with 1 atm hydrogen gas in the presence of excess $CF_3CO_2^-$ (eq 3.13), Peters and coworkers observed the formation of a Co(I) species by UV–Vis, that they believed to be cobalt anion **3.5a** (presumably made when $CF_3CO_2^-$ (CF_3CO_2H pK_a = 12.7 in CH_3CN)[64] deprotonates **3.3a**.[24]) However, when I repeated this experiment, the ^{19}F NMR of reaction 3.13 (Figure 3.8) showed different ^{1}H, ^{19}F, and ^{11}B NMR spectra than those of **3.5a** (see Appendix II). The new species had a CF_3 group (δ −76.56, 3F) and two BF_2 peaks (δ −149.07 2F, −149.10 2F) in a ratio of 3:2:2. This spectrum can be attributed to compound **3.9**.

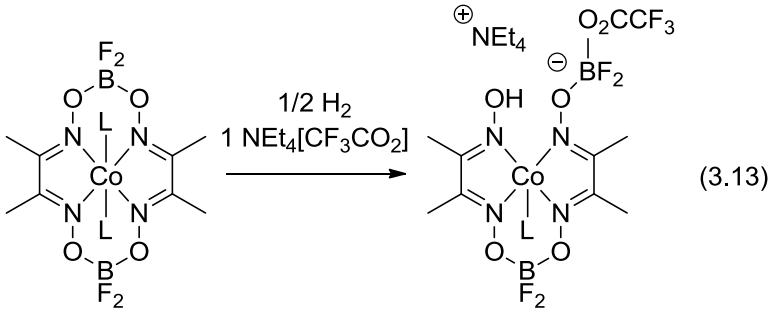

3.1a **3.9** (3.13)

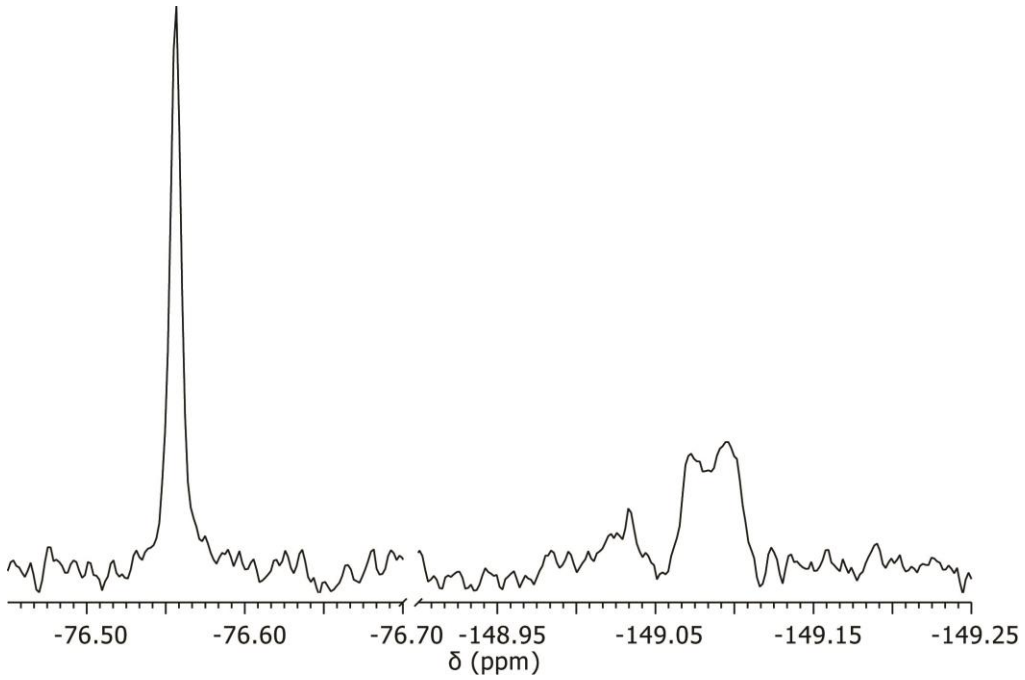

Figure 3.9. ^{19}F NMR of **3.1a** in CD_3CN with 1 atm H_2 in the presence of excess $NEt_4[CF_3CO_2]$ (relevant portions shown, full spectrum in Appendix II).

Compound **3.7** may also be the kinetic product of the protonation of **3.5**. Upon rapid mixing of **3.5** with acid, Bakac and coworkers observed an intermediate with λ_{max} of 610 nm, similar to **3.5** but less intense (10^4 $M^{-1}cm^{-1}$).[30] They attributed this feature to **3.3**. This assignment is doubtful based on our findings here;[27] the Norton group has shown that metal protonation is usually slow.[65] I propose that the Bakac spectrum is due to the ligand-protonated complex **3.6**, based on its similarities to our spectra.

3.3 Experimental Details

Use caution when performing reactions under pressure! All manipulations were performed under an argon atmosphere using standard schlenk or inert atmosphere box techniques. High pressure NMR spectra were taken using a sapphire NMR tube similar to the design of Owen and Bercaw,[66] outfitted with 1/16" o.d. PEEK tubing leading to a pressure gauge

and a valve connected to a high pressure manifold, a hydrogen tank connected to a pressure gauge, a rotary vacuum pump, and the sample tube. After evacuation of the manifold and sample tube, the sample was pressurized with the desired amount of gas and a vortex mixer was used to saturate the solution. This sample tube was then lowered manually into a 300 MHz NMR spectrometer using a custom–made shield designed to minimize exposure to the pressurized tube. ***Caution: Working with high gas pressures in sapphire tubes is very dangerous. Steps should be taken to minimize exposure to the tube and the manifold. For your safety, the equipment should be regularly tested well above operating pressures.*** Other NMR spectra were recorded on either a Bruker 300 or 400 MHz instrument.

High Pressure UV-Visible spectra were recorded with a custom-made stainless steel cell equipped with one 2 mm thick sapphire window and one 10 mm thick CaF_2 window (resulting optical path length = 1 cm). This cell was manufactured in the University of Nottingham, Nottingham, UK and was donated to the BNL group by Prof. Michael W. George. It has been described previously (see Fig. 3 in Poliakoff, M. *et al.*, *Angew. Chem. Int. Ed.* **1995**, *34*, 1275-1295). The cell was equipped with a magnetic stir bar and a thermocouple was inserted into one of the ports to allow measurement of the internal cell temperature. A CH_3CN or THF solution was loaded into the cell via a syringe inside an argon glovebox and the cell was sealed. It was then transferred to a high-pressure filling station consisting of a network of 1/16" o.d. stainless steel tubing, high-pressure valves and fittings (Scientific Systems, Inc.), pressure transducers (Omega Engineering, Inc., PX61V1-5KGV), a rotary vacuum pump, and a hydrogen cylinder equipped with a high-pressure regulator. After evacuating all of the tubing and refilling with H_2 several times, the tubing was then filled with H_2 to the desired pressure. The top valve of the high-pressure cell was then opened to saturate the solution with H_2 to the desired pressure. After

stirring the solution for several minutes and allowing the pressure to stabilize, the cell was sealed again and taken to an Agilent 8453 diode-array spectrophotometer for acquisition of UV/visible spectra.

X-ray diffraction data were obtained using a X-ray diffraction data were collected on a Bruker Apex II diffractometer. Crystal data, data collection and refinement parameters are summarized in the SI (Table S1). The structures were solved using direct methods and standard difference map techniques, and were refined by full matrix least squares procedures on F^2 with SHELXTL (Version 6.1).[67-68]

Rapid mixing experiments were performed using a HiTech anaerobic stopped flow spectrometer fitted with an Olis rapid scanning monochromator with a 1 cm path length, wavelength range of 300 – 700 nm, a mixing time of less than 3 ms, and 1 ms time resolution. Kinetic data were fitted using global analysis.

Spectro–electrochemical reductions were performed using a Pt honeycomb electrode from Pine Instrument Company in a quartz cell with 1.7 mm path length containing either 0.1 M solutions of NBu_4PF_6 in CH_3CN or 0.1 M $NBu_4[B(C_6F_5)_4]$ in THF referenced to a Ag wire pseudo-reference electrode. The correct potential for reduction was found in a preliminary experiment in which the potential was gradually lowered (100 mV increments) until the desired reduction went to completion.

Solution magnetic moments were measured using Evan's Method. Unless otherwise specified they were performed using a saturated solution of the analyte in 5% toluene in $CDCl_3$, this solution was placed in a coaxial insert and submerged in an NMR tube containing 5% toluene in $CDCl_3$. The difference in the toluene Me peak positions was measured on a 500 MHz

NMR spectrometer and this peak separation used to calculated the solution magnetic moment. The measured magnetic moments were corrected for the diamagnetic susceptibility of the solvent.[69]

Benzene and THF were distilled from Na/benzophenone ketyl and stored over 3 Å molecular sieves. Acetonitrile was purified by a previously published procedure.[70] Deuterated solvents were purified analogously to their proteo counterparts. Complexes **1c**, **2c,** and **5a** were made by known procedures.[24, 46] The hydrogen and deuterium gas were purchased as ultra-high purity grade (99.999% pure).

3.4 References

1. Schrauzer, G. N.; Windgassen, R. J., Über Cobaloxime(II) und deren Beziehung zum Vitamin B12r. *Chem. Ber.* **1966,** *99,* 602-610.

2. Schrauzer, G. N.; Windgassen, R. J., Alkylcobaloximes and Their Relation to Alkylcobalamins. *J. Am. Chem. Soc.* **1966,** *88,* 3738-3743.

3. Schrauzer, G. N.; Kohnle, J., Coenzym B12-Modelle. *Chem. Ber.* **1964,** *97,* 3056-3064.

4. Schrauzer, G. N.; Sibert, J. W., Coenzyme B_{12} and coenzyme B_{12} model compounds in the catalysis of the dehydration of glycols. *J. Am. Chem. Soc.* **1970,** *92,* 1022-1030.

5. Schrauzer, G. N.; Weber, J. H.; Beckham, T. M., Cobalt-carbon bond cleavage in substituted alkylcobalamins and alkylcobaloximes. Evidence for d-orbital participation and olefin pi complexes of cobalt(I) nucleophiles. *J. Am. Chem. Soc.* **1970,** *92,* 7078-7086.

6. Schrauzer, G. N., The Chemistry of Co(I) Derivatives of Vitamin B_{12} and of Related Chelates. *Ann. N. Y. Acad. Sci.* **1969,** *158,* 526-539.

7. Schrauzer, G. N.; Sibert, J. W.; Windgassen, R. J., Photochemical and thermal cobalt-carbon bond cleavage in alkylcobalamins and related organometallic compounds. Comparative study. *J. Am. Chem. Soc.* **1968,** *90,* 6681-6688.

8. Schrauzer, G. N., *Inorg. Synth.* **1968,** *11,* 61-70.

9. Schrauzer, G. N.; Holland, R. J., Hydridocobaloximes. *J. Am. Chem. Soc.* **1971,** *93*, 1505-1506.

10. Bhattacharjee, A.; Chavarot-Kerlidou, M.; Andreiadis, E. S.; Fontecave, M.; Field, M. J.; Artero, V., Combined Experimental–Theoretical Characterization of the Hydrido-Cobaloxime [$HCo(dmgH)_2(PnBu_3)$]. *Inorg. Chem.* **2012,** *51*, 7087-7093.

11. Chao, T.-H.; Espenson, J. H., Mechanism of hydrogen evolution from hydridocobaloxime. *J. Am. Chem. Soc.* **1978,** *100*, 129-33.

12. Zhang, P.; Jacques, P.-A.; Chavarot-Kerlidou, M.; Wang, M.; Sun, L.; Fontecave, M.; Artero, V., Phosphine Coordination to a Cobalt Diimine-Dioxime Catalyst Increases Stability during Light-Driven H_2 Production. *Inorg. Chem.* **2012,** *51*, 2115-2120.

13. Artero, V.; Chavarot-Kerlidou, M.; Fontecave, M., Splitting Water with Cobalt. *Angew. Chem., Int. Ed.* **2011,** *50*, 7238-7266.

14. Jacques, P.-A.; Artero, V.; Pecaut, J.; Fontecave, M., Cobalt and nickel diimine-dioxime complexes as molecular electrocatalysts for hydrogen evolution with low overvoltages. *Proc. Natl. Acad. Sci. U. S. A., Early Ed.* **2009**, 1-6.

15. Fihri, A.; Artero, V.; Pereira, A.; Fontecave, M., Efficient H_2-Producing Photocatalytic Systems Based on Cyclometalated Iridium- and Tricarbonylrhenium-Diimine Photosensitizers and Cobaloxime Catalysts. *Dalton Trans.* **2008**, 5567-5569.

16. Fihri, A.; Artero, V.; Razavet, M.; Baffert, C.; Leibl, W.; Fontecave, M., Cobaloxime-Based Photocatalytic Devices for Hydrogen Production. *Angew. Chem., Int. Ed.* **2008,** *47*, 564-567.

17. Baffert, C.; Artero, V.; Fontecave, M., Cobaloximes as Functional Models for Hydrogenases. 2. Proton Electroreduction Catalyzed by Difluoroborylbis(dimethylglyoximato)cobalt(II) Complexes in Organic Media. *Inorg. Chem.* **2007,** *46*, 1817-1824.

18. Razavet, M.; Artero, V.; Fontecave, M., Proton Electroreduction Catalyzed by Cobaloximes: Functional Models for Hydrogenases. *Inorg. Chem.* **2005,** *44*, 4786-4795.

19. Du, P.; Schneider, J.; Luo, G.; Brennessel, W. W.; Eisenberg, R., Visible Light-Driven Hydrogen Production from Aqueous Protons Catalyzed by Molecular Cobaloxime Catalysts. *Inorg. Chem.* **2009,** *48*, 4952-4962.

20. Lazarides, T.; McCormick, T.; Du, P.; Luo, G.; Lindley, B.; Eisenberg, R., Making Hydrogen from Water Using a Homogeneous System Without Noble Metals. *J. Am. Chem. Soc.* **2009,** *131*, 9192-9194.

21. Du, P.; Schneider, J.; Luo, G.; Brennessel, W. W.; Eisenberg, R., Visible Light-Driven Hydrogen Production from Aqueous Protons Catalyzed by Molecular Cobaloxime Catalysts. *Inorg. Chem.* **2009,** *48*, 4952-4962.

22. Du, P.; Knowles, K.; Eisenberg, R., A Homogeneous System for the Photogeneration of Hydrogen from Water Based on a Platinum(II) Terpyridyl Acetylide Chromophore and a Molecular Cobalt Catalyst. *J. Am. Chem. Soc.* **2008,** *130*, 12576-12577.

23. McCormick, T. M.; Han, Z.; Weinberg, D. J.; Brennessel, W. W.; Holland, P. L.; Eisenberg, R., Impact of Ligand Exchange in Hydrogen Production from Cobaloxime-Containing Photocatalytic Systems. *Inorg. Chem.* **2011,** *50*, 10660-10666.

24. Hu, X. L.; Brunschwig, B. S.; Peters, J. C., Electrocatalytic Hydrogen Evolution at Low Overpotentials by Cobalt Macrocyclic Glyoxime and Tetraimine Complexes. *J. Am. Chem. Soc.* **2007,** *129*, 8988-8998.

25. Hu, X.; Cossairt, B. M.; Brunschwig, B. S.; Lewis, N. S.; Peters, J. C., Electrocatalytic Hydrogen Evolution by Cobalt Difluoroboryl-diglyoximate Complexes. *Chem. Commun.* **2005**, 4723-4725.

26. Dempsey, J. L.; Winkler, J. R.; Gray, H. B., Kinetics of Electron Transfer Reactions of H_2-Evolving Cobalt Diglyoxime Catalysts. *J. Am. Chem. Soc.* **2010,** *132*, 1060-1065.

27. Dempsey, J. L.; Winkler, J. R.; Gray, H. B., Mechanism of H_2 Evolution from a Photogenerated Hydridocobaloxime. *J. Am. Chem. Soc.* **2010,** *132*, 16774-16776.

28. Dempsey, J. L.; Brunschwig, B. S.; Winkler, J. R.; Gray, H. B., Hydrogen Evolution Catalyzed by Cobaloximes. *Acc. Chem. Res.* **2009,** *42*, 1995-2004.

29. Valdez, C. N.; Dempsey, J. L.; Brunschwig, B. S.; Winkler, J. R.; Gray, H. B., Catalytic Hydrogen Evolution from a Covalently Linked Dicobaloxime. *Proc. Natl. Acad. Sci.* **2012,** *109*, 15589-15593.

30. Szajna-Fuller, E.; Bakac, A., Catalytic Generation of Hydrogen with Titanium Citrate and a Macrocyclic Cobalt Complex. *Eur. J. Inorg. Chem.* **2010**, 2488-2494.

31. Muckerman, J. T.; Fujita, E., Theoretical Studies of the Mechanism of Catalytic Hydrogen Production by a Cobaloxime. *Chem. Commun.* **2011,** *47*, 12456-12458.

32. Niklas, J.; Mardis, K. L.; Rakhimov, R. R.; Mulfort, K. L.; Tiede, D. M.; Poluektov, O. G., The Hydrogen Catalyst Cobaloxime: A Multifrequency EPR and DFT Study of Cobaloxime's Electronic Structure. *J. Phys. Chem. B* **2012,** *116*, 2943-2957.

33. Simándi, L. I.; Budó-Záhonyi, É.; Szeverényi, Z., Effect of Strong Base on the Activation of Molecular Hydrogen by Pyridinebis(dimethylglyoximato)cobalt(II). *Inorg. Nucl. Chem. Lett.* **1976,** *12*, 237-41.

34. Simándi, L. I.; Szeverényi, Z.; Budó-Záhonyi, É., Activation of molecular hydrogen by cobaloxime(II) derivatives. *Inorg. Nucl. Chem. Letters* **1975,** *11*, 773-777.

35. Sun, Y. A. The Anions of C_{60} and Its Pyrrolidine Derivatives. B. The Search for Hydridocobaloximes. Ph.D. Thesis, University of Southern California, Los Angeles, CA, 1997.

36. Burczyk, A. F.; O'Driscoll, K. F.; Rempel, G. L., Cobaloxime as a Catalytic Chain Transfer Agent. *J. Polym. Sci., Polym. Chem. Ed.* **1984,** *22*, 3255–3262.

37. Szeverényi, Z.; Budó-Záhonyi, É.; Simándi, L. I., Autocatalytic reduction of pyridinecobaloxime(III) by molecular hydrogen. *J. Coord. Chem.* **1980,** *10*, 41-5.

38. Simándi, L. I.; Budó-Záhonyi, É.; Szeverényi, Z.; Németh, S., Kinetics and mechanism of the activation of molecular hydrogen by bis(dimethylglyoximato)cobalt(II) derivatives. *J. Chem. Soc., Dalton Trans.* **1980**, 276-83.

39. Ittel, S. D.; Gridnev, A. A. Initiation of Polymerization by Hydrogen Atom Donation. U.S. Patent 7022792, April 4, 2006.

40. Gridnev, A. A.; Ittel, S. D., Catalytic Chain Transfer in Free-Radical Polymerizations. *Chem. Rev.* **2001,** *101*, 3611–3659.

41. Gridnev, A., The 25th Anniversary of Catalytic Chain Transfer. *J. Polym. Sci., Part A: Polym. Chem.* **2000,** *38*, 1753–1766.

42. Gridnev, A. A.; Ittel, S. D.; Wayland, B. B.; Fryd, M., Isotopic Investigation of Hydrogen Transfer Related to Cobalt-Catalyzed Free-Radical Chain Transfer. *Organometallics* **1996,** *15*, 5116-5126.

43. Gridnev, A. A., Features of the Radical Polymerization of Styrene and Methyacrylates in the Presence of Cobalt-oximes. *Polym. Sci. U.S.S.R.* **1989,** *31*, 2369–2376.

44. Li, G.; Han, A.; Pulling, M. E.; Estes, D. P.; Norton, J. R., Evidence for Formation of a Co-H Bond from $(H_2O)_2Co(dmgBF_2)_2$ under H_2. Application to Radical Cyclizations. *J. Am. Chem. Soc.* **2012,** *134*, 14662-14665.

45. Estes, D. P.; Norton, J. R.; Jockusch, S.; Sattler, W., Mechanisms by which Alkynes React with $CpCr(CO)_3H$. Application to Radical Cyclization. *J. Am. Chem. Soc.* **2012,** *134*, 15512-15518.

46. Bakac, A.; Brynildson, M. E.; Espenson, J. H., Characterization of the structure, properties, and reactivity of a cobalt(II) macrocyclic complex. *Inorg. Chem.* **1986,** *25*, 4108-4114.

47. Bakac, A.; Iowa State University, Ames, IA; *Personal Communication;* January 19, 2014.

48. Lide, D. R., *CRC Handbook of Chemistry and Physics*. 87th Edition ed.; CRC Taylor and Francis: Boca Raton, FL, 2006.

49. Cotton, F. A.; Caulton, K. G., Crystal and molecular structure of bis(triphenyylphosphine)tetrakis(dimethylglyoximato)dirhodium. Length of a rhodium(II)-to-rhodium(II) single bond. *J. Am. Chem. Soc.* **1971,** *93*, 1914-1918.

50. Collman, J. P.; Elliott, C. M.; Halbert, T. R.; Tovrog, B. S., Synthesis and characterization of "face-to-face" porphyrins. *Proc. Natl. Acad. Sci.* **1977,** *74*, 18-22.

51. Collman, J. P.; Wagenknecht, P. S.; Hutchison, J. E., Molecular Catalysts for Multielectron Redox Reactions of Small Molecules: The “Cofacial Metallodiporphyrin” Approach. *Angew. Chem. Int. Ed. Engl.* **1994,** *33*, 1537-1554.

52. Eaton, S. S.; Eaton, G. R.; Chang, C. K., Synthesis and geometry determination of cofacial diporphyrins. EPR spectroscopy of dicopper diporphyrins in frozen solution. *J. Am. Chem. Soc.* **1985,** *107*, 3177-3184.

53. Chang, C. K., Stacked double-macrocyclic ligands III. Spectral properties of cofacial diporphyrins as a function of the inter-chromophore separation. *J. Heter. Chem.* **1977,** *14*, 1285-1288.

54. Live, D. H.; Chan, S. I., Bulk susceptibility corrections in nuclear magnetic resonance experiments using superconducting solenoids. *Anal. Chem.* **1970,** *42*, 791-792.

55. Harvey, J. N., Understanding the kinetics of spin-forbidden chemical reactions. *Phys. Chem. Chem. Phys.* **2007,** *9*, 331-343.

56. Schweiger, A.; Jeschke, G., *Principles of Pulse Electron Paramagnetic Resonance*. Oxford University Press: Oxford, UK, 2001.

57. Li, G.; Estes, D. P.; Norton, J. R.; Sattler, A.; Ruccolo, S., Dihydrogen Activation and Hydrogen Atom Transfer by Cobaloxime: A Kinetic Study. *J. Am. Chem. Soc.* **2014,** *in preparation*.

58. Ram, M. S.; Riordan, C. G.; Yap, G. P. A.; LiableSands, L.; Rheingold, A. L.; Marchaj, A.; Norton, J. R., Kinetics and mechanism of alkyl transfer from organocobalt(III) to nickel(I): Implications for the synthesis of acetyl coenzyme A by CO dehydrogenase. *J. Am. Chem. Soc.* **1997,** *119*, 1648-1655.

59. Norton, J. R.; Spataru, T.; Camaoni, D.; Lee, S.-J.; Li, G.; Choi, J.; Franz, J. A., Kinetics and Mechanism of the Hydrogenation of $CpCr(CO)_3$• to $CpCr(CO)_3H$. *Organometallics* **2014,** *33*, 2496.

60. Drago, R. S., *Physical Methods for Chemists, 2nd Ed.* Saunders College Publishing: 1992.

61. Purwanto; Deshpande, R. M.; Chaudhari, R. V.; Delmas, H., Solubility of Hydrogen, Carbon Monoxide, and 1-Octene in Various Solvents and Solvent Mixtures. *J. Chem. Eng. Data* **1996,** *41*, 1414-1417.

62. Wayner, D. D. M.; Parker, V. D., Bond Energies in Solution from Electrode Potentials and Thermochemical Cycles - A Simplified and General Approach. *Acc. Chem. Res.* **1993,** *26*, 287-294.

63. Kaljurand, I.; Kutt, A.; Soovali, L.; Rodima, T.; Maemets, V.; Leito, I.; Koppel, I. A., Extension of the self-consistent spectrophotometric basicity scale in acetonitrile to a full span of 28 pK_a units: Unification of different basicity scales. *J. Org. Chem.* **2005,** *70*, 1019-1028.

64. Eckert, F.; Leito, I.; Kaljurand, I.; Kütt, A.; Klamt, A.; Diedenhofen, M., Prediction of acidity in acetonitrile solution with COSMO-RS. *J. Comput. Chem.* **2009,** *30*, 799-810.

65. Kristjánsdóttir, S. S.; Norton, J. R., Acidity of Hydrido Transition Metal Complexes in Solution. In *Transition Metal Hydrides*, Dedieu, A., Ed. VCH: New York, 1992.

66. Owen, J. S.; Labinger, J. A.; Bercaw, J. E., Kinetics and Mechanism of Methane, Methanol, and Dimethyl Ether C−H Activation with Electrophilic Platinum Complexes. *J. Am. Chem. Soc.* **2006,** *128*, 2005-2016.

67. Sheldrick, G. M. *SHELXTL, An Integrated System for Solving, Refining, and Displaying Crystal Structures from Diffraction Data*, University of Gottingen: Gottingen, 1981.

68. Sheldrick, G., A short history of SHELX. *Acta Crystallogr., Sect. A: Found. Crystallogr.* **2008,** *64*, 112-122.

69. Bain, G. A.; Berry, J. F., Diamagnetic Corrections and Pascal's Constants. *J. Chem. Educ.* **2008,** *85*, 532.

70. Estes, D. P.; Vannucci, A. K.; Hall, A. R.; Lichtenberger, D. L.; Norton, J. R., Thermodynamics of the Metal-Hydrogen Bonds in $(\eta^5\text{-}C_5H_5)M(CO)_2H$ (M = Fe, Ru, Os). *Organometallics* **2011,** *30*, 3444-3447.

Chapter 4. Catalytic Regeneration of Vanadium Hydrides

4.1 MOHAT from vanadium hydrides

As was noted in Chapter 1, the MOHAT reactivity of transition metal hydrides is controlled by the M–H BDFE and steric accessibility of the hydride ligand. A third important factor to make these reactions *catalytic* is that the metalloradical created after transfer of H• must react with H_2 to regenerate the M–H bond. All three of these qualities are necessary in order to perform catalytic radical reactions with hydrides.

As we saw in Section 1.4, vanadium hydrides are good candidates for mediating radical cyclizations. Landis and coworkers calculated the BDE's of several homoleptic transition metal hydrides and predicted that the V–H bonds would be the weakest.[1] The Norton group measured the V–H BDFE's for the compounds $HV(CO)_4$dppx (x = m,e,p,b) using the method described in section 2.2. The results are shown in table 4.1.

Table 4.1. Thermodynamic Parameters of V–H bonds

Compound	pK_a (est in CH_3CN)	E^o_{ox} (V vs Fc/Fc^+)	V–H BDFE (kcal/mol)
$HV(CO)_4$dppm	18.7	-1.18	52.0
$HV(CO)_4$dppe	17.4	-1.12	51.6
$HV(CO)_4$dppp	17.1	-1.17	50.1
$HV(CO)_4$dppb	16.7	-1.19	49.0

The V–H bonds are indeed very weak, with BDFE values between 52 –49 kcal/mol. The vanadium hydrides above transfer H• to styrene (eq 4.1) faster than $CpCr(CO)_3H$ (BDFE = 57 kcal/mol). The rate of these reactions varies inversely with the bite angle of the chelating phosphine (i.e. dppm is faster than dppb) — in opposition to the trend in BDFE. This means that

the vanadium hydrides are sterically demanding. The rates and bite angles are shown in Table 4.2.

Table 4.2. MOHAT rate constants and natural bite angles of vanadium hydrides

Compound	$k_H \times 10^3$ $M^{-1}s^{-1}$	Bite angle[2]
$HV(CO)_4$(dppm)	17	—
$HV(CO)_4$(dppe)	9.0	78.1
$HV(CO)_4$(dppp)	5.7	86.2
$HV(CO)_4$(dppb)	0.85	98.6

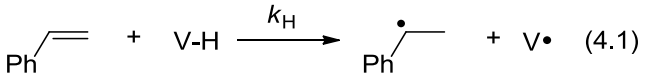

Vanadium hydrides were found to initiate radical cyclizations of appropriate α – ω dienes.[3-4] With two equiv $HV(CO)_4$(dppe), **1.18** was converted to **1.19** in 77% yield (eq 4.2). However, no product appeared under catalytic conditions (7 mol% VH and up to 70 atm H_2) (Scheme 4.1).

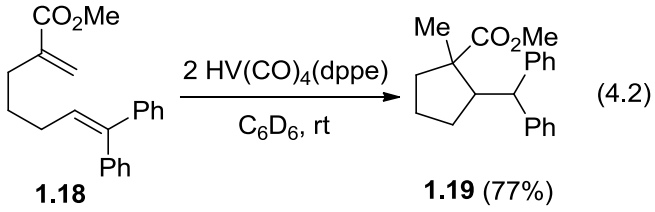

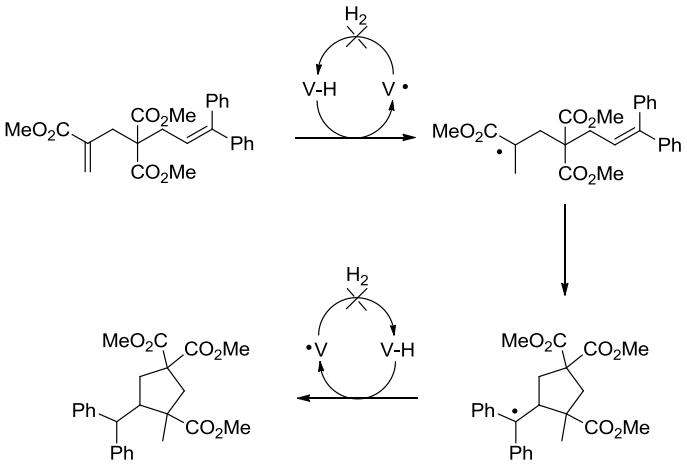

Scheme 4.1. Radical cyclization of a 1,6 diene using stoichiometric vanadium hydride

4.1.1 Possibilities for Catalytic Regeneration of Vanadium Hydrides

In the above example, the vanadium hydride was not able to act as a catalytic reagent for hydrogen atom transfers because the hydride could not be regenerated under H_2. The V–H BDFE's (52-49 kcal/mol) are small enough that these hydrides are thermodynamically unstable toward hydrogen loss, i.e. the equilibrium of eq 4.3 lies to the right. However, they are kinetically stable (k_f is very small). Thus k_r must also be small (since $K_{4.3} = k_f/k_r$).

$$2\ \text{V-H} \underset{k_r}{\overset{k_f}{\rightleftharpoons}} 2\ \text{V}\bullet + \text{H}_2 \quad (4.3)$$

4.2 Regenerating Vanadium Hydrides without H_2

One way around the problem of low V–H BDFE is to reform the hydride by sequential reduction and protonation of the metalloradical (Scheme 4.2). Addition of a one electron reductant and an acid could be able to regenerate the vanadium hydride from the vanadium radical. This would avoid the need to break a strong H–H bond. These reactions could also be done at atmospheric pressure, much better from a safety standpoint. However, adding other

reagents to the reaction does make the reaction less green, since more waste will be produced to regenerate the V–H bond.

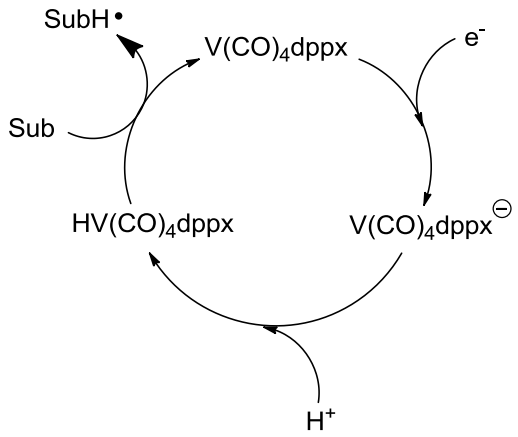

Scheme 4.2. Proposed electrocatalytic HAT scheme

There are a few requirements for the reagents used in this transformation. Firstly, the reductant added must be a strong enough reducing agent to reduce V• to $[V]^-$. Second, the acid used must be a strong enough acid to protonate $[V]^-$ to give V–H. Third, the acid and the reductant must not react with each other. As we have seen in Chapter 3, the concentration of hydride does not need to be very high as long as MOHAT is sufficiently fast.

We have shown that the bite angle of the ligand controls the pK_a and the BDFE of these vanadium hydride complexes. But, they all have similar reduction potentials. As of now there is no explanation of this but it should make finding a suitable reductant easy. The different pK_a's of these hydrides allows suitable acids to be chosen.

4.3 Results

For my initial studies, I chose Cp^*_2Co (–1.94 V vs FcH/FcH^+)[5] and $PhNH_3BF_4$ (pK_a = 11.6 in CH_3CN),[6] both of which meet all the concerns listed above. Upon mixing $NEt_4[V(CO)_4dppe]$ with Cp^*_2Co and $PhNH_3BF_4$, gas bubbled violently out of the solution. Other

one electron reductants, namely Cp_2Co (–1.33 V vs FcH/FcH^+)[5] and $(C_6H_6)_2Cr$ (–1.15 V vs FcH/FcH^+)[5] gave similar results. Control experiments showed that gas was only evolved when the reductant and vanadium hydride were both present (mixtures of only acid and reductant, or only acid and the vanadium hydride, were stable). The IR spectrum in the CO region was unchanged during this gas expulsion, suggesting that the gas is H_2 and not CO. I was never able to observe MOHAT or radical cyclization using these systems.

These hydrides are competent hydrogen production catalysts. Mixing equimolar amounts of $PhNH_3BF_4$ and Cp_2Co with 2 mol% $NEt_4[V(CO)_4dppe]$ in CH_3CN gave 54% yield of hydrogen (27 turnovers) in 14 minutes (measured by a Toepler pump). This leads to a lower limit TOF = 0.032 s^{-1}. This is much slower than hydrogenase enzymes and the recently synthesized $Ni(P_2N)_2$ complexes which can achieve TOF's of 3000 s^{-1} and 10^5 s^{-1}, respectively.[7]

$$PhNH_3BF_4 + Cp_2Co \xrightarrow[CH_3CN,\ 14\ min]{2\ mol\ \%\ NEt_4[V(CO)_4(dppe)]} \underset{54\ \%}{H_2} \qquad (4.4)$$

Given that the only mixtures which evolve hydrogen contain reductant and vanadium hydride, the key step in hydrogen production is probably one electron reduction of the vanadium hydride to produce the vanadium hydride radical cation (**4.1**). A catalytic cycle for this reaction is shown in Scheme 4.3. The key step in this cycle is reduction of the vanadium hydride to make the 19 e^- $V–H^{\bullet-}$. This species can be protonated to release hydrogen and reform V• which can then reenter the cycle.

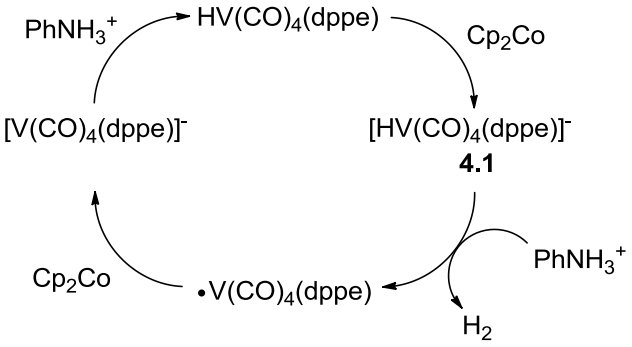

Scheme 4.3. Catalytic cycle for hydrogen production

This mechanism is operative for many hydrogen evolution cycles including $Co(dmgBF_2)_2(L)_2$[8] and Ni(cyclam).[9] Koelle noted that hydrides are often more easily reduced than their corresponding metalloradicals.[10] He rationalized this by thinking of protonation as oxidation of the metal by 2 e^-, so that any conditions that reduce V• would also reduce VH.

Changing the bite angle of the chelating phosphine has been shown to have a profound impact on the electron transfer chemistry of metal complexes.[11] DuBois and coworkers showed that varying the bite angle of the chelating phosphines in $[Pd(P—P)_2]^{2+}$ (**4.2**) complexes changed the reduction potentials by up to 0.6 V. They proposed that this was due to a structural change from square planar toward a pseudo–tetrahedral structure caused by the large bite angle of the chelate, seen in **4.2**.

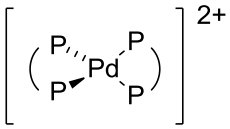

4.2

With this in mind, I attempted the syntheses of vanadium hydrides with larger bite angles. Using the synthesis in scheme 4.4, I was able to synthesize $HV(CO)_4(dppf)$. I was not able to make vanadium hydrides from ligands with larger bite angles like Xantphos (natural bite angle = 111.4°).[2] Other ligands such as phenanthroline also proved unsuitable.

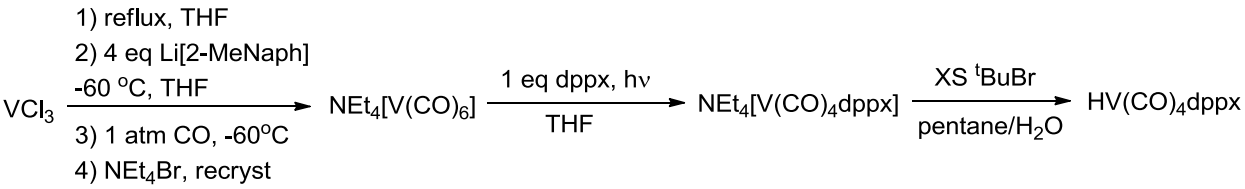

Scheme 4.4. Synthesis of $HV(CO)_4dppx$

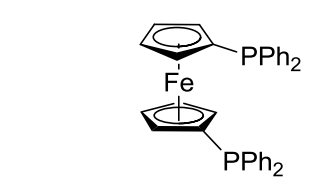

dppf

Measured Bite Angle = 100.8°

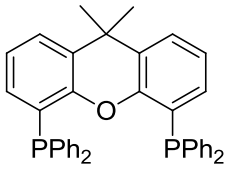

XantPhos

Natural Bite Angle = 111.4°

Crystals of $HV(CO)_4dppf$ were grown by diffusion of pentane into a concentrated solution in benzene. The structure is shown in Figure 4.1 on the right. These vanadium hydrides are octahedral complexes with the hydride ligand residing in the interstices between ligands as seen in the structure of $HV(CO)_4dppe$.[12-13] (The hydride in $HV(CO)_4dppf$ was not found in the X–ray structure. But the disorder in the CO ligands suggests that the hydride is disordered, being either between the two CO ligands or between one CO and one phosphine. This behavior has been seen for other vanadium hydrides.[12]) The observed bite angle of the dppe ligand, 79.3°, fits into an octahedral coordination environment, which means its deviation from octahedral to a prismatic structure is small. The dihedral angle between the OC–V–CO plane and the P–V–P plane (henceforth referred to as the distortion angle) for the dppe complex is only 6°. However dppf, with an observed bite angle of 100.8°, is too large to fit into an octahedral environment. Its distortion angle is 30.4°.

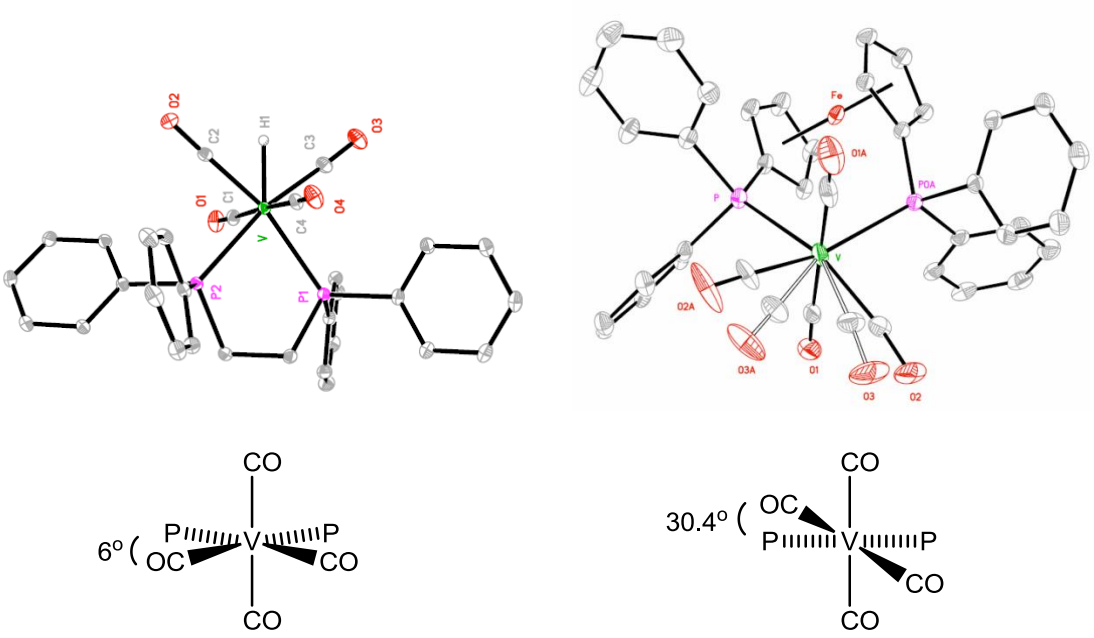

Figure 4.1. Molecular structures of $HV(CO)_4dppe$ (top left) and $HV(CO)_4dppf$ (top right) with pictorial representations below

Distortions from an octahedral coordination environment can change the bonding of the metal. For example, distortion of the carbonyls out of the equatorial plane interrupts backbonding to those carbonyls. The average ν_{CO} for $NEt_4[V(CO)_4dppe]$[14] is 1807 cm^{-1} while that of $NEt_4[V(CO)_4dppf]$ is 1836 cm^{-1}.

The increased bite angle of the phosphine will increase the overlap of the P lone pairs with the d_{xy} orbital, pushing it up in energy (Figure 4.2). Since the d_{xy} orbital is the LUMO orbital, any electron added to $HV(CO)_4dppx$ would end up in d_{xy}. Increasing its energy would make it more difficult to add an electron to the complex. The interruption to the CO backbonding will have a similar effect by raising the energy of all of the back bonding orbitals, including d_{xy}. Hence, increasing the bite angle of the chelate can serve to make the hydride more difficult to reduce by one electron.

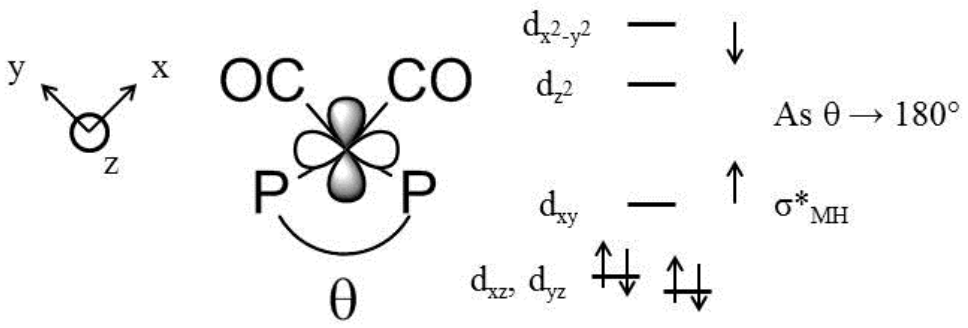

Figure 4.2. Effect of the chelate bite angle on the d_{xy} orbital energy in $HV(CO)_4$dppx

The CV of $NEt_4[V(CO)_4dppf]$ in CH_3CN (figure 4.3, left) shows a reversible wave at −1.14 V vs Fc/Fc^+, which I assign to the V•/V^- redox process. The CV of $HV(CO)_4$dppf in CH_2Cl_2 is shown in figure 4.3 on the right. Scanning in the cathodic direction produces an irreversible reduction wave at −1.59 V vs Fc/Fc^+. This peak is not present on the return wave, but a different oxidation peak is seen at −1.22 V vs Fc/Fc^+. We presume that the reductive peak is probably the $VH/VH^{\bullet-}$ couple. The $VH^{\bullet-}$ will react with VH to produce V•, which is quickly reduced to V^-, as in eq 4.5. The oxidation peak observed on the return wave is probably the oxidation of this V^-.

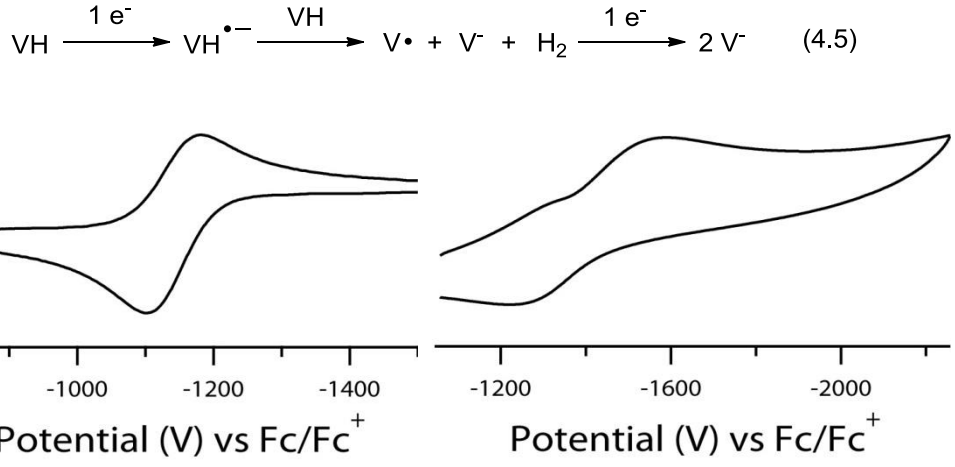

Figure 4.3. CV's of $NEt_4[V(CO)_4dppf]$ in CH_3CN (left) and $HV(CO)_4$dppf in CH_2Cl_2(right)

Using the by now familiar thermodynamic cycle (eq 2.10), I determined the V–H BDFE from the V–H pK_a and the potential of the V•/V$^-$ couple. Equilibrating a mixture of 4-amino-pyridinium (pK_a = 17.62, $K_{homoconjugation}$ = 57.5)[6] with NEt_4[$V(CO)_4$dppf] in acetonitrile gave a pK_a = 16.8 for $HV(CO)_4$dppf (eq 4.6). This combined with the potential of the V•/V$^-$ couple (−1.14 V vs Fc/Fc^+) leads to a V–H BDFE of 50 kcal/mol. The BDFE's of the other V–H bonds are correlated to the ligand bite angle,[4] but the BDFE of $HV(CO)_4$dppf is higher than that of $HV(CO)_4$dppb by about 1 kcal/mol, despite having a much larger bite angle.

$$\begin{array}{ccc} HV(CO)_4dppf & & V(CO)_4dppf^{\ominus} \\ + & \rightleftharpoons & + \\ NH_2Py & & NH_2PyH^+ \end{array} \qquad (4.6)$$

Due to solubility, the pK_a's of $HV(CO)_4$dppx (x = m, e, p, b) were determined by equilibration of VH with $[Cp^*Cr(CO)_3]^-$ in CH_2Cl_2 (eq 4.7) with the assumption that the relative pK_a would be the same in CH_3CN. Ion pairing in CH_2Cl_2 may have introduced error into the original pK_a measurements. Despite these quantitative issues, the V–H bond in $HV(CO)_4$dppf is plainly very weak.

$$V\text{-}H + [Cp^*Cr(CO)_3]^- \underset{CD_2Cl_2}{\overset{K_{eq}}{\rightleftharpoons}} [V]^- + Cp^*Cr(CO)_3H \qquad (4.7)$$

We showed above that $HV(CO)_4$dppf is more difficult to reduce than $V(CO)_4$dppf. Thus this system should be amenable to our reductive protonation scheme. No gas was produced when $HV(CO)_4$dppf was mixed with Cp_2Co or $(C_6H_6)_2Cr$. However, $HV(CO)_4$dppf slowly decomposed in solution to give metalloradical $V(CO)_4$dppf and H_2 as in eq 4.4.

Since $HV(CO)_4$dppf is stable to the appropriate reductants, it should serve as an electrocatalyst for HAT reactions. Attempted cyclization of substrate **1.18** at 50°C gave 19%

yield (by NMR) of hydrogenated product **1.20**, after two days of heating. Free dppf ligand was present in the solution, meaning that the hydride is not stable at the temperature used.

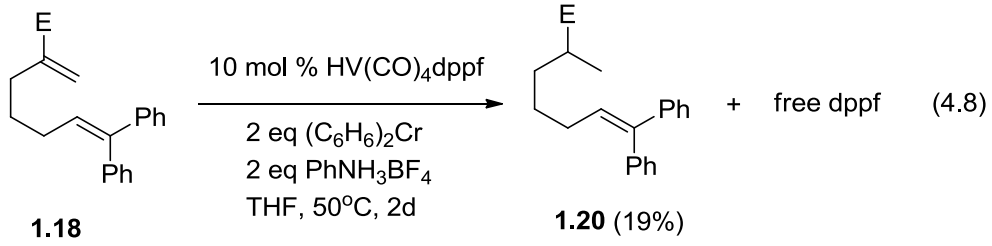

1.18 **1.20** (19%)

I was never able to obtain cyclized product from the reaction. The excess reductant may interfere with the cyclization. The radical **4.3** is fairly electrophilic and could be reduced by 1 e^- to form the enolate **4.4**, which would react rapidly with acid to form **1.20** (eq 4.8).

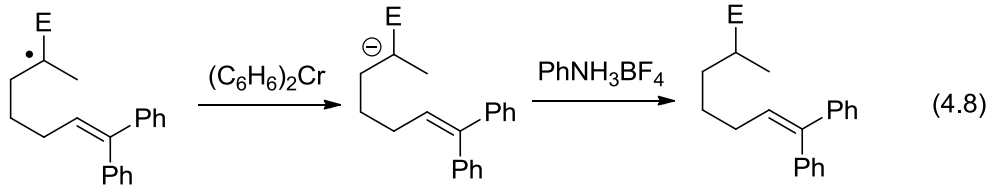

4.3 **4.4** **1.20**

4.4 Experimental Details

All reactions were done under argon atmosphere with standard schlenk technique or in an inert atmosphere box. THF and benzene were purified by distillation from potassium benzophenone ketyl. Acetonitrile was purified as described previously.[15] NMR spectra were taken on a Bruker 300, 400, or 500 MHz spectrometer. IR spectra were taken on a Perkin-Elmer Spectrum 2 spectrometer in CH_3CN solution in a 0.1 mm path length CaF_2 solution cell. X-ray diffraction data were collected on a Bruker Apex II diffractometer. Crystal data, data collection and refinement parameters are summarized in the SI (Table S1). The structures were solved using direct methods and standard difference map techniques, and were refined by full matrix least squares procedures on F^2 with SHELXTL (Version 6.1).[16-17] CV's were obtained using a

BASi potentiostat with a vitreous carbon working electrode (0.5 cm^2) and $Ag/AgNO_3$ reference electrode using 0.1 M NBu_4PF_6 in CH_3CN or 0.1 M $NBu_4B(C_6F_5)_4$ in CH_2Cl_2 as solvent with Cp_2Fe as a reference.[18]

The anion $NEt_4[V(CO)_4dppf]$ was made by the same procedure used to make the analogous known compounds $NEt_4[V(CO)_4dppx]$(x = m, e, p, b).[14] Crystals of the anion $NEt_4[V(CO)_4dppf]$ were obtained by dissolving the compound in a minimal amount of CH_2Cl_2 and layering in benzene. X-ray diffraction data and the molecular structure can be found in Appendix III.

$NEt_4[V(CO)_4dppf]$. ^{1}H NMR (CD_3CN) δ (ppm) 7.69 (bs, 8H, meta CH), 7.35-7.31 (bm, 12H, ortho, para CH), 4.20 (bs, 4H, CpH) 4.17 (bs, 4H, CpH), 3.18 (q (J = 7.2 Hz), 8H, CH_2), 1.23 (t (J = 7.2 Hz), 12 H, CH_3). IR (CH_3CN) ν_{CO} = 1897, 1774, 1741 cm^{-1}. $C_{49}H_{51}O_4NP_2FeV$ calc. (66.37 %C, 5.80 %H, 1.58 %N) found (63.01 %C, 5.95 %H, 1.48 %N).

The vanadium hydrides $HV(CO)_4dppm$, $HV(CO)_4dppe$, $HV(CO)_4dppp$, and $HV(CO)_4dppb$ were synthesized by known procedures and identified by IR and NMR spectroscopy. $HV(CO)_4dppf$ was synthesized by the same procedure.

$HV(CO)_4dppf$. ^{1}H NMR (C_6D_6) δ (ppm) 7.80 (bs, 8H, meta CH), 7.04 (bs, 12H, ortho/para CH), 4.30 (bs, 4H, CpH), 3.85 (bs, 4H, CpH), −4.37 (t (J = 30.4 Hz), 1H, V–H). Crystals of the hydride were obtained by slow diffusion of pentane into a concentrated benzene solution (20 mg in 3 mL) of $HV(CO)_4dppf$. X-ray diffraction data and the molecular structure can be found in Appendix III.

4.4 References

1. Uddin, J.; Morales, C. M.; Maynard, J. H.; Landis, C. R., Computational studies of metal-ligand bond enthalpies across the transition metal series. *Organometallics* **2006,** *25*, 5566-5581.

2. Casey, C. P.; Whiteker, G. T., The Natural Bite Angle of Chelating Diphosphines. *Israel J. Chemistry* **1990,** *30*, 299-304.

3. Hartung, J.; Pulling, M. E.; Smith, D. M.; Yang, D. X.; Norton, J. R., Initiating Radical Cyclizations by H• Transfer from Transition Metals. *Tetrahedron* **2008,** *64*, 11822-11830.

4. Choi, J.; Pulling, M. E.; Smith, D. M.; Norton, J. R., Unusually Weak Metal-Hydrogen Bonds in $HV(CO)_4(P\text{-}P)$ and Their Effectiveness as H• Donors. *J. Am. Chem. Soc.* **2008,** *130*, 4250-4252.

5. Connelly, N. G.; Geiger, W. E., Chemical Redox Agents for Organometallic Chemistry. *Chem. Rev.* **1996,** *96*, 877-910.

6. Kaljurand, I.; Kutt, A.; Soovali, L.; Rodima, T.; Maemets, V.; Leito, I.; Koppel, I. A., Extension of the self-consistent spectrophotometric basicity scale in acetonitrile to a full span of 28 pK_a units: Unification of different basicity scales. *J. Org. Chem.* **2005,** *70*, 1019-1028.

7. Helm, M. L.; Stewart, M. P.; Bullock, R. M.; DuBois, M. R.; DuBois, D. L., A Synthetic Nickel Electrocatalyst with a Turnover Frequency Above 100,000 s^{-1} for H2 Production. *Science* **2011,** *333*, 863-866.

8. Dempsey, J. L.; Winkler, J. R.; Gray, H. B., Mechanism of H_2 Evolution from a Photogenerated Hydridocobaloxime. *J. Am. Chem. Soc.* **2010,** *132*, 16774-16776.

9. Kelly, C. A.; Blinn, E. L.; Camaioni, N.; D'Angelantonio, M.; Mulazzani, Q. G., Mechanism of CO2 and H+ Reduction by Ni(cyclam)+ in Aqueous Solution. A Pulse and Continuous Radiolysis Study. *Inorg. Chem.* **1999,** *38*, 1579-1584.

10. Koelle, U., Transition Metal Catalyzed Proton Reduction. *New J. Chem.* **1992,** *16*, 157-169.

11. Raebiger, J. W.; Miedaner, A.; Curtis, C. J.; Miller, S. M.; Anderson, O. P.; DuBois, D. L., Using Ligand Bite Angles To Control the Hydricity of Palladium Diphosphine Complexes. *J. Am. Chem. Soc.* **2004,** *126*, 5502-5514.

12. Choi, J. Thermodynamics and Kinetics of Hydrogen Atom Transfer from Transition-Metal Hydrides and Their Applications. Ph.D. Thesis, Columbia University, New York, 2007.

13. Puttfarcken, U.; Rehder, D., Carbonylhydridophosphinevanadium complexes, a novel route to hydrido complexes by ion exchange on silica silica gel. *J. Organomet. Chem.* **1978,** *157*, 321-325.

14. Rehder, D.; Dahlenburg, L.; Muller, I., Substitution Products of $[V(CO)_6]$- AND $[ETA^5\text{-}CPV(CO)_4]$ with di-tertiary and tetra-tertiary phosphines. *J. Organomet. Chem.* **1976,** *122*, 53-61.

15. Estes, D. P.; Vannucci, A. K.; Hall, A. R.; Lichtenberger, D. L.; Norton, J. R., Thermodynamics of the Metal-Hydrogen Bonds in (η^5-C_5H_5)M$(CO)_2$H (M = Fe, Ru, Os). *Organometallics* **2011,** *30*, 3444-3447.

16. Sheldrick, G. M. *SHELXTL, An Integrated System for Solving, Refining, and Displaying Crystal Structures from Diffraction Data*, University of Gottingen: Gottingen, 1981.

17. Sheldrick, G., A short history of SHELX. *Acta Crystallogr., Sect. A: Found. Crystallogr.* **2008,** *64*, 112-122.

18. Pavlishchuk, V. V.; Addison, A. W., Conversion constants for redox potentials measured versus different reference electrodes in acetonitrile solutions at 25°C. *Inorg. Chim. Acta* **2000,** *298*, 97-102.

Chapter 5. Metal to Alkyne Hydrogen Atom Transfer (MAHAT)

5.1 Introduction

5.1.1 Stereochemistry in the Reactions of Metal Hydrides with Alkynes

A variety of mechanisms have been proposed for the reactions of alkynes with transition-metal hydrides. The most common of these (eq 5.1) involves coordination of the alkyne to the metal, followed by its insertion into the M-H bond.[1-4] This mechanism results in syn addition of the M–H to the triple bond, and gives a *Z* alkene after proteolytic cleavage of the M–C bond.

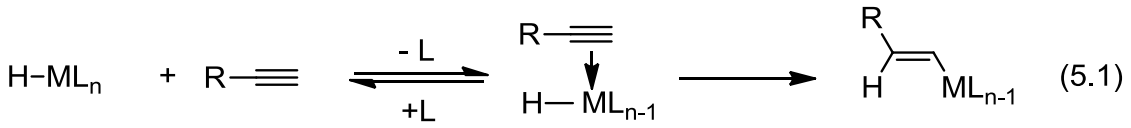

(5.1)

However, there are a number of reports of the anti addition of M–H to alkynes, resulting in E olefins after hydrolysis.[5-13] Several mechanisms have been offered to explain this, one of which involves radicals. For example, the reaction of $Cp_2Mo(H)_2$ with electron poor alkynes produced vinyl hydride **5.1** with trans geometry. Jones and coworkers showed that $Cp^*Rh(PMe_3)(H)_2$ reacts with hexafluoro-2-butyne to give the vinyl species **5.2** with trans selectivity (eq 5.2). The stereochemistry was found to vary with the nature of the alkyne: the more electron poor the alkyne, the more trans product. Both proposed that trans addition goes through transition state **5.3**.[14]

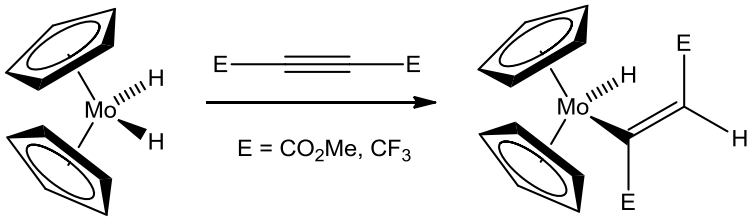

(5.2)

5.1

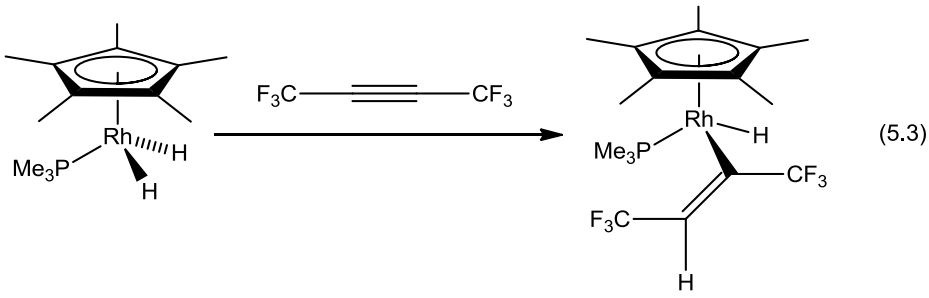

(5.3)

5.2

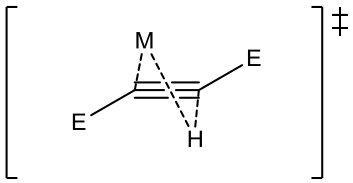

5.3

A different mechanism was proposed by Bergman and Huggins.[15] The trans addition of Ni–Me species 5**.4** was thought to proceed by initial cis addition, followed by an isomerization step catalyzed by phosphine nucleophilic attack to give the trans addition product 5**.5** (Scheme 5.1).

Scheme 5.1

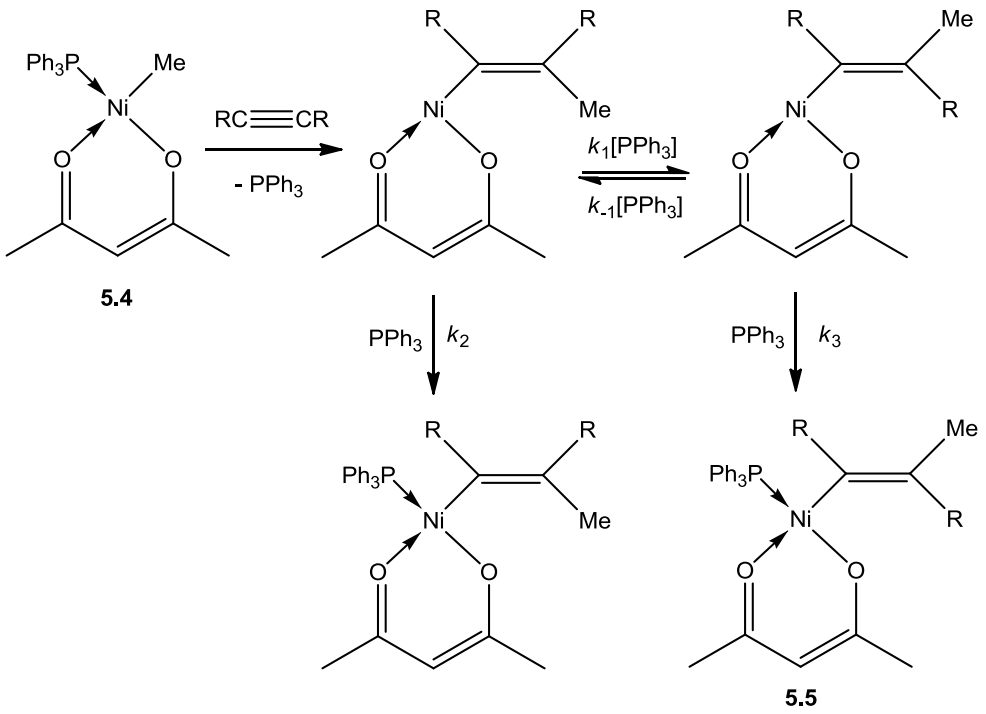

Crabtree showed that hydrosilylation of internal alkynes by **5.6** gives initial cis insertion (Scheme 5.2).[8] Subsequent cis–trans isomerization gives a mixture of stereochemical outcomes. He proposed that this involves isomerization through an η^2-vinyl complex (5.**7**) which was observed by Green previously.[16]

Scheme 5.2

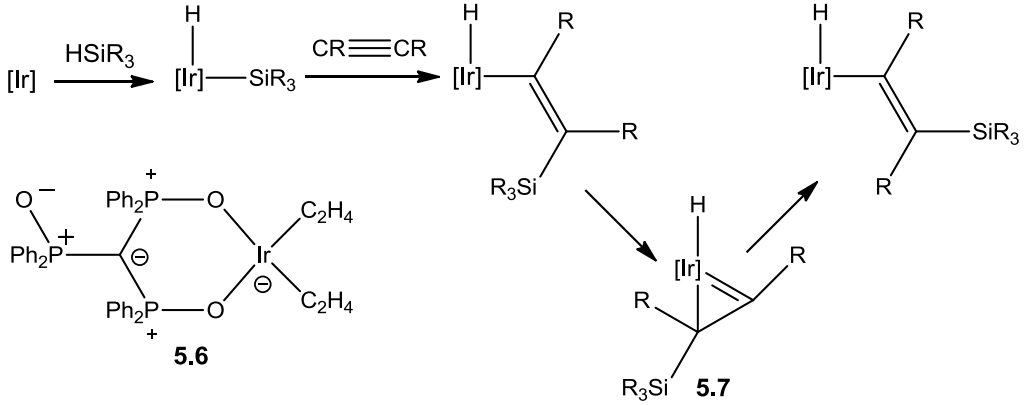

Trost and coworkers found that **5.8** catalyzes the trans hydrosilylation of internal alkynes.[7] Yamamoto also observed trans hydrosilylation of terminal alkynes with catalytic lewis acids such as $AlCl_3$.[17] They proposed that trans selectivity comes from hydride transfer to the Lewis acid–activated alkyne, which would prefer attack from the opposite side. This attack is followed by silylation of the resulting M–C bond.

Scheme 5.3

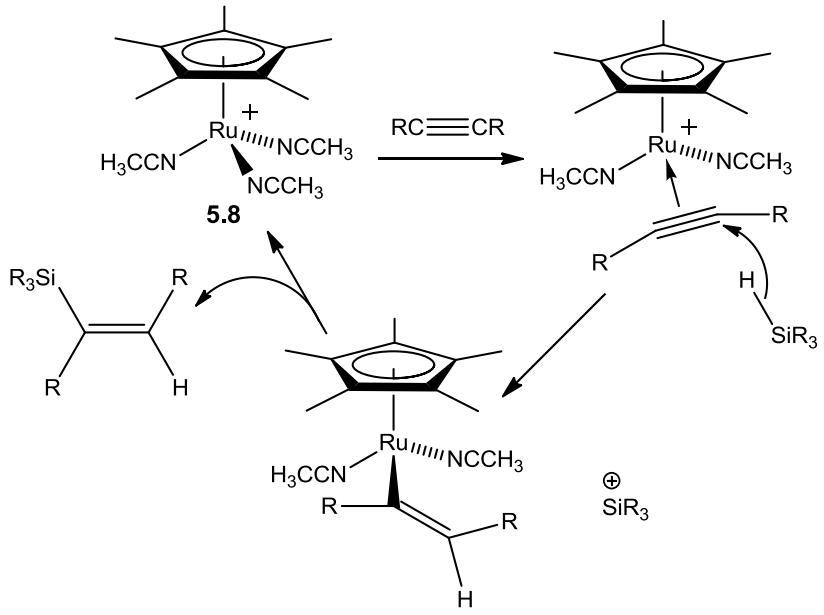

5.1.2 Electron Transfer to Alkynes

The reduction of alkynes can also happen via one electron mechanisms. Of course the best known example is the alkali metal (Na, Li) reduction of alkynes in liquid ammonia to give trans-olefins.[18] This reaction presumably occurs through a single electron transfer to the alkyne to give an alkyne radical anion **5.9**, shown in its more stable trans geometry.[19]

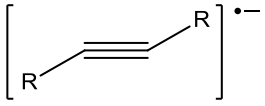

5.9

Clark observed that the platinum dihydride **5.10** reacts with electron–poor alkynes to give the trans vinyl product **5.11**. Based on a variety of data, including spin trapping of the vinyl radical species **5.12**, he proposed that **5.10** first transfers an electron and then a proton to an electron poor alkyne, producing a vinyl radical; isomerization of that radical, coordination, and reductive elimination from the alkyl hydride complex **5.11** give an E olefin.[6]

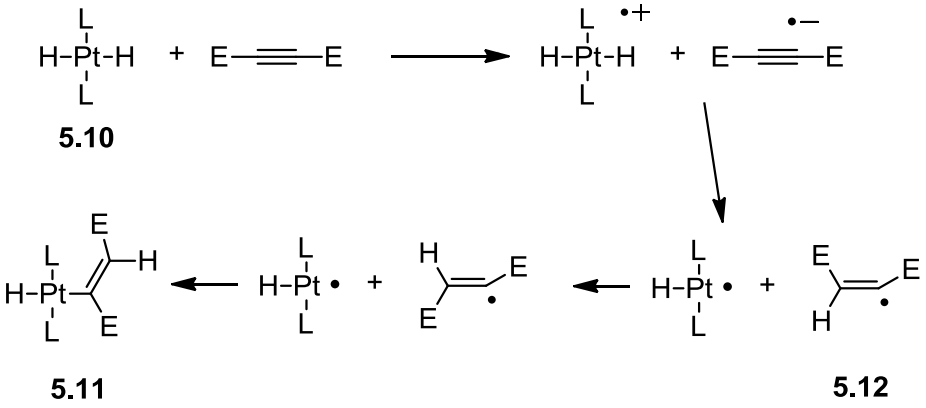

5.1.3 Radical Additions to Alkynes

Alkyl radicals are well known to react with alkynes. One common type of radical cyclization is the so called "dig" cyclization in which the accepting bond is an alkyne.[20] These "dig" cyclizations are popular due to the functionality of the olefin created in the product.

Radicals in sp^2 orbitals are more difficult to make than ones in sp^3 orbitals, as demonstrated by the higher BDE's of sp^2 C–H bonds. The enthalpies of reaction of H• and ethylene (eq 5.5) or acetylene (eq 5.6) are available from the appropriate heats of formation[21-22] (shown below each species). Addition of H• to ethylene is more favorable by about 1.5 kcal/mol. By applying the Marcus cross relation and assuming that both ethyl and vinyl radical have the same self–exchange rate (no data is available on self–exchange rates of carbon radicals), this

difference in driving force should result in HAT to ethylene being about 3.5 times faster than HAT to acetylene (eq 5.7).

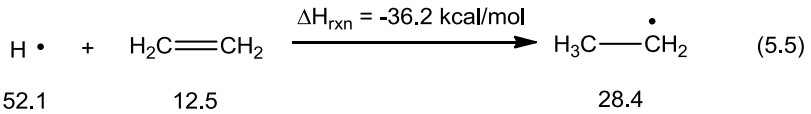

(5.5)

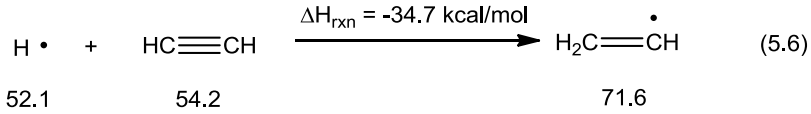

(5.6)

$$\frac{k_{ethylene}}{k_{acetylene}} \propto \sqrt{\frac{K_{eth}}{K_{acet}}} \approx 3.5 \qquad (5.7)$$

Contrary to what was seen for ethylene/acetylene, the addition of H• to propyne (−41 kcal/mol) is more exothermic than to propene (−35.9 kcal/mol).[21-22] Addition of methyl radicals to alkynes are always slower than to alkenes, despite the alkyne addition being more exothermic.[23] A variety of explanations have been used to explain this: error in thermodynamic measurements, entropic effects, and the large single triplet gap of alkynes.[23-24] Whatever the reason, alkynes react with radicals slower than olefins.[23] The *tert*–butyl radical reacts six times faster with styrene than with phenyl acetylene (eq 5.8).

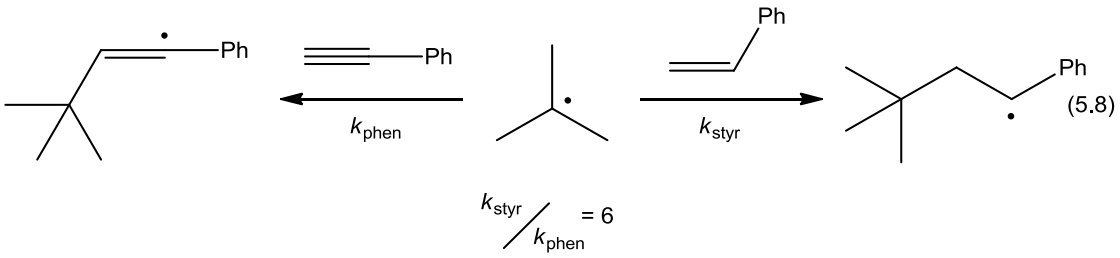

(5.8)

Metal to Alkyne HAT (MAHAT), forming vinyl radicals, has been observed.[12-13] Ungváry reported, based on CIDNP evidence, the transfer of H• to phenylacetylene during hydroformylation by $HCo(CO)_4$ (eq 5.9).[13] Gridnev and Wayland also observed trans selectivity in the reaction of cobalt porphyrin hydrides (made in situ) with various alkynes and assumed a

radical mechanism (eq 5.10).[12] We could possibly use these MAHAT's in catalytic radical cyclizations.

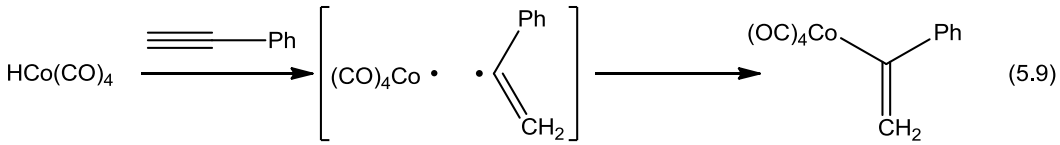

(5.9)

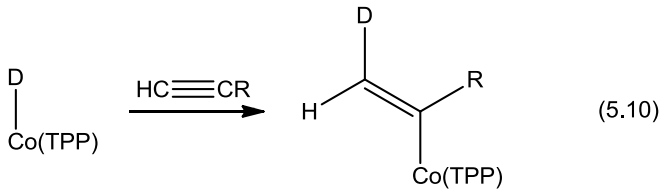

(5.10)

5.2 Results

We considered the possibility of catalyzing radical cyclizations via vinyl radicals generated by HAT to alkynes, similar to those seen in chapter 1. Despite the fact that alkynes react more slowly, vinyl radicals are less stable and should cyclize faster (see Scheme 1.3) than the $RO_2C(Me)C•$ radicals made previously by this method. Since the initial MAHAT is the rate determining step this should lead to a slower overall reaction with better selectivity for cyclization.

5.2.1 Reactions of unactivated alkynes with $CpCr(CO)_3H$

Alkyl substituted alkynes were found to be unreactive. Both 1-octyne and trimethylsilylacetylene gave no reaction when heated with $CpCr(CO)_3H$ (from now on referred to as Cr–H) at 50 ºC for 24 h. The reaction of trimethylsilylacetylene was followed by ^1H NMR, and no relative change in integrals was seen over the course of five hours. An upper limit of the rate constant could not be estimated.

5.2.2 Reaction of phenylacetylene with $CpCr(CO)_3H$

Aryl alkynes, such as phenylacetylene, are readily consumed by Cr–H. The reaction of phenylacetylene (0.044M) with two equiv of Cr–H (0.088M) yields the products shown in eq 5.11. The major products are styrene (**5.13**, 44%), ethylbenzene (**5.14**, 5%) and the organometallic complex **5.15** (51%). Crystals of **5.15** were identified by crystallography as the fulvene complex (Figure 5.1). Its structure was similar to that of known fulvene complexes.[25]

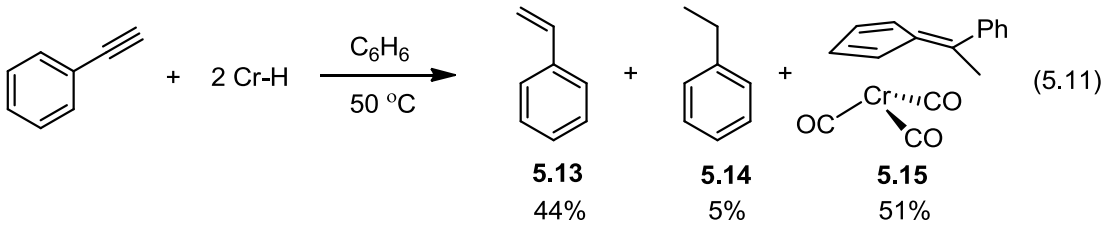

Figure 5.1. Molecular structure of **5.15** (20% ellipsoids, hydrogens omitted for clarity)

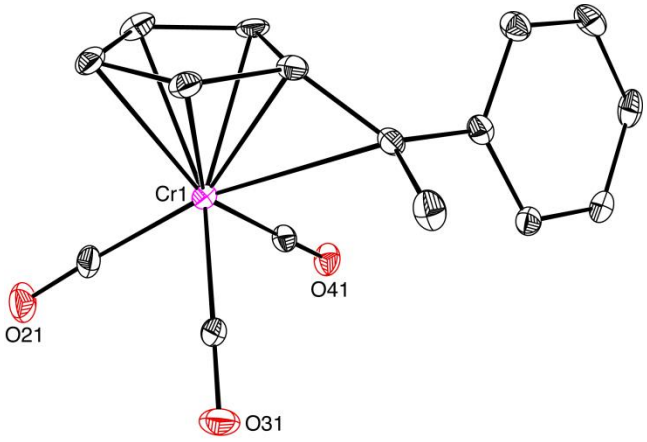

Complex **5.15** could form by two different pathways, one involving reductive elimination from vinyl chromium species **5.16**, and one in which the intermediate radical **5.17** attacks the Cp ring directly. Calculations on $CpCr(CO)_3$ show that there is only ~5% spin density on the Cp ring. This makes the mechanism involving **5.16** more plausible. However, we never observe **5.16** and the role of the metal carbon bond (if any) in these cases is unknown.

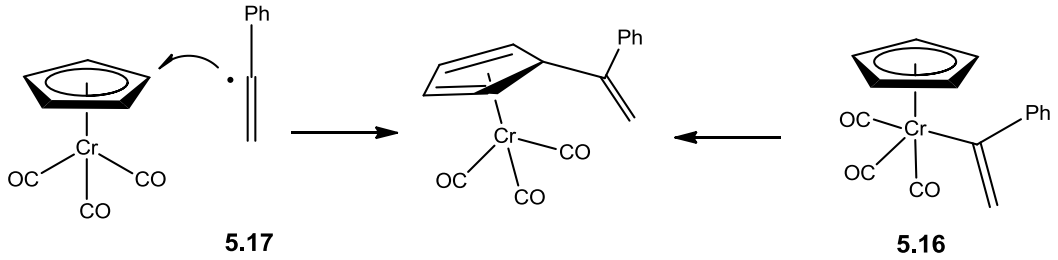

5.17 **5.16**

Support for a HAT mechanism was given by the reaction of Cr–H with phenylacetylene-d_1. We obtained cis and trans styrene-d_1 in a 1:1 ratio, consistent with the mechanism in Scheme 5.4. Donation of an H• to the terminal carbon of phenyl acetylene will give the vinyl radical **5.17**, which is linear.[26-27] Transfer of a second H• from Cr–H will not be affected by the position of the deuterium, so there will be a 1:1 *E*:*Z* (**5.19**:**5.18**) ratio for the resulting styrene-d_1. The same result has been reported by Ungváry for the reaction of phenylacetylene-d_1 with $HCo(CO)_4$.[13]

Scheme 5.4

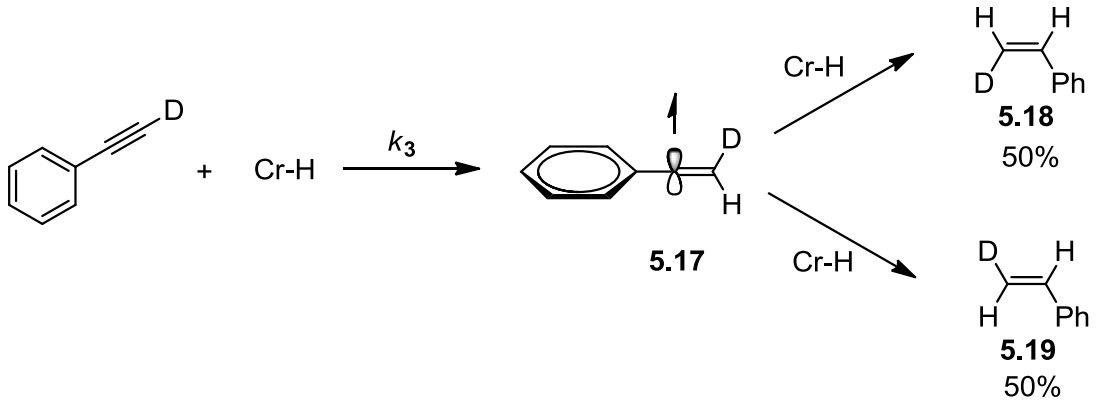

Further evidence for a radical mechanism is offered by the rate of the reaction of phenylacetylene with Cr–H. When we treat Cr–H (0.012M) with a tenfold excess of phenylacetylene (≥ 0.124M) the amounts of **5.14** and **5.15** that form are very small, i.e., the yield of styrene is greater than 95%. The disappearance of Cr–H is first order, and k_{obs} is linear in [PhC≡CH] (Figure 2), showing the rate law to be that in eq 5.12.

$$-\frac{d[Cr-H]}{dt} = 2k_3[Cr-H][\mathrm{PhC}\equiv\mathrm{CH}] \qquad \textbf{(5.12)}$$

Figure 5.2. Kinetics of HAT from **CrH** to phenyl acetylene

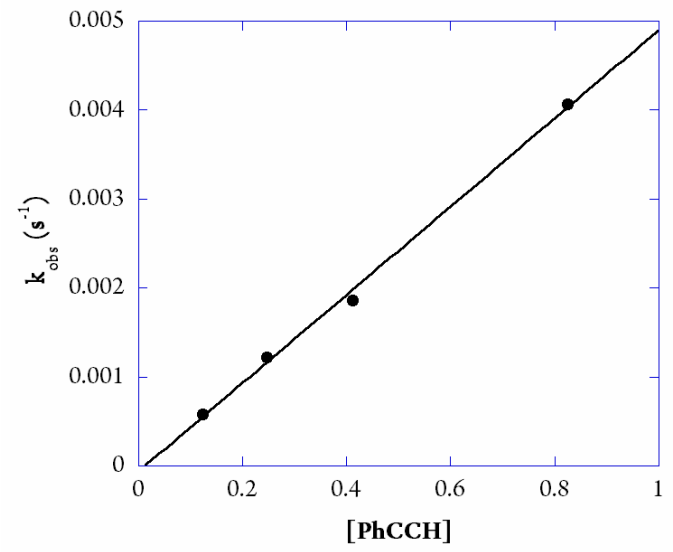

The resulting rate constant (k_3) (2.5(± 0.1) × 10^{-3} $M^{-1}s^{-1}$) for HAT to PhC≡CH is six times slower than HAT from Cr–H to styrene.[28] The ratio is very similar to that (1:6) for the addition of the ^{t}Bu radical to PhC≡CH/PhCH=CH_2.[23]

The Cr–H/ Cr–D isotope effect cannot be measured accurately because of the competition between back transfer and hydrogenation after the initial D• transfer. With Cr–D, for example, back transfer of H• competes not only with back transfer of D• but also with addition of a second D•; both styrene and phenylacetylene-d_1 are products. Addition of excess $CpCr(CO)_3$ favors exchange over hydrogenation and allows estimation of k_H/k_D as 0.2 — substantially inverse. The similarity in the PhC≡CH/PhCH=CH_2 rate constant ratio and the inverse isotope effect support our description of eq 5.11 as a H• transfer process.

5.2.3 Catalytic Cyclization Using a Vinyl Radical

Since Cr–H does transfer H• to phenylacetylene we designed a substrate that could be cyclized by that reaction. The ease of transfer to phenylacetylene suggested the enyne **5.20**. **5.20** has a triple bond that accepts H• more rapidly (k_1 = 2.5×10^{-3} $M^{-1}s^{-1}$) than the double bond (k_3 = 5.9×10^{-4} $M^{-1}s^{-1}$).[28] This radical cyclization should proceed through an intermediate vinyl radical.

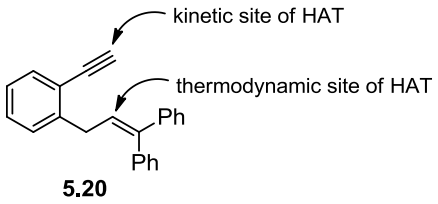

5.20

Compound **5.20** was synthesized by nucleophilic attack of the Gilman reagent derived from **5.21** on the appropriate allyl bromide. The resulting molecule was then deprotected using tetrabutylammonium fluoride, to give **5.20** in 83% yield. The synthesis is shown in Scheme 5.5.

Scheme 5.5. Synthesis of 5.21

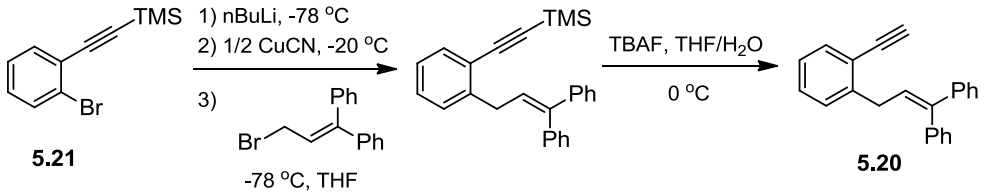

5.21 **5.20**

When we treated **5.20** with a stoichiometric amount (2 equiv) of Cr–H (eq 5.13) we obtained the indene product **5.22** in 42% yield, with the balance being the hydrogenated product **5.23**.

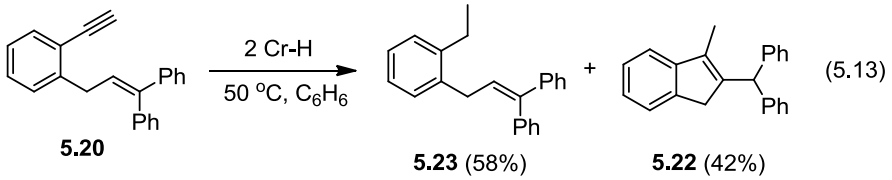

5.20 **5.23** (58%) **5.22** (42%) (5.13)

Under H_2 (2.4 atm) in the presence of a catalytic amount of Cr–H**, 5.22** was formed in 43% yield along with 22% of **5.23** and 35% of the double bond isomer **5.24**, for a total of 78% cyclized material.

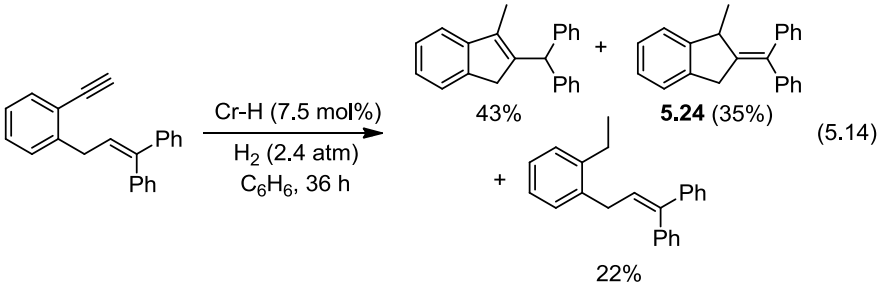

(5.14)

With our recently discovered cobaloxime catalyst (**1.34**), **2.20** gives only **2.22** and **2.24** in 48% and 52% yields respectively (eq 5.15).[29] This is expected since the cobalt hydride is created in situ in very small concentrations, making this catalyst good at suppressing hydrogenation. The results are shown in Table 5.1.

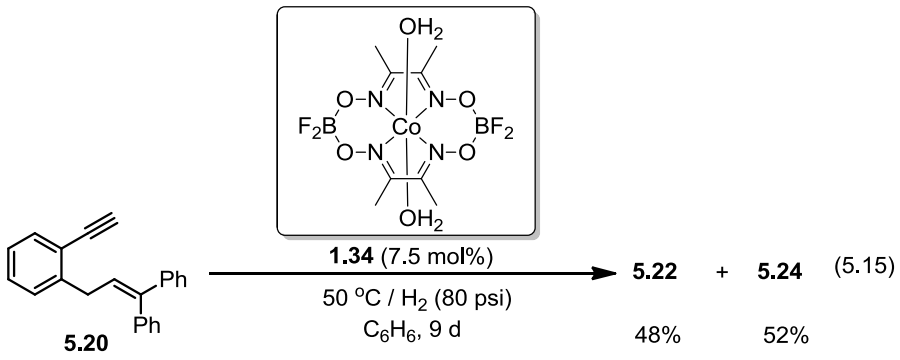

(5.15)

Table 5.1. Cyclization reactions of **5.20**

Catalyst	Loading (mol %)	H_2 (atm)	Reaction time	% **5.23**	% **5.22**	% **5.24**
$CpCr(CO)_3H$	200	—		58	42	—
$CpCr(CO)_3H$	7.5	2.4	36 h	22	43	35
$Co(dmgBF_2)_2(OH_2)_2$	7.5	5.4	9 d	—	48	52

The mechanism is surely that shown in Scheme 5.5. The vinyl radical produced by the initial H• transfer cyclizes to make **5.25**. A second H• transfer, from Cr–H to the methylene in **5.25,** isomerizes the double bond in **5.25** to an internal position, giving **5.22**; the fact that no **5.25** accumulates implies that the second H• transfer is faster than the first. The same vinyl radical that made **5.25** can also react with Cr–H to form styryl compound **5.26**, which can further hydrogenate to form **5.23** or cyclize to form **5.24**.

Scheme 5.6 Cyclization Mechanism of 5.20

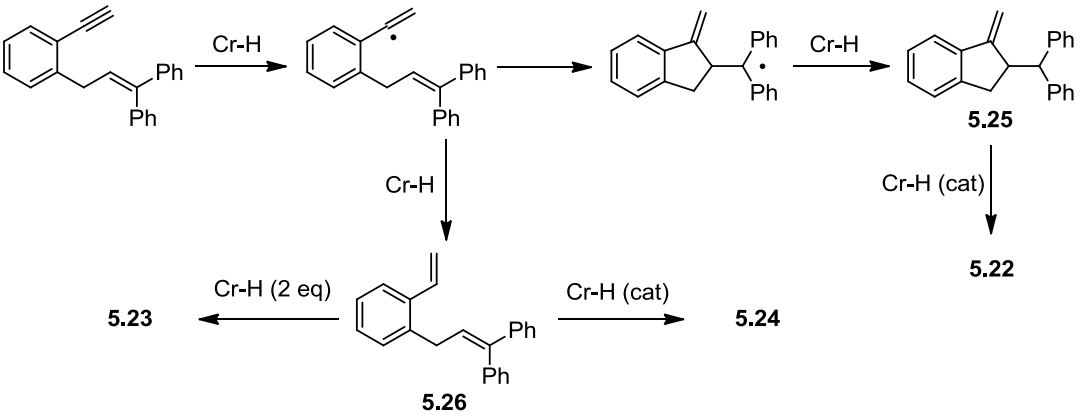

5.2.4 Reactions with Diphenylacetylene

In order to study the effect of substitution we next studied diphenylacetylene. Treating PhC≡CPh with Cr–H gave only the expected hydrogenation products, *E*- and Z-stilbene, as observed by GC, with no further hydrogenation.

Figure 5.3. Time dependence of Cis/Trans ratio in diphenyl acetylene hydrogenation

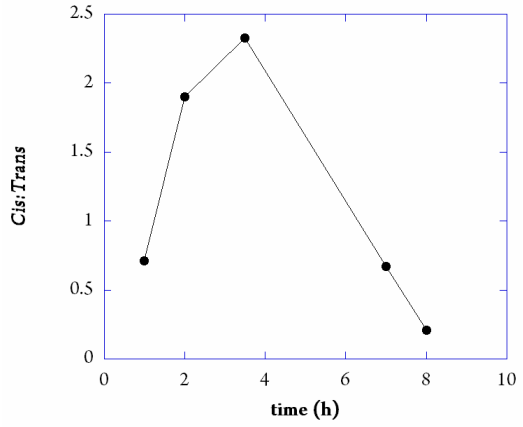

The rate constant for HAT (k_6 = 1.4(± 0.3) × 10^{-4} $M^{-1}s^{-1}$) was approximately 20 times smaller than that of PhC≡CH, similar to the substitution effect seen with substituted alkenes.[28] This trend suggests that the key step is HAT.

The *cis:trans* ratio was not constant over the course of the reaction. At first there is a slight preference for trans, then cis formation is favored, but by the end of the reaction the product is predominantly trans (Figure 5.3).

Scheme 5.7 Caged Radical Pair in Diphenylacetylene Hydrogenation

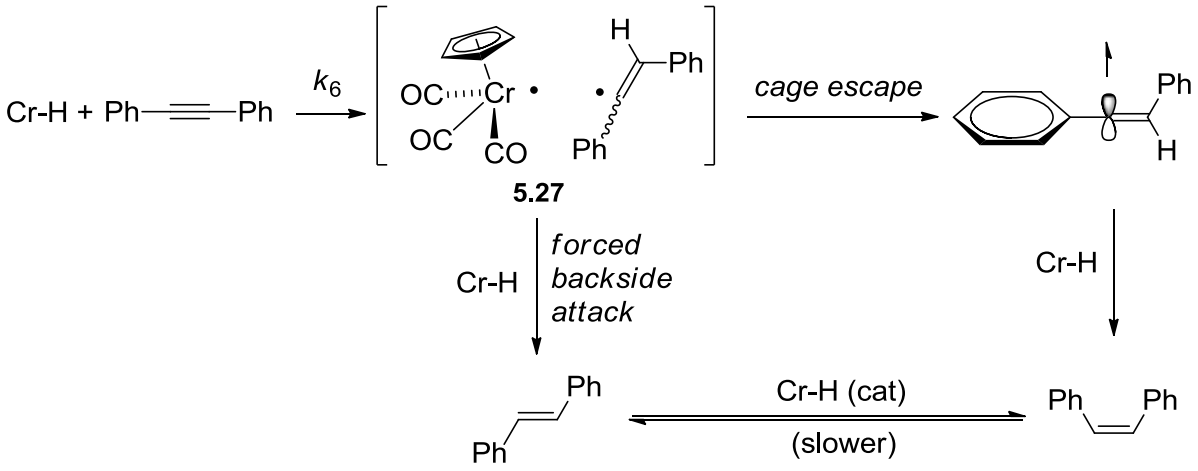

We propose the mechanism in Scheme 5.7 to explain this variation over time. The initial product of the MAHAT from $CpCr(CO)_3H$ to PhC≡CPh is presumably a caged radical pair (**5.27**), with the Cr remaining near the hydrogen it has just transferred; the second Cr–H will prefer to approach the *caged* vinyl radical on the side away from the first Cr (and the H), and will give predominantly trans (*E*) product. Later, when lower [Cr–H] permits cage escape, the *free* vinyl radical will prefer approach away from the second Ph, on the same side as the first hydrogen, and give largely *Z* stilbene. Eventually cis/trans isomerization, catalyzed by reversible H• transfer, will move toward the largely *E* equilibrium mixture (the thermodynamic ratio is known[30] to be 99.8:0.2).

5.2.5 Reaction of $CpCr(CO)_3H$ with Electron-Poor Alkynes

5.2.5.1 Methyl Propiolate

Treating methyl propiolate (0.0365M) with stoichiometric Cr–H produced methyl acrylate (39%) as well as small oligomers of methyl propiolate (confirmed by mass spectrometry and ^{1}H NMR). Larger concentrations (0.58M) of propiolate gave lower yields of acrylate, because the amount of oligomerization increased.

When we treat Cr–D with excess methyl propiolate, we do not observe H/D exchange. When we carry out this reaction in the presence of excess $CpCr(CO)_3$• **(5.28)** (in equilibrium with the dimer $[CpCr(CO)_3]_2$[31]) we do observe H/D exchange at the start of the reaction, showing the intermediacy of a vinyl radical (Scheme 5.8). (We have found the addition of the metalloradical **5.28** to be a useful general method for observing H/D exchange in the absence of other reactions.) The vinyl radical will *not* be linear, but will invert rapidly,[26] so both cis and trans acrylate esters will be formed (a cis trans ratio of 1.4 is observed).

Scheme 5.8 H/D Exchange in Methyl Propiolate Hydrogenation

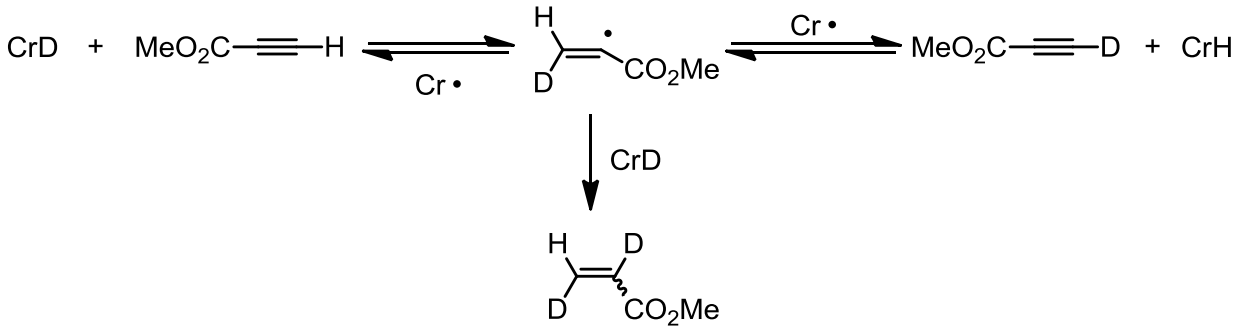

In the presence of a large excess of methyl propiolate, the reaction is first order in Cr–H. Given the small chain length of the oligomers and assuming rapid chain propagation, the rate law for Scheme 5.8 will be the same as that for phenyl acetylene (eq 5.12), with k_9 = 3.2(± 0.3) × 10^{-4} $M^{-1}s^{-1}$. The overall mechanism is that in Scheme 5.9: after rate determining MAHAT, the vinyl radical either hydrogenates by reaction with a second Cr–H or adds to propiolate to make dimer.

Scheme 5.9 Methyl Propiolate Oligomerization

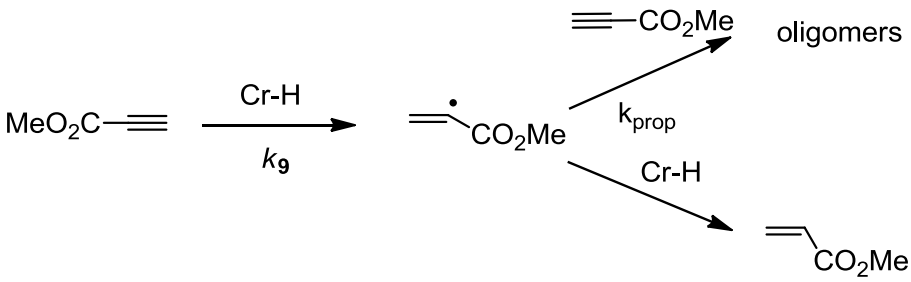

5.2.5.2 Dimethyl Acetylenedicarboxylate

Treating dimethyl acetylenedicarboxylate (DMAD) with Cr–H (eq 5.16) gave **5.29** as the major product (76%) in addition to **5.30** (17%), **5.31** (5%), and oligomers as big as tetramers

(2%). There was a 4:1 preference for the cis hydrogenation product **5.30** over the trans product **5.31**.

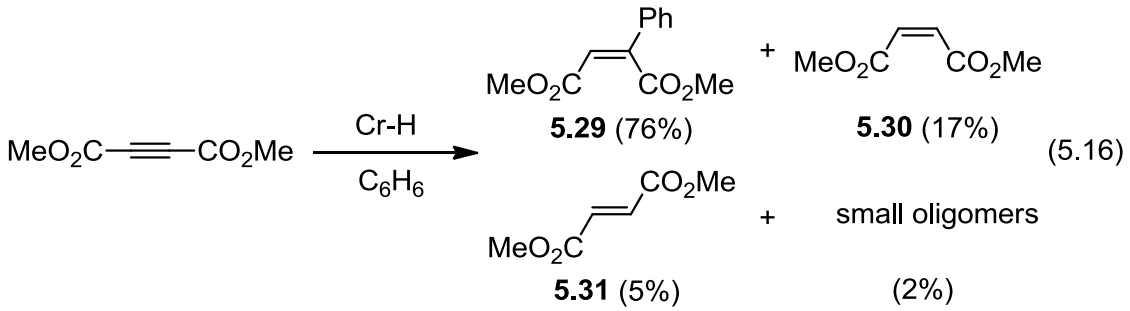

(5.16)

The appearance of **5.29** makes a HAT mechanism seem less likely; no phenyl substituted product was seen with methyl propiolate. Radicals are known to attack benzene,[32-33] but this often occurs reversibly, only at high temperatures, and is generally intramolecular (although more reactive radicals like HO• readily attack benzene).[34] In one example, •CF_3 only adds to benzene reversibly above 140 °C.[35] A SET mechanism (similar to that of Clark)[6] could explain the presence of **5.29** (Scheme 5.10).

Scheme 5.10 Reaction of DMAD and CrH

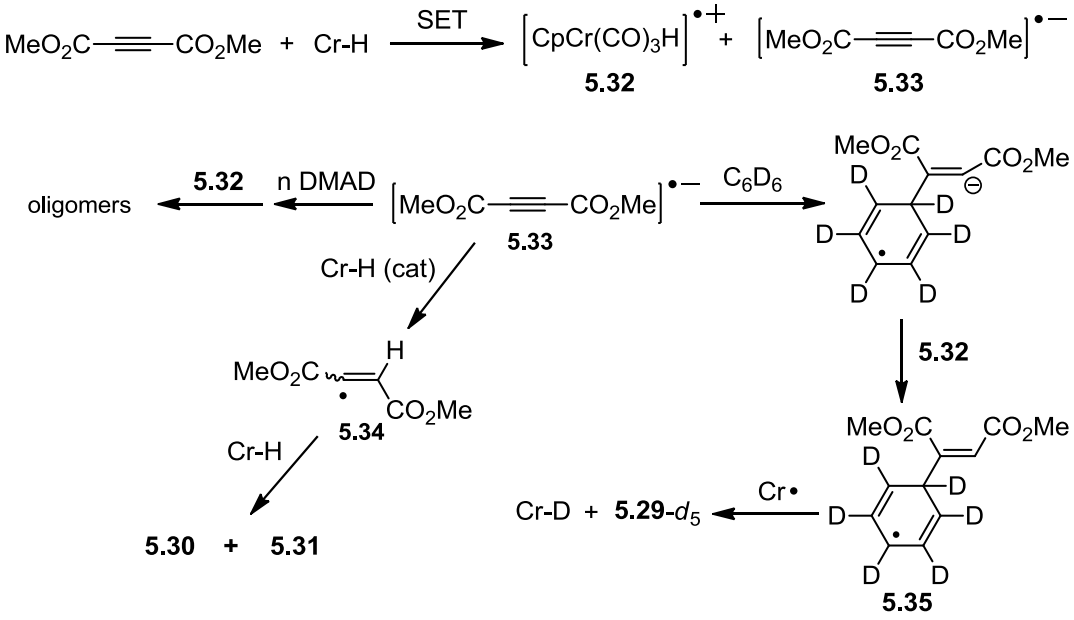

Concentration profiles of **5.29**, **5.30**, and **5.31** were fit to the kinetic model shown in Scheme 5.11. Kintecus kinetic modeling software[36] was used to fit kinetic parameters to the data.

The ratio of **5.30** to **5.31** remains constant throughout the reaction, but the ratio of **5.29** to the sum of **5.30** and **5.31** gets larger as the reaction continues. This variation in product ratio excludes a HAT (giving **5.30**, **5.31**) parallel to SET (giving **5.29**). Indeed, it proved impossible to simulate the kinetics[36] on this basis.

In the kinetic model (Scheme 5.11) the rate constants of reactions 5.17, 5.18, and 5.20 were optimized while the other rate constants were specified as constant in order to keep the model as simple as possible. Reactions 5.19 and 5.21 are certainly diffusion controlled ($\approx 10^{10}$ $M^{-1}s^{-1}$) because of the very acidic nature of the radical cation. The rates of reactions similar to 5.22 and 5.23[37] have been measured and since the product ratio **5.30**:**5.31** is constant (4:1), the ratio of the rate constants of reactions 5.22 and 5.23 is also 4:1. An approximate value similar to those previously measured (10^9 $M^{-1}s^{-1}$) was chosen for reaction 5.22 and the ratio was used to calculate a rate constant (2.5×10^8 $M^{-1}s^{-1}$) for reaction 5.23. (Since oligomers accounted for less than 2% of the product under these conditions, they were not included for simplicity.) A sample fit is shown below (k_{17} = 9.9(±0.2)×10^{-3} $M^{-1}s^{-1}$, k_{18} = 12.5(±0.3) s^{-1}, k_{20} = 850(±10) $M^{-1}s^{-1}$, R^2 = 0.9975). The rate constant k_{17} for electron transfer to DMAD is over 30 times *greater* than the rate constant k_9 for HAT to methyl propiolate.

Scheme 5.11 Mechanistic Scheme Used in Kinetic Modelling

$$\mathrm{DMAD} + \mathrm{CrH} \xrightarrow{k_{17}} \mathrm{DMAD}^{\bullet-} + \mathrm{CrH}^{\bullet+} \quad (5.17)$$

$$\mathrm{DMAD}^{\bullet-} + \mathrm{solvent} \xrightarrow{k_{18}} \mathrm{DMADPh}^{\bullet-} \quad (5.18)$$

$$\mathrm{DMADPh}^{\bullet-} + \mathrm{CrH}^{\bullet+} \xrightarrow{10^{10}\,M^{-1}s^{-1}} \mathbf{5.29} + \mathrm{Cr}\bullet \quad (5.19)$$

$$\mathrm{DMAD}^{\bullet-} + \mathrm{CrH} \xrightarrow{k_{20}} \mathrm{DMADH}\bullet + \mathrm{Cr}^{-} \quad (5.20)$$

$$\mathrm{Cr}^{-} + \mathrm{CrH}^{\bullet+} \xrightarrow{10^{10}\,M^{-1}s^{-1}} \mathrm{CrH} + \mathrm{Cr}\bullet \quad (5.21)$$

$$\mathrm{DMADH}\bullet + \mathrm{CrH} \xrightarrow{10^{9}\,M^{-1}s^{-1}} \mathbf{5.30} + \mathrm{Cr}\bullet \quad (5.22)$$

$$\mathrm{DMADH}\bullet + \mathrm{CrH} \xrightarrow{2.5x10^{8}\,M^{-1}s^{-1}} \mathbf{5.31} + \mathrm{Cr}\bullet \quad (5.23)$$

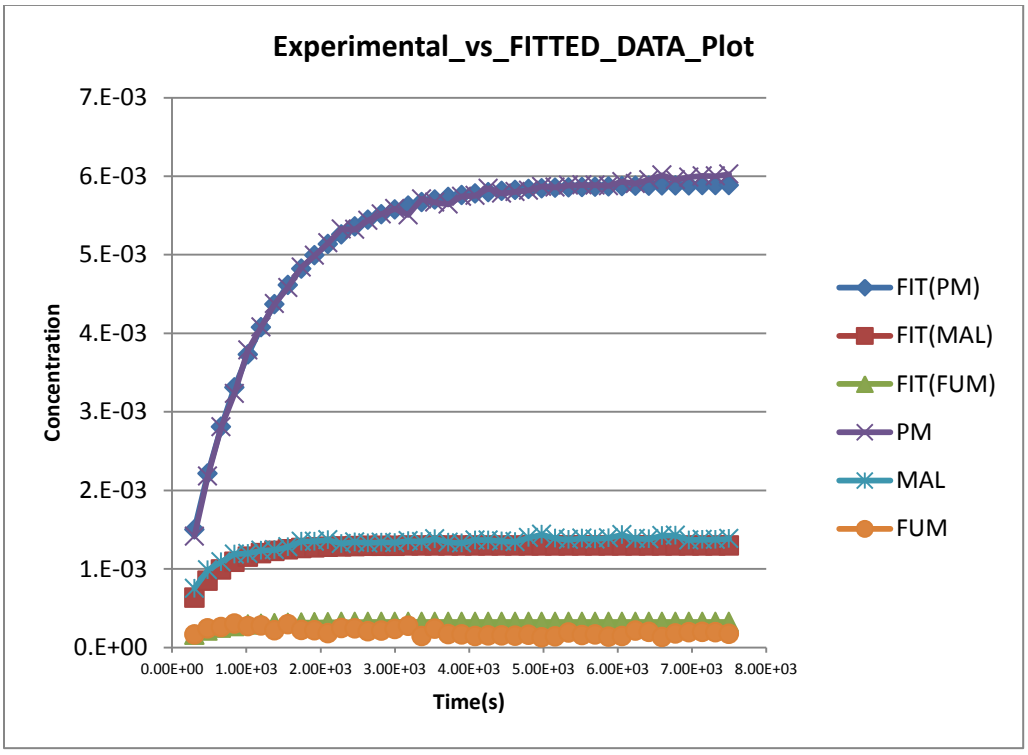

The initial reaction is probably formation of an ion pair **5.32**:**5.33** (Tilset and Parker observed an irreversible two electron oxidation potential for $CpCr(CO)_3H$ at 0.633 V vs Fc/Fc^+ and found that the cation **5.32** is very acidic.[38]) After escape, the free radical anion **5.33** will react with either benzene, Cr–H, or DMAD (the three predominant species in solution). With benzene, **5.33** will give **5.35** and eventually **5.29**. With Cr–H**, 5.33** will be protonated to the vinyl radical **5.34** (presumably nonlinear, cf. the radical from methyl propiolate above). With DMAD, **5.33** will give oligomers (vide infra).

There is literature precedent for the attack of anion radicals ($SO_4^{\bullet-}$,[39-41] $HPO_4^{\bullet-}$,[42] and $O^{\bullet-}$[40]) on aromatics (including benzene), and for the formation of oligomers from **5.33** and DMAD.[43] Electron transfer from inorganic reductants like iodide and thiocyanate has been observed to be 2000 times faster to DMAD than to methyl propiolate.[43] Irreversible reduction potentials[44] are available for many alkynes, although they do not tell us the thermodynamics of electron transfer to these alkynes. A plot of these irreversible potentials vs the rate constants k_H (Figure 5.4) offers a strong argument for a change in mechanism between phenylacetylene and DMAD.

Since the electron transfer from Cr−H to DMAD is quite endergonic, the barrier to electron transfer is largely determined by the thermodynamics of the reaction. The rate constant k_H measured for DMAD would correspond to a barrier height of 22 kcal/mol and an electrochemical potential difference of 0.95 V. The irreversible potentials for $CrH/CrH^{\bullet+}$ (0.633 V) and $DMAD/DMAD^{\bullet-}$ (−0.80 V) would cause a barrier of 37 kcal/mol. However, the overpotentials caused by irreversibility, changes in solvation energy, and junction potentials will cause this calculated barrier to be artificially high, shifting the peaks away from each other. If

each of the electrochemical events had overpotentials of 200 mV, the calculated reaction barrier (27 kcal/mol) would be close to that obtained in my experiment.

Table 5.2. Summary of reactions of alkynes with Cr–H

Alkyne	$k_H(\times 10^3)(M^{-1}s^{-1})$	Cis:Trans
Ph—	2.5(± 0.1)	1
CO_2Me—	0.32(± 0.03)	1.4
Ph— —Ph	0.14(± 0.03)	—
MeO_2C— —CO_2Me	9.9(± 2)	4

Figure 5.4. Rate Constants (k_H) vs. Alkyne Reduction Potential

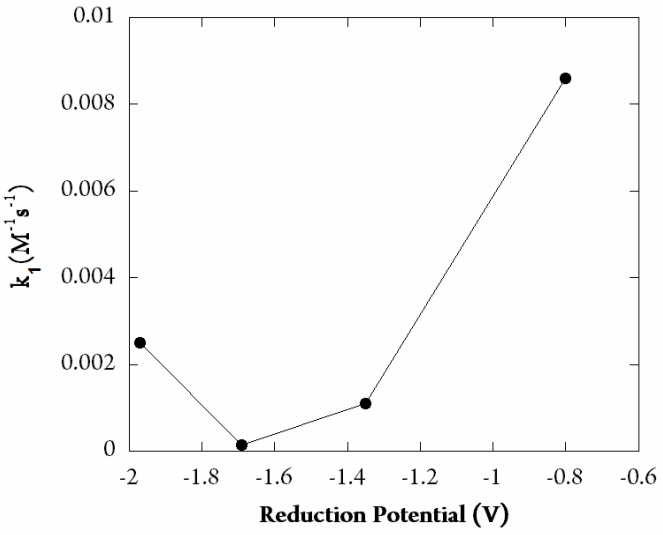

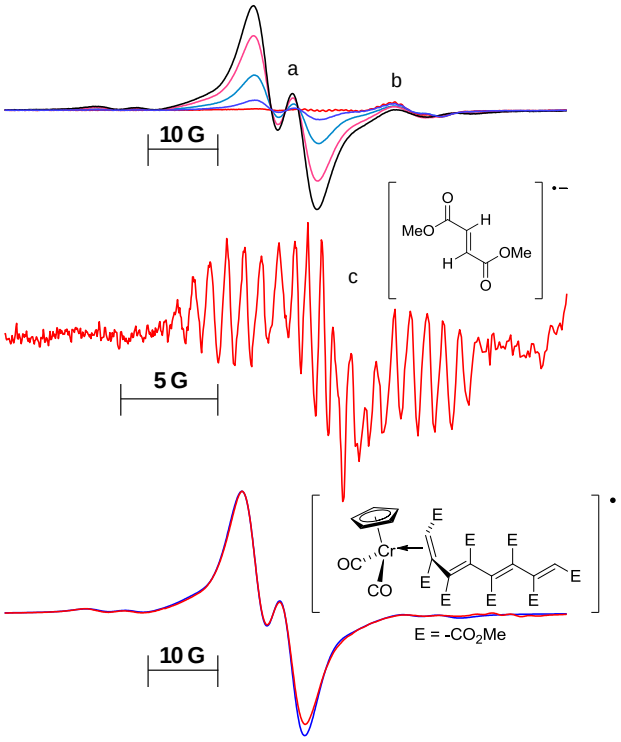

Figure 5.5: EPR spectra from reaction of DMAD with Cr–H. (top) Stacked spectra over time; (middle) Signal attributed to the fumarate radical anion (obtained by scaled subtraction of other signals); (bottom) Doublet signal attributed to the oligomer spin adduct (Simulation in blue)

In order to further study the reaction of DMAD with Cr–H, we followed the reaction by EPR spectroscopy at room temperature. The EPR spectra produced during the course of the reaction are shown in figure 5.5 as a function of time. The first signal to appear (radical c) is a triplet of septets (a_1 = 1.0 G (6H), a_2 = 5.4 G (2H) Figure 5.5(middle)) which has a g value of 2.0044. When the reaction is run with Cr–D, the larger (triplet) coupling disappears. When the methyl esters are replaced with tBu esters the septet coupling disappears. These data match the EPR spectrum of the dimethyl fumarate radical anion, previously reported in liquid ammonia at −50 °C.[45-46] Observation of the dimethyl fumarate radical anion supports our claim that electron transfer from Cr–H to electron poor alkenes and alkynes is possible. This signal is not observed

when Cr–H reacts directly with dimethyl fumarate. The mechanism above involves formation of $[CpCr(CO)_3]^-$ which may be the reductant that makes the dimethyl fumarate radical anion.

Two more major EPR signals appear over the course of the reaction. The first (signal b) is a broad singlet with g value of 1.9990 whose appearance coincides with the disappearance of the fumarate radical anion. The second (signal a) is a broad doublet with g value 2.0093 which persists after the reaction is over. This second signal shows coupling to one proton (which disappears when reaction is run with Cr–D) and satellites due to coupling to one chromium atom (^{53}Cr I = 3/2, 9.55% abundance). Appearance of this radical coincides with disappearance of the previous radical. Simulated parameters for all Cr centered radicals are given in Table 5.3.

$CpCr(CO)_3$• (**5.28**) is known to form complexes (so called "spin adducts") with alkenes under ambient conditions (probably by substitution of CO) that have similar ^{53}Cr coupling and g values to that of both these radicals.[47] Assignment of signals a and b as “spin adducts” makes sense given the amount of **5.28** which is being produced in this reaction. However, spin adducts with **5.29**, **5.30**, and **5.31** do not match the observed spectra (see Table 5.3).

The assignment of signal b as a spin adduct with solvent, similar to the one seen with toluene,[47] is tentative but reasonable. Oligomer could displace benzene to create the final signal. Since only one of the double bonds could be coordinated at a time coordinating to an end group of the oligomer would give rise to a doublet due to coupling with only one vinyl proton. This signal was reproduced with low intensity from a mixture of **5.28** with DMAD laced with a trace of the oligomer. Under the conditions of the EPR experiment (1.35M DMAD), oligomers are one of the major products and thus more likely to form a spin adduct with **5.28**.

Table 5.3. Spin adducts of $CpCr(CO)_3$• with Alkenes

Alkene	g[a]	a_H (G)	a_{Cr}(G)
Signal a	2.0093	4.95 (d)	14.85
Signal b[b]	1.9990	—	—
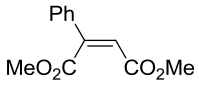	2.0095	6.60 (d)	14.45
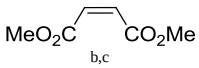	—	5.1 (t)	—
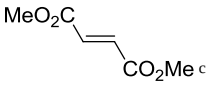	—	4.6 (t)	14.7

(a) Referenced to TEMPO.[48] (b) ^{53}Cr satellites were too low in intensity to obtain an accurate *a* value. (c) Since their multiplicity automatically ruled them out as candidates for the identity of c and d, their *g* value was not determined.

5.3 Experimental Details

All manipulations were performed under an argon atmosphere using standard Schlenk or inert atmosphere box techniques. NMR spectra were taken on either a Bruker 300, 400, or 500 MHz spectrometer. IR spectra were taken with a Perkin-Elmer Spectrum 2000 FT-IR spectrometer. Gas chromatography was performed on a HP-5890A gas chromatograph utilizing a DB-5 column with He as the carrier gas. X-ray diffraction data were collected on a Bruker Apex II diffractometer. Crystal data, data collection and refinement parameters are summarized in Appendix IV. The structures were solved using direct methods and standard difference map techniques, and were refined by full matrix least squares procedures on F^2 with SHELXTL (Version 6.1).[49-50] Benzene and THF were distilled from Na/benzophenone ketyl and stored over

3 Å molecular sieves. Benzene-d_6 (Cambridge Isotope Laboratories) was dried by distillation from CaH_2 and then deoxygenated by three freeze-pump-thaw cycles. All other liquids were dried by distillation from CaH_2 and then deoxygenated by three freeze-pump-thaw cycles and stored under an argon atmosphere. Phenylacetylene, phenylacetylene-d_1, methyl propiolate, diphenylacetylene, dimethyl acetylenedicarboxylate, and di-^{t}butyl acetylenedicarboxylate were purchased from commercial sources.

Materials. $CpCr(CO)_3H$ and $CpCr(CO)_3D$ were synthesized by known procedures and sublimed prior to use.[51] Methyl propiolate-d_1[52], dimethylphenylmaleate,[53] and **2.25**[54] were also synthesized by literature procedures.

(3-(2-Ethynylphenyl)prop-1-ene-1,1-diyl)dibenzene **(5.20)**. To a solution of 2-bromo-phenylethynyltrimethylsilane (1.58 mmol) in THF (16 mL) was added ^{n}BuLi (1.74 mmol, 1.1 eq) at -78 °C and stirred for twenty min. CuCN (71 mg, 0.79 mmol) was then added to the solution and the temperature raised to -20 °C for twenty minutes, after which time the solution turned from yellow to pale pink. The solution was returned to -78 °C, and 3-bromo-1,1-diphenyl-prop-1-ene (431 mg, 1.58 mmol in 1 mL THF) was added dropwise, and the mixture was brought to room temperature slowly and stirred overnight. The reaction was quenched with NH_4Cl, extracted with ether (50 mL, 3 times), and dried with $MgSO_4$. The solvent was removed in vacuo.

To this crude mixture, in 5 mL of 10:1 THF:H_2O, was added dropwise a solution of 0.45 g tetrabutylammonium fluoride dissolved in 2 mL of the same solvent mixture at 0 °C. The reaction was stirred for 12 hours and worked up in the same manner as before. The product was then isolated (clear oil, 199 mg, 43% yield) from a silica column, using a 4% toluene in hexane

mixture as the mobile phase (R_f = 0.19). ^{1}H NMR (300 MHz, $CDCl_3$, δ), 7.49-7.13 (m, 14H, ArH), 6.27 (t (*J* = 7.5 Hz), 1H, =C-H), 3.66 (d (*J* = 7.5 Hz), 2H, CH_2) 3.19 (s, 1H, ≡C-H). ^{13}C NMR (100 MHz, $CDCl_3$, δ) 143, 142.7, 142.4, 139.8, 132.9, 130.0, 129.0, 128.6, 128.3, 128.1, 127.4, 127.1, 127.04, 127.00, 126.0, 121.6, 82.2, 81.3, 34.5 ppm. IR (neat) 3293 (≡C-H stretch), 2104 (C≡C stretch), 1598 (ring stretch), 700 (≡C-H bend). MS (APCI) 295 $[M+1]^+$.

Procedure for Cyclizations. *Caution! All reactions under gas pressure should be properly shielded!* A solution of (3-(2-ethynylphenyl)prop-1-ene-1,1-diyl)dibenzene **(5.20)** (0.187 mmol) and $CpCr(CO)_3H$ (0.014 mmol) in benzene (0.5 mL) was added to a Fischer-Porter reactor that was subsequently charged with an appropriate pressure of H_2. This reaction was then heated with vigorous stirring until the reaction was over; the green color changed to brown, then to green once the starting material had been consumed (no color change was observed with **1.34**). Solvent was then removed in vacuo, and catalyst removed by filtration through silica plug to yield a crude mixture of products. Compound **5.23** was identified by comparison to an authentic sample synthesized by a method similar to **5.20**. Compounds **5.22** and **5.24** were nearly inseparable from each other and both were inseparable from grease. Compound **5.22** was purified by preparative TLC; only the bottom part of the overlapping bands was taken (20% toluene/hexane). Compound **5.24** was purified on a silica column using a solvent gradient (0 - 6% Toluene in hexane) and combining the first few fractions. Purification of **5.22** and **5.24** could also be accomplished by Semi-prep HPLC (C18 - (CH_3CN: H_2O) Gradient 10 – 80% CH_3CN over 80 minutes; retention time: (**5.22**) = 62.0 min (**5.24**) = 64.2 min). Column shedding contaminated the products with a considerable amount of grease.

***2-Benzhydryl-3-methyl-1H-indene* (5.22)**. ^{1}H NMR (300 MHz, $CDCl_3$, δ) 7.30-7.16 (m, 14H, ArH), 5.53 (s, 1H, CPh_2H), 3.19 (q (*J* = 1.9 Hz), 2H, CH_2), 2.08 (t (*J* = 1.9 Hz), 3H, CH_3)

(long range coupling confirmed by COSY). ^{13}C NMR (75 MHz, $CDCl_3$) 146.9, 143.75, 143.0, 135.2, 129.2, 128.4, 128.0, 126.4, 124.4, 123.4, 118.8, 50.2, 39.8, 10.8 IR (neat) 3056, 3024 (sp^2 C-H stretch), 2962, 2918(sp^3 C-H stretch) cm^{-1} MS (APCI) 167 $[CH(Ph)_2]^+$, 295 $[M-1]^+$, 329 $[M+MeOH_2]^+$.

(3-(2-Ethynylphenyl)prop-1-ene-1,1-diyl)dibenzene **(5.23)**. ^{1}H NMR (300 MHz, $CDCl_3$, δ) 7.41 - 7.16 (m, 14H, ArH), 6.20 (t (*J* = 7.5 Hz), 1H, =C-H), 3.47 (d (*J* = 7.5 Hz), 2H, **CH_2**-CH=), 2.54 (q (*J* = 7.5 Hz), 2H, **CH_2**-CH_3), 1.12 (t (*J* = 7.5 Hz), 3H, CH_3). ^{13}C NMR (100 MHz, $CDCl_3$, δ) 142.50, 142.25, 142.19, 139.88, 138.59, 129.90, 129.04, 128.40, 128.28, 128.12, 127.96, 127.36, 127.17, 127.02, 126.40, 125.99, 33.12, 25.70, 14.96. IR (neat) 3060, 3023 (sp^2 C-H stretch), 2962, 2922, 2852 (sp^3 C-H stretch), MS (APCI) 299 [M+1].

2-(Diphenylmethylene)-1-methyl-2,3-dihydro-1H-indene **(5.24)**. ^{1}H NMR (300 MHz, $CDCl_3$, δ) 7.37-7.14 (m, 14H, ArH), 4.14 (q (*J* = 7.0 Hz), 1H, C-H), 3.81 (AB system (*J* = 21 Hz, Δν = 263.7 Hz), 2H, inequivalent CH_2 pair) 1.08 (d (*J* = 7.0 Hz), 3H, CH_3). ^{13}C NMR (125 MHz, $CDCl_3$, δ) 147.6, 144.3, 143.0, 142.5, 141.1, 136.3, 129.5, 129.0, 128.5, 128.2, 126.71, 127.66, 126.60, 124.4, 123.8, 43.6, 37.9, 21.4 IR (neat) 3079, 3056, 3020 (sp^2 C-H stretch), 2962, 2922, 2860 (sp^3 C-H stretch) cm^{-1}. MS (FAB) 295 [M-1]

Isolation and characterization of (6-methyl-6-phenylfulvene)Cr(CO)$_3$ **(5.15).** A stoichiometric mixture of phenylacetylene and $CpCr(CO)_3H$ was heated in benzene at 50°C until the color turned from green to brown. The product was crystallized by vapor diffusion of pentane into a solution of the mixture in dichloromethane to yield red air-stable crystals of the fulvene complex. These crystals were then studied by X-ray diffraction. ^{1}H NMR (500 MHz, C_6D_6, δ) 7.31 (s, 2H, PhH), 7.00 (s, 3H, PhH) 4.68 (s, 1H, CpH) 4.57 (s, 1H, CpH), 4.25 (s, 1H, CpH),

4.06 (s, 1H, CpH), 1.84 (s, 3H, CH_3). CCDC 886281 contains the supplementary crystallographic data for **5.15**. These data can be obtained free of charge from The Cambridge Crystallographic Data Centre via http://www.ccdc.cam.ac.uk/data_request/cif. X-ray structural parameters are in Appendix IV:

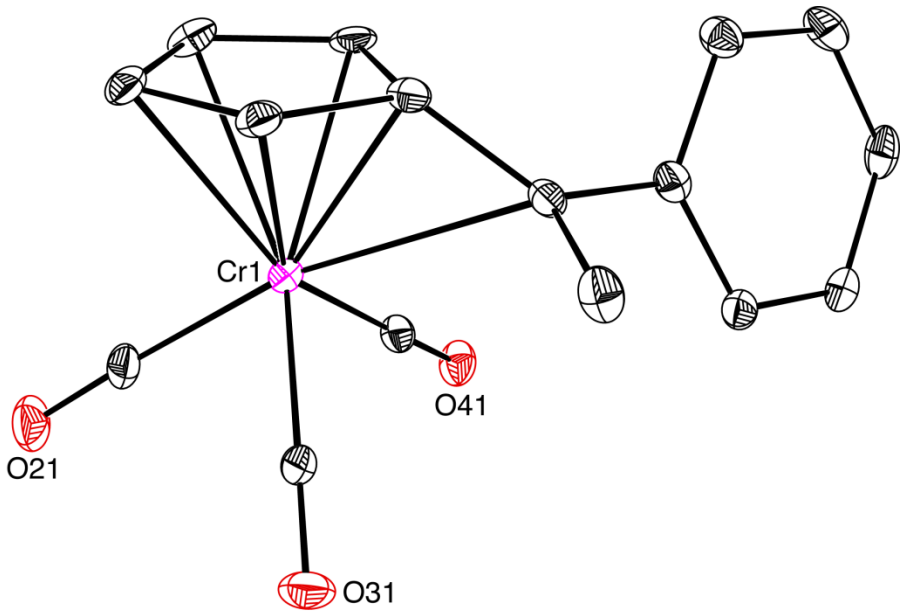

Too little material was isolated to fully characterize this complex. The ^{1}H NMR spectrum was matched to that of an authentic sample of the compound made by stirring 100 mg of tris(acetonitrile)tricarbonylchromium with 65 mg of 6-methyl-6-phenylfulvene in 7 mL of THF overnight. The solvent was then removed in vacuo and dark red crystals obtained by dissolving in a minimal amount (1 mL) of pentane and letting stand at room temperature for 10 min. This compound was incorrectly characterized in the literature previously.[55]

^{1}H NMR (300 MHz, $CDCl_3$, δ) 7.45-7.31 (m, 5H, PhH), 5.44 (s, 1H, CpH), 5.34 (s, 1H, CpH), 4.75 (s, 1H, CpH), 4.70 (s, 1H, CpH), 2.26 (s, 3H, CH_3). ^{1}H NMR (300 MHz, C_6D_6, δ)

7.106 - 7.00 (m, 5H, PhH), 4.69 (s, 1H, CpH), 4.58 (s, 1H, CpH), 4.25 (s, 1H, CpH), 4.07 (s, 1H, CpH), 1.85 (s, 3H, CH_3). ^{13}C NMR (125 MHz, $CDCl_3$, δ) 237.8, 141.7, 128.49, 128.40, 128.23, 123.6, 105.0, 93.6, 93.5, 89.4, 88.1, 25.7. IR (CH_3CN) ν_{CO} = 1978, 1897 cm^{-1} MS (FAB) 304 $[M]^+$, 276 $[M\text{-}CO]^+$, 248 $[M\text{-}2CO]^+$. Anal: $C_{16}H_{12}CrO_3$ Calc. 63.16 % C, 3.98 % H: Found 63.42 % C, 4.10 % H.

Kinetic measurements. Stock solutions (C_6D_6) of both $CpCr(CO)_3H$ and the appropriate alkyne were added separately to a J-Young NMR tube and frozen in two layers with concentrations appropriate to achieve a 10–fold excess of alkyne. At the beginning of the experiment it was quickly melted, mixed, and inserted into the probe of a 500 MHz NMR spectrometer preequilibrated to 50.0 (±0.5)°C (using an ethylene glycol chemical shift thermometer). Spectra were taken every 3 minutes and the intensity of the hydride resonance (δ −5.6 ppm) was compared with that of an internal standard (hexamethylcyclotrisiloxane). Reactions were monitored through at least three half-lives and fit to a first–order exponential. The product peaks from the reaction with DMAD were fit to the model in Scheme 10 using Kintecus kinetic modeling software.[36] Reported rate constants other than that for phenylacetylene are the average of those from three kinetic runs.

EPR measurements. X-band EPR spectra were taken on a Bruker EMX spectrometer at ambient temperature in benzene in 5 mm J-Young style tubes (concentrations of organic reactants were ≈ 1M). *g* values were calculated by comparison with an internal sample of TEMPO (g = 2.00623).[48] EPR simulations were done with Bruker's Simphonia software.[56] EPR spectra not included in the text can be found in Appendix IV.

5.4 Refences

1. Foo, T.; Bergman, R. G., Migratory insertion reactions of indenyliridium dialkyls and alkyl and aryl hydrides. *Organometallics* **1992,** *11*, 1811-1819.

2. Roddick, D. M.; Fryzuk, M. D.; Seidler, P. F.; Hillhouse, G. L.; Bercaw, J. E., Halide, hydride, alkyl, and dinitrogen complexes of bis(pentamethylcyclopentadienyl)hafnium. *Organometallics* **1985,** *4*, 97-104.

3. Frohnapfel, D. S.; White, P. S.; Templeton, J. L., Insertion Products from Photolysis of Tp‘(CO)3WH and Alkynes. *Organometallics* **2000,** *19*, 1497-1506.

4. Bassetti, M.; Casellato, P.; Gamasa, M. P.; Gimeno, J.; González-Bernardo, C.; Martín-Vaca, B., Insertion Reactions of Alkynes into the Ru−H Bond of Indenylruthenium(II) Hydride Complexes. Mechanism of the Reaction of Phenylacetylene with [RuH(η5-C9H7)(dppm)] (dppm = Bis(diphenylphosphino)methane). *Organometallics* **1997,** *16*, 5470-5477.

5. Clark, H. C.; Wong, C. S., Free-radical Participation in the Insertion Reaction of Acetylene with Platinum Hydride. *J. Am. Chem. Soc.* **1977,** *99*, 7073-7074.

6. Clark, H. C.; Ferguson, G.; Goel, A. B.; Janzen, E. G.; Ruegger, H.; Siew, P. Y.; Wong, C. S., Chemistry of Metal Hydrides. 27. Kinetic and ESR Studies of Acetylene Insertion Reactions with Platinum(II) Dihydrides and the Crystal Structure Determination of *trans*-PtH[P-*t*-Bu_2-*n*-Bu]$_2$($CH_3O_2CC{=}CHCO_2CH_3$). *J. Am. Chem. Soc.* **1986,** *108*, 6961-6972.

7. Trost, B. M.; Ball, Z. T.; Jöge, T., A Chemoselective Reduction of Alkynes to (E)-Alkenes. *J. Am. Chem. Soc.* **2002,** *124*, 7922-7923.

8. Tanke, R. S.; Crabtree, R. H., Unusual activity and selectivity in alkyne hydrosilylation with an iridium catalyst stabilized by an oxygen-donor ligand. *J. Am. Chem. Soc.* **1990,** *112*, 7984-7989.

9. Nakamura, A.; Otsuka, S., Reactions of transition—metal dihydrides VI. Stereochemistry of the insertion of substituted acetylenes into the metal-hydrogen bond in dihydrido- bis(η-cyclopentadienyl)-molybdenum and -tungsten. *J. Mol. Catal.* **1976,** *1*, 285-307.

10. Herberich, G. E.; Barlage, W., Trans insertion of activated, symmetrically disubstituted acetylenes into the metal-hydrogen bond of bis(cyclopentadienyl)metal hydrides of rhenium, tungsten, and molybdenum. *Organometallics* **1987,** *6*, 1924-1930.

11. Selmeczy, A. D.; Jones, W. D., Insertions of electrophiles into metal hydride bonds. Reactions of (C5Me5)Rh(PMe3)H2 with activated alkynes to produce η2-alkene complexes. *Inorg. Chim. Acta* **2000,** *300-302*, 138-150.

12. Gridnev, A. A.; Ittel, S. D.; Wayland, B. B.; Fryd, M., Isotopic Investigation of Hydrogen Transfer Related to Cobalt-Catalyzed Free-Radical Chain Transfer. *Organometallics* **1996,** *15*, 5116-5126.

13. Bockman, T. M.; Garst, J. F.; Ungváry, F., Reaction of Cobalt Tetracarbonyl Hydride with Phenylacetylene. *J. Organomet. Chem.* **1999,** *586*, 41-47.

14. Nakamaura, A.; Otsuka, S., Reaction of transition metal dihydrides. I. Insertion and substitution at the metal-hydride bonds in dihydridobis(.pi.-cyclopentadienyl)molybdenum. *J. Am. Chem. Soc.* **1972,** *94*, 1886-1894.

15. Huggins, J. M.; Bergman, R. G., Mechanism, regiochemistry, and stereochemistry of the insertion reaction of alkynes with methyl(2,4-pentanedionato)(triphenylphosphine)nickel. A cis insertion that leads to trans kinetic products. *J. Am. Chem. Soc.* **1981,** *103*, 3002-3011.

16. Allen, S. R.; Beevor, R. G.; Green, M.; Norman, N. C.; Orpen, A. G.; Williams, I. D., Reactions of co-ordinated ligands. Part 33. Mononuclear [small eta]2-vinyl complexes: synthesis, structure, and reactivity. *J. Chem. Soc., Dalton Trans.* **1985**, 435-450.

17. Sudo, T.; Asao, N.; Gevorgyan, V.; Yamamoto, Y., Lewis Acid Catalyzed Highly Regio- and Stereocontrolled Trans-Hydrosilylation of Alkynes and Allenes. *J. Org. Chem.* **1999,** *64*, 2494-2499.

18. Smith, M. B.; March, J., *March's Advanced Organic Chemistry: Reactions, Mechanisms, and Structure*. 6th ed.; John Wiley & Sons, Inc.: Hoboken, NJ, 2007.

19. Huang, M.-B.; Liu, Y., The Trans-Bent Structures of the Acetylene and Methylacetylene Radical Anions. *J. Phys. Chem. A* **2001,** *105*, 923-929.

20. Alabugin, I. V.; Gilmore, K.; Manoharan, M., Rules for Anionic and Radical Ring Closure of Alkynes. *J. Am. Chem. Soc.* **2011,** *133*, 12608-12623.

21. Luo, Y.-R., *Handbook of bond dissociation energies in organic compounds*. CRC Press: Boca Raton, Florida, 2002; p 380.

22. Lide, D. R., *CRC Handbook of Chemistry and Physics*. 87th Edition ed.; CRC Taylor and Francis: Boca Raton, FL, 2006.

23. Fischer, H.; Radom, L., Factors Controlling the Addition of Carbon-Centered Radicals to Alkenes—An Experimental and Theoretical Perspective. *Angew. Chem., Int. Ed.* **2001,** *40*, 1340-1371.

24. Pross, A., *Theoretical and Physical Principles of Organic Reactivity*. Wiley-Interscience: New York, NY, 1995.

25. Gleiter, R.; Bleiholder, C.; Rominger, F., α-Metallocenylmethylium Ions and Isoelectronic Fulvene Complexes of d6 to d9 Metals. Structural Considerations§. *Organometallics* **2007,** *26*, 4850-4859.

26. Korth, H.-G.; Lusztyk, J.; Ingold, K. U., Electron Paramagnetic Resonance Spectroscopic Study of the Radicals Formed During the Photodecomposition of some bis(alkenoyl)peroxides, a bis(alkenoyl)peroxide and Some Peroxydicarbonates. *J. Chem. Soc., Perkin Trans. 2* **1990**, 1997-2007.

27. Rhodes, C. J.; Roduner, E., Muonated Radicals formed from Phenyl- and Silyl-Substituted Acetylenes. *J. Chem. Soc., Perkin. Trans. 2* **1990**, 1729-1733.

28. Choi, J.; Tang, L.; Norton, J. R., Kinetics of Hydrogen Atom Transfer from (η^5-C_5H_5)$Cr(CO)_3H$ to Various Olefins: Influence of Olefin Structure. *J. Am. Chem. Soc.* **2007,** *129*, 234-240.

29. Li, G.; Han, A.; Pulling, M. E.; Estes, D. P.; Norton, J. R., Evidence for Formation of a Co-H Bond from $(H_2O)_2Co(dmgBF_2)_2$ under H_2. Application to Radical Cyclizations. *J. Am. Chem. Soc.* **2012,** *134*, 14662-14665.

30. Fischer, G.; Muszkat, K. A.; Fischer, E., The thermodynamic equilibrium between cis- and trans-isomers in stilbene and some derivatives. *J. Chem. Soc. B., Phys. Org.* **1968**, 1156-1158.

31. McLain, S. J., Equilibrium between $[CpCr(CO)_3]_2$ and $CpCr(CO)_3$. Thermodynamics of chromium-chromium single-bond cleavage. *J. Am. Chem. Soc.* **1988,** *110*, 643-644.

32. Mawson, S. D.; Routledge, A.; Weavers, R. T., Iodomethylene lactone formation An improved synthesis. *Tetrahedron* **1995,** *51*, 4665-4678.

33. Montevecchi, P. C.; Navacchia, M. L., Substituent Effects on Vinyl Radical Cyclizations onto Aryl Rings. *J. Org. Chem.* **1998,** *63*, 537-542.

34. Fessenden, R. W.; Eiben, K., Electron spin resonance studies of transient radicals in aqueous solutions. *J. Phys. Chem.* **1971,** *75*, 1186-1201.

35. Chamberlain, G. A.; Whittle, E., Reactions of CF3 radicals with aromatics. Part 4.-Hydrogen abstraction from benzene at high temperatures and the bond dissociation energy D(C6H5-H). *Transactions of the Faraday Society* **1971,** *67*, 2077-2084.

36. Ianni, J. C. *Kintecus*, Windows Version 4.00; www.kintecus.com: 2010.

37. Franz, J. A.; Linehan, J. C.; Birnbaum, J. C.; Hicks, K. W.; Alnajjar, M. S., Absolute Rate Expressions for Hydrogen Atom Abstraction from Molybdenum Hydrides by Carbon-Centered Radicals. *J. Am. Chem. Soc.* **1999,** *121*, 9824–9830.

38. Ryan, O. B.; Tilset, M.; Parker, V. D., Chemical and Electrochemical Oxidation of Group 6 Cyclopentadienyl Metal Hydrides. *J. Am. Chem. Soc.* **1990,** *112*, 2618-2626.

39. Merga, G.; Aravindakumar, C. T.; Rao, B. S. M.; Mohan, H.; Mittal, J. P., Pulse radiolysis study of the reactions of SO with some substituted benzenes in aqueous solution. *J. Chem. Soc., Faraday Trans.* **1994,** *90*, 597-604.

40. Sharma, S. B.; Mudaliar, M.; Rao, B. S. M.; Mohan, H.; Mittal, J. P., Radiation Chemical Oxidation of Benzaldehyde, Acetophenone, and Benzophenone. *J. Phys. Chem. A* **1997,** *101*, 8402-8408.

41. Steenken, S., One-electron redox reactions between radicals and organic molecules. An addition/elimination (inner-sphere) path [1]

Electron Transfer II. Mattay, J., Ed. Springer Berlin / Heidelberg: 1996; Vol. 177, pp 125-145.

42. Rosso, J. A.; Caregnato, P.; Mora, V. C.; Gonzalez, M. C.; Mártire, D. O., Reactions of Phosphate Radicals with Monosubstituted Benzenes. A Mechanistic Investigation. *Helv. Chim. Acta* **2003,** *86*, 2509-2524.

43. Dvorko, G. F.; Shilov, A. E., Electron transfer to a carbon triple bond. *Theor. Exp. Chem.* **1970,** *3*, 364-368.

44. Utley, J. H. P.; Lines, R., The Electrochemistry of the Carbon–Carbon Triple bond. In *The Carbon–Carbon Triple Bond (1978)*, John Wiley & Sons, Ltd.: 2010; pp 739-753.

45. Elson, I. H.; Kemp, T. J.; Greatorex, D.; Jenkins, H. D. B., Electron Spin Resonance Studies of Reduction by Solvated Electrons in Liquid Ammonia. Part 7. α,β-Unsaturated Carboxylic Acids, Esters and Nitriles. *J. Chem. Soc., Faraday Trans. 2* **1973,** *69*, 1402-1415.

46. Nelsen, S.; Gillespie, J., Conformations of the Radical Anions from Dialkyl Maleates and Fumarates. *J. Org. Chem.* **1975,** *40*, 2391-2394.

47. Sokolov, V. I.; Gasanov, R. G.; Goh, L. Y.; Weng, Z.; Chistyakov, A. L.; Stankevich, I. V., (Cyclopentadienyl)chromiumtricarbonyl dimers as a source of metal-centered free-radicals to form stable η2-bonded spin-adducts with fullerenes. *J. Organomet. Chem.* **2005,** *690*, 2333-2338.

48. Rockenbauer, A.; Gyor, M.; Hideg, K.; Hankovszky, H. O., Investigation of naturally abundant 17O hyperfine satellites in the electron spin resonance spectrum of 5- and 6-membered cyclic nitroxide (aminoxyl) radicals. *J. Chem. Soc., Chem. Commun.* **1985**, 1651-1653.

49. Sheldrick, G. M. *SHELXTL, An Integrated System for Solving, Refining, and Displaying Crystal Structures from Diffraction Data*, University of Gottingen: Gottingen, 1981.

50. Sheldrick, G., A short history of SHELX. *Acta Crystallogr., Sect. A: Found. Crystallogr.* **2008,** *64*, 112-122.

51. Choi, J.; Tang, L. H.; Norton, J. R., Kinetics of hydrogen atom transfer from (eta(5)-C5H5)Cr(CO)(3)H to various olefins: Influence of olefin structure. *J. Am. Chem. Soc.* **2007,** *129*, 234-240.

52. Švenda, J.; Myers, A. G., Anti-Selective Epoxidation of Methyl α-Methylene-β-tert-butyldimethylsilyloxycarboxylate Esters. Evidence for Stereospecific Oxygen Atom Transfer in a Nucleophilic Epoxidation Process. *Org. Lett.* **2009,** *11*, 2437-2440.

53. Zeng, H.; Hua, R., Palladium-Catalyzed Hydrophenylation of Alkynes with Sodium Tetraphenylborate under Mild Conditions. *J. Org. Chem.* **2007,** *73*, 558-562.

54. Bakac, A.; Brynildson, M. E.; Espenson, J. H., Characterization of the structure, properties, and reactivity of a cobalt(II) macrocyclic complex. *Inorg. Chem.* **1986,** *25*, 4108-4114.

55. Edelmann, F.; Wormsbächer, D.; Behrens, U., Übergangsmetall-Fulven-Komplexe, VIII: Photochemische Substitution des Aromaten in (Aromat)Cr(CO)3-Komplexen durch Fulvene. *Chem. Ber.* **1978,** *111*, 817-818.

56. *WINEPR SimFonia*, 1.25; Bruker Analytische Messtechnik GmbH: 1996.

Appendix I. Relevant Spectral Data and Calculations for Chapter 2

Selected IR Spectra.

$CpFe(CO)_2H$ in CH_3CN *(CO stretches marked are within 3 cm^{-1} of the actual maximum value)*

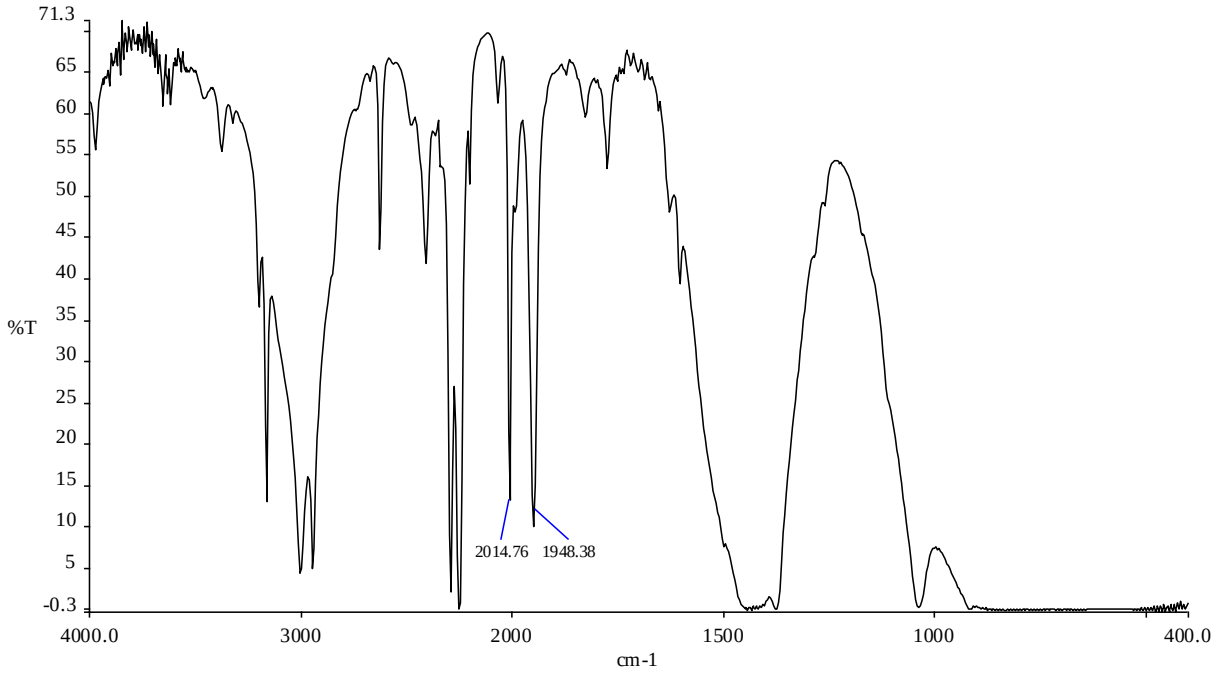

$K[CpFe(CO)_2]$ in CH_3CN

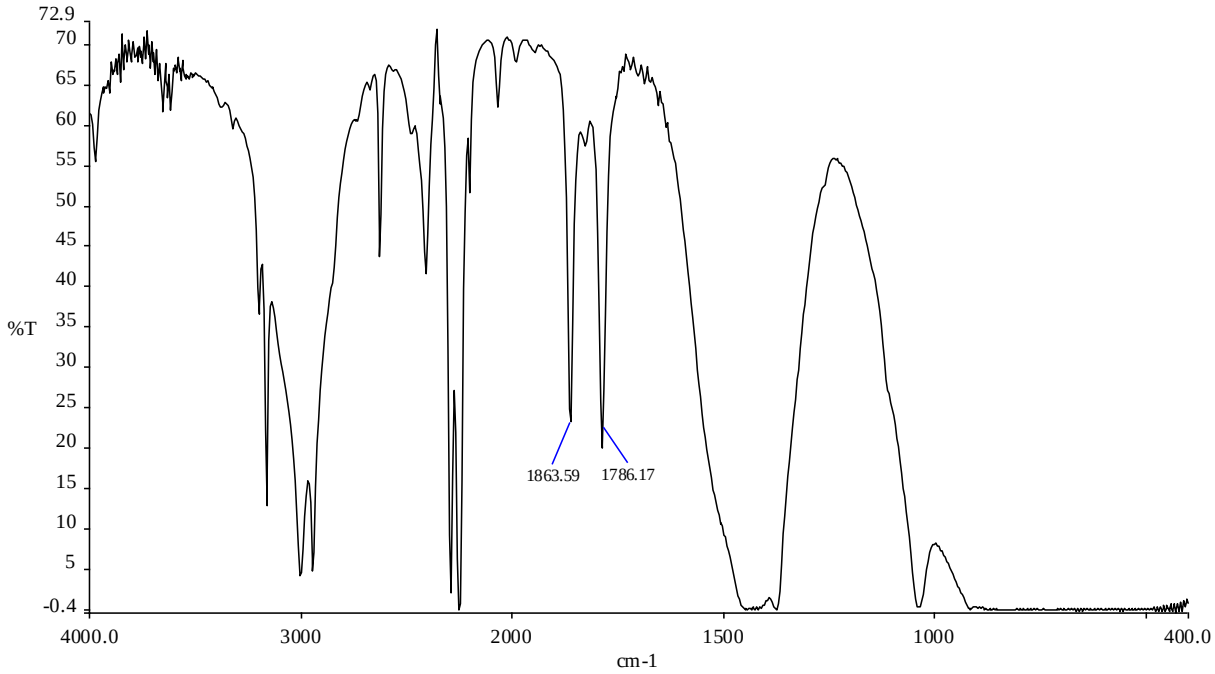

FpH equilibrated with TBD

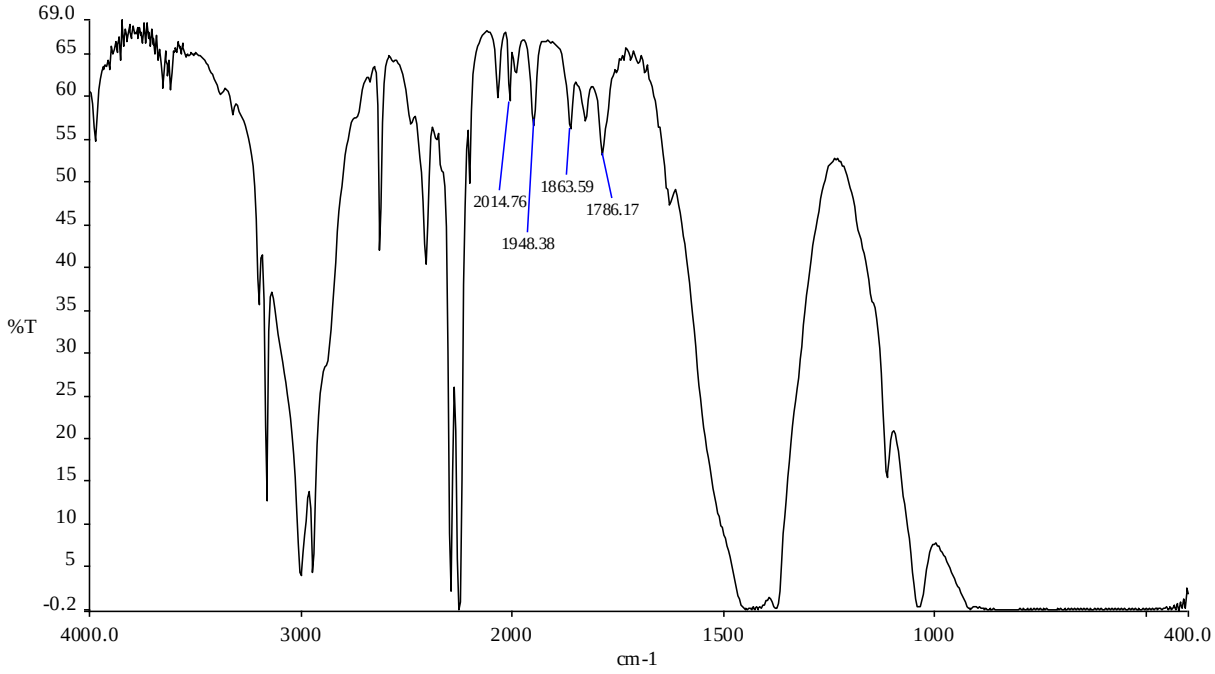

Absorbance vs. Cocentration (Beer's Law) Plots for Exemplary Complexes

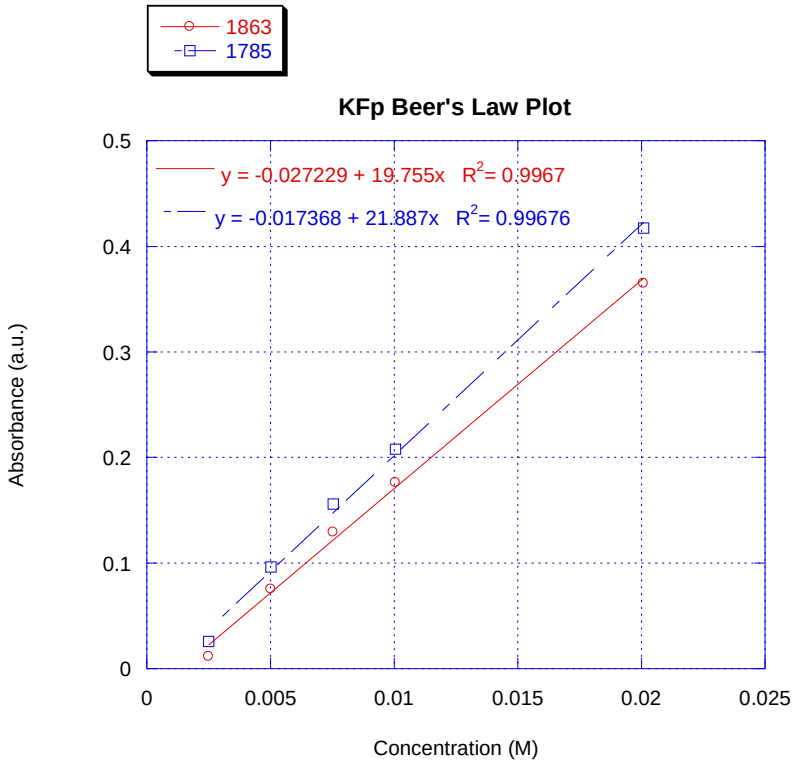

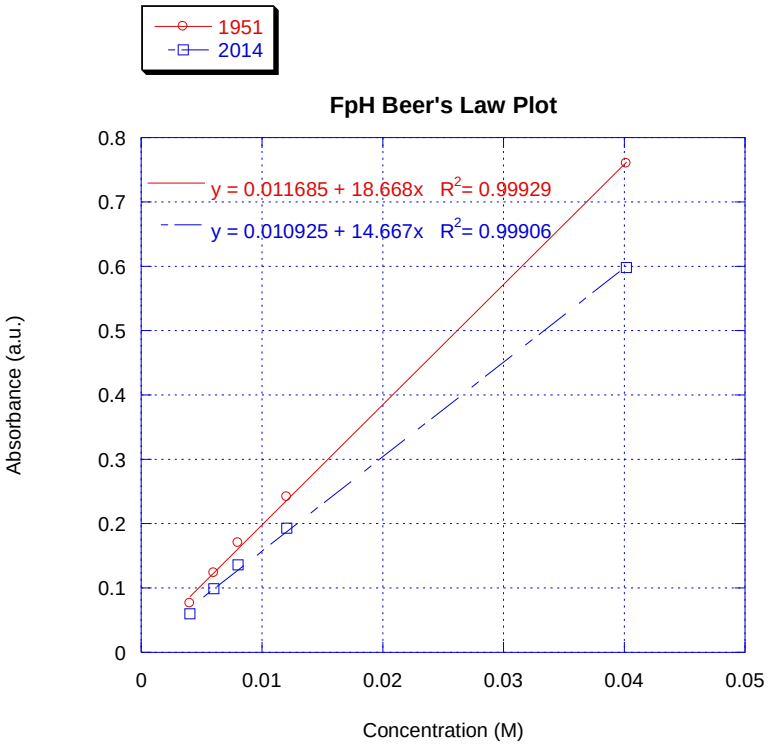
1951
2014
FpH Beer's Law Plot
y = 0.011685 + 18.668x R2= 0.99929
y = 0.010925 + 14.667x R2= 0.99906
Absorbance (a.u.)
Concentration (M)
0
0.1
0.2
0.3
0.4
0.5
0.6
0.7
0.8
0.01
0.02
0.03
0.04
0.05

Appendix II. Selected Spectra and Crystallographic data for Chapter 3

Crystallographic data for complexes **3.1a** and **3.1b**

Compound	**3.1a**	**3.1b**	$[Co(dmgBF_2)_2(H_2O)]_2$
Lattice	Monoclinic	Monoclinic	Hexagonal
Formula	$C_{12}H_{18}B_2CoF_4N_6O_4$	$C_{16}H_{28}B_2CoF_4N_4O_6$	$C_{16}H_{28}B_4CoF_8N_8O_{10}$
Formula Weight	466.87	528.97	746.61
Space Group	$P2_1/c$	$P2_1/c$	P622
a (Å)	8.5877(19)	9.179(8)	18.287(4)
b (Å)	11.747(3)	9.762(8)	18.287(4)
c (Å)	9.730(2)	15.465(10)	9.958(2)
α (°)	90	90	90
β (°)	114.822(3)	126.03(3)	90
γ (°)	90	90	120
V ($Å^3$)	890.9(3)	1120.7(15)	2883.95
Z	2	2	3
Temperature (K)	150(2)	293(2)	283-303
Radiation (λ, Å)	0.71073	0.71073	0.71073
ρ (calc.) (g cm^{-3})	1.740	1.568	1.394
θ max (deg)	31	31.29	30.68
μ (Mo Kα) (mm^{-1})	1.039	0.840	0.951
no. of data collected	14370	17714	45867
no. of data used	2830	3642	3006
no. of parameters	136	151	116
R_1 [I > 2σ(I)]	0.0269	0.0886	0.1151
wR_2 [I > 2σ(I)]	0.0701	0.2670	0.2506
R_1 [all data]	0.0326	0.1736	0.1906
wR_2 [all data]	0.0735	0.3346	0.3231
GOF	1.041	1.047	0.9920

Table 2. Atomic coordinates (× 10^4) and equivalent isotropic displacement parameters (A^2 × 10^3) for **3.1a**. U(eq) is defined as one third of the trace of the orthogonalized Uij tensor.

	x	y	z	U(eq)
Co	0	0	0	14(1)
F(1)	-3212(1)	1708(1)	-4368(1)	26(1)
F(2)	-3875(1)	1298(1)	-2370(1)	26(1)
O(1)	-1128(1)	1932(1)	-1998(1)	19(1)
O(2)	2318(1)	-14(1)	3166(1)	19(1)
N(1)	-212(1)	1542(1)	-561(1)	15(1)
N(2)	1539(1)	606(1)	1863(1)	16(1)
N(3)	-2034(2)	225(1)	880(1)	21(1)
C(1)	692(2)	3521(1)	276(2)	21(1)
C(2)	695(2)	2263(1)	475(1)	16(1)
C(3)	1750(2)	1701(1)	1932(1)	16(1)
C(4)	2936(2)	2349(1)	3273(1)	20(1)
C(5)	-2920(2)	547(1)	1398(1)	19(1)
C(6)	-4069(2)	940(1)	2055(2)	26(1)
B	-2653(2)	1230(1)	-2951(2)	19(1)

Table 3. Bond lengths [A] and angles [^{o}] for **3.1a**.

Co-N(1)	1.8779(11)
Co-N(1)	1.8779(11)
Co-N(2)	1.8784(10)
Co-N(2)	1.8784(10)
Co-N(3)	2.2603(12)
Co-N(3)	2.2603(12)
F(1)-B	1.3747(16)
F(2)-B	1.3868(16)
O(1)-N(1)	1.3645(13)
O(1)-B	1.4948(17)
O(2)-N(2)	1.3683(13)
O(2)-B	1.4900(16)
N(1)-C(2)	1.2973(15)
N(2)-C(3)	1.2971(16)
N(3)-C(5)	1.1394(17)
C(1)-C(2)	1.4897(17)
C(2)-C(3)	1.4791(17)
C(3)-C(4)	1.4841(17)
C(5)-C(6)	1.4576(18)
B-O(2)	1.4900(16)

N(1)-Co-N(1)	180.0
N(1)-Co-N(2)	98.16(4)
N(1)-Co-N(2)	81.84(4)
N(1)-Co-N(2)	81.84(4)
N(1)-Co-N(2)	98.16(4)
N(2)-Co-N(2)	180.0
N(1)-Co-N(3)	89.93(4)
N(1)-Co-N(3)	90.07(4)
N(2)-Co-N(3)	86.15(5)
N(2)-Co-N(3)	93.85(5)
N(1)-Co-N(3)	90.07(4)
N(1)-Co-N(3)	89.93(4)
N(2)-Co-N(3)	93.85(5)
N(2)-Co-N(3)	86.15(5)
N(3)-Co-N(3)	180.00(2)
N(1)-O(1)-B	115.31(9)
N(2)-O(2)-B	115.37(9)
C(2)-N(1)-O(1)	118.44(10)
C(2)-N(1)-Co	116.81(8)
O(1)-N(1)-Co	124.49(8)
C(3)-N(2)-O(2)	118.45(10)
C(3)-N(2)-Co	116.90(8)
O(2)-N(2)-Co	124.38(8)
C(5)-N(3)-Co	166.45(10)
N(1)-C(2)-C(3)	112.30(10)
N(1)-C(2)-C(1)	125.41(11)
C(3)-C(2)-C(1)	122.28(11)
N(2)-C(3)-C(2)	112.15(10)
N(2)-C(3)-C(4)	125.67(11)
C(2)-C(3)-C(4)	122.15(11)
N(3)-C(5)-C(6)	179.04(13)
F(1)-B-F(2)	112.30(11)
F(1)-B-O(2)	104.90(10)
F(2)-B-O(2)	109.59(10)
F(1)-B-O(1)	104.07(10)
F(2)-B-O(1)	109.38(11)
O(2)-B-O(1)	116.48(10)

Symmetry transformations used to generate equivalent atoms:

Table 4. Anisotropic displacement parameters [A^2 × 10^3]
for **3.1a**. The anisotropic displacement factor exponent takes the form:
-2pi^2 [h^2 a^2 U11 + ... + 2 hka*bU12]

U11	U22	U33	U23	U13	U12

Co	16(1)	11(1)	15(1)	0(1)	6(1)	0(1)
F(1)	29(1)	22(1)	20(1)	5(1)	4(1)	3(1)
F(2)	23(1)	21(1)	37(1)	0(1)	17(1)	1(1)
O(1)	21(1)	16(1)	16(1)	4(1)	6(1)	0(1)
O(2)	23(1)	16(1)	15(1)	1(1)	5(1)	3(1)
N(1)	16(1)	14(1)	16(1)	2(1)	7(1)	1(1)
N(2)	16(1)	15(1)	16(1)	0(1)	7(1)	1(1)
N(3)	22(1)	18(1)	23(1)	-1(1)	11(1)	-1(1)
C(1)	27(1)	13(1)	26(1)	-1(1)	13(1)	-2(1)
C(2)	17(1)	13(1)	20(1)	0(1)	10(1)	0(1)
C(3)	16(1)	16(1)	18(1)	-2(1)	9(1)	-1(1)
C(4)	19(1)	18(1)	22(1)	-5(1)	8(1)	-3(1)
C(5)	20(1)	16(1)	20(1)	0(1)	8(1)	-2(1)
C(6)	27(1)	23(1)	36(1)	-5(1)	20(1)	-3(1)
B	19(1)	17(1)	19(1)	1(1)	7(1)	2(1)

Table 5. Hydrogen coordinates (x 10^4) and isotropic displacement parameters (A^2 x 10^3) for **3.1a**.

	x	y	z	U(eq)
H(1A)	70	3709	-800	32
H(1B)	1876	3795	645	32
H(1C)	127	3885	851	32
H(4A)	3500	1825	4123	30
H(4B)	2286	2919	3552	30
H(4C)	3804	2730	3031	30
H(6A)	-4820	1538	1413	39
H(6B)	-3391	1246	3070	39
H(6C)	-4767	302	2123	39

Table 6. Atomic coordinates (× 10^4) and equivalent isotropic displacement parameters (A^2 × 10^3) for **3.1b**. U(eq) is defined as one third of the trace of the orthogonalized Uij tensor.

	x	y	z	U(eq)
Co	1.0000	0.5000	0.5000	0.0475
B	0.7261(9)	0.2588(8)	0.4446(7)	0.0704
F1	0.6904(6)	0.2468(6)	0.3421(4)	0.1116
F2	0.6277(6)	0.1664(4)	0.4524(5)	0.1233
N1	1.0350(6)	0.3084(5)	0.5198(4)	0.0557
N2	0.7543(6)	0.5036(4)	0.4459(4)	0.0495
O1	0.9160(6)	0.2253(5)	0.5187(5)	0.0998
O2	0.6621(5)	0.3967(4)	0.4455(4)	0.0762

O3	0.9326(7)	0.4887(5)	0.3299(4)	0.0794
C1	0.6802(7)	0.6231(6)	0.4245(5)	0.0568
C2	0.7995(8)	0.7335(6)	0.4335(6)	0.0672
C3	0.4947(8)	0.6477(7)	0.3916(6)	0.0761
H5A	0.4420	0.5624	0.3910	0.1140
H5B	0.4234	0.6871	0.3213	0.1140
H5C	0.4984	0.7094	0.4412	0.1140
C4	0.7375(8)	0.8738(6)	0.3994(6)	0.0709
H4A	0.8350	0.9288	0.4120	0.1070
H4B	0.6966	0.9103	0.4394	0.1070
H4C	0.6402	0.8748	0.3246	0.1070
C5	0.7614(11)	0.5065(12)	0.2335(7)	0.1190
H7A	0.6865	0.5606	0.2458	0.1430
H7B	0.7041	0.4181	0.2053	0.1430
C6	1.0527(14)	0.4931(11)	0.3022(9)	0.1290
H3A	1.0994	0.4019	0.3078	0.1550
H3B	1.1534	0.5521	0.3519	0.1550
C7	0.7791(13)	0.5739(16)	0.1592(9)	0.1491
H2A	0.7615	0.6718	0.1597	0.1790
H2B	0.6917	0.5393	0.0875	0.1790
C8	0.9667(13)	0.5435(14)	0.1951(9)	0.1279
H1A	0.9671	0.4748	0.1500	0.1540
H1B	1.0258	0.6256	0.1947	0.1540

Table 7. Bond lengths [A] and angles [^{o}] for **3.1b**.

Co	N1	1.892
Co	N2	1.889
Co	O3	2.324
B	F1	1.42(1)
B	F2	1.33(1)
B	O1	1.452(8)
B	O2	1.472(9)
N1	O1	1.353(9)
N2	O2	1.341(7)
N2	C1	1.292(7)
O3	C5	1.402(8)
O3	C6	1.40(2)
C1	C2	1.48(1)
C1	C3	1.48(1)
C2	C4	1.458(8)
C3	H5A	0.960
C3	H5B	0.960
C3	H5C	0.960
C4	H4A	0.960
C4	H4B	0.96

C4	H4C	0.959
C5	H7A	0.97
C5	H7B	0.97
C5	C7	1.41(2)
C6	H3A	0.97
C6	H3B	0.97
C6	C8	1.44(2)
C7	H2A	0.97
C7	H2B	0.97
C7	C8	1.50(2)
C8	H1A	0.97
C8	H1B	0.97

Table 8. Anisotropic displacement parameters [A^2 × 10^3]
for **3.1b**. The anisotropic displacement factor exponent takes the form:
-2pi^2 [h^2 a^2 U11 + ... + 2 hka*bU12]

	U11	U22	U33	U23	U13	U12
Co	0.0391	0.0479	0.0653	-0.0038	0.0362	-0.0029
B	0.0490	0.0580	0.1100	-0.0130	0.0500	-0.0110
F1	0.0890	0.1230	0.1190	-0.0410	0.0590	-0.0110
F2	0.0710	0.0680	0.2370	0.0060	0.0940	-0.0109
N1	0.0480	0.0540	0.0800	-0.0030	0.0460	-0.0041
N2	0.0420	0.0550	0.0590	-0.0050	0.0339	-0.0068
O1	0.0610	0.0600	0.1780	0.0050	0.0700	-0.0080
O2	0.0560	0.0590	0.1290	-0.0030	0.0630	-0.0067
O3	0.0610	0.1210	0.0650	0.0070	0.0420	-0.0050
C1	0.0460	0.0520	0.0820	-0.0010	0.0430	0.0030
C2	0.0450	0.0600	0.0970	0.0060	0.0420	0.0020
C3	0.0550	0.0670	0.1270	0.0150	0.0650	0.0120
C4	0.0550	0.0590	0.1020	0.0060	0.0480	0.0020
C5	0.0540	0.2210	0.0820	-0.0050	0.0400	-0.0270
C6	0.0890	0.2220	0.0990	0.0280	0.0680	0.0470
C7	0.0810	0.2730	0.1200	0.0740	0.0740	0.0460
C8	0.0770	0.2160	0.1210	0.0090	0.0750	-0.0010

Table 9. Atomic coordinates (× 10^4) and equivalent isotropic displacement parameters (A^2 × 10^3) for $[Co(dmgBF_2)_2(H_2O)]_2$. U(eq) is defined as one third of the trace of the orthogonalized Uij tensor.

	x	y	z	U(eq)
Co5	-0.54946(4)	-0.45054(4)	0.000000	0.0578(6)
N4	-0.5343(4)	-0.4389(5)	-0.1870(8)	0.0457(19)
N3	-0.6495(4)	-0.5567(4)	0.0094(7)	0.0444(17)
O5	-0.6903(5)	-0.5964(6)	-0.1041(5)	0.084(3)

O6	-0.5933(5)	-0.4977(6)	-0.2745(6)	0.076(2)
O4	-0.6120(4)	-0.3880(4)	0.000000	0.126(6)
C1	-0.6807(6)	-0.5890(6)	0.1200(9)	0.050(2)
C2	-0.7668(7)	-0.6731(10)	0.1533(9)	0.097(5)
H2a	-0.774(4)	-0.680(4)	0.2489(9)	0.146(8)
H2b	-0.8132(9)	-0.670(3)	0.116(10)	0.146(8)
H2c	-0.765(3)	-0.7207(12)	0.115(10)	0.146(8)
C4	-0.6478(10)	-0.5534(6)	0.3814(13)	0.093(5)
H4a	-0.623(6)	-0.586(6)	0.409(3)	0.140(7)
H4b	-0.624(6)	-0.5022(6)	0.4330(17)	0.140(7)
H4c	-0.7078(10)	-0.585(6)	0.396(2)	0.140(7)
C3	-0.6291(10)	-0.5307(5)	0.2257(11)	0.089(5)
H4	-0.646(4)	-0.406(4)	-0.031(6)	0.000(14)
F2a	-0.7130(7)	-0.4965(6)	-0.1979(9)	0.119(4)
B2a	-0.6831(13)	-0.5603(10)	-0.221(3)	0.126(10)
F1a	-0.7271(7)	-0.6074(8)	-0.3303(9)	0.140(5)

Table 10. Bond lengths [A] and angles [^{o}] for [Co(dmgBF$_2$)$_2$(H$_2$O)]$_2$.

Co5 N4	1.879(7)
Co5 N4	1.879(7)
Co5 N3	1.890(7)
Co5 N3	1.890(7)
Co5 O4	1.982(13)
N4 O6	1.386(11)
N4 C3	1.276(12)
N3 O5	1.348(11)
N3 C1	1.246(12)
O5 B2a	1.31(3)
O6 B2a	1.554(17)
C1 C2	1.591(16)
C1 C3	1.459(15)
C4 C3	1.597(15)
F2a B2a	1.532(18)
B2a F1a	1.37(3)

N4 Co5 N4	176.6(4)
N3 Co5 N4	100.2(3)
N3 Co5 N4	79.6(3)
N3 Co5 N4	79.6(3)
N3 Co5 N4	100.2(3)
N3 Co5 N3	174.2(3)
O4 Co5 N4	91.71(17)
O4 Co5 N4	91.71(17)
O4 Co5 N3	92.91(16)

O4 Co5 N3	92.91(16)
O6 N4 Co5	121.4(5)
C3 N4 Co5	115.0(8)
C3 N4 O6	123.4(8)
O5 N3 Co5	120.1(5)
C1 N3 Co5	120.6(7)
C1 N3 O5	119.2(8)
B2a O5 N3	125.7(14)
B2a O6 N4	118.8(13)
C2 C1 N3	129.8(8)
C3 C1 N3	108.4(9)
C3 C1 C2	121.5(8)
C1 C3 N4	115.8(10)
C4 C3 N4	121.2(11)
C4 C3 C1	122.2(8)
O6 B2a O5	119(2)
F2a B2a O5	105.5(17)
F2a B2a O6	97.9(9)
F1a B2a O5	120.6(13)
F1a B2a O6	105.1(17)
F1a B2a F2a	106.0(19)

Table 11. Anisotropic displacement parameters [A^2 × 10^3]
for $[Co(dmgBF_2)_2(H_2O)]_2$. The anisotropic displacement factor exponent takes the form:
-2pi^2 [h^2 a^2 U11 + ... + 2 hka*bU12]

	U11	U22	U33	U12	U13	U23
Co5	0.0888(12)	0.0888(12)	0.0406(8)	0.0779(12)	0.0028(9)	0.0028(9)
N4	0.031(4)	0.060(5)	0.062(4)	0.034(4)	0.000(3)	0.025(4)
N3	0.050(3)	0.069(4)	0.044(4)	0.052(3)	0.035(3)	0.001(4)
O5	0.090(5)	0.206(9)	0.012(2)	0.118(6)	0.031(3)	0.041(4)
O6	0.070(5)	0.105(6)	0.040(3)	0.034(4)	-0.028(3)	0.031(4)
O4	0.071(5)	0.071(5)	0.230(17)	0.032(7)	-0.051(10)	-0.051(10)
C1	0.074(6)	0.065(6)	0.040(5)	0.056(5)	-0.009(4)	-0.010(4)
C2	0.077(7)	0.174(14)	0.022(4)	0.048(9)	0.024(5)	-0.024(6)
C4	0.143(12)	0.027(4)	0.082(8)	0.022(6)	0.049(8)	0.010(5)
C3	0.126(10)	0.012(4)	0.063(6)	-0.014(5)	0.042(7)	0.001(4)
F2a	0.185(10)	0.096(6)	0.109(6)	0.095(6)	-0.033(6)	-0.015(5)
B2a	0.105(13)	0.048(8)	0.23(3)	0.042(9)	0.092(17)	0.065(12)
F1a	0.121(8)	0.199(12)	0.088(6)	0.070(8)	-0.050(6)	-0.039(6)

UV-Vis Spectra Under High Pressure

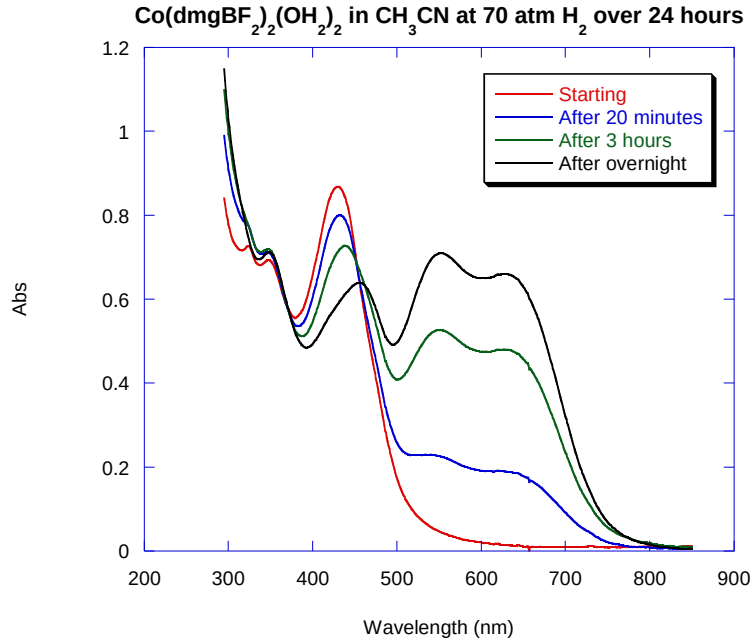

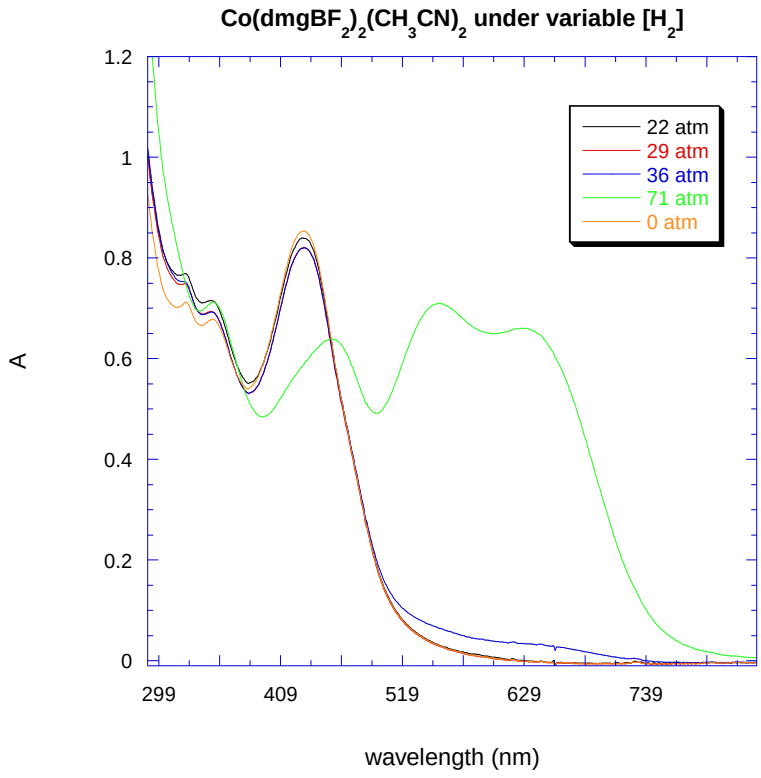

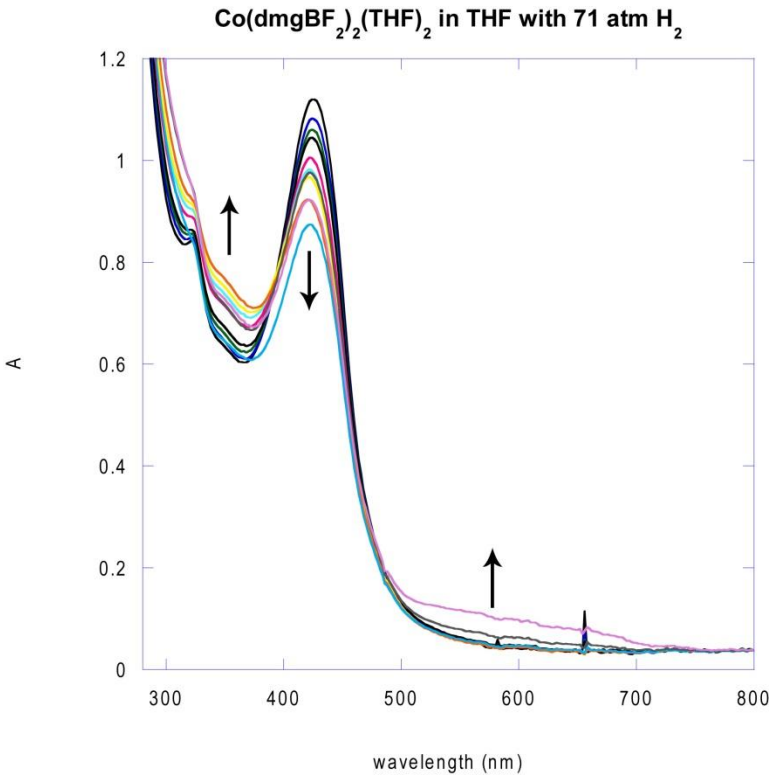

Plot of absorbances vs time in the hydrogenation of 3.1b in THF

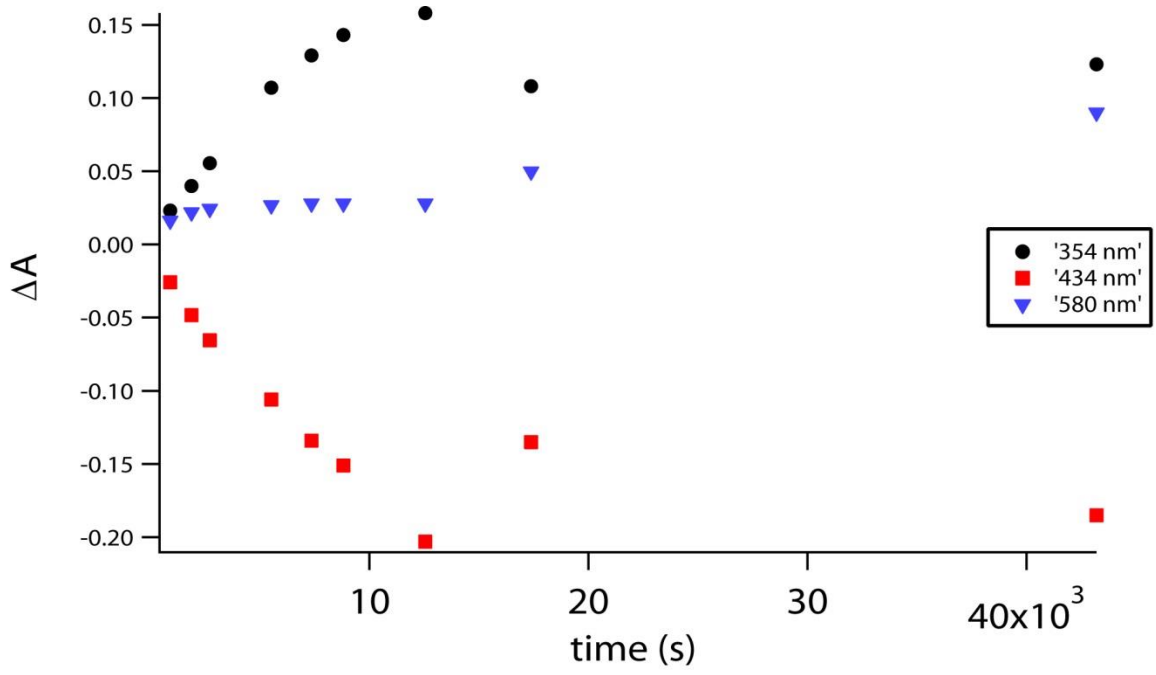

Derivation of the Equilibrium Expression

$$K_{eq} = \frac{[CoH]^2}{[Co]^2[H_2]}, \text{where} [H_2] >> [Co]_0$$

$$[Co] = [Co]_0 - [CoH] \Rightarrow K_{eq}[H_2] = \left(\frac{[CoH]}{[Co]_0 - [Co]}\right)^2 \Rightarrow \frac{1}{K_{eq}[H_2]} = \left(\frac{[Co]_0}{[CoH]} - 1\right)^2$$

$$A_{430} = \varepsilon_{Co}[Co] + \varepsilon_{CoH}[CoH] = \varepsilon_{Co}\left([Co]_0 - [CoH]\right) + \varepsilon_{CoH}[CoH]$$

$$[CoH] = \frac{A_{430} - A^0_{430}}{\varepsilon_{CoH} - \varepsilon_{Co}} \equiv \frac{\Delta}{\Delta\varepsilon} \Rightarrow \frac{1}{[H_2]} = K_{eq}\left[\left([Co]_0 \Delta\varepsilon\right)^2 \frac{1}{\Delta^2} - 2\left([Co]_0 \Delta\varepsilon\right)\frac{1}{\Delta} + 1\right]$$

H/D Exchange Reactions with complex 3.2a

Complex **3.2a** in CD_3CN under 4 atm D_2**:** ^{1}H NMR

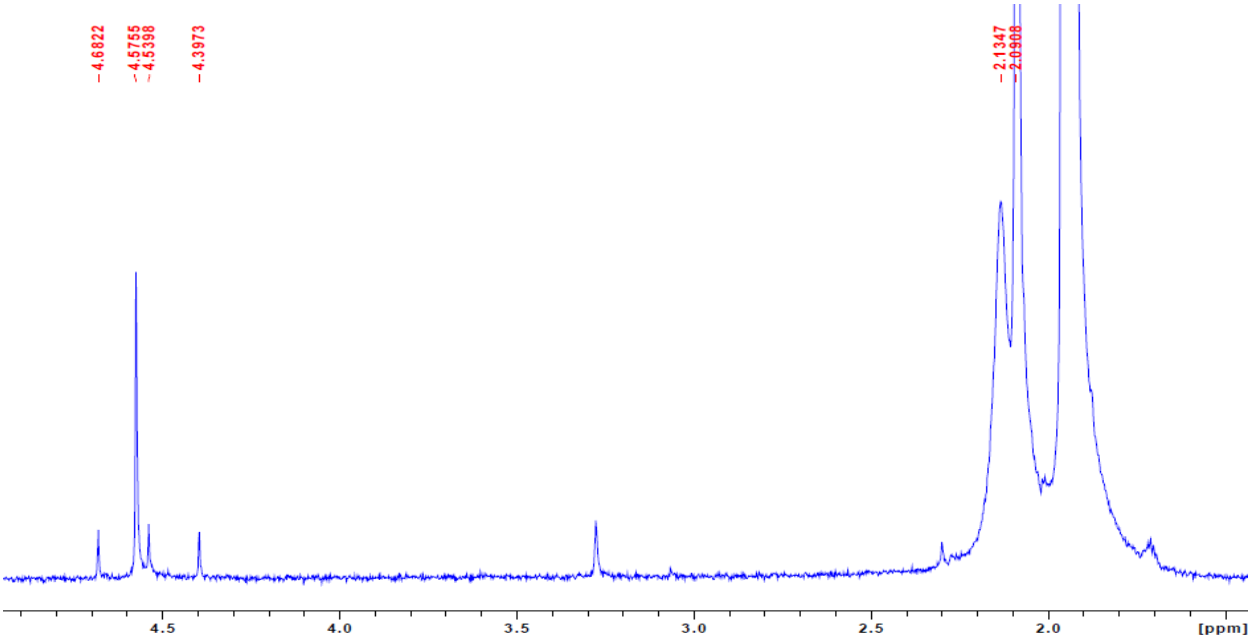

Complex **3.2a** in CH_3CN under 4 atm D_2**:** ^2H NMR

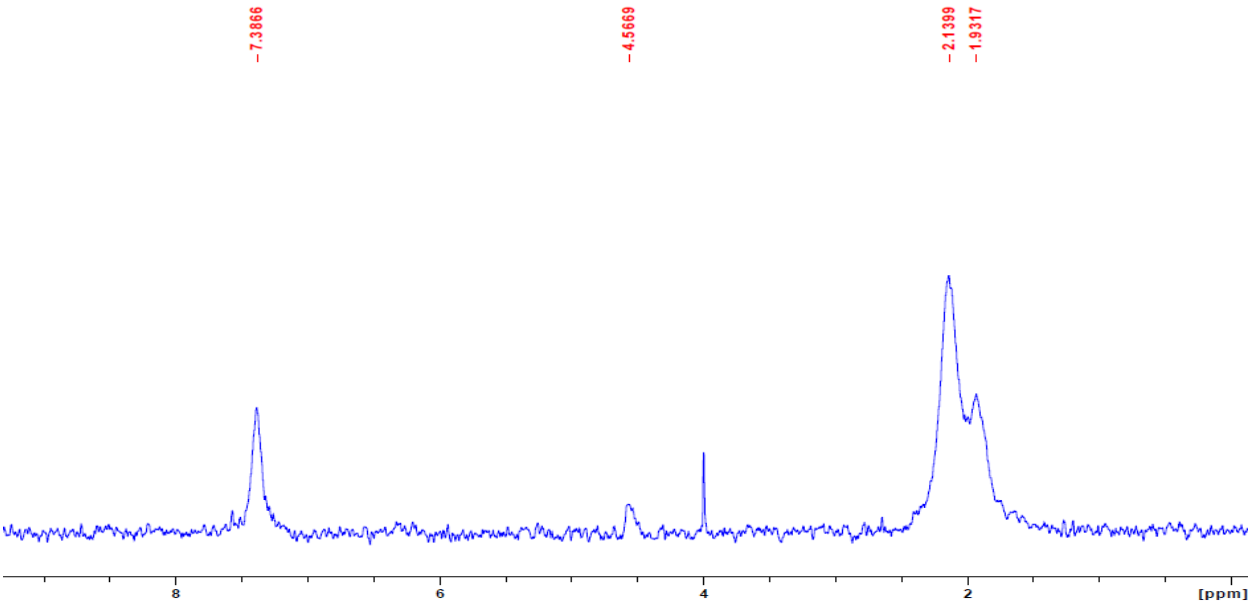

Complex **3.1a** in CH_3CN after stirring for 24 hours under 5.4 atm D_2: ^2H NMR

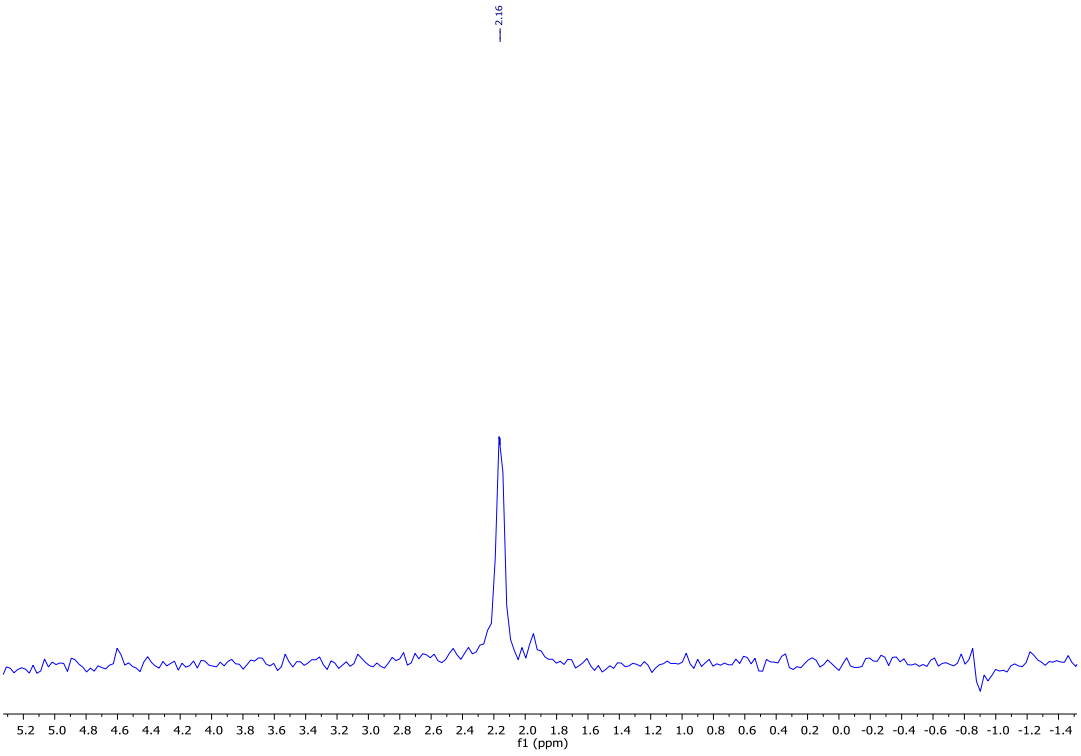

Stopped Flow Reaction of 3.5b with $HNEt_3BF_4$ in THF:

A 0.001 M solution of $Na[Co(dmgBF_2)_2(THF)]$ (**3.5b**) in THF was rapidly mixed with 0.01 – 0.037 M solutions of $HNEt_3BF_4$ in THF in a stopped flow spectrometer and monitored over the course of 8 s. These reactions did not result in complete protonation of **3.5b** over the course of the entire reaction time.

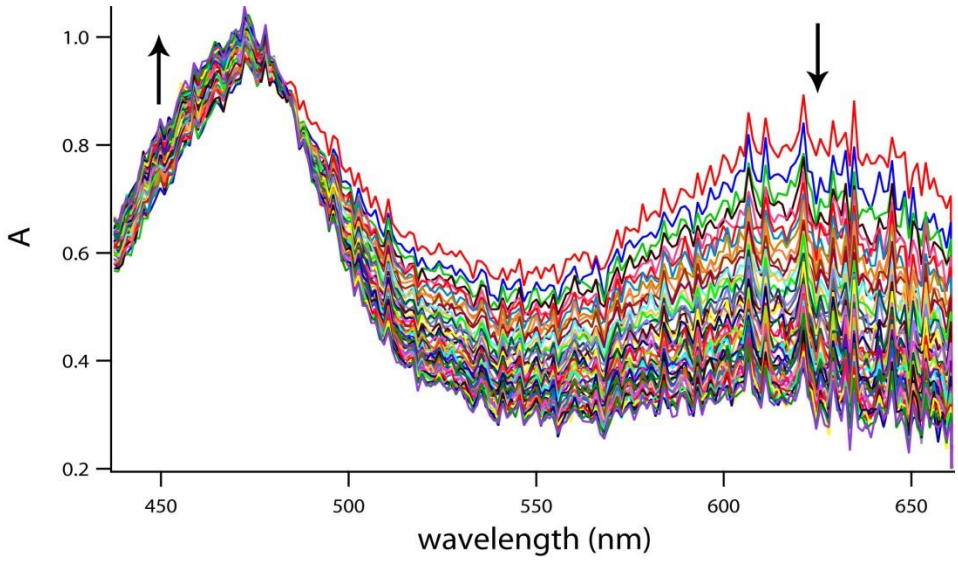
1.0
0.8
0.6
0.4
0.2
A
450
500
550
600
650
wavelength (nm)

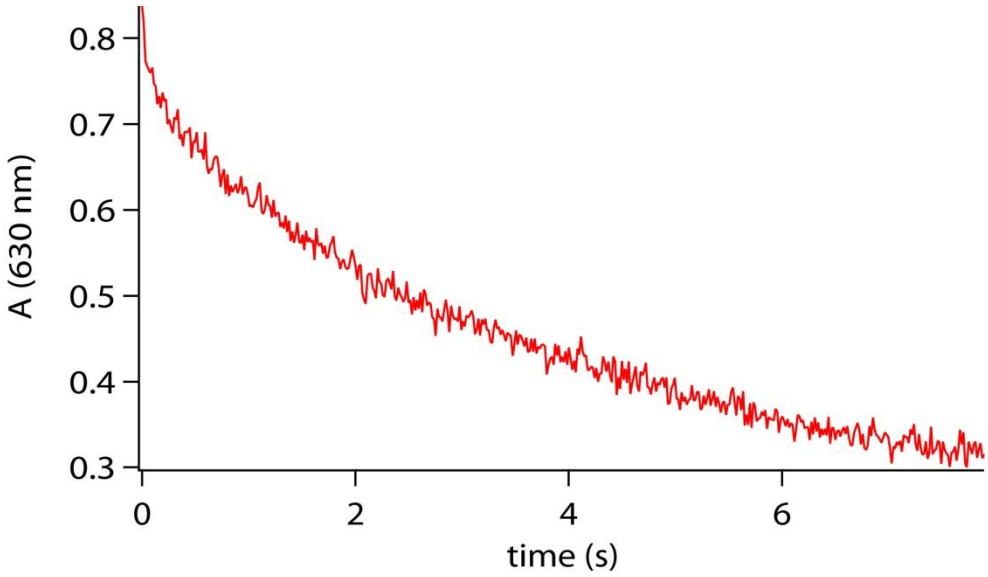
0.8
0.7
0.6
0.5
0.4
0.3
A (630 nm)
0
2
4
6
time (s)

^{19}F NMR of 3.1a with 17 eq of $NEt_4[CF_3CO_2]$ under 1 atm H_2:

A solution which was 5 mM in **3.1a** and 79 mM in $NEt_4[CF_3CO_2]$ in CD_3CN was thoroughly degassed and then placed under atmospheric pressure of H_2 gas. The reaction was monitored by ^{19}F NMR using fluorobenzene (δ = –113.5 ppm)[1] as a standard. After 5 days a color change from orange to purple was observed and two new peaks in the ^{19}F NMR were seen (δ = –76.56 s 3F, –149.07 bs 2F, and –149.10 bs 2F). This spectrum is shown below with new peaks marked with *.

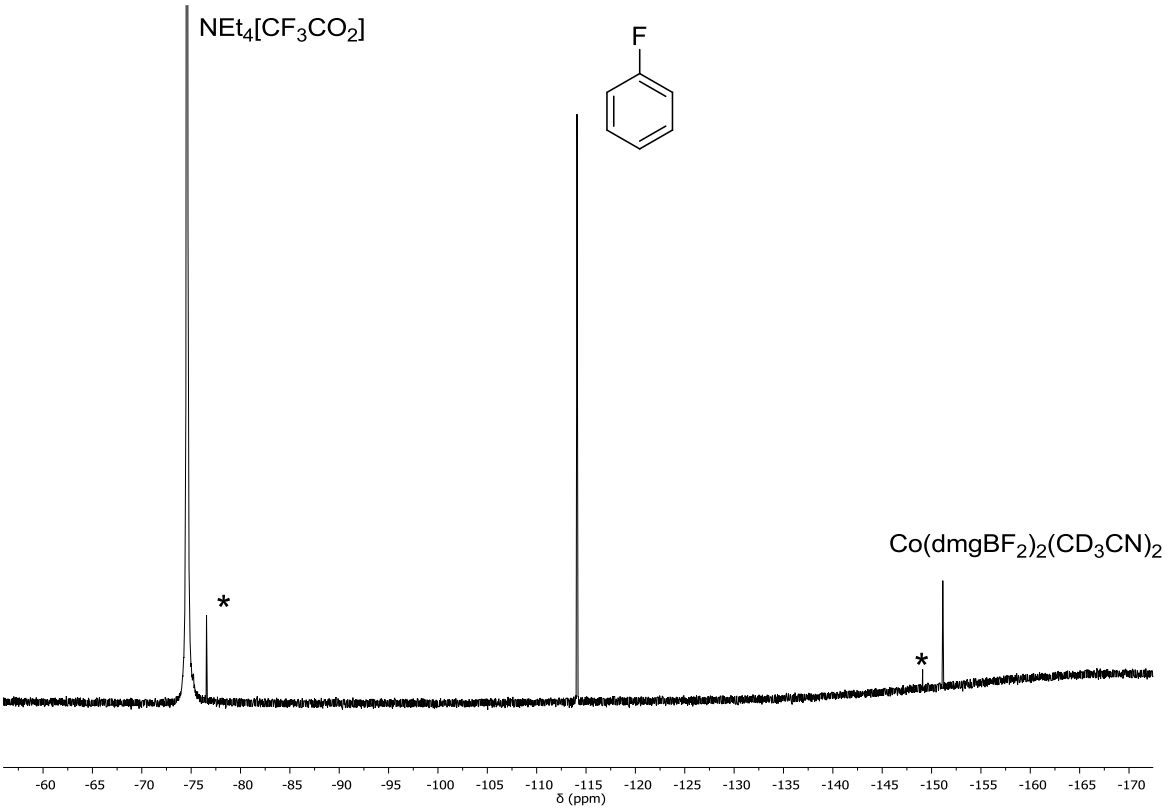

^{1}H NMR of **3.5a** in CD_3CN: δ 1.96 (s, 3H), 1.67 (s, 12H)

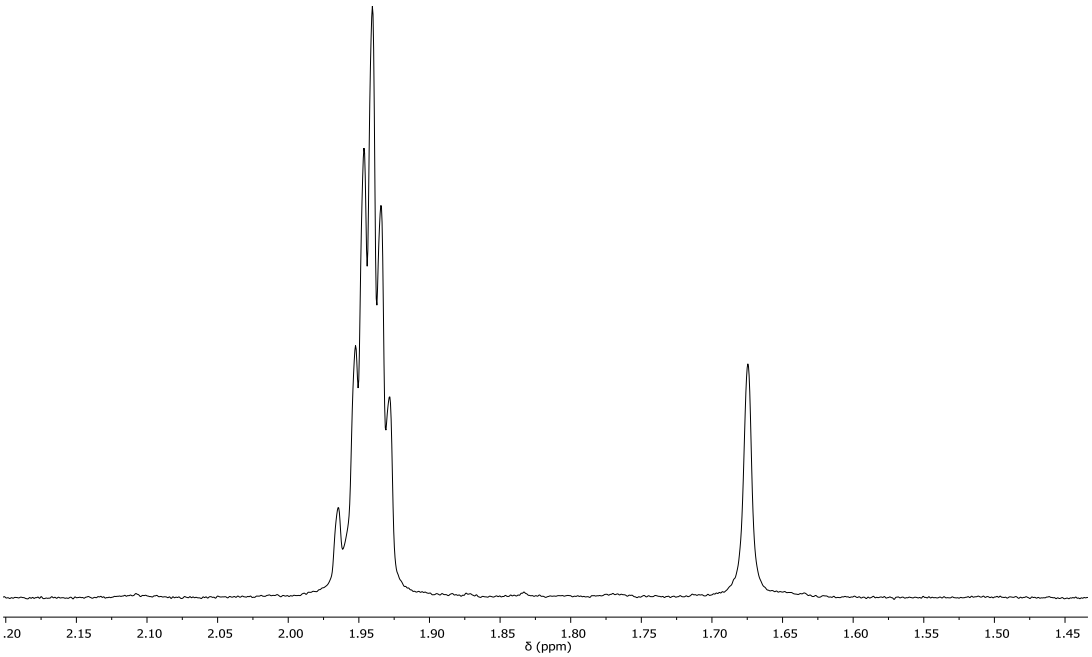

^{19}F NMR of **3.5a** in CD_3CN: δ -150.375 (1:1:1:1 quartet, J_{B-F} = 9.8 Hz)

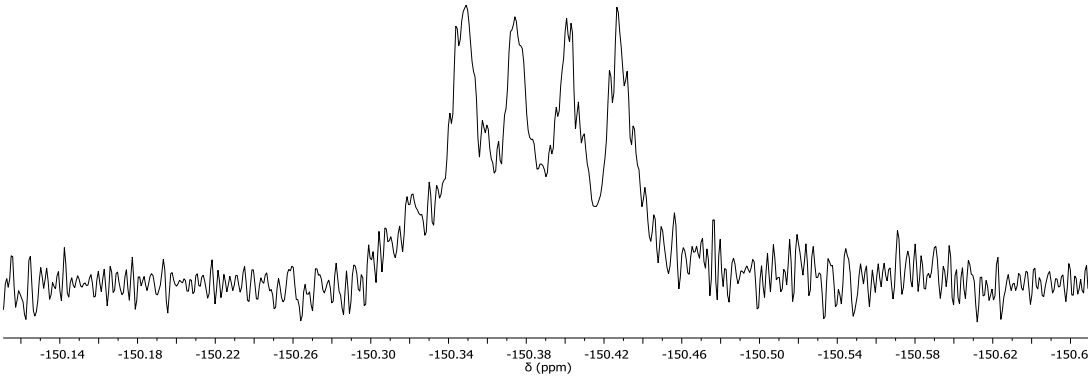

^{11}B NMR of **3.5a** in CD_3CN: δ 3.64 (t, J_{B-F} = 10.0 Hz)

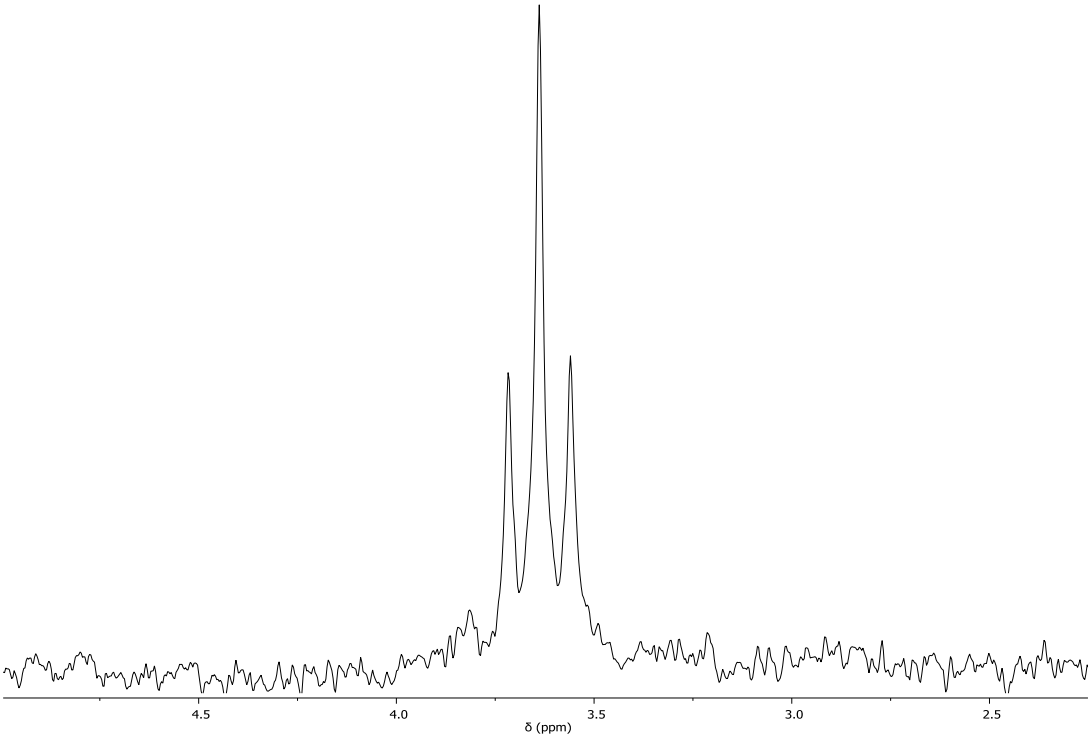

References

1. Silverstein, R. M.; Webster, F. X.; Kiemle, D. J., *Spectrometric Identification of Organic Compounds*. 7th ed.; John Wiley & Sons: Hoboken, NJ, 2005.

Appendix III. Crystallographic and Spectral Data for Chapter 4

Crystallographic Data

Compound	$HV(CO)_4dppf$	$NEt_4[V(CO)_4dppf]$
Lattice	Monoclinic	Monoclinic
Formula	$C_{38}H_{28}FeO_4P_2V$	$C_{49}H_{51}FeNO_4P_2V$
Formula Weight	717.33	886.64
Space Group	C2/c	C2/c
a (Å)	14.417(2)	37.168(5)
b (Å)	12.0665(18)	13.1193(16)
c (Å)	18.700(3)	18.579(2)
α (°)	90	90
β (°)	95.955(2)	112.440(2)
γ (°)	90	90
V ($Å^3$)	3235.5(9)	8373.6(18)
Z	4	8
Temperature (K)	130(2)	130(2)
Radiation (λ, Å)	0.71073	0.71073
ρ (calc.) (g cm^{-3})	1.473	1.407
θ max (deg)	31.04	30.52
μ (Mo Kα) (mm^{-1})	0.877	0.693
no. of data collected	25118	104496
no. of data used	5117	12757
no. of parameters	228	568
R_1 [$I > 2\sigma(I)$]	0.0514	0.0407
wR_2 [$I > 2\sigma(I)$]	0.1159	0.0911
R_1 [all data]	0.0816	0.0586
wR_2 [all data]	0.1308	0.0988
GOF	1.068	1.031

Table III.1. Atomic coordinates (x 10^4) and equivalent isotropic displacement parameters (A^2 x 10^3) for $NEt_4[V(CO)_4dppf]$. U(eq) is defined as one third of the trace of the orthogonalized Uij tensor.

	x	y	z	U(eq)
V	938(1)	2523(1)	587(1)	13(1)
Fe	2233(1)	2534(1)	1479(1)	15(1)
P(1)	1389(1)	3928(1)	1142(1)	14(1)
P(2)	1383(1)	1132(1)	661(1)	14(1)
O(1)	226(1)	1303(1)	-438(1)	33(1)
O(2)	938(1)	1733(1)	2159(1)	32(1)
O(3)	222(1)	3666(1)	585(1)	29(1)
O(4)	877(1)	3355(1)	-1016(1)	31(1)
N(1)	0	-139(2)	-2500	23(1)
N(2)	0	4994(2)	-2500	26(1)
C(1)	2576(1)	1250(2)	1725(1)	24(1)
C(2)	2232(1)	1092(2)	1050(1)	20(1)
C(3)	1901(1)	1237(1)	1260(1)	16(1)
C(4)	2052(1)	1478(2)	2074(1)	19(1)
C(5)	2466(1)	1476(2)	2354(1)	24(1)
C(6)	2567(1)	3840(2)	1666(1)	22(1)
C(7)	2418(1)	3577(2)	869(1)	23(1)
C(8)	2004(1)	3559(2)	602(1)	18(1)
C(9)	1895(1)	3816(1)	1238(1)	15(1)
C(10)	2248(1)	3996(2)	1899(1)	19(1)
C(11)	1463(1)	4385(2)	2126(1)	17(1)
C(12)	1610(1)	3724(2)	2753(1)	25(1)
C(13)	1664(1)	4039(2)	3501(1)	32(1)
C(14)	1563(1)	5017(2)	3627(1)	30(1)
C(15)	1417(1)	5679(2)	3012(1)	30(1)
C(16)	1371(1)	5373(2)	2268(1)	25(1)
C(17)	1262(1)	5141(1)	595(1)	17(1)
C(18)	872(1)	5440(2)	271(1)	22(1)
C(19)	763(1)	6356(2)	-127(1)	25(1)
C(20)	1043(1)	6978(2)	-218(1)	25(1)
C(21)	1430(1)	6701(2)	103(1)	25(1)
C(22)	1540(1)	5791(2)	511(1)	21(1)
C(23)	1280(1)	-88(2)	1039(1)	17(1)
C(24)	897(1)	-359(2)	894(1)	22(1)
C(25)	806(1)	-1294(2)	1128(1)	26(1)
C(26)	1098(1)	-1974(2)	1522(1)	25(1)

C(27)	1482(1)	-1725(2)	1669(1)	24(1)
C(28)	1572(1)	-793(2)	1427(1)	20(1)
C(29)	1414(1)	686(2)	-254(1)	17(1)
C(30)	1348(1)	-318(2)	-511(1)	24(1)
C(31)	1364(1)	-599(2)	-1219(1)	28(1)
C(32)	1450(1)	104(2)	-1676(1)	26(1)
C(33)	1522(1)	1111(2)	-1425(1)	23(1)
C(34)	1499(1)	1396(2)	-725(1)	21(1)
C(35)	515(1)	1706(2)	-26(1)	19(1)
C(36)	953(1)	2019(2)	1576(1)	19(1)
C(37)	512(1)	3302(2)	591(1)	19(1)
C(38)	915(1)	3052(2)	-402(1)	19(1)
C(40)	277(1)	507(2)	-2730(1)	26(1)
C(41)	489(1)	1323(2)	-2150(1)	28(1)
C(42)	-247(1)	-784(2)	-3192(2)	34(1)
C(43)	-24(1)	-1440(2)	-3556(2)	48(1)
C(51)	462(1)	5204(3)	-2051(3)	23(1)
C(52)	605(2)	6145(5)	-2304(6)	26(2)
C(53)	-193(1)	5909(3)	-2408(3)	27(1)
C(54)	-643(2)	5784(6)	-2770(6)	41(2)
C(55)	-48(1)	4847(4)	-3362(3)	27(1)
C(56)	195(2)	4039(10)	-3534(6)	42(3)
C(57)	-75(2)	4021(3)	-2196(3)	27(1)
C(58)	-68(2)	4063(9)	-1367(5)	29(2)
C(100)	2657(1)	3419(2)	4932(2)	52(1)
C(101)	2408(1)	1798(3)	4400(2)	51(1)
C(102)	2566(1)	2717(3)	4334(2)	55(1)

Table III.2. Bond lengths [A] and angles [deg] for $NEt_4[V(CO)_4dppf]$.

V-C(35)	1.885(2)
V-C(37)	1.889(2)
V-C(36)	1.934(2)
V-C(38)	1.934(2)
V-P(2)	2.4306(6)
V-P(1)	2.4398(6)
Fe-C(8)	2.033(2)
Fe-C(4)	2.040(2)
Fe-C(9)	2.0456(19)
Fe-C(3)	2.0483(19)
Fe-C(2)	2.052(2)
Fe-C(1)	2.055(2)
Fe-C(7)	2.056(2)
Fe-C(5)	2.060(2)

Fe-C(10)	2.063(2)
Fe-C(6)	2.065(2)
P(1)-C(9)	1.8239(19)
P(1)-C(11)	1.843(2)
P(1)-C(17)	1.850(2)
P(2)-C(3)	1.825(2)
P(2)-C(29)	1.841(2)
P(2)-C(23)	1.846(2)
O(1)-C(35)	1.180(3)
O(2)-C(36)	1.169(3)
O(3)-C(37)	1.176(2)
O(4)-C(38)	1.164(3)
N(1)-C(40)#1	1.514(3)
N(1)-C(40)	1.514(3)
N(1)-C(42)#1	1.521(3)
N(1)-C(42)	1.521(3)
N(2)-C(53)	1.440(5)
N(2)-C(53)#1	1.440(5)
N(2)-C(57)#1	1.465(4)
N(2)-C(57)	1.465(4)
N(2)-C(55)	1.555(4)
N(2)-C(55)#1	1.555(4)
N(2)-C(51)#1	1.619(4)
N(2)-C(51)	1.619(4)
C(1)-C(5)	1.409(3)
C(1)-C(2)	1.424(3)
C(2)-C(3)	1.436(3)
C(3)-C(4)	1.432(3)
C(4)-C(5)	1.425(3)
C(6)-C(7)	1.412(3)
C(6)-C(10)	1.423(3)
C(7)-C(8)	1.425(3)
C(8)-C(9)	1.430(3)
C(9)-C(10)	1.433(3)
C(11)-C(12)	1.386(3)
C(11)-C(16)	1.391(3)
C(12)-C(13)	1.390(3)
C(13)-C(14)	1.381(3)
C(14)-C(15)	1.372(4)
C(15)-C(16)	1.388(3)
C(17)-C(22)	1.394(3)
C(17)-C(18)	1.398(3)
C(18)-C(19)	1.388(3)
C(19)-C(20)	1.383(3)
C(20)-C(21)	1.380(3)
C(21)-C(22)	1.390(3)

C(23)-C(24)	1.392(3)
C(23)-C(28)	1.399(3)
C(24)-C(25)	1.385(3)
C(25)-C(26)	1.380(3)
C(26)-C(27)	1.386(3)
C(27)-C(28)	1.387(3)
C(29)-C(30)	1.390(3)
C(29)-C(34)	1.396(3)
C(30)-C(31)	1.388(3)
C(31)-C(32)	1.372(3)
C(32)-C(33)	1.393(3)
C(33)-C(34)	1.385(3)
C(40)-C(41)	1.511(3)
C(42)-C(43)	1.522(4)
C(51)-C(52)	1.490(7)
C(53)-C(54)	1.555(8)
C(55)-C(56)	1.503(10)
C(57)-C(58)	1.532(10)
C(100)-C(101)#2	1.381(5)
C(100)-C(102)	1.382(5)
C(101)-C(102)	1.368(5)
C(101)-C(100)#2	1.381(5)

C(35)-V-C(37)	78.57(9)
C(35)-V-C(36)	95.39(9)
C(37)-V-C(36)	84.22(9)
C(35)-V-C(38)	84.57(9)
C(37)-V-C(38)	94.37(9)
C(36)-V-C(38)	178.57(9)
C(35)-V-P(2)	90.04(7)
C(37)-V-P(2)	163.71(6)
C(36)-V-P(2)	85.32(6)
C(38)-V-P(2)	96.12(6)
C(35)-V-P(1)	164.88(6)
C(37)-V-P(1)	91.82(6)
C(36)-V-P(1)	95.22(6)
C(38)-V-P(1)	84.55(6)
P(2)-V-P(1)	101.54(2)
C(8)-Fe-C(4)	139.46(8)
C(8)-Fe-C(9)	41.05(8)
C(4)-Fe-C(9)	111.99(8)
C(8)-Fe-C(3)	110.75(8)
C(4)-Fe-C(3)	41.01(8)
C(9)-Fe-C(3)	111.48(7)
C(8)-Fe-C(2)	111.13(8)
C(4)-Fe-C(2)	68.41(8)

C(9)-Fe-C(2)	139.75(8)
C(3)-Fe-C(2)	41.01(8)
C(8)-Fe-C(1)	138.99(9)
C(4)-Fe-C(1)	68.20(9)
C(9)-Fe-C(1)	179.64(9)
C(3)-Fe-C(1)	68.87(8)
C(2)-Fe-C(1)	40.59(8)
C(8)-Fe-C(7)	40.79(8)
C(4)-Fe-C(7)	178.99(9)
C(9)-Fe-C(7)	68.82(8)
C(3)-Fe-C(7)	138.26(9)
C(2)-Fe-C(7)	110.59(9)
C(1)-Fe-C(7)	111.00(9)
C(8)-Fe-C(5)	178.97(9)
C(4)-Fe-C(5)	40.68(8)
C(9)-Fe-C(5)	139.91(9)
C(3)-Fe-C(5)	68.74(8)
C(2)-Fe-C(5)	67.88(9)
C(1)-Fe-C(5)	40.05(9)
C(7)-Fe-C(5)	139.05(9)
C(8)-Fe-C(10)	68.31(8)
C(4)-Fe-C(10)	113.14(8)
C(9)-Fe-C(10)	40.82(7)
C(3)-Fe-C(10)	140.69(8)
C(2)-Fe-C(10)	178.26(8)
C(1)-Fe-C(10)	138.84(9)
C(7)-Fe-C(10)	67.86(9)
C(5)-Fe-C(10)	112.67(9)
C(8)-Fe-C(6)	68.06(8)
C(4)-Fe-C(6)	140.66(9)
C(9)-Fe-C(6)	68.52(8)
C(3)-Fe-C(6)	178.31(8)
C(2)-Fe-C(6)	137.96(8)
C(1)-Fe-C(6)	111.14(8)
C(7)-Fe-C(6)	40.06(9)
C(5)-Fe-C(6)	112.42(9)
C(10)-Fe-C(6)	40.33(8)
C(9)-P(1)-C(11)	99.91(9)
C(9)-P(1)-C(17)	99.23(9)
C(11)-P(1)-C(17)	100.07(9)
C(9)-P(1)-V	119.79(6)
C(11)-P(1)-V	118.86(6)
C(17)-P(1)-V	115.34(6)
C(3)-P(2)-C(29)	99.49(9)
C(3)-P(2)-C(23)	99.04(9)
C(29)-P(2)-C(23)	99.79(9)

C(3)-P(2)-V	120.98(6)
C(29)-P(2)-V	117.83(7)
C(23)-P(2)-V	115.88(6)
C(40)#1-N(1)-C(40)	112.0(2)
C(40)#1-N(1)-C(42)#1	109.20(14)
C(40)-N(1)-C(42)#1	107.09(13)
C(40)#1-N(1)-C(42)	107.09(13)
C(40)-N(1)-C(42)	109.20(14)
C(42)#1-N(1)-C(42)	112.4(3)
C(53)-N(2)-C(53)#1	67.2(4)
C(53)-N(2)-C(57)#1	161.4(3)
C(53)#1-N(2)-C(57)#1	120.3(3)
C(53)-N(2)-C(57)	120.3(3)
C(53)#1-N(2)-C(57)	161.4(3)
C(57)#1-N(2)-C(57)	58.7(4)
C(53)-N(2)-C(55)	111.1(3)
C(53)#1-N(2)-C(55)	81.2(3)
C(57)#1-N(2)-C(55)	57.2(3)
C(57)-N(2)-C(55)	109.0(3)
C(53)-N(2)-C(55)#1	81.2(3)
C(53)#1-N(2)-C(55)#1	111.1(3)
C(57)#1-N(2)-C(55)#1	109.0(3)
C(57)-N(2)-C(55)#1	57.2(3)
C(55)-N(2)-C(55)#1	165.7(4)
C(53)-N(2)-C(51)#1	56.1(2)
C(53)#1-N(2)-C(51)#1	106.0(3)
C(57)#1-N(2)-C(51)#1	105.6(3)
C(57)-N(2)-C(51)#1	91.5(3)
C(55)-N(2)-C(51)#1	79.0(2)
C(55)#1-N(2)-C(51)#1	103.5(2)
C(53)-N(2)-C(51)	106.0(3)
C(53)#1-N(2)-C(51)	56.1(2)
C(57)#1-N(2)-C(51)	91.5(3)
C(57)-N(2)-C(51)	105.6(3)
C(55)-N(2)-C(51)	103.5(2)
C(55)#1-N(2)-C(51)	79.0(2)
C(51)#1-N(2)-C(51)	160.5(4)
C(5)-C(1)-C(2)	108.24(19)
C(5)-C(1)-Fe	70.17(12)
C(2)-C(1)-Fe	69.57(12)
C(1)-C(2)-C(3)	108.42(18)
C(1)-C(2)-Fe	69.84(12)
C(3)-C(2)-Fe	69.37(11)
C(4)-C(3)-C(2)	106.62(18)
C(4)-C(3)-P(2)	123.85(15)
C(2)-C(3)-P(2)	129.53(15)

C(4)-C(3)-Fe	69.18(11)
C(2)-C(3)-Fe	69.62(11)
P(2)-C(3)-Fe	126.79(10)
C(5)-C(4)-C(3)	108.54(19)
C(5)-C(4)-Fe	70.44(12)
C(3)-C(4)-Fe	69.81(11)
C(1)-C(5)-C(4)	108.18(19)
C(1)-C(5)-Fe	69.78(12)
C(4)-C(5)-Fe	68.88(12)
C(7)-C(6)-C(10)	108.41(19)
C(7)-C(6)-Fe	69.61(12)
C(10)-C(6)-Fe	69.75(11)
C(6)-C(7)-C(8)	107.93(19)
C(6)-C(7)-Fe	70.33(12)
C(8)-C(7)-Fe	68.74(12)
C(7)-C(8)-C(9)	108.53(18)
C(7)-C(8)-Fe	70.47(12)
C(9)-C(8)-Fe	69.94(11)
C(8)-C(9)-C(10)	106.88(17)
C(8)-C(9)-P(1)	123.03(15)
C(10)-C(9)-P(1)	130.03(15)
C(8)-C(9)-Fe	69.00(11)
C(10)-C(9)-Fe	70.26(11)
P(1)-C(9)-Fe	127.72(10)
C(6)-C(10)-C(9)	108.24(18)
C(6)-C(10)-Fe	69.92(12)
C(9)-C(10)-Fe	68.93(11)
C(12)-C(11)-C(16)	118.06(19)
C(12)-C(11)-P(1)	119.46(15)
C(16)-C(11)-P(1)	122.48(16)
C(11)-C(12)-C(13)	121.0(2)
C(14)-C(13)-C(12)	120.1(2)
C(15)-C(14)-C(13)	119.6(2)
C(14)-C(15)-C(16)	120.4(2)
C(15)-C(16)-C(11)	120.8(2)
C(22)-C(17)-C(18)	118.19(18)
C(22)-C(17)-P(1)	122.89(15)
C(18)-C(17)-P(1)	118.90(15)
C(19)-C(18)-C(17)	121.1(2)
C(20)-C(19)-C(18)	119.7(2)
C(21)-C(20)-C(19)	120.1(2)
C(20)-C(21)-C(22)	120.2(2)
C(21)-C(22)-C(17)	120.7(2)
C(24)-C(23)-C(28)	117.75(19)
C(24)-C(23)-P(2)	119.63(15)
C(28)-C(23)-P(2)	122.48(15)

C(25)-C(24)-C(23)	121.3(2)
C(26)-C(25)-C(24)	120.2(2)
C(25)-C(26)-C(27)	119.7(2)
C(26)-C(27)-C(28)	120.1(2)
C(27)-C(28)-C(23)	121.0(2)
C(30)-C(29)-C(34)	117.93(19)
C(30)-C(29)-P(2)	123.67(16)
C(34)-C(29)-P(2)	118.39(15)
C(31)-C(30)-C(29)	120.8(2)
C(32)-C(31)-C(30)	120.8(2)
C(31)-C(32)-C(33)	119.3(2)
C(34)-C(33)-C(32)	119.9(2)
C(33)-C(34)-C(29)	121.2(2)
O(1)-C(35)-V	171.91(19)
O(2)-C(36)-V	175.79(18)
O(3)-C(37)-V	171.18(18)
O(4)-C(38)-V	175.96(18)
C(41)-C(40)-N(1)	114.96(18)
N(1)-C(42)-C(43)	115.8(2)
C(52)-C(51)-N(2)	114.5(4)
N(2)-C(53)-C(54)	111.3(5)
C(56)-C(55)-N(2)	117.7(5)
N(2)-C(57)-C(58)	115.1(5)
C(101)#2-C(100)-C(102)	120.8(3)
C(102)-C(101)-C(100)#2	119.5(3)
C(101)-C(102)-C(100)	119.7(3)

Symmetry transformations used to generate equivalent atoms:
#1 -x,y,-z-1/2 #2 -x+1/2,-y+1/2,-z+1

Table III.3. Anisotropic displacement parameters (A^2 x 10^3) for $NEt_4[V(CO)_4dppf]$. The anisotropic displacement factor exponent takes the form:
-2 pi^2 [h^2 a*^2 U11 + ... + 2 h k a* b* U12]

	U11	U22	U33	U23	U13	U12
V	12(1)	14(1)	12(1)	0(1)	4(1)	0(1)
Fe	12(1)	17(1)	15(1)	0(1)	4(1)	1(1)
P(1)	13(1)	15(1)	14(1)	0(1)	4(1)	1(1)
P(2)	14(1)	15(1)	13(1)	0(1)	5(1)	0(1)
O(1)	26(1)	36(1)	28(1)	-2(1)	-1(1)	-10(1)
O(2)	42(1)	34(1)	22(1)	8(1)	15(1)	6(1)
O(3)	20(1)	32(1)	37(1)	4(1)	14(1)	8(1)
O(4)	40(1)	36(1)	19(1)	6(1)	13(1)	1(1)
N(1)	18(1)	23(1)	26(1)	0	6(1)	0
N(2)	35(1)	24(1)	15(1)	0	5(1)	0
C(1)	16(1)	22(1)	31(1)	3(1)	6(1)	5(1)
C(2)	19(1)	19(1)	24(1)	-2(1)	9(1)	2(1)
C(3)	17(1)	15(1)	17(1)	1(1)	6(1)	1(1)
C(4)	22(1)	19(1)	17(1)	1(1)	6(1)	0(1)
C(5)	21(1)	24(1)	20(1)	4(1)	-1(1)	1(1)
C(6)	15(1)	22(1)	26(1)	1(1)	6(1)	-2(1)
C(7)	22(1)	24(1)	26(1)	2(1)	14(1)	-2(1)
C(8)	20(1)	18(1)	17(1)	1(1)	7(1)	0(1)
C(9)	14(1)	14(1)	15(1)	-1(1)	5(1)	-1(1)
C(10)	17(1)	18(1)	19(1)	-1(1)	5(1)	-1(1)
C(11)	14(1)	19(1)	17(1)	-3(1)	6(1)	-2(1)
C(12)	28(1)	28(1)	18(1)	1(1)	10(1)	6(1)
C(13)	35(1)	42(1)	18(1)	2(1)	10(1)	4(1)
C(14)	29(1)	42(1)	21(1)	-11(1)	11(1)	-9(1)
C(15)	39(1)	25(1)	34(1)	-11(1)	23(1)	-6(1)
C(16)	30(1)	21(1)	25(1)	-3(1)	13(1)	0(1)
C(17)	20(1)	14(1)	16(1)	-1(1)	5(1)	1(1)
C(18)	20(1)	18(1)	26(1)	1(1)	5(1)	-1(1)
C(19)	23(1)	19(1)	25(1)	1(1)	-1(1)	3(1)
C(20)	36(1)	16(1)	21(1)	3(1)	7(1)	3(1)
C(21)	35(1)	18(1)	25(1)	1(1)	16(1)	-2(1)
C(22)	22(1)	20(1)	23(1)	-1(1)	11(1)	1(1)
C(23)	23(1)	16(1)	15(1)	-1(1)	10(1)	1(1)
C(24)	23(1)	17(1)	29(1)	2(1)	11(1)	2(1)
C(25)	28(1)	20(1)	35(1)	1(1)	17(1)	-2(1)
C(26)	38(1)	16(1)	24(1)	-1(1)	16(1)	-2(1)

C(27)	33(1)	17(1)	19(1)	3(1)	8(1)	6(1)
C(28)	22(1)	19(1)	17(1)	1(1)	6(1)	2(1)
C(29)	14(1)	21(1)	14(1)	-2(1)	4(1)	2(1)
C(30)	31(1)	20(1)	20(1)	-2(1)	9(1)	-2(1)
C(31)	39(1)	25(1)	20(1)	-7(1)	10(1)	-2(1)
C(32)	27(1)	37(1)	17(1)	-6(1)	11(1)	2(1)
C(33)	21(1)	31(1)	19(1)	0(1)	9(1)	-1(1)
C(34)	20(1)	22(1)	20(1)	-2(1)	8(1)	-3(1)
C(35)	21(1)	20(1)	17(1)	2(1)	7(1)	0(1)
C(36)	19(1)	21(1)	19(1)	0(1)	7(1)	3(1)
C(37)	19(1)	19(1)	18(1)	3(1)	6(1)	1(1)
C(38)	18(1)	17(1)	21(1)	-3(1)	6(1)	-2(1)
C(40)	22(1)	30(1)	25(1)	1(1)	8(1)	-3(1)
C(41)	22(1)	28(1)	31(1)	-2(1)	6(1)	-5(1)
C(42)	25(1)	32(1)	43(2)	-12(1)	9(1)	-6(1)
C(43)	43(2)	38(2)	65(2)	-25(1)	24(2)	-7(1)
C(51)	19(2)	24(2)	21(2)	3(2)	3(2)	-1(2)
C(52)	15(3)	34(4)	29(3)	6(3)	7(2)	7(2)
C(53)	25(2)	26(2)	37(3)	5(2)	19(2)	7(2)
C(54)	16(3)	66(6)	38(4)	10(5)	7(3)	-17(4)
C(55)	24(2)	40(3)	17(2)	3(2)	7(2)	-5(2)
C(56)	42(6)	63(5)	19(3)	-13(3)	12(4)	-17(5)
C(57)	37(3)	23(2)	24(2)	2(2)	14(2)	-9(2)
C(58)	30(5)	31(3)	23(3)	6(2)	9(3)	3(3)
C(100)	36(2)	42(2)	71(2)	6(2)	14(2)	-2(1)
C(101)	39(2)	52(2)	53(2)	-5(2)	6(1)	7(1)
C(102)	51(2)	61(2)	57(2)	10(2)	24(2)	7(2)

Table III.4. Hydrogen coordinates (x 10^4) and isotropic displacement parameters (A^2 x 10^3) for $NEt_4[V(CO)_4dppf]$.

	x	y	z	U(eq)
H(1B)	2849	1210	1748	29
H(2A)	2222	920	518	24
H(4A)	1893	1621	2392	23
H(5A)	2648	1625	2900	29
H(6A)	2849	3897	2011	26
H(7A)	2576	3425	550	27
H(8A)	1821	3398	59	22
H(10A)	2267	4183	2434	22
H(12A)	1676	3046	2670	30
H(13A)	1770	3582	3926	38
H(14A)	1595	5229	4137	36
H(15A)	1346	6351	3097	36
H(16A)	1277	5845	1849	30
H(18A)	678	5009	324	27
H(19A)	497	6555	-336	30
H(20A)	969	7596	-503	30
H(21A)	1622	7134	46	30
H(22A)	1808	5609	734	26
H(24A)	693	106	629	27
H(25A)	542	-1467	1017	31
H(26A)	1036	-2609	1692	30
H(27A)	1684	-2194	1936	28
H(28A)	1836	-631	1527	23
H(30A)	1292	-817	-199	29
H(31A)	1315	-1287	-1388	34
H(32A)	1460	-94	-2160	32
H(33A)	1586	1601	-1732	28
H(34A)	1542	2088	-564	25
H(40A)	472	53	-2807	31
H(40B)	128	837	-3235	31
H(41A)	647	1731	-2360	43
H(41B)	658	1004	-1661	43
H(41C)	300	1764	-2053	43
H(42A)	-421	-325	-3599	41
H(42B)	-414	-1236	-3024	41
H(43A)	-207	-1855	-3974	71
H(43B)	156	-1886	-3158	71

H(43C)	124	-1000	-3771	71
H(51A)	521	5252	-1486	27
H(51B)	606	4612	-2134	27
H(52A)	884	6227	-1996	40
H(52B)	463	6737	-2225	40
H(52C)	562	6089	-2857	40
H(53A)	-116	6485	-2664	33
H(53B)	-109	6070	-1847	33
H(54A)	-766	6418	-2702	61
H(54B)	-720	5225	-2509	61
H(54C)	-726	5631	-3327	61
H(55A)	-325	4692	-3671	33
H(55B)	12	5506	-3553	33
H(56A)	131	4010	-4097	62
H(56B)	140	3377	-3354	62
H(56C)	471	4202	-3265	62
H(57A)	123	3522	-2208	33
H(57B)	-333	3766	-2548	33
H(58A)	-107	3376	-1202	43
H(58B)	-276	4512	-1355	43
H(58C)	184	4328	-1012	43
H(100)	2766	4058	4884	62
H(101)	2344	1313	3991	61
H(102)	2613	2874	3878	66

Table III.5. Atomic coordinates (x 10^4) and equivalent isotropic displacement parameters (A^2 x 10^3) for $HV(CO)_4$dppf. U(eq) is defined as one third of the trace of the orthogonalized Uij tensor.

	x	y	z	U(eq)
V	0.0000	1.31197(5)	0.2500	0.0364
Fe	0.0000	0.94808(4)	0.2500	0.0326
P	-0.02432(5)	1.17864(5)	0.35035(3)	0.0273
O1	0.2059(2)	1.3244(2)	0.31732(13)	0.0618
C1	-0.0263(2)	0.9379(2)	0.35539(16)	0.0387
H1A	-0.0891	0.9302	0.3731	0.0460
C2	0.0329(2)	0.8496(2)	0.33863(18)	0.0450
H2A	0.0185	0.7689	0.3420	0.0540
C3	0.1150(2)	0.8948(2)	0.31523(17)	0.0428
H3A	0.1685	0.8517	0.2995	0.0510
C4	0.1071(2)	1.0122(2)	0.31641(15)	0.0339

H4A	0.1546	1.0662	0.3025	0.0410
C5	0.01893(19)	1.03951(19)	0.34107(14)	0.0297
C6	-0.1393(2)	1.1506(2)	0.37990(15)	0.0320
C7	-0.2174(2)	1.1460(2)	0.33047(17)	0.0376
H7A	-0.2117	1.1638	0.2816 0.0450	
C8	-0.3039(2)	1.1160(3)	0.3506(2)	0.0475
H8A	-0.3567	1.1122	0.3158	0.0570
C9	-0.3123(2)	1.0915(3)	0.4220(2)	0.0526
H9A	-0.3711	1.0705	0.4363	0.0630
C10	-0.2364(3)	1.0975(3)	0.4719(2)	0.0539
H10A	-0.2430	1.0818	0.5209	0.0650
C11	-0.1496(2)	1.1262(3)	0.45177(17)	0.0420
H11A	-0.0971	1.1294	0.4869	0.0500
C12	0.04000(19)	1.2248(2)	0.43442(13)	0.0285
C13	0.0152(2)	1.3244(2)	0.46513(15)	0.0390
H13A	-0.0349	1.3669	0.4423	0.0470
C14	0.0627(2)	1.3619(2)	0.52841(15)	0.0409
H14A	0.0448	1.4296	0.5490	0.0490
C15	0.1362(2)	1.3013(2)	0.56196(15)	0.0385
H15A	0.1696	1.3280	0.6050	0.0460
C16	0.1606(2)	1.2023(2)	0.53270(15)	0.0361
H16A	0.2104	1.1599	0.5561	0.0430
C17	0.11295(19)	1.1639(2)	0.46914(14)	0.0320
H17A	0.1304	1.0955	0.4493	0.0380
C18	0.1298(3)	1.3147(2)	0.29398(15)	0.0446
C19	0.0695(8)	1.4175(6)	0.1936(3)	0.0461
O2	0.1122(8)	1.4837(7)	0.1672(3)	0.0900
C20	0.0216(7)	1.4505(7)	0.2130(5)	0.0456
O3	0.0446(7)	1.5383(7)	0.1948(5)	0.0771

Table III.6. Bond lengths [A] and angles [deg] for $HV(CO)_4$dppf.

V	P	2.5237
V	C18	1.965
V	C19	1.989
Fe	C1	2.049
Fe	C2	2.054
Fe	C3	2.057
Fe	C4	2.032
Fe	C5	2.024
P	C5	1.805(2)
P	C6	1.832(3)
P	C12	1.827(2)
O1	C18	1.144(5)
C1	H1A	1.000

C1	C2	1.420(4)
C1	C5	1.427(4)
C2	H2A	0.999
C2	C3	1.413(4)
C3	H3A	0.999
C3	C4	1.422(3)
C4	H4A	0.999
C4	C5	1.435(4)
C6	C7	1.382(4)
C6	C11	1.399(4)
C7	H7A	0.951
C7	C8	1.388(4)
C8	H8A	0.950
C8	C9	1.385(5)
C9	H9A	0.949
C9	C10	1.364(5)
C10	H10A	0.950
C10	C11	1.388(5)
C11	H11A	0.950
C12	C13	1.394(4)
C12	C17	1.388(4)
C13	H13A	0.950
C13	C14	1.381(4)
C14	H14A	0.950
C14	C15	1.383(4)
C15	H15A	0.950
C15	C16	1.375(4)
C16	H16A	0.951
C16	C17	1.389(4)
C17	H17A	0.949
C19	O2	1.15(1)

P	V	C18	84.2
P	V	C19	156.7
P	V	P	100.79
P	V	C18	97.0
P	V	C19	84.1
C18	V	C19	72.6
C18	V	P	97.0
C18	V	C18	178.1
C18	V	C19	106.1
C19	V	P	84.1
C19	V	C18	106.1
C19	V	C19	100.4
P	V	C18	84.2
P	V	C19	156.7

C18	V	C19	72.6
C1	Fe	C2	40.5
C1	Fe	C3	68.2
C1	Fe	C4	68.9
C1	Fe	C5	41.0
C1	Fe	C1	173.1
C1	Fe	C2	133.7
C1	Fe	C3	109.5
C1	Fe	C4	114.0
C1	Fe	C5	145.1
C2	Fe	C3	40.2
C2	Fe	C4	68.3
C2	Fe	C5	68.7
C2	Fe	C1	133.7
C2	Fe	C2	109.3
C2	Fe	C3	113.7
C2	Fe	C4	144.2
C2	Fe	C5	173.7
C3	Fe	C4	40.7
C3	Fe	C5	69.0
C3	Fe	C1	109.5
C3	Fe	C2	113.7
C3	Fe	C3	143.6
C3	Fe	C4	175.1
C3	Fe	C5	134.4
C4	Fe	C5	41.4
C4	Fe	C1	114.0
C4	Fe	C2	144.2
C4	Fe	C3	175.1
C4	Fe	C4	135.2
C4	Fe	C5	109.5
C5	Fe	C1	145.1
C5	Fe	C2	173.7
C5	Fe	C3	134.4
C5	Fe	C4	109.5

Table III.7. Anisotropic displacement parameters (A^2 x 10^3) for $HV(CO)_4dppf$. The anisotropic displacement factor exponent takes the form:
-2 pi^2 [h^2 a*^2 U11 + ... + 2 h k a* b* U12]

	U11	U22	U33	U23	U13	U12
V	0.0703	0.0187	0.0209	0.0000	0.0087	0.0000
Fe	0.0468	0.0163	0.0389	0.0000	0.0238	0.0000
P	0.0378	0.0197	0.0256	0.0028	0.0095	0.0055
O1	0.0805	0.0630	0.0406	-0.0024	-0.0006	-0.0284
C1	0.0509	0.0231	0.0459	0.0071	0.0238	0.0055
C2	0.0650	0.0217	0.0529	0.0100	0.0279	0.0086
C3	0.0534	0.0272	0.0516	0.0074	0.0234	0.0144
C4	0.0444	0.0256	0.0341	0.0047	0.0157	0.0072
C5	0.0407	0.0215	0.0291	0.0046	0.0140	0.0062
C6	0.0400	0.0200	0.0382	0.0023	0.0142	0.0075
C7	0.0405	0.0293	0.0445	-0.0058	0.0112	0.0051
C8	0.0402	0.0355	0.0680	-0.0121	0.0111	0.0052
C9	0.0444	0.0383	0.0800	0.0048	0.0299	0.0070
C10	0.0540	0.0511	0.0620	0.0170	0.0316	0.0131
C11	0.0432	0.0417	0.0435	0.0133	0.0160	0.0080
C12	0.0383	0.0247	0.0238	0.0050	0.0100	0.0033
C13	0.0560	0.0314	0.0297	0.0025	0.0047	0.0121
C14	0.0620	0.0324	0.0287	0.0003	0.0071	0.0036
C15	0.0468	0.0414	0.0282	0.0045	0.0082	-0.0086
C16	0.0366	0.0429	0.0299	0.0093	0.0092	0.0024
C17	0.0373	0.0313	0.0294	0.0065	0.0130	0.0063
C18	0.0790	0.0311	0.0248	0.0001	0.0110	-0.0164
C19	0.0780	0.0320	0.0250	0.0100	-0.0110	-0.0170
O2	0.1340	0.0850	0.0420	0.0390	-0.0340	-0.0730
C20	0.0500	0.0380	0.0460	0.0100	-0.0090	-0.0120
O3	0.0840	0.0550	0.0850	0.0440	-0.0260	-0.0330

NMR Spectra

$NEt_4[V(CO)_4dppf]$ in CD_3CN

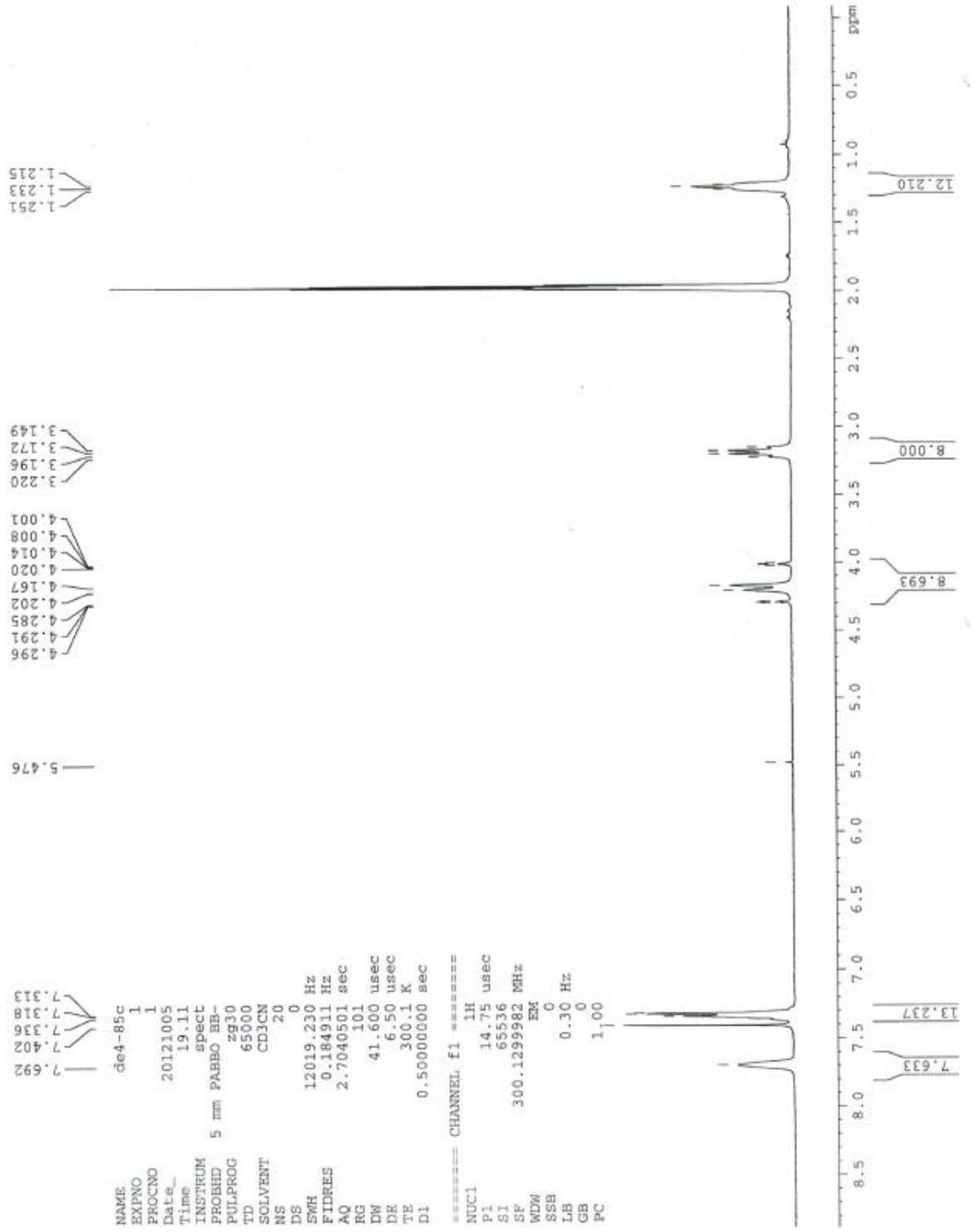

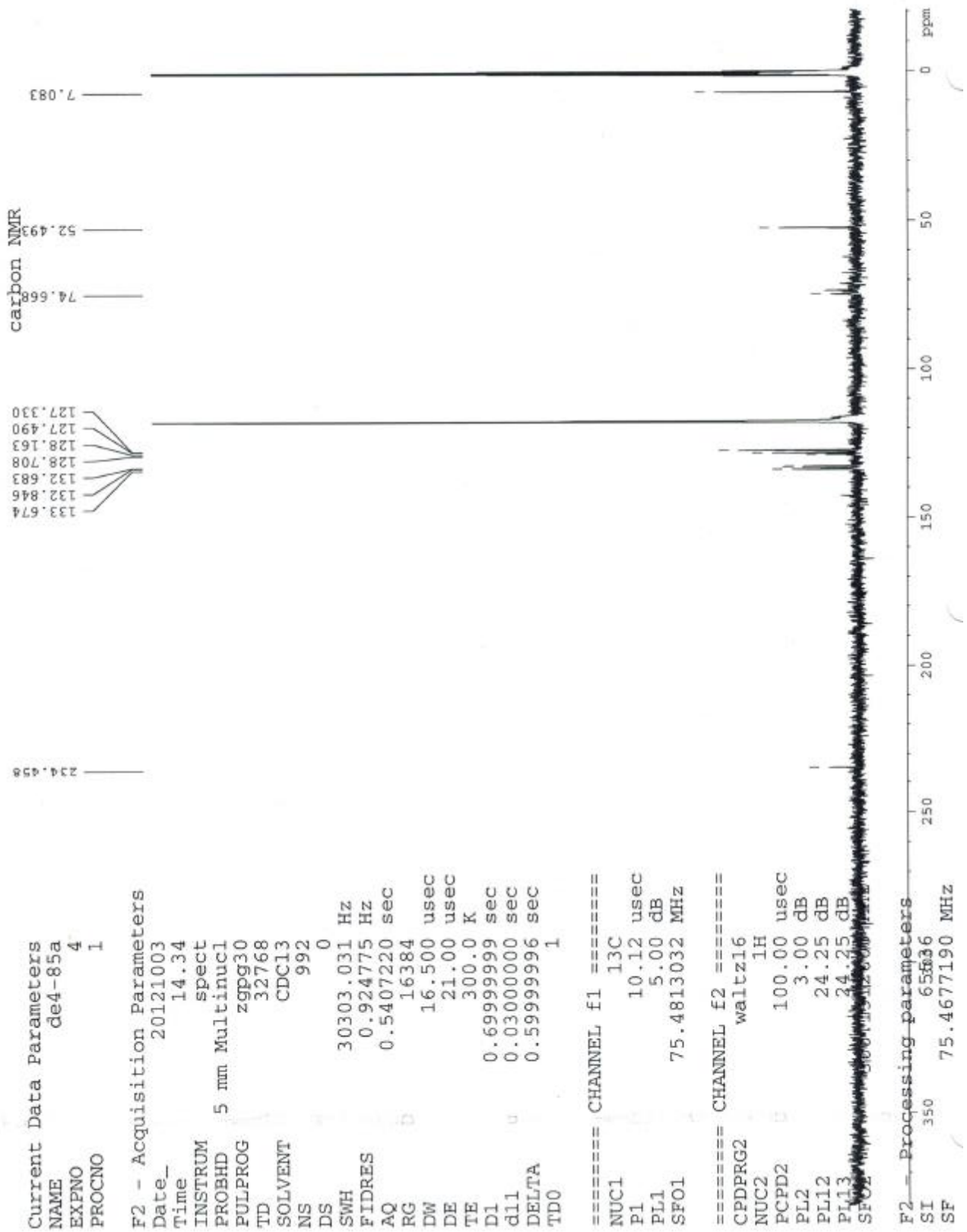
carbon NMR
234.458
133.674
132.846
132.683
128.708
128.163
127.490
127.330
74.668
52.493
7.083
ppm
Current Data Parameters
NAME de4-85a
EXPNO 4
PROCNO 1
F2 - Acquisition Parameters
Date_ 20121003
Time 14.34
INSTRUM spect
PROBHD 5 mm Multinucl
PULPROG zgpg30
TD 32768
SOLVENT CDCl3
NS 992
DS 0
SWH 30303.031 Hz
FIDRES 0.924775 Hz
AQ 0.5407220 sec
RG 16384
DW 16.500 usec
DE 21.00 usec
TE 300.0 K
D1 0.69999999 sec
d11 0.03000000 sec
DELTA 0.59999996 sec
TD0 1
======== CHANNEL f1 ========
NUC1 13C
P1 10.12 usec
PL1 5.00 dB
SFO1 75.4813032 MHz
======== CHANNEL f2 ========
CPDPRG2 waltz16
NUC2 1H
PCPD2 100.00 usec
PL2 3.00 dB
PL12 24.25 dB
PL13 24.25 dB
F2 - Processing parameters
SI 65536
SF 75.4677190 MHz

$HV(CO)_4dppf$

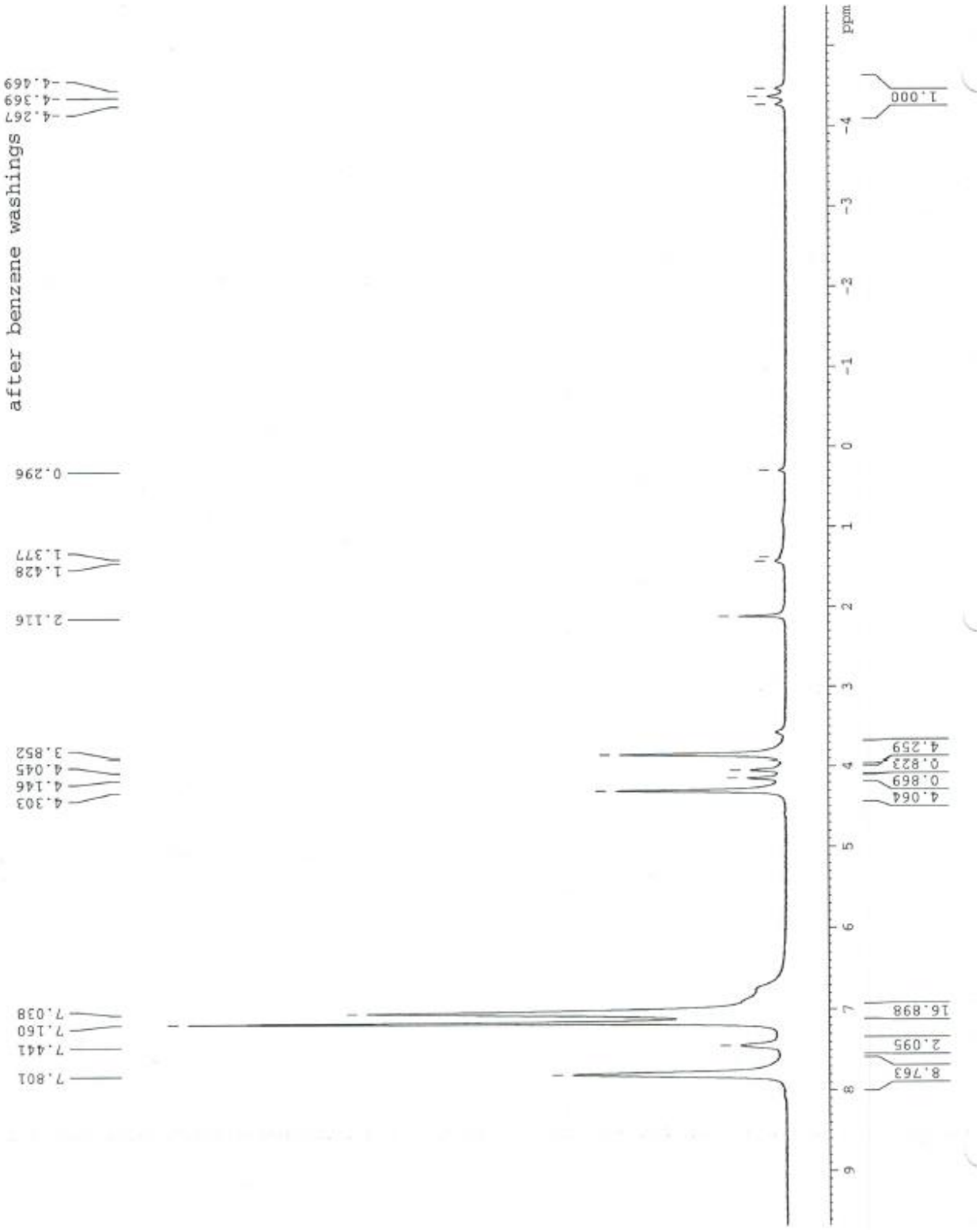
after benzene washings
-4.469
-4.369
-4.267
0.296
1.377
1.428
2.116
3.852
4.045
4.146
4.303
7.038
7.160
7.441
7.801
1.000
4.259
0.823
0.869
4.064
16.898
2.095
8.763
ppm

IR Spectra

$NEt_4[V(CO)_4dppf]$ in CH_3CN (carbonyl region)

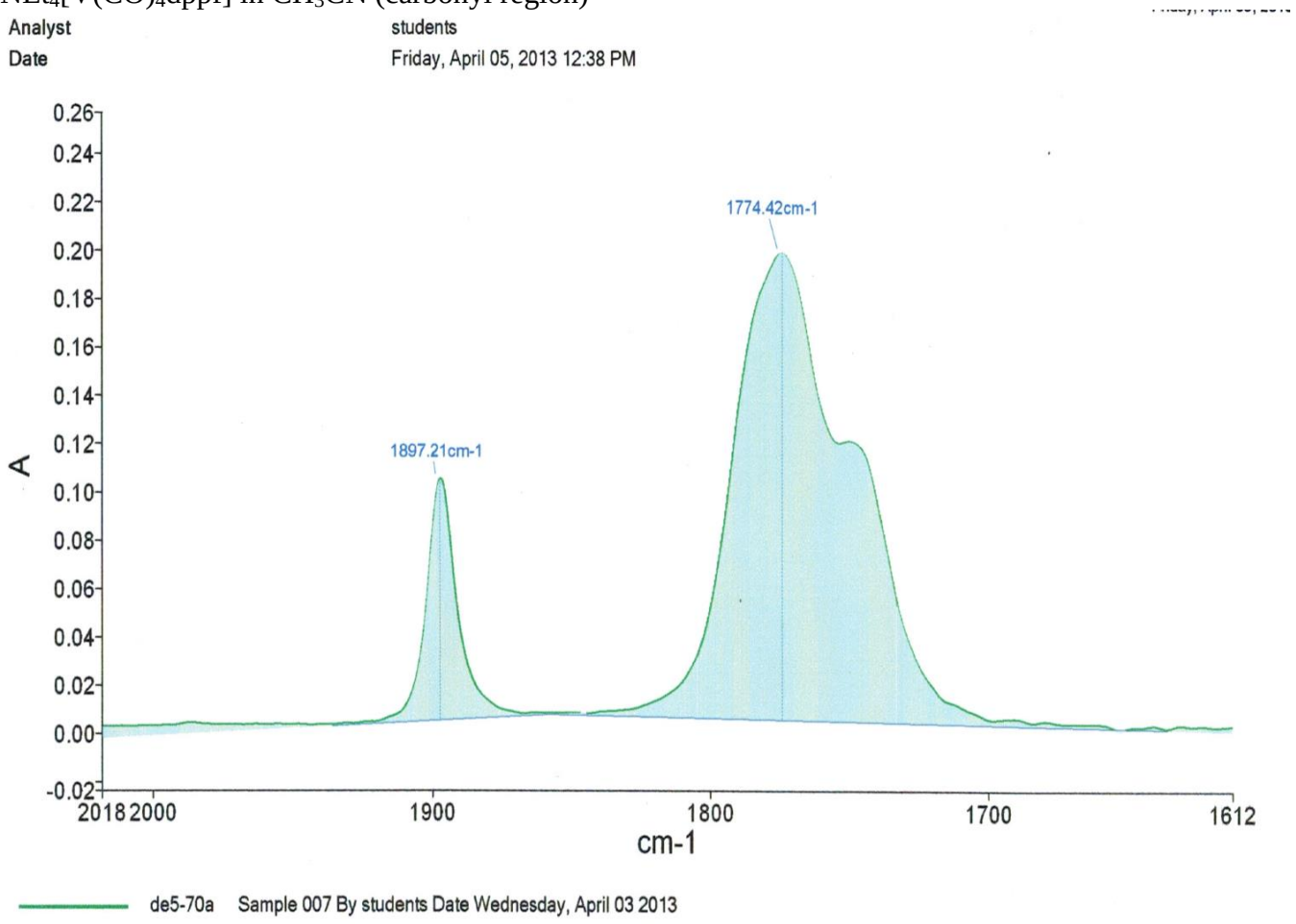

$HV(CO)_4dppf$ in CH_3CN (carbonyl region)

Equilibration of $NEt_4[V(CO)_4dppf]$ with NH_2PyH^+ (three trials)

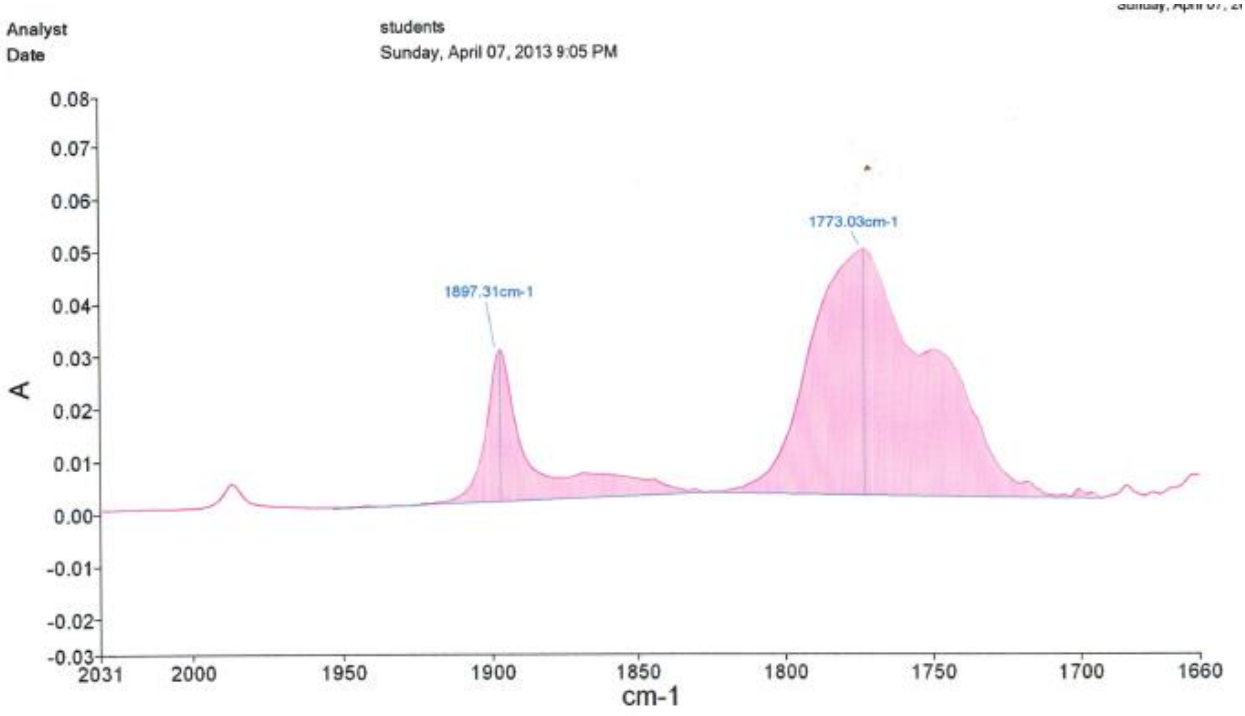
Analyst
students
Date
Sunday, April 07, 2013 9:05 PM
1773.03cm-1
1897.31cm-1
A
cm-1

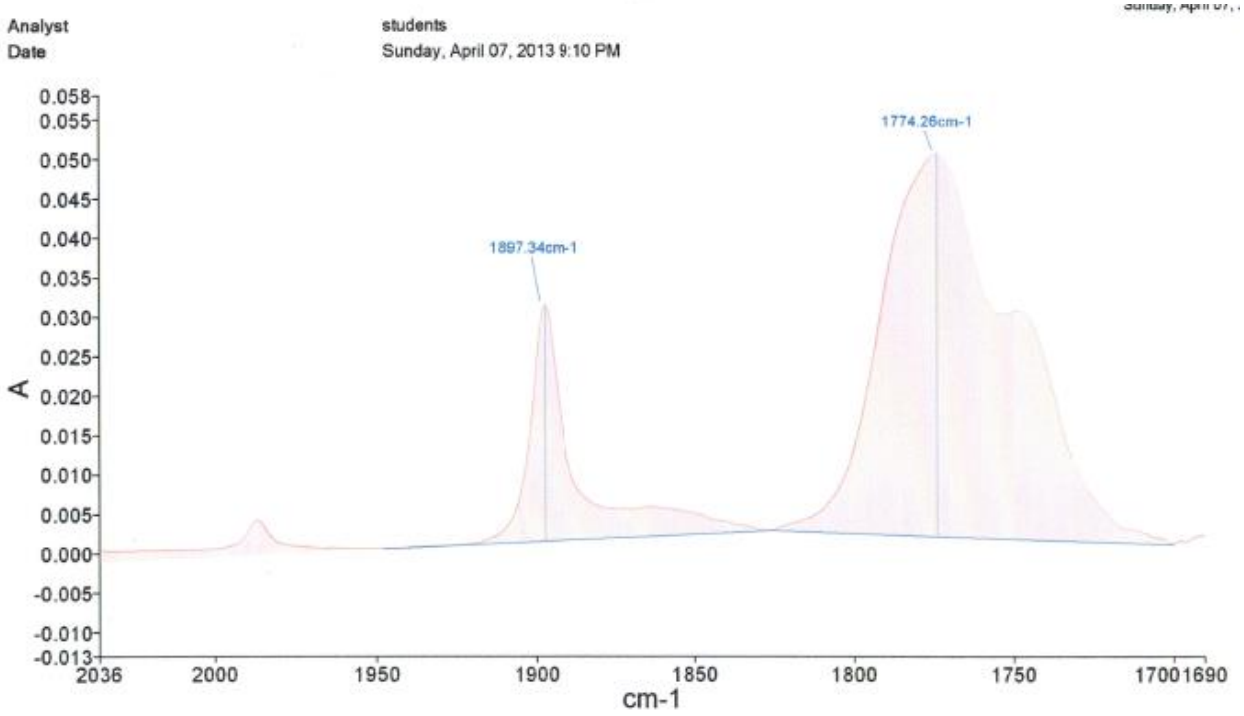
Analyst
students
Date
Sunday, April 07, 2013 9:10 PM
1774.26cm-1
1897.34cm-1
A
cm-1

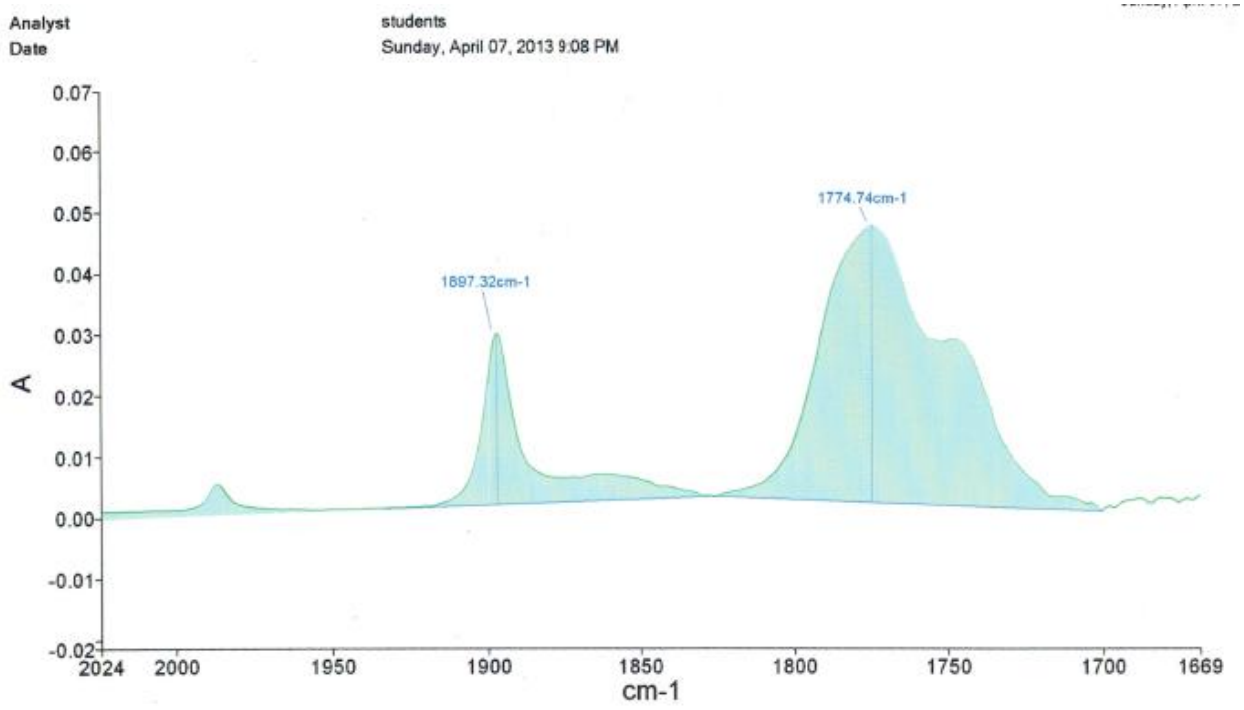
Analyst
students
Date
Sunday, April 07, 2013 9:08 PM
1774.74cm-1
1697.32cm-1
A
0.07
0.06
0.05
0.04
0.03
0.02
0.01
0.00
-0.01
-0.02
2024
2000
1950
1900
1850
1800
1750
1700
1669
cm-1

Appendix IV. Crystallographic Data, Selected Spectral Data, and Kinetic Traces for Chapter 5

Crystallographic Data for 5.15

Structural Parameters	
Lattice	Monoclinic
Formula	$C_{16}H_{12}O_3Cr$
Formula Weight	304.26
Space Group	$P2_1/n$
a (Å)	10.281(4)
b (Å)	11.029(4)
c (Å)	12.894(4)
α (°)	90
β (°)	112.791(5)
γ (°)	90
V (Å^3)	1347.9(8)
Z	4
Temperature (K)	150(2)
Radiation (λ, Å)	0.71073
ρ (calc.) (g cm^{-3})	1.499
θ max (deg)	31.01
μ (Mo Kα) (mm^{-1})	0.851
no. of data collected	20776
no. of data used	4225
no. of parameters	182
R_1 [I > 2σ(I)]	0.0636
wR_2 [I > 2σ(I)]	0.1289
R_1 [all data]	0.1868

wR_2 [all data]	0.1663
GOF	1.005

Table 1. Atomic coordinates (× 10^4) and equivalent isotropic displacement parameters (A^2 × 10^3) for **5.4**. U(eq) is defined as one third of the trace of the orthogonalized Uij tensor.

	x	y	z	U(eq)
Cr(1)	120(1)	702(1)	2332(1)	25(1)
C(1)	1408(4)	-156(4)	3881(3)	32(1)
C(2)	1791(5)	1061(4)	4026(3)	36(1)
C(3)	577(5)	1764(4)	3906(3)	34(1)
C(4)	-556(4)	977(4)	3696(3)	29(1)
C(5)	-98(4)	-243(4)	3628(3)	27(1)
C(6)	-966(4)	-1094(4)	2848(3)	26(1)
C(7)	-2552(4)	-1030(4)	2439(4)	36(1)
C(11)	-406(4)	-2290(4)	2692(3)	28(1)
C(12)	-803(4)	-2802(4)	1628(4)	31(1)
C(13)	-286(4)	-3922(4)	1493(4)	34(1)
C(14)	623(5)	-4552(4)	2420(4)	39(1)
C(15)	991(5)	-4066(4)	3471(4)	38(1)
C(16)	490(5)	-2948(4)	3613(4)	33(1)
C(21)	716(5)	1948(4)	1657(4)	36(1)
C(31)	-1656(4)	994(4)	1263(3)	28(1)
C(41)	767(4)	-351(4)	1508(4)	29(1)
O(21)	1052(4)	2704(3)	1207(3)	52(1)
O(31)	-2785(3)	1185(3)	622(2)	42(1)
O(41)	1197(3)	-989(3)	1018(3)	37(1)

Table 3. Bond lengths [A] and angles [^{o}] for **3.1a**.

Cr(1)-C(31)	1.841(4)
Cr(1)-C(21)	1.854(5)
Cr(1)-C(41)	1.862(5)
Cr(1)-C(5)	2.055(4)
Cr(1)-C(1)	2.142(4)
Cr(1)-C(4)	2.149(4)
Cr(1)-C(2)	2.230(4)
Cr(1)-C(3)	2.231(4)
Cr(1)-C(6)	2.488(4)
C(1)-C(2)	1.391(6)

C(1)-C(5)	1.457(6)
C(2)-C(3)	1.426(6)
C(3)-C(4)	1.393(6)
C(4)-C(5)	1.440(6)
C(5)-C(6)	1.412(6)
C(6)-C(11)	1.484(6)
C(6)-C(7)	1.508(6)
C(11)-C(12)	1.391(6)
C(11)-C(16)	1.392(5)
C(12)-C(13)	1.382(6)
C(13)-C(14)	1.386(6)
C(14)-C(15)	1.366(6)
C(15)-C(16)	1.376(6)
C(21)-O(21)	1.143(5)
C(31)-O(31)	1.154(5)
C(41)-O(41)	1.142(5)

C(31)-Cr(1)-C(21)	86.05(19)
C(31)-Cr(1)-C(41)	98.74(18)
C(21)-Cr(1)-C(41)	86.45(19)
C(31)-Cr(1)-C(5)	107.98(18)
C(21)-Cr(1)-C(5)	156.70(18)
C(41)-Cr(1)-C(5)	108.88(17)
C(31)-Cr(1)-C(1)	148.34(18)
C(21)-Cr(1)-C(1)	124.60(19)
C(41)-Cr(1)-C(1)	91.62(18)
C(5)-Cr(1)-C(1)	40.56(16)
C(31)-Cr(1)-C(4)	92.66(17)
C(21)-Cr(1)-C(4)	123.40(17)
C(41)-Cr(1)-C(4)	148.82(17)
C(5)-Cr(1)-C(4)	39.98(15)
C(1)-Cr(1)-C(4)	65.06(16)
C(31)-Cr(1)-C(2)	150.06(17)
C(21)-Cr(1)-C(2)	93.38(19)
C(41)-Cr(1)-C(2)	111.11(17)
C(5)-Cr(1)-C(2)	65.08(17)
C(1)-Cr(1)-C(2)	37.04(17)
C(4)-Cr(1)-C(2)	62.85(16)
C(31)-Cr(1)-C(3)	112.79(17)
C(21)-Cr(1)-C(3)	92.67(18)
C(41)-Cr(1)-C(3)	148.34(17)
C(5)-Cr(1)-C(3)	64.97(17)
C(1)-Cr(1)-C(3)	63.09(16)
C(4)-Cr(1)-C(3)	37.03(16)
C(2)-Cr(1)-C(3)	37.28(15)
C(31)-Cr(1)-C(6)	85.52(16)

C(21)-Cr(1)-C(6)	168.62(16)
C(41)-Cr(1)-C(6)	87.29(16)
C(5)-Cr(1)-C(6)	34.58(15)
C(1)-Cr(1)-C(6)	65.06(15)
C(4)-Cr(1)-C(6)	64.67(15)
C(2)-Cr(1)-C(6)	97.74(16)
C(3)-Cr(1)-C(6)	97.63(16)
C(2)-C(1)-C(5)	108.3(4)
C(2)-C(1)-Cr(1)	74.9(3)
C(5)-C(1)-Cr(1)	66.5(2)
C(1)-C(2)-C(3)	108.7(4)
C(1)-C(2)-Cr(1)	68.0(2)
C(3)-C(2)-Cr(1)	71.4(2)
C(4)-C(3)-C(2)	108.2(4)
C(4)-C(3)-Cr(1)	68.3(2)
C(2)-C(3)-Cr(1)	71.3(2)
C(3)-C(4)-C(5)	109.0(4)
C(3)-C(4)-Cr(1)	74.7(3)
C(5)-C(4)-Cr(1)	66.5(2)
C(6)-C(5)-C(4)	122.2(4)
C(6)-C(5)-C(1)	121.8(4)
C(4)-C(5)-C(1)	105.6(4)
C(6)-C(5)-Cr(1)	89.8(3)
C(4)-C(5)-Cr(1)	73.5(2)
C(1)-C(5)-Cr(1)	72.9(2)
C(5)-C(6)-C(11)	121.1(3)
C(5)-C(6)-C(7)	121.1(4)
C(11)-C(6)-C(7)	114.7(3)
C(5)-C(6)-Cr(1)	55.7(2)
C(11)-C(6)-Cr(1)	115.7(3)
C(7)-C(6)-Cr(1)	113.9(3)
C(12)-C(11)-C(16)	118.4(4)
C(12)-C(11)-C(6)	120.9(4)
C(16)-C(11)-C(6)	120.7(4)
C(13)-C(12)-C(11)	120.4(4)
C(12)-C(13)-C(14)	120.2(4)
C(15)-C(14)-C(13)	119.6(4)
C(14)-C(15)-C(16)	120.6(4)
C(15)-C(16)-C(11)	120.7(4)
O(21)-C(21)-Cr(1)	177.7(4)
O(31)-C(31)-Cr(1)	177.7(4)
O(41)-C(41)-Cr(1)	178.3(4)

Table 4. Anisotropic displacement parameters [A^2 × 10^3] for **3.1a**. The anisotropic displacement factor exponent takes the form:

-2pi^2 [h^2 a^2 U11 + ... + 2 hka*bU12]

	U11	U22	U33	U23	U13	U12
Cr(1)	28(1)	22(1)	21(1)	-2(1)	5(1)	-1(1)
C(1)	30(2)	39(3)	15(2)	1(2)	-4(2)	7(2)
C(2)	30(2)	47(3)	25(2)	-11(2)	3(2)	-3(2)
C(3)	44(3)	28(2)	23(2)	-10(2)	3(2)	5(2)
C(4)	30(2)	32(3)	20(2)	-4(2)	6(2)	5(2)
C(5)	30(2)	29(2)	20(2)	2(2)	8(2)	7(2)
C(6)	29(2)	24(2)	26(2)	6(2)	10(2)	1(2)
C(7)	31(2)	30(3)	51(3)	4(2)	18(2)	2(2)
C(11)	27(2)	25(2)	32(2)	4(2)	12(2)	2(2)
C(12)	28(2)	27(2)	34(2)	2(2)	6(2)	-3(2)
C(13)	34(2)	29(2)	39(3)	-7(2)	13(2)	-8(2)
C(14)	36(2)	22(2)	60(3)	-10(2)	20(2)	-1(2)
C(15)	37(3)	31(3)	45(3)	15(2)	14(2)	14(2)
C(16)	41(3)	30(2)	31(2)	3(2)	16(2)	6(2)
C(21)	49(3)	22(2)	36(3)	-6(2)	16(2)	-4(2)
C(31)	38(2)	21(2)	24(2)	-4(2)	9(2)	-1(2)
C(41)	30(2)	26(2)	30(2)	3(2)	11(2)	-4(2)
O(21)	76(3)	31(2)	55(2)	-1(2)	32(2)	-16(2)
O(31)	40(2)	45(2)	28(2)	3(1)	0(2)	14(2)
O(41)	49(2)	29(2)	40(2)	-8(1)	24(2)	-2(1)

Table 5. Hydrogen coordinates (x 10^4) and isotropic displacement parameters (A^2 x 10^3) for **3.1a**.

	x	y	z	U(eq)
H(1A)	2061	-854	3962	38
H(2A)	2753	1390	4177	44
H(3A)	543	2667	3960	41
H(4A)	-1528	1219	3616	34
H(7A)	-2878	-1589	2878	54
H(7B)	-2973	-1258	1642	54
H(7C)	-2835	-202	2530	54
H(12A)	-1433	-2379	989	38
H(13A)	-554	-4261	762	41
H(14A)	988	-5317	2327	47
H(15A)	1599	-4505	4109	46
H(16A)	758	-2621	4348	40

NMR Spectra

Compound Synthesis and Characterization

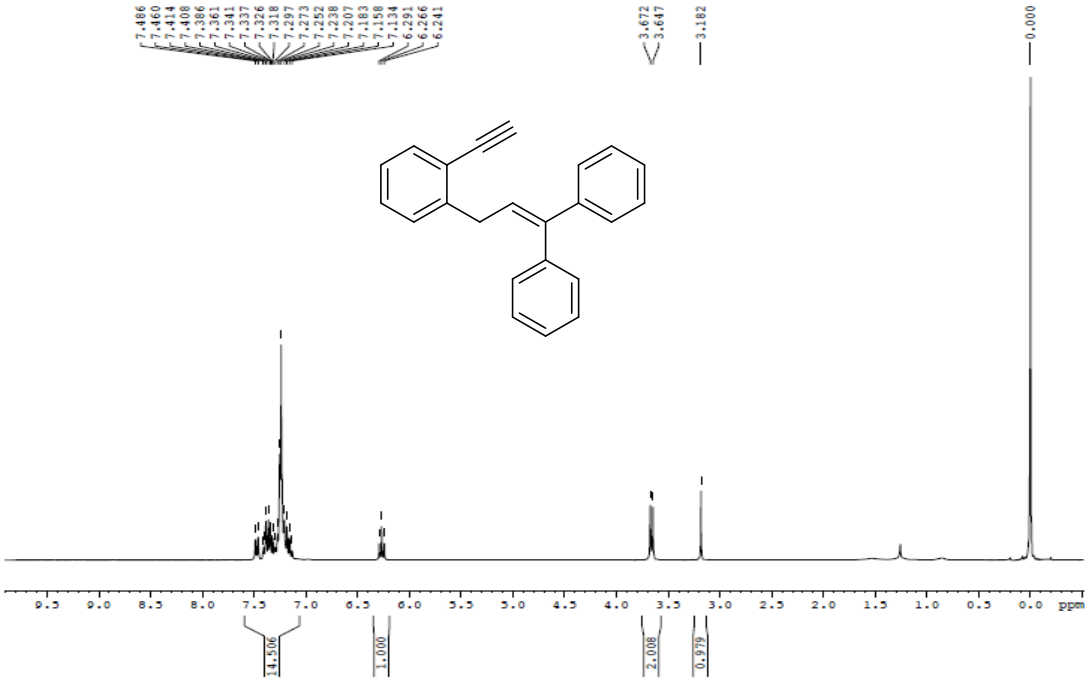

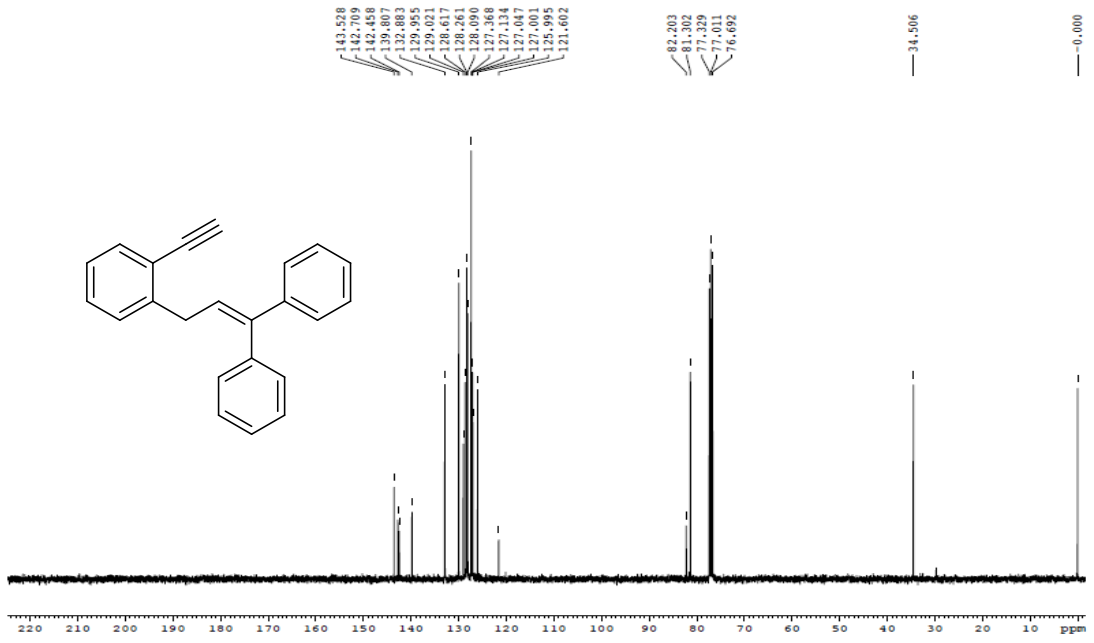
143.528
142.709
142.458
139.807
132.883
129.955
129.021
128.617
128.261
128.090
127.368
127.134
127.047
127.001
125.995
121.602
82.203
81.302
77.329
77.011
76.692
34.506
0.000
220 210 200 190 180 170 160 150 140 130 120 110 100 90 80 70 60 50 40 30 20 10 ppm

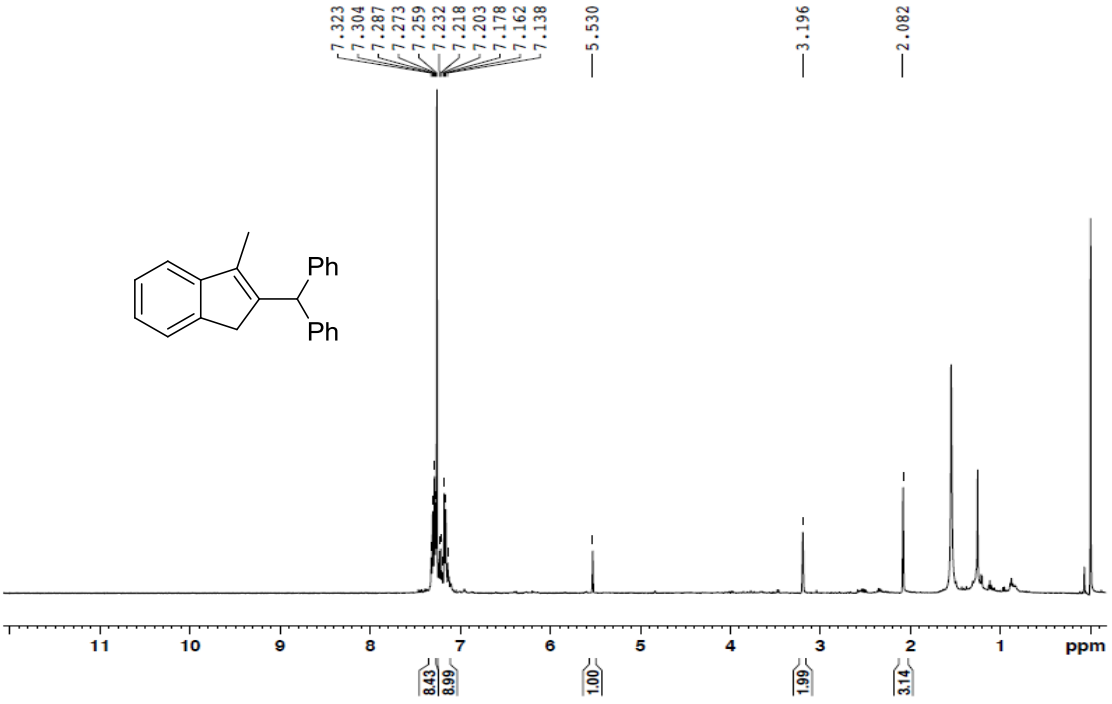
7.323
7.304
7.287
7.273
7.259
7.232
7.218
7.203
7.178
7.162
7.138
5.530
3.196
2.082
Ph
Ph
11 10 9 8 7 6 5 4 3 2 1 ppm
8.43
8.99
1.00
1.99
3.14

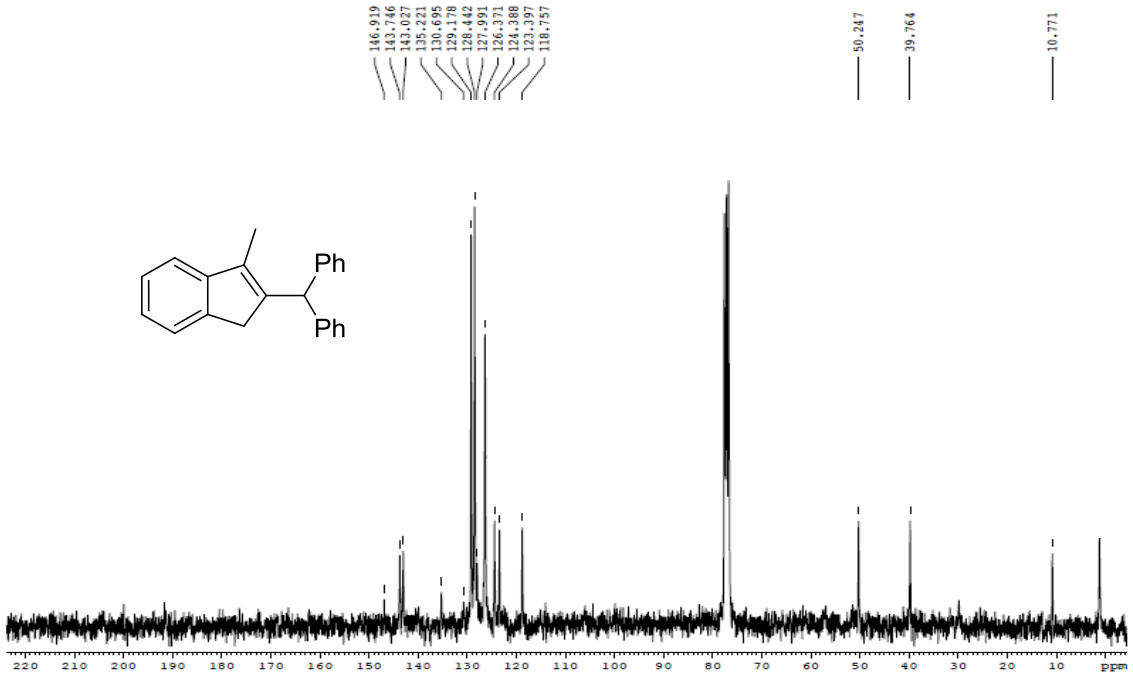
146.919
143.746
143.027
135.221
130.695
129.178
128.442
127.991
126.371
124.388
123.397
118.757
50.247
39.764
10.771
Ph
Ph
220 210 200 190 180 170 160 150 140 130 120 110 100 90 80 70 60 50 40 30 20 10 ppm

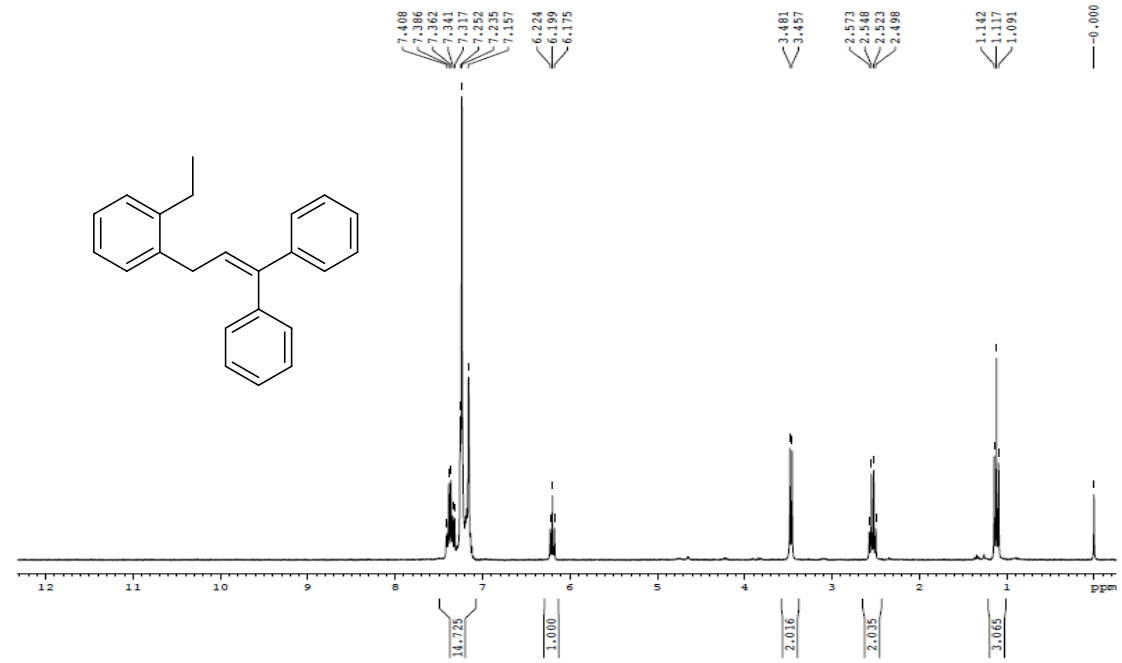
7.408
7.386
7.362
7.341
7.317
7.252
7.235
7.157
6.224
6.199
6.175
3.481
3.457
2.573
2.548
2.523
2.498
1.142
1.117
1.091
-0.000
12 11 10 9 8 7 6 5 4 3 2 1 ppm
14.725
1.000
2.016
2.035
3.065

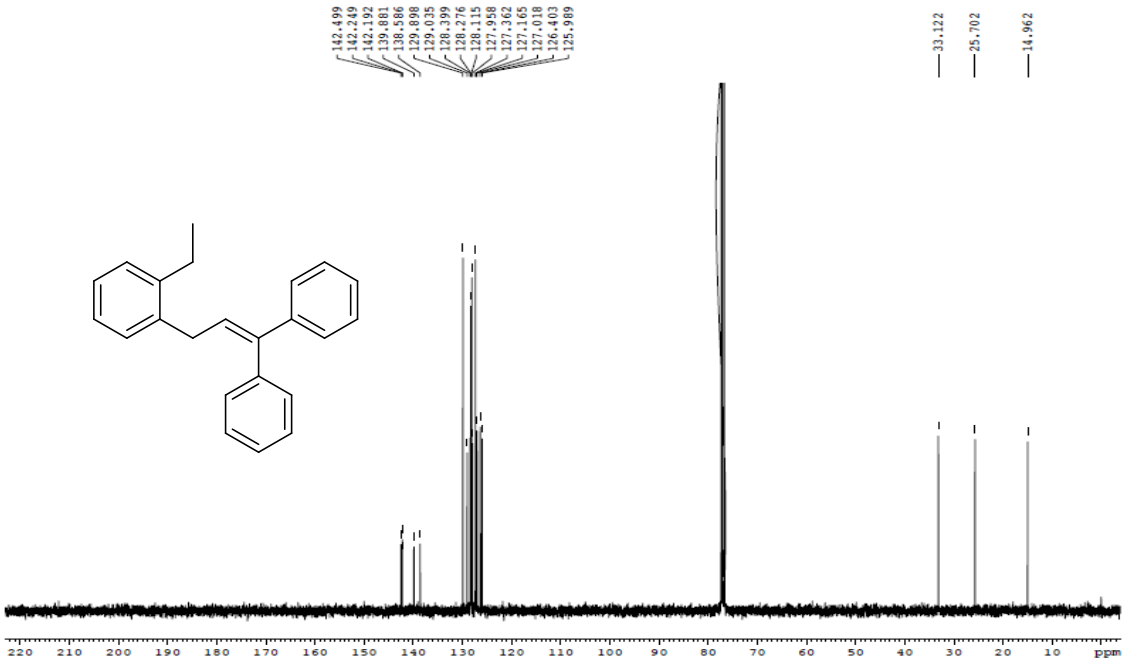
142.499
142.249
142.192
139.881
138.586
129.898
129.035
128.399
128.276
128.115
127.958
127.362
127.165
127.018
126.403
125.989
33.122
25.702
14.962
220 210 200 190 180 170 160 150 140 130 120 110 100 90 80 70 60 50 40 30 20 10 ppm

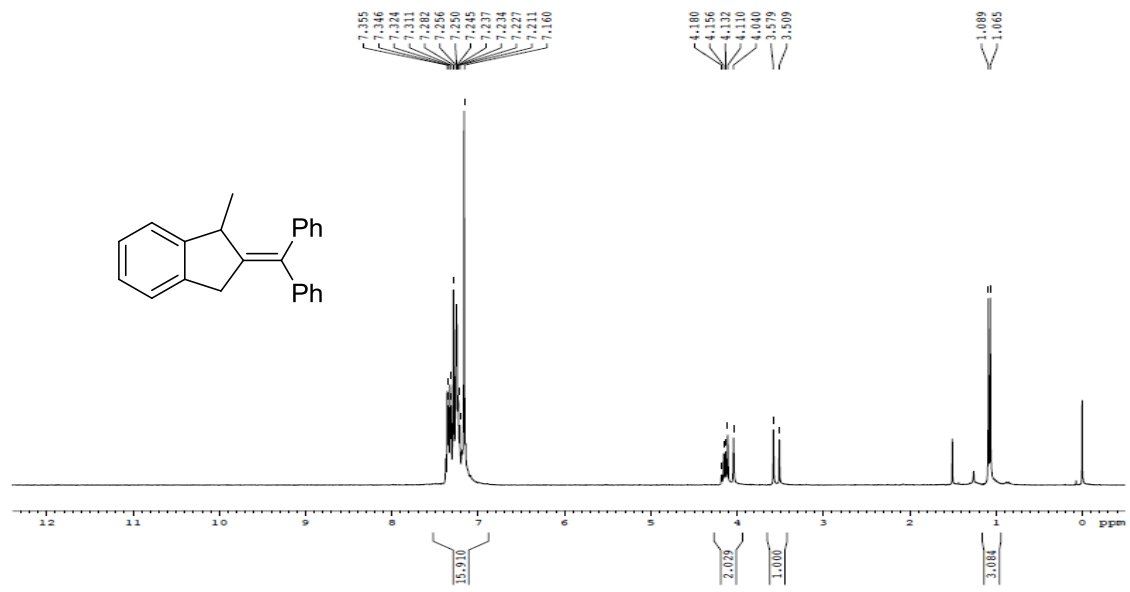
7.355
7.346
7.324
7.311
7.282
7.256
7.250
7.245
7.237
7.234
7.227
7.211
7.160
4.180
4.156
4.132
4.110
4.040
3.579
3.509
1.089
1.065
Ph
Ph
12 11 10 9 8 7 6 5 4 3 2 1 0 ppm
15.910
2.029
1.000
3.084

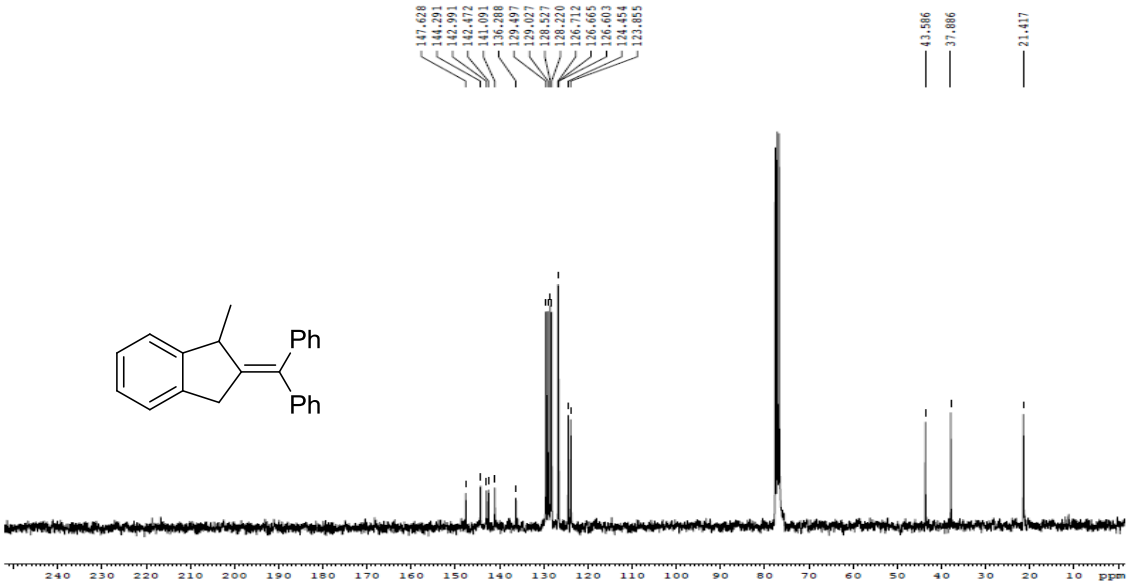
147.628
144.291
142.991
142.472
141.091
136.288
129.497
129.027
128.527
128.220
126.712
126.665
126.603
124.454
123.855
43.586
37.886
21.417
Ph
Ph
240 230 220 210 200 190 180 170 160 150 140 130 120 110 100 90 80 70 60 50 40 30 20 10 ppm

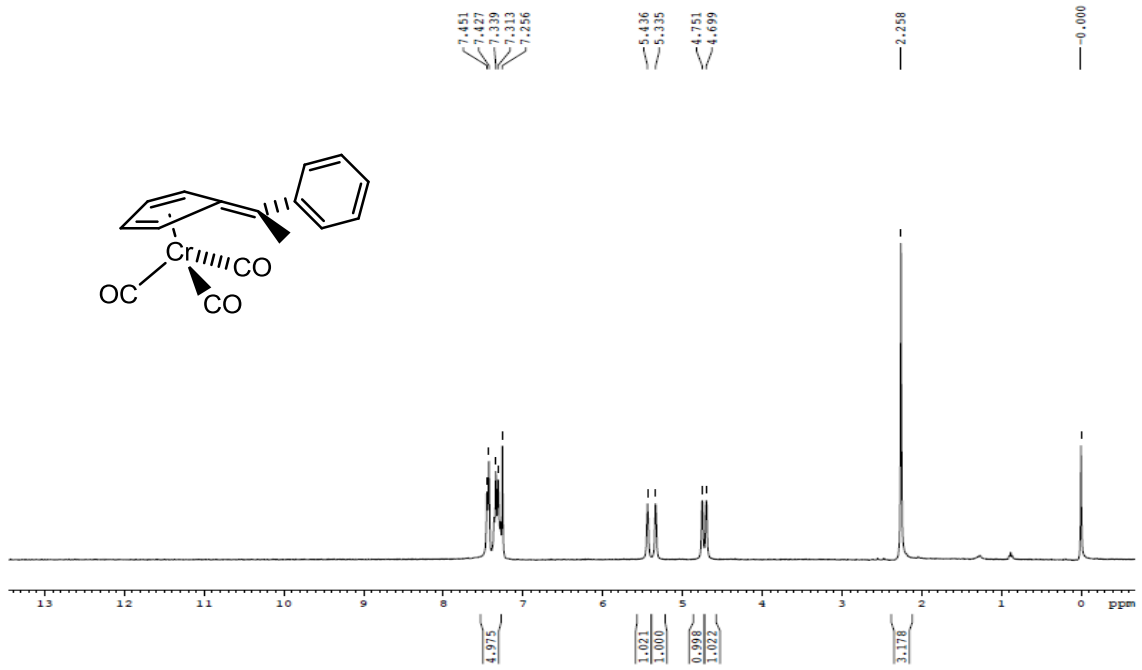
7.451
7.427
7.339
7.313
7.256
5.436
5.335
4.751
4.699
2.258
0.000
Cr
CO
OC
CO
13
12
11
10
9
8
7
6
5
4
3
2
1
0
ppm
4.975
1.021
1.000
0.398
1.022
3.178

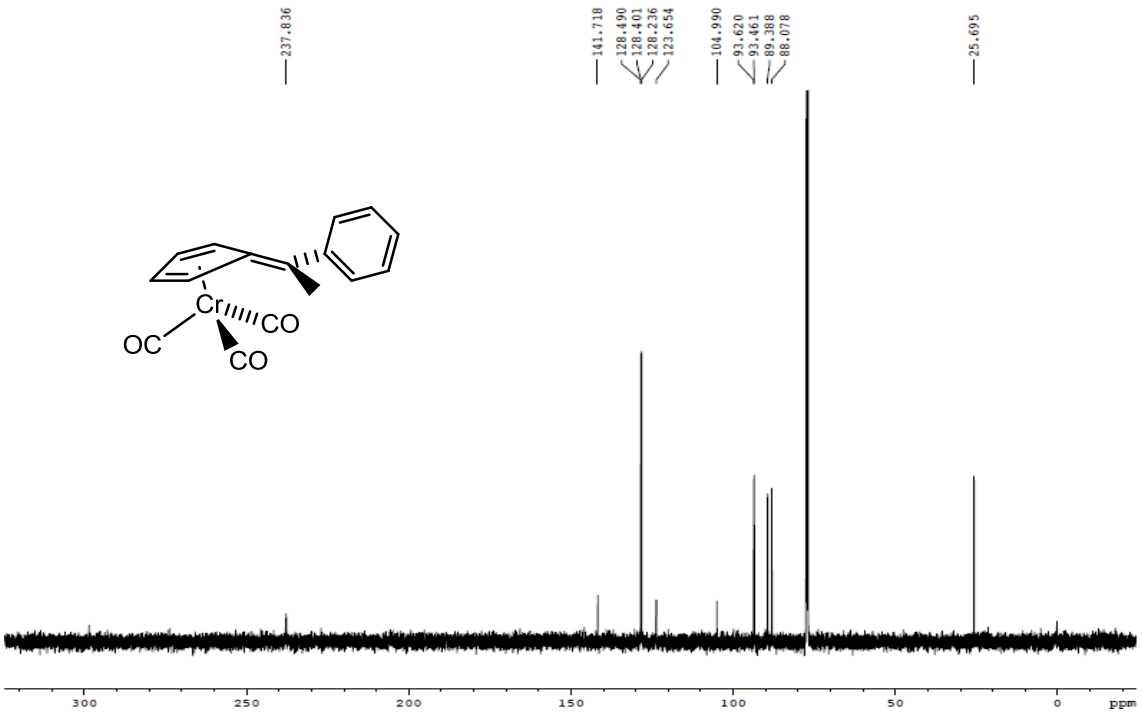
237.836
141.718
128.490
128.401
128.236
123.654
104.990
93.620
93.461
89.388
88.078
25.695
Cr
CO
OC
CO
300
250
200
150
100
50
0
ppm

Kinetic Traces (1 = CrH)

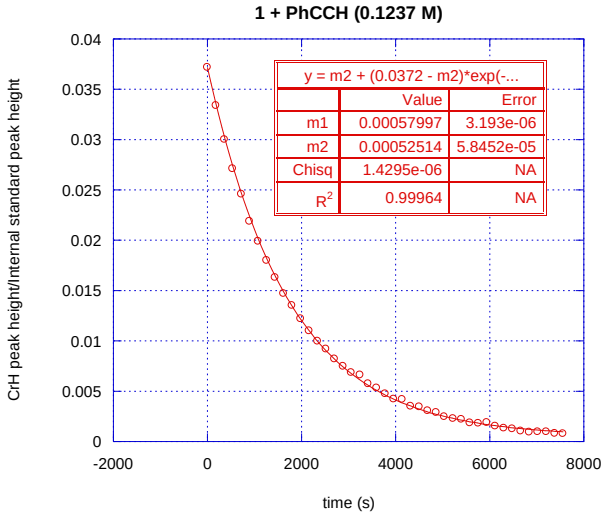

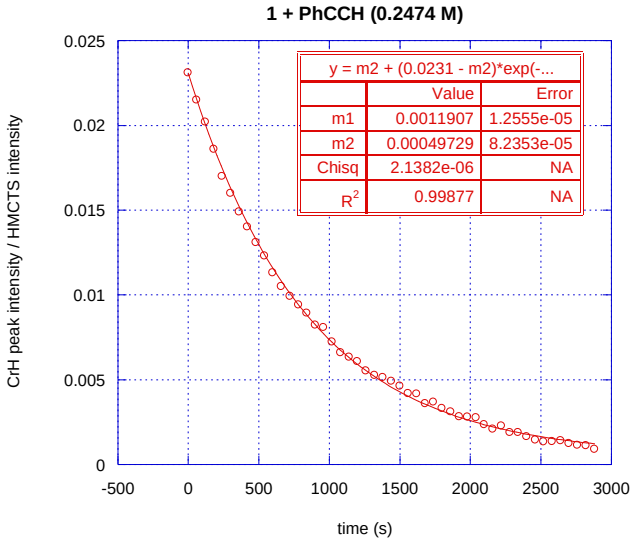

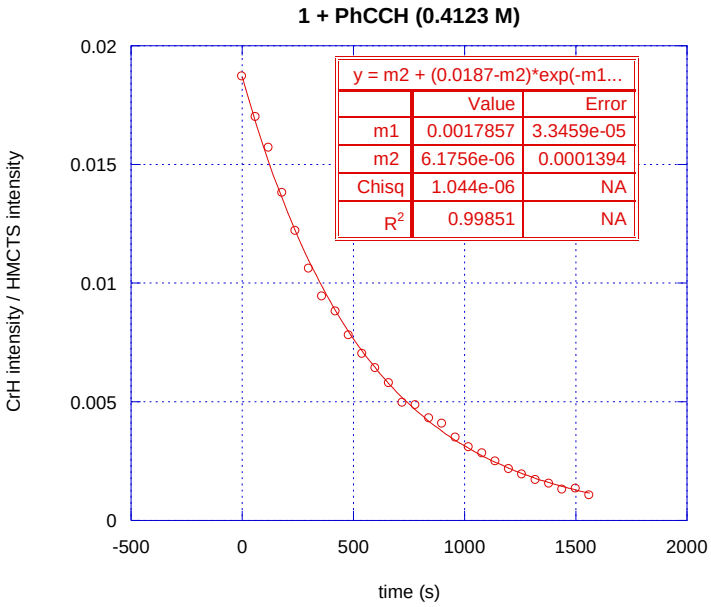
1 + PhCCH (0.4123 M)
y = m2 + (0.0187-m2)*exp(-m1...
Value
Error
m1
0.0017857
3.3459e-05
m2
6.1756e-06
0.0001394
Chisq
1.044e-06
NA
R2
0.99851
NA
CrH intensity / HMCTS intensity
time (s)
0.02
0.015
0.01
0.005
0
-500
0
500
1000
1500
2000

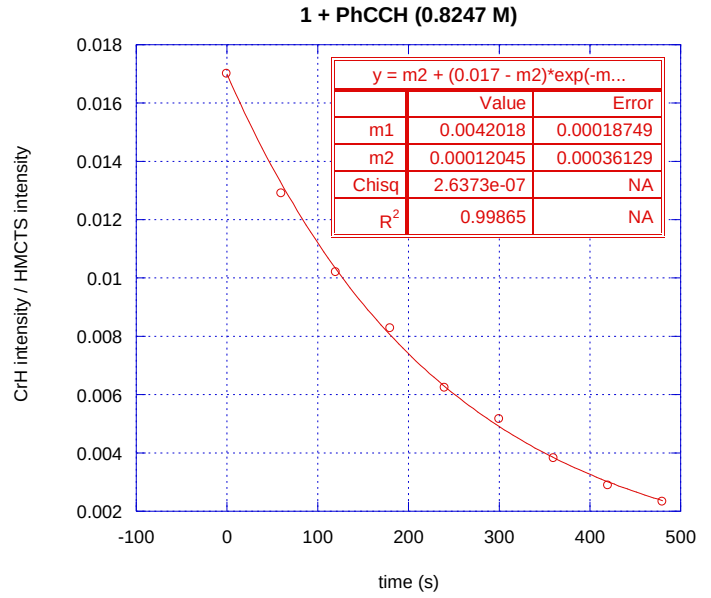
1 + PhCCH (0.8247 M)
y = m2 + (0.017 - m2)*exp(-m...
Value
Error
m1
0.0042018
0.00018749
m2
0.00012045
0.00036129
Chisq
2.6373e-07
NA
R2
0.99865
NA
CrH intensity / HMCTS intensity
time (s)
0.018
0.016
0.014
0.012
0.01
0.008
0.006
0.004
0.002
-100
0
100
200
300
400
500

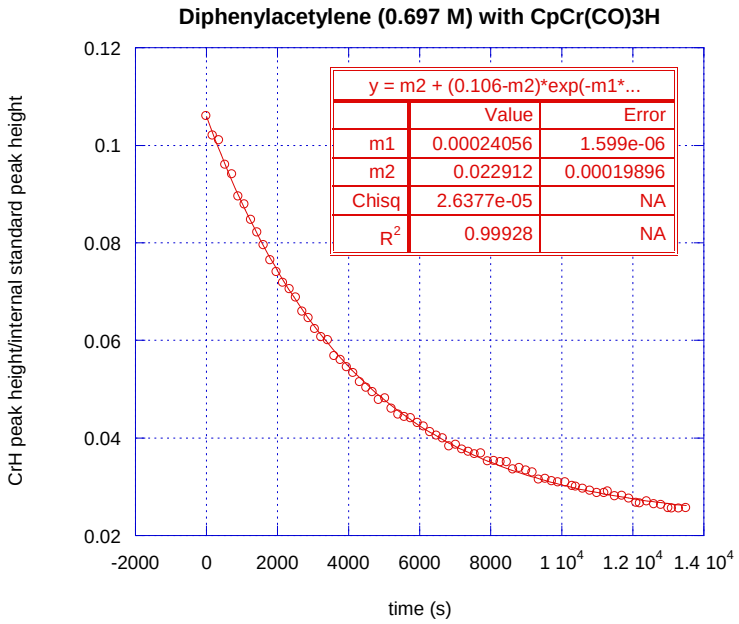
Diphenylacetylene (0.697 M) with CpCr(CO)3H
y = m2 + (0.106-m2)*exp(-m1*...
Value Error
m1 0.00024056 1.599e-06
m2 0.022912 0.00019896
Chisq 2.6377e-05 NA
R² 0.99928 NA
CrH peak height/internal standard peak height
time (s)
0.12
0.1
0.08
0.06
0.04
0.02
-2000
0
2000
4000
6000
8000
1 10⁴
1.2 10⁴
1.4 10⁴

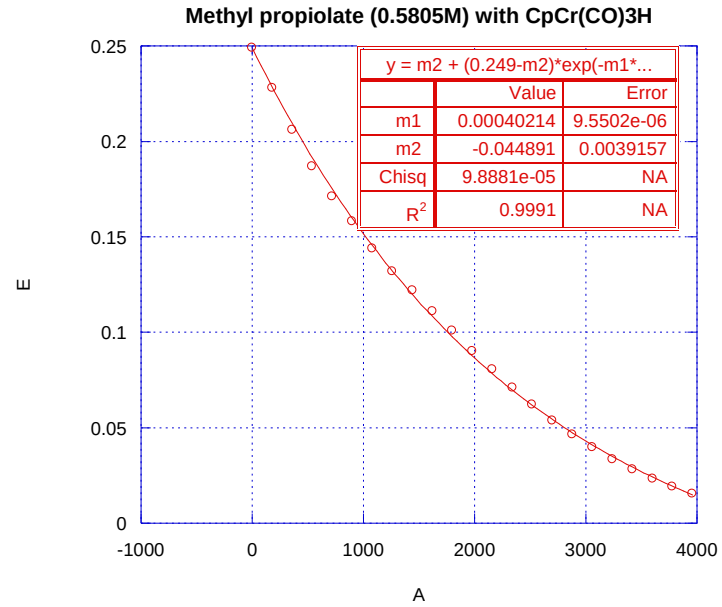
Methyl propiolate (0.5805M) with CpCr(CO)3H
y = m2 + (0.249-m2)*exp(-m1*...
Value Error
m1 0.00040214 9.5502e-06
m2 -0.044891 0.0039157
Chisq 9.8881e-05 NA
R² 0.9991 NA
E
A
0.25
0.2
0.15
0.1
0.05
0
-1000
0
1000
2000
3000
4000

EPR Spectra

$CpCr(CO)_3H$ + $MeO_2C{\equiv}CO_2Me$ ⟶

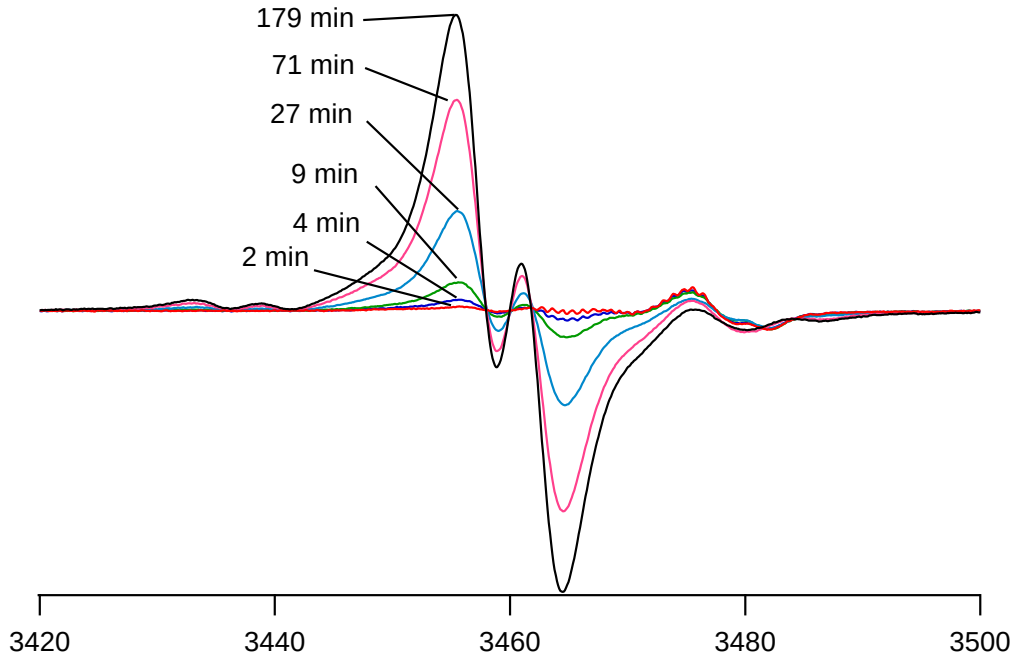

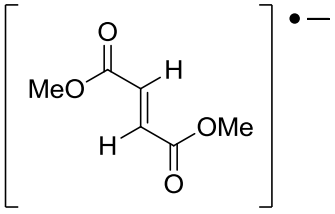

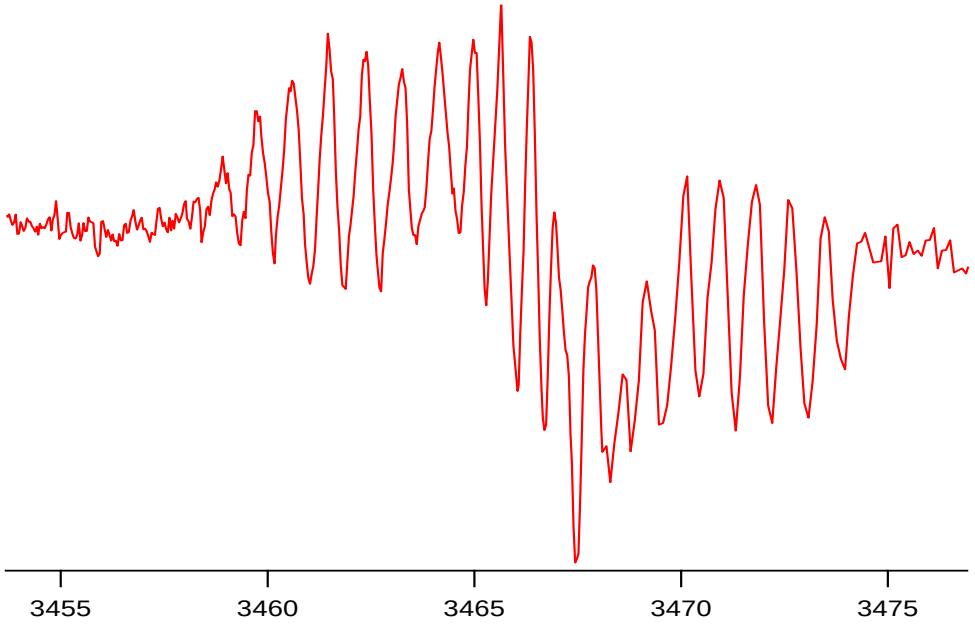

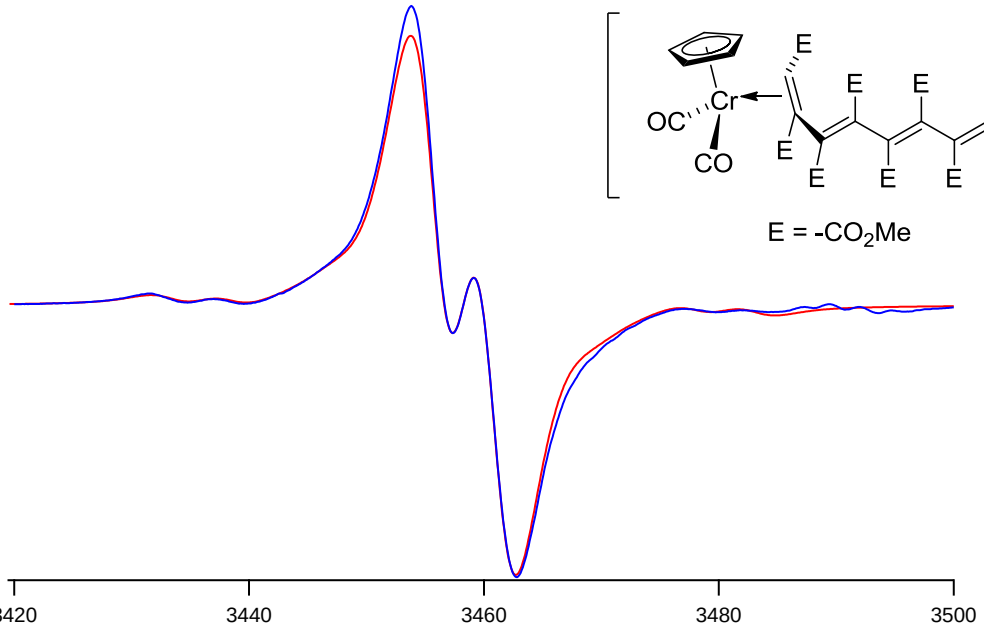

$CpCr(CO)_3D$ + $MeO_2C{-}{\equiv}{-}CO_2Me$ ⟶


3450
3460
3470
3480
3490

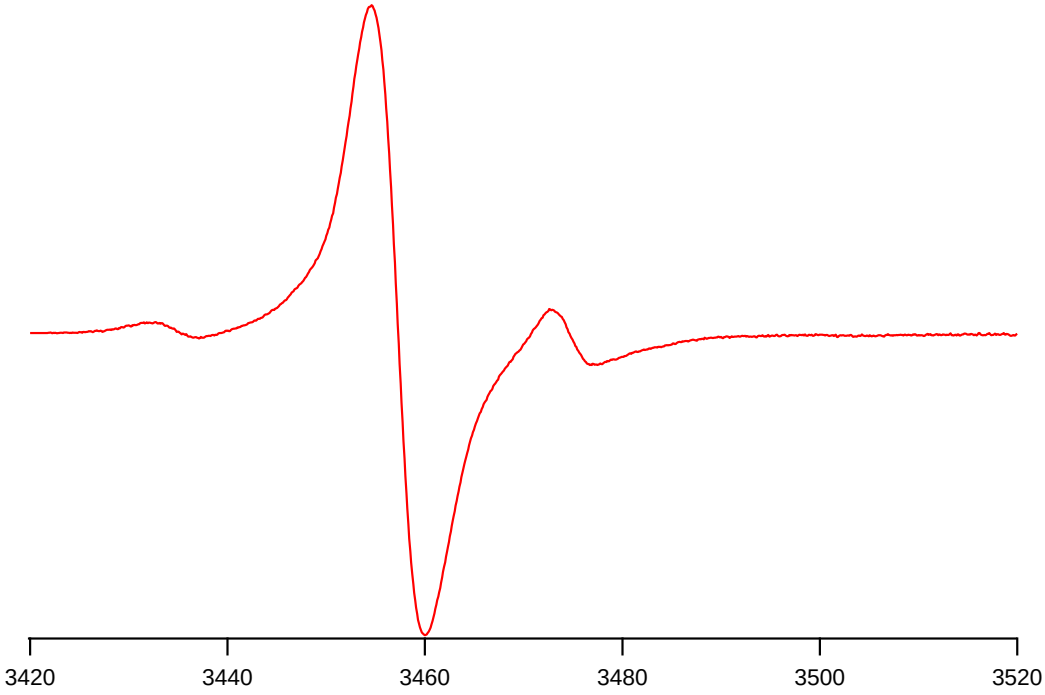
3420
3440
3460
3480
3500
3520

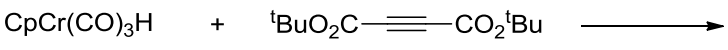
CpCr(CO)3H
+
tBuO2C
CO2tBu

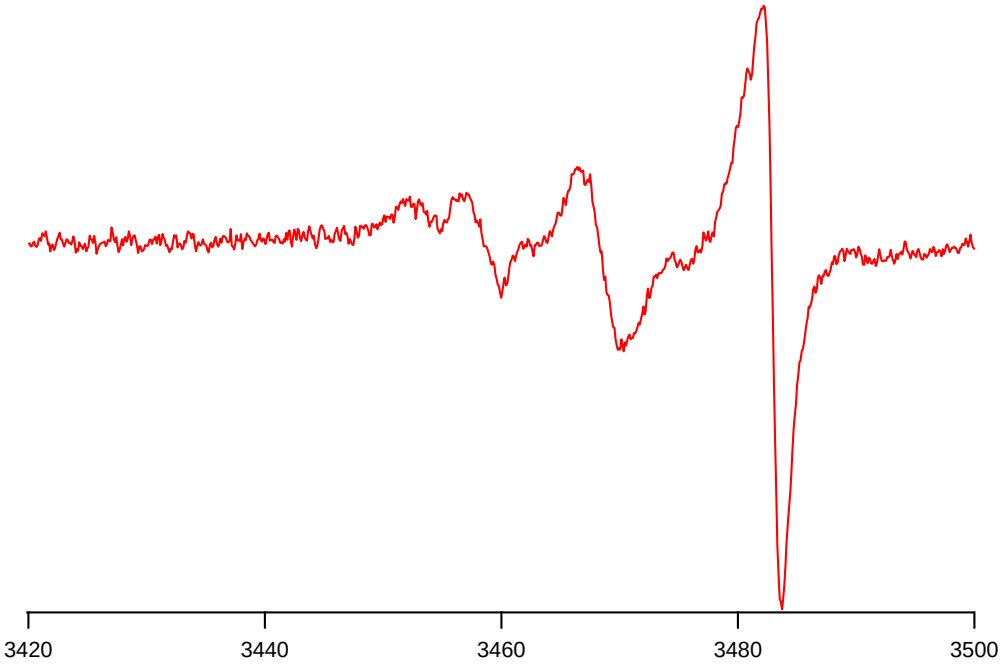
3420
3440
3460
3480
3500

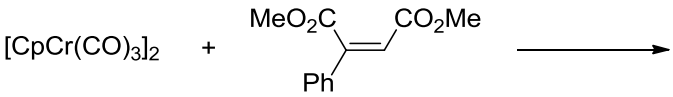
[CpCr(CO)3]2
+
MeO2C
CO2Me
Ph

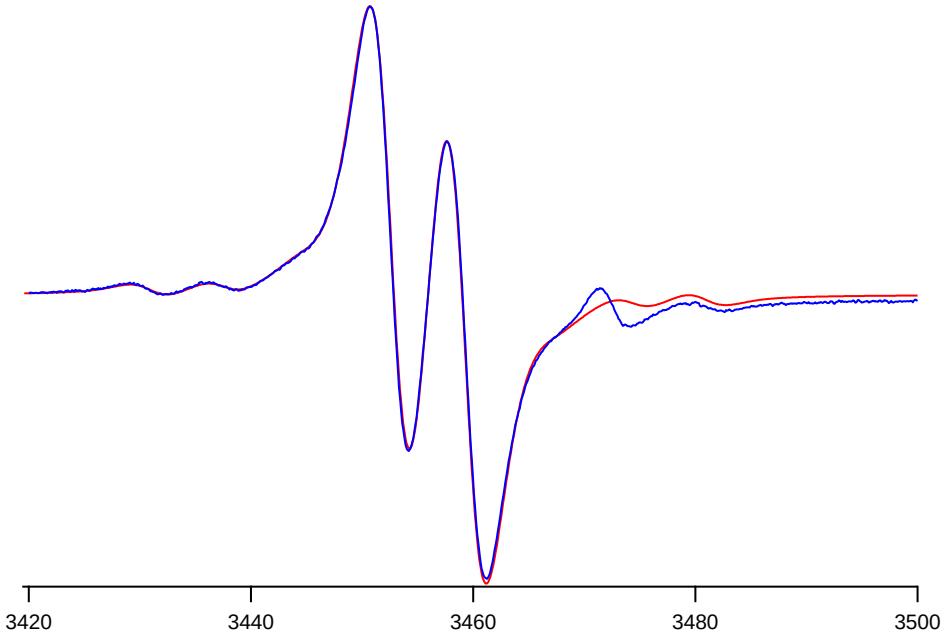
3420
3440
3460
3480
3500

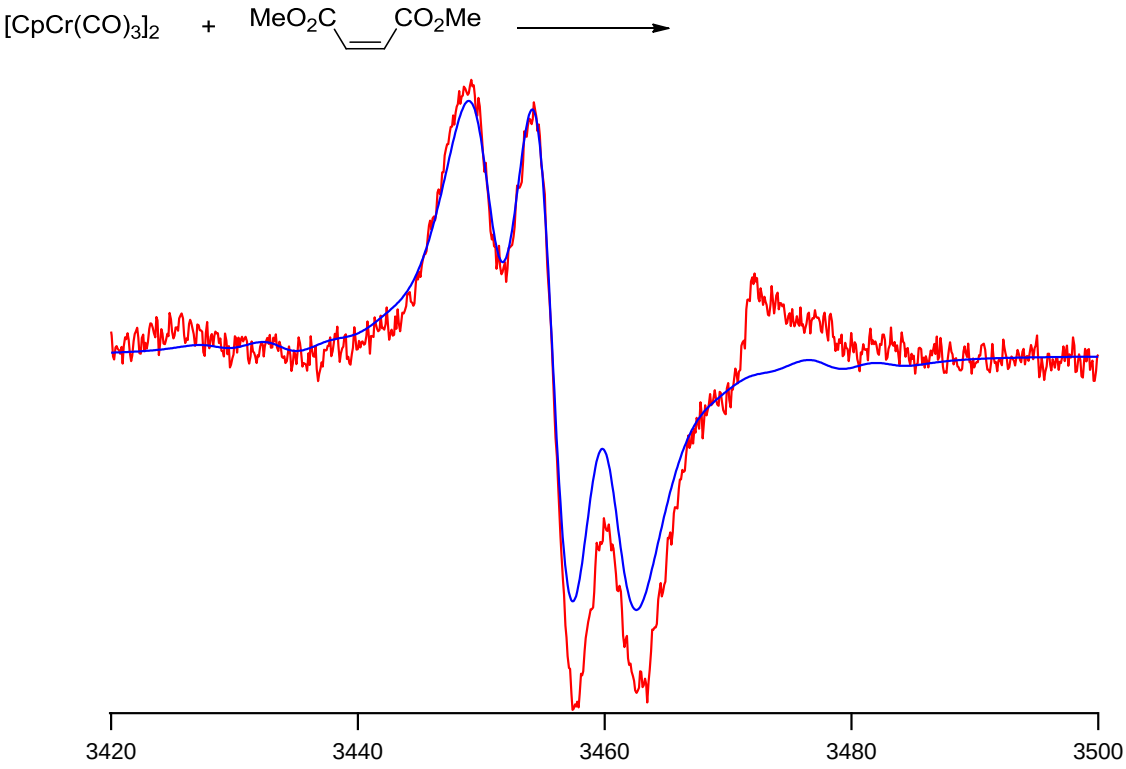
[CpCr(CO)3]2
+
MeO2C
CO2Me
3420
3440
3460
3480
3500

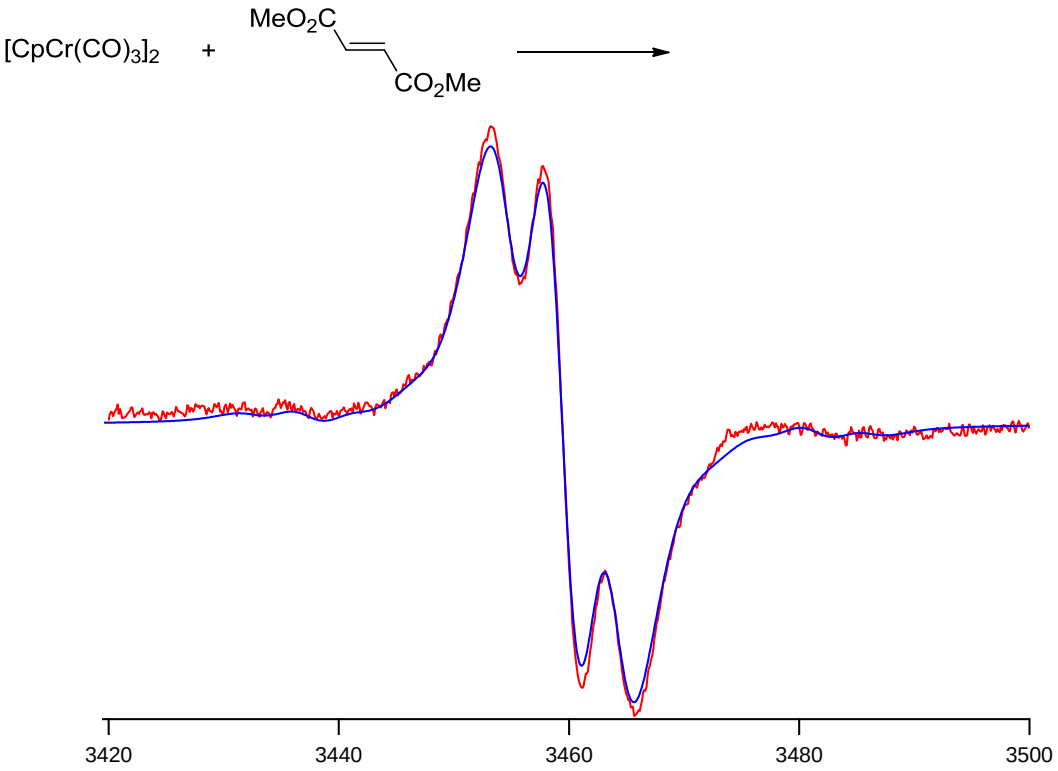
[CpCr(CO)3]2
+
MeO2C
CO2Me
3420
3440
3460
3480
3500

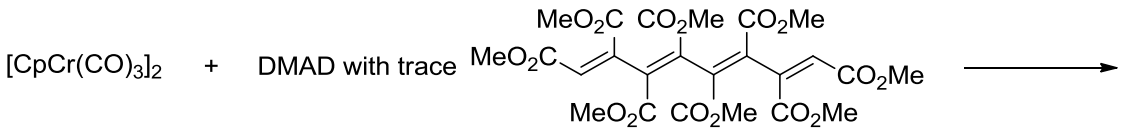
[CpCr(CO)3]2
+
DMAD with trace
MeO2C CO2Me CO2Me
MeO2C
CO2Me
MeO2C CO2Me CO2Me

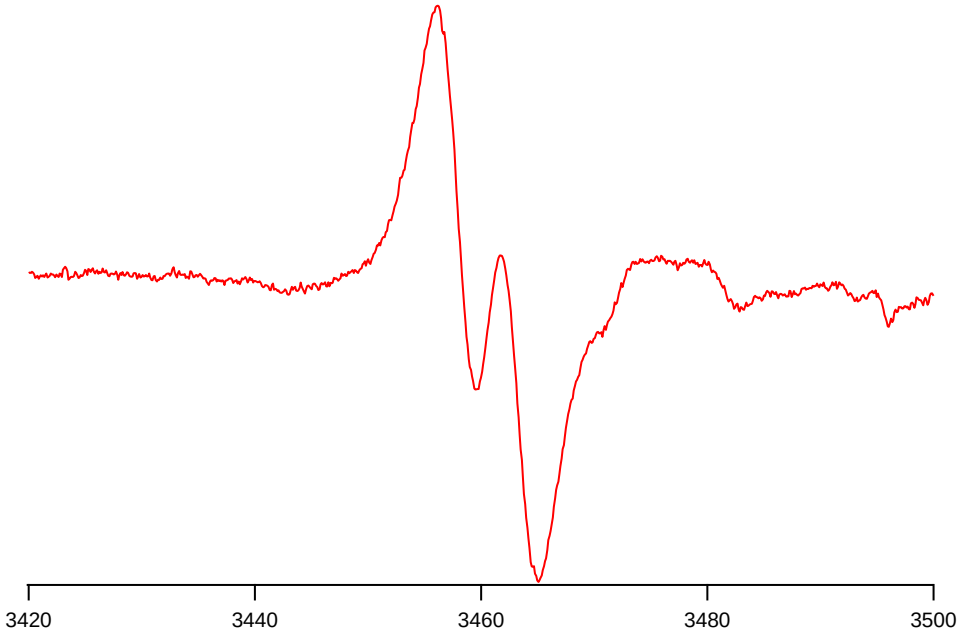
3420
3440
3460
3480
3500